



# **Plasma-Initiated Polymerization and Copolymerization and Analysis of Products**

vorgelegt von  
**M.Sc. Alaa Fahmy Mohamed**  
aus Kairo, Ägypten

Von der der Fakultät III - Institut für Werkstoffwissenschaften und -technologien  
Fachgebiet Polymertechnik und Polymerphysik  
der Technischen Universität Berlin  
zur Erlangung des akademischen Grades  
Doktor der Naturwissenschaften  
Dr. rer. nat.

genehmigte Dissertation

Promotionsausschuss:  
Vorsitzender: Prof. Dr. rer. nat. Walter Reimers  
Berichter: Prof. Dr. rer. nat. Jörg F. Friedrich  
Berichter: Prof. Dr.-Ing. Manfred H. Wagner

Tag der wissenschaftlichen Aussprache: 07.10.2011

Berlin 2011



# **Plasma-Initiated Polymerization and Copolymerization and Analysis of Products**

Submitted by  
Alaa Fahmy Mohamed  
from Cairo, Egypt

**Inaugural-Dissertation**  
In order to obtain the academic degree of  
Doctor of Natural Science (Dr. rer. nat.)

submitted to Faculty III  
Institute of Materials Science and Technology  
Department of Polymer Engineering and Polymer Physics  
Technical University of Berlin

Vorsitzender: Prof. Dr. rer. nat. Walter Reimers  
Gutachter: Prof. Dr. rer. nat. Jörg F. Friedrich  
Gutachter: Prof. Dr.-Ing. Manfred H. Wagner

07.10.2011

Berlin 2011

D 83

## **Statement of authenticity**

The undersigned declare that this Ph. D. thesis is based on research performed by the candidate for the Ph. D. of material science and technology degree Alaa Fahmy Mohamed, under the supervision of Prof. Dr. rer. nat. Jörg F. Friedrich within the Department of Polymer Surfaces at Federal Institute for Materials Research and Testing.

.....

.....

Alaa Fahmy Mohamed

Prof. Dr. rer. nat. Jörg F. Friedrich

Date:.....

## Acknowledgement

First of all, I would like to sincerely thank Prof. Dr. rer. nat. Jörg F. Friedrich (BAM-Federal Institute for Materials Research and Testing) for giving me the opportunity to join his group and finish my Ph. D. thesis under his supervision. I appreciate that he helped me a lot and gave me great support during my study at BAM. I also would like to thank Prof. Dr. rer. nat. Andreas Schönhals and Dr. Renate Mix (BAM-Federal Institute for Materials Research and Testing). They supervised me patiently and encouraged me during my whole thesis work. They gave me much knowledge about both theoretical and experimental skills of chemical and physical for polymers. Moreover, I was inspired by them giving me many good ideas and helped me a lot with data analysis and documentation.

I also would like to give special thanks to Prof. Dr. Manfred H. Wagner (Technical University-Berlin) for his supported for completing the thesis work as the second reviewer of my thesis.

It is my pleasant duty to thank my confreres Mrs. Gundula Hidde for her support to measure XPS, Mr. Milczewski for his cheerful laboratory support and Mr. Neubert who was always nice to help me with DSC analysis. I would like to thank ours department secretary Ms Haske and Ms Schulz for their understanding support and help at numerous times.

I thank all my friends for their good reviews and advices, especially Mr. Purohit, Mr. Yin and Mrs. Krause. At last but not least, I thank my God. He gave me senior professors in Germany. They were supported me in every things.

Last but not the least thanks are to parents and my family for the moral support and encouragement I received during the course of my work and studies. I could not have concentrate and focus on my studies without enduring patient support from my wife Marwa. In fact I owe special thanks to her towards understanding my working habits and allowing me to remain involved with my studies at maximal.

## Abstract

Plasma deposited polymer films from simple organic molecules with a polymerizable C=C bond (vinyl, acrylic, diene..., also with limitations allyl), such as acrylic acid, allyl alcohol and styrene with a thickness of about 150 nm were deposited by pulse plasma polymerization onto different substrates (inorganic and organic).

The structure-property relationships of these samples were studied with respect to the duty cycle [ $DC=t_{on}/(t_{on}+t_{off})$ ] of the pulsed plasma by a broad combination of different techniques and probes. For the first time volume-sensitive methods such as Fourier Transmittance Infrared (FTIR) and Dielectric Relaxation Spectroscopy (DRS) are combined with surface analytics by employing X-ray Photoelectron Spectroscopy (XPS). For an unambiguous identification of COOH and OH groups by XPS, derivatizations with trifluoroethanol (TFE) and trifluoroacetic anhydride (TFAA) were accomplished. FTIR gives in principal the same dependence of the concentration of COOH and OH groups on DC like XPS. The observed differences are discussed considering the different sampling depths of both methods.

The dielectric measurements reveal that the structure of the plasma deposited films is different from that of chemically produced reference polymers. In particular a lower glass transition temperature is observed.

The structure of plasma polymer films varies in dependence on the DC. This result refers to a highly branched structure of the plasma deposited (co)polymer with a high number of dangling chains. Moreover, the dielectric measurements show that the plasma deposited polymer films are not thermally stable but undergo a post-plasma chemical reaction during heating, where the reaction kinetics depends on the DC.

The retention of the monomer structure or its relevant units in the deposited film, e.g. aromatic rings in the case of styrene, COOH and OH groups in the case of acrylic acid and allyl alcohol plasma deposited polymers, decreases when the duty cycle becomes higher.

Plasma polymers with high functional group retention ( $FG_{\text{retention}} = FG_{\text{polymer}}/FG_{\text{monomer}}$ ) and a minimum degree of branching and cross-linking were obtained at low duty cycle applied in this study, i.e. with minimal duration of plasma pulses.

The idea was to minimize the plasma exposure as much as possible for suppressing the monomer fragmentation in the plasma and to improve the chance of chemical chain propagation in the plasma-off periods. Thus, it was expected that the number of defects and irregularities could be minimized and therefore the structure and composition of plasma polymers is nearer to that of classic (reference) polymers. Chemical polymerization was expected to produce regular structured and composed polymers, in contrast to plasma polymerization that was responsible for irregular structures produced by monomer fragmentation and random recombination of all fragments and atoms. The (short) plasma pulse should adopt the role of an initiator of the chemical (radical) chain growth in the monomer adsorption layer. General problem of chemical gas phase polymerization under low-pressure conditions is the deficiency in monomer molecules present at the chain propagation centers. Thus, chain terminations occur (recombination, chain transfer, disproportionation, rearrangement etc.) very rapidly and hinder the formation of linear polymer molecules of higher molar mass. The next plasma pulse creates a new radical center followed by very short chain propagation. Thus, branched and crosslinked polymers were produced.

Polystyrene (PS) spin coated thin films were modified by O<sub>2</sub> and Ar plasma and UV irradiation treatments for each one second. The modified PS samples were compared with plasma (pPS) and commercial (cPS) polystyrene. The effects of O<sub>2</sub> and Ar plasma and UV irradiation treatments on a surface and bulk of polymer layers were discussed. An important result was that one second exposure to the plasma or its radiation was sufficient to modify the surface significantly. However, this study was also dedicated to understand the effects of plasma particle shower and plasma irradiation on the already deposited layers of plasma polymers within the layer growing process.

The surface properties were evaluated by XPS and Contact Angle Measurements (CAM) and the bulk properties were investigated by FTIR and DRS. It was found that oxygen incorporation seems to proceed more rapidly with O<sub>2</sub> than with Ar plasma as well as with plasma polymerization and plasma UV irradiation, respectively.

Spin-coated PS thin films exposed to plasma UV irradiation and plasma deposited PS films did not show many differences in the XPS spectrum and CAM in comparison to commercial reference polystyrene. The dielectric measurements showed that the plasma deposited films were not thermally stable and underwent an undesired post-plasma chemical oxidation. However, the chemical structure of plasma deposited films is different from that of the reference PS.

Copolymers of acrylic acid and styrene (AA/S) were prepared by pulsed plasma deposition and their structures were studied with respect to the DC and feed gas ratio (comonomer ratio). It is known that low energy doses enhance the structural retention of comonomer and high energy doses prefer fragmentation and loss in regular structure. Additionally, it was found that through a proper selection of the feed gas composition the concentration of the surface functional groups in plasma deposited films can be controlled. The FTIR spectra of the plasma-deposited copolymer films were found to be partially different from a superposition of the spectra of the respective plasma homopolymers. This suggests that interactions and fragmentation followed by recombination reactions are taking place between the monomer molecules in the plasma or during their respective plasma deposition process.

Plasma deposited acrylic acid-styrene copolymer films were prepared and characterized using XPS, FTIR, differential scanning calorimetry (DSC) and DRS. The relative partial flow rates of the comonomer are used for adjustment of the copolymer composition. Process parameters were fixed to conditions optimized for retention of functional groups. By doing this it is possible to control undesired chemical properties of the copolymer films such as concentration of unsaturations or oxygen-containing functional groups.

The results obtained by dielectric spectroscopy are discussed in detail together with the data from FTIR and XPS measurements.



## **Zusammenfassung**

In dieser Arbeit wurden im Plasma abgeschiedene Polymerfilme von einfachen organischen Molekülen mit polymerisierbaren C=C-Bindungen (Vinyl, Acryl, Dien, ..., mit Einschränkungen auch Allyl), wie in Acrylsäure, Allylalkohol und Styrol vorhanden, mit einer Dicke von etwa 150 nm durch Pulsplasmapolymerisation auf verschiedenen anorganischen und organischen Substraten erzeugt.

Die Struktur-Eigenschaftsbeziehungen dieser Proben wurden in Abhängigkeit vom Tastverhältnis  $[DC=t_{on}/(t_{on}+t_{off})]$  des Hochfrequenzplasmas mittels einer weit gefächerten Kombination von verschiedenen Techniken und Prüfmethoden untersucht. Es wurden zum einen volumensensitive Methoden wie die Fourier-Transform-Infrarotspektroskopie (FTIR) und die dielektrische Relaxationsspektroskopie (DRS) eingesetzt, die mit Oberflächenanalysetechniken wie die Röntgenphotoelektronenspektroskopie (XPS) kombiniert werden. Um eine eindeutige Identifizierung der COOH- und OH-Gruppen in den abgeschiedenen Schichten ermöglichen zu können, wurden diese mit 2,2,2-Trifluorethanol (TFE) bzw. Trifluoressigsäureanhydrid (TFAA) derivatisiert. Die FTIR-Analytik zeigt prinzipiell dieselbe Abhängigkeit der COOH-bzw. OH-Gruppenkonzentration vom Tastverhältnis DC wie die XPS. Die beobachteten Unterschiede werden im Hinblick auf die verschiedenen Eindringtiefen der beiden Analysemethoden diskutiert.

Die DRS-Messungen offenbaren, daß sich die im Plasma abgeschiedenen Polymerfilme von den chemisch erzeugten Referenzpolymeren strukturell unterscheiden. Zum Beispiel wird eine niedrigere Glasübergangstemperatur beobachtet.

Die Struktur der im Plasma abgeschiedenen Polymerfilme variiert in Abhängigkeit von DC. Dieses Ergebnis kann mit der hochverzweigten Struktur der plasmaabgeschiedenen (Co)-Polymere erklärt werden, die eine große Anzahl an Seitenketten besitzen. Überdies zeigen die DRS-Messungen, daß die plasmaerzeugten Polymerfilme thermisch instabil sind;

nach der Plasmabehandlung gehen sie chemische Reaktionen während ihrer Erwärmung ein, wobei die Reaktionskinetik von gewählten DC abhängt.

Die Monomerstruktur bzw. die relevanten funktionellen Einheiten wie aromatische Ringe im Fall von Styrol, COOH- und OH-Gruppen im Fall von Acrylsäure und Allylalkohol werden in immer geringerem Maße als stabile Einheiten in die Polymerstruktur der Filme übernommen, je höher das Tastverhältnis DC wird. Im Plasma erzeugte Polymere mit hoher Retention der funktionellen Gruppen ( $FG_{\text{retention}} = FG_{\text{polymer}}/FG_{\text{monomer}}$ ) und einem minimalen Verzweigungsgrad bzw. minimaler Anzahl an Querverzweigungen können dann erhalten werden, wenn ein niedriges Tastverhältnis angewendet wird, also kurze Plasmapulsdauer und lange plasmalose Pausen.

Die Absicht war, die Plasmaexposition der Monermoleküle so gering wie möglich zu halten, um die Monomerfragmentierung im Plasma zu unterdrücken und die Wahrscheinlichkeit der chemischen Kettenfortpflanzungen besonders nach Ende jeden Plasmapulses zu erhöhen. Dadurch sollte die Defektdichte und die Strukturirregularitäten minimiert werden, um plasmaabgeschiedene Polymere zu erhalten, die sich strukturell und von der Zusammensetzung her kaum oder gar nicht mehr von den klassischen Referenzpolymeren unterscheiden. Die chemische Polymerisation sollte regelmäßig strukturierte und einheitliche Polymere bilden, ganz im Gegensatz zur fragmentierenden Plasmapolymerisation, welche die unregelmäßigen Strukturen durch Monomerzerfall und zufällige Rekombinationen aller Fragmente und Atome verursacht.

Ein (kurzer) Plasmapuls sollte dabei die Rolle des Initiators bei der chemischen Radikalkettenwachstumsreaktion in der obersten Monomeradsorptionsschicht übernehmen. Jedoch liegt das generelle Problem der chemischen Gasphasenniederdruckpolymerisation in der geringen Monomerkonzentration direkt an den radikalischen Kettenfortpflanzungszentren. Dementsprechend kommt es sehr schnell zu Kettenabbrüchen (Rekombinationen, Kettenübertragungen, Disproportionierungen, Umlagerungen etc.), die die Bildung linearer Polymere

hoher Molmasse verhindern. Der nächste Plasmapulss erzeugt ein neues Radikalzentrum gefolgt von einem sehr kurzen Kettenwachstum. Daher werden verzweigte und kreuzverknüpfte Polymere erzeugt.

Diese Studie war ebenso dazu gedacht, die Einwirkungen des Plasmapartikelstromes und der Strahlung auf bereits gebildete Polymerfilme während der Polymerfilmwachstumsphase zu verstehen.

Dazu wurden dünne Polystyrolfilme (PS, spin-coated) einem Sauerstoff- oder Argonplasma als auch UV-Strahlung ausgesetzt. Die so veränderten PS-Filme wurden mit plasmopolymerisiertem PS und kommerziellen (cPS) Polystyrol verglichen. Die Effekte der Sauerstoff- und Argonplasma als auch UV-Strahlungsbehandlung auf die Polymeroberfläche und das Polymer als Ganzes wurden diskutiert. Ein wichtiges Ergebnis war, daß die Polymeroberfläche nach nur einer Sekunde Plasma- oder Strahlungsexposition signifikant modifiziert ist.

Die Oberflächeneigenschaften wurden mittels XPS und durch Kontaktwinkelmessungen (CAM) analysiert und die Eigenschaften des Polymers als Ganzes wurden mittels FTIR und DRS bestimmt. Es wurde gefunden, daß der Sauerstoffeinbau schneller unter Benutzung eines Sauerstoff- anstelle eines Argonplasmas geschieht; ebenso gut funktionieren die Plasmapolymerisation und die Plasma-UV-Bestrahlung.

Dünne PS spin-coated Filme, die der Plasma-UV-Strahlung ausgesetzt waren und die rein plasmachemisch erzeugten Filme sind nicht sehr verschieden von den käuflichen Referenzpolystyrolen, wenn man die XPS-Spektren und die Kontaktwinkelmessergebnisse vergleicht. Die DRS-Messungen zeigten, daß plasmaerzeugte Filme nicht besonders temperaturstabil sind und störende chemische Oxidationen nach der Plasmabehandlung eingeht. Damit ist auch die chemische Struktur der plasmaerzeugten Polymerfilme von der der Referenzpolystyrole verschieden.

Plasmaerzeugte Acrylsäure/Styrol Copolymere (AA/S) wurden abgeschieden und die Strukturen untersucht in Abhängigkeit von DC und vom Comonomerverhältnis. Bekannterweise erhöht ein geringer Energieeintrag die strukturelle Stabilität des Comonomers, während hohe Energieeinträge zu bevorzugter Fragmentierung und zum Verlust der strukturellen Integrität und Regularität führen. Zudem wurde gefunden, daß die Oberflächenkonzentrationen der funktionellen Gruppen auf plasmaerzeugten Polymerfilmen über das Comonomerverhältnis gesteuert werden kann. Die FTIR Spektren der plasmaerzeugten Homopolymere unterschieden sich teilweise von denen der Copolymere. Dies deutet darauf hin, daß zwischen den Monomermolekülen im Plasma bzw. während des Abscheidungsprozesses gewisse Wechselwirkungen, auftreten, die zu Fragmentierungen und Rekombinationen auftreten.

Die relativen partiellen Flußraten der Comonomere wurden zur Beeinflussung der Copolymerzusammensetzung benutzt. Die Prozeßparameter wurden dabei auf einen optimalen Wert konstant gehalten, um die Stabilität der funktionellen Gruppen zu gewährleisten. Somit ist es möglich, unerwünschte chemische Eigenschaften der Copolymerfilme unter Kontrolle zu halten wie die Anzahl von ungesättigten Funktionalitäten und sauerstoffhaltigen funktionellen Gruppen.

Im Plasma abgeschiedene Acrylsäure-Styrol-Copolymerfilme wurden hergestellt und mittels XPS, FTIR, Differential Scanning Calorimetry (DSC) und DRS untersucht. Die Ergebnisse der dielektrischen Spektroskopie werden im Detail behandelt zusammen mit den Daten der FTIR und XPS Messungen.

## Contents

<b>Contents.....</b>	<b>I</b>
<b>List of abbreviations.....</b>	<b>VI</b>
<b>List of Figures .....</b>	<b>VIII</b>
<b>List of Tables.....</b>	<b>XVIII</b>
<b>List of Schemes .....</b>	<b>XVIII</b>
<b>CHAPTER 1 .....</b>	<b>1</b>
<b>Introduction .....</b>	<b>1</b>
1. Background and basics.....	1
1.1. Plasma state .....	1
1.2. Classification of plasmas.....	3
1.2.1. Cold plasmas .....	3
1.2.1.1. Low-pressure .....	3
1.2.1.2. Atmospheric pressure .....	8
1.2.1.3. Low-pressure high-density plasmas .....	8
1.3. Applications of plasma low-pressure .....	8
1.3.1. Functionalization of organic and inorganic polymeric surfaces .....	8
1.3.2. Plasma deposition of biocompatible layers .....	9
1.3.3. Etching of polymer surfaces.....	10
1.3. Surface functionalization.....	10
1.3.1. Plasma treatment .....	10
1.3.2. Plasma polymerization .....	12

1.3.2.1. Basics of plasma polymerization.....	12
1.3.2.2. External plasma parameters .....	14
1.3.2.3. Radicals generation and polymerization .....	17
2. Review of literatures related to plasma (co)polymerization .....	18
2.1. Homopolymerization.....	19
2.2. Copolymerization .....	24
3. Motivation .....	29
3.1. Plasma polymerization .....	29
3.2. Plasma copolymerization .....	31
3.3. Organic and inorganic substrates .....	32
4. Enrichment of functional groups at substrate surfaces.....	34
5. Approach and perspective of the work.....	35
5.1. Brief overview of proposed work.....	35
<b>CHAPTER 2 .....</b>	<b>37</b>
<b>Experimental.....</b>	<b>37</b>
1. Chemical structures .....	37
2. Materials.....	38
3. Sample preparation.....	39
3.1. Plasma deposited thin films.....	39
3.1.1. Plasma deposited thin polymer films .....	39
3.1.2. Plasma deposited thin copolymer films .....	42
3.2. Spin coated thin films.....	42
4. Characterization methods .....	43
4.1. Surface functionality .....	43
4.1.1. Derivatization of functional groups for improved XPS analysis .....	44

4.1.1.1. Carboxylic group derivatization.....	44
4.1.1.2. Hydroxyl group derivatization .....	46
4.2. Contact angle measurements (CAM) .....	47
4.3. Chemical composition estimated by FTIR.....	47
4.4. Thermal measurements .....	48
4.5. Dynamic mobility and dielectric properties .....	48
<b>CHAPTER 3 .....</b>	<b>50</b>
<b>Results and discussion.....</b>	<b>50</b>
1. Acrylic acid plasma deposited thin polymer films.....	50
1.1. Kinetics of polymer deposition .....	50
1.2. Estimation of the surface functionality by derivatization and XPS .....	52
1.3. Investigation of the chemical composition by FTIR.....	54
1.4. Thermal properties .....	57
1.5. Dynamic mobility and thermal stability.....	58
2. Allyl alcohol plasma deposited thin polymer films .....	70
2.1. Kinetics of polymer deposition .....	70
2.2. Estimation of the surface functionality by derivatization and XPS .....	72
2.3. Investigation of the functionality of films on different substrates by FTIR.....	75
2.4. Dynamic mobility and thermal stability.....	80
3. Plasma deposited and spin coated thin polystyrene films .....	89
3.1. Functionalization.....	89
3.2. Chemical composition of the films .....	92
3.3. Contact angle measurement (CAM).....	94
3.4. Dynamic mobility and thermal stability.....	95
4. Acrylic acid-styrene plasma deposited thin copolymer films .....	103

4.1. Influence of the Duty Cycle .....	104
4.1.1. Kinetics of the copolymer deposition.....	104
4.1.2. Retention of functional groups during copolymerization .....	106
4.1.3. Investigation of the chemical composition by FTIR .....	110
4.1.4. Thermal analysis .....	114
4.1.5. Dynamic mobility and thermal stability .....	115
4.2. Influence of the comonomer ratio .....	123
4.2.1. Kinetics of the copolymer deposition.....	123
4.2.2. Retention of functional groups during copolymerization .....	124
4.2.3. Investigation of the chemical composition by FTIR .....	126
4.2.4. Thermal analysis .....	131
4.2.5. Dynamic mobility and thermal stability .....	132
<b>CHAPTER 4 .....</b>	<b>139</b>
<b>Conclusions .....</b>	<b>139</b>
Fields of Application .....	147
1. Thin films (micro...) .....	147
2. Ultra-thin films (nano...) .....	147
<b>CURRICULUM VITAE .....</b>	<b>148</b>
1) Personal Information.....	148
2) Experiences .....	148
Publications from this work .....	149
Conferences and Seminars .....	149
Publications .....	150
<b>CHAPTER 5 .....</b>	<b>152</b>



<b>REFERENCES.....</b>	<b>152</b>
------------------------	------------

## List of abbreviations

cps	counts per second
eV	electron volt ( $1 \text{ eV} = 1.6022 \times 10^{-19} \text{ J}$ )
cw	constant wave
rf	radio frequency
Pa	Pascal ( $1 \text{ Pa} = 1 \text{ N/m}^2$ )
W	Watt ( $W = 1 \text{ J/s}$ )
$W_{\text{eff}}$	effective power
UV	ultra violet
Ar	Argon
O <sub>2</sub>	Oxygen
T	temperature
kJ	kilo joules ( $1 \text{ joule} = 10^7 \text{ ergs} = 0.2388 \text{ calorie}$ )
Hz	hertz
DC	duty cycle
PP	Polypropylene
PE	Polyethylene
Al	aluminum
Si	silicon wafer
S	styrene monomer
PS	polystyrene
AA	acrylic acid monomer
cPAA	conventional poly(acrylic acid)
pPAA	plasma poly(acrylic acid)
AAI	allyl alcohol monomer

PAAI	plasma poly(allyl alcohol)
AA/S	acrylic acid–styrene copolymer
TFAA	trifluoroacetic anhydride
TFE	2, 2, 2-trifluoroethanol
XPS	X-ray photoelectron spectroscopy
ESCA	electron spectroscopy for chemical analysis
ATR-FTIR	attenuated total reflectance –Fourier transforms infrared
CAM	contact angle measurements
DSC	differential scanning calorimetry
DRS	dielectric relaxation spectroscopy

## List of Figures

Figure 1: Interactions of plasma-generated species with the substrate .....	4
Figure 2: Druvesteyn electron energy distribution of the cold plasma (average electron energy: 3 eV) adapted from Ref. [16] .....	5
Figure 3: Evolution of main parameters of pulsed plasma.....	7
Figure 4: Model of a plasma deposited styrene film, as proposed by Friedrich et al. <sup>[27]</sup> .....	13
Figure 5: (a) Chemical structure of styrene (S), acrylic acid (AA) and allyl alcohol (AAl), (b) It is in 3D, (c) homopolymers of it and (d) acrylic acid styrene tentative copolymer (AA/S). 37	
Figure 6: Plasma reactor.....	40
Figure 7: Shows the dielectric relaxation's sample.....	42
Figure 8: Presentation of the different samples for O <sub>2</sub> , Ar plasmas and UV irradiation treated spin coated PS in comparison to plasma PS and commercial PS as a blank.....	43
Figure 9: Diamond golden gate apparatus (FTIR) .....	48
Figure 10: Deposition rate for AA and propionic acid versus DC. The error of the data is smaller than the size of the symbols. The inset gives thickness of the plasma polymerised layer versus deposition time for various DC .....	51
Figure 11: Deposition rate of PAA normalised to the duty cycle versus DC .....	52
Figure 12: High resolution XPS spectra of the sample PAA01 after derivatization with TEF. The solid line represents the experimental data. The dashed line is a fit of a sum of five Lorentz/Gauss functions (Lorentz fraction 72 %) to the data. The dotted lines represent the individual contributions.....	53
Figure 13: Concentration of the carboxylic groups per 100 carbon atoms for PAA versus DC. The error bars results from three different measurements at the same sample. The dotted line indicates the maximal possible concentration of carboxylic groups.....	54

Figure 14: FTIR spectra for the plasma PAA deposited with a duty cycle of 0.5 in comparison to conventional PAA. The inset enlarges the wavenumber region for the carbonyl stretching vibration. The dashed line is a fit of two Gaussians to the data where the dashed-dotted lines are the individual contributions.....	55
Figure 15: FTIR spectra for the plasma PAA deposited with a duty cycle of 0.2 (sample PAA02, solid line) in the wavenumber region for the carbonyl stretching vibration. The dashed line is a fit of three Gaussians to the data where the dashed-dotted lines are the individual contributions.....	56
Figure 16: Measure concentration of COOH groups of PAA from FTIR $\frac{A_{1703}}{A_{1735}}$ versus DC.	
The inset gives $\frac{A_{1703}}{A_{1735}}$ versus the concentration of COOH estimated from the XPS measurements .....	57
Figure 17: Glass transition temperature $T_g$ versus DC for conventionally and plasma deposited PAA. The dashed line is the extrapolation of the dependence obtained for plasma deposited PAA to cPAA18. The inset gives the heat flow versus temperature for conventional and plasma deposited PAA for the second heating run at a rate of 10 K/min .....	58
Figure 18: Dielectric loss $\epsilon''$ for the sample cPAA45 vs. frequency and temperature in a 3D representation. The inset gives the dielectric loss for cPAA45 vs. temperature at a fixed frequency of 1 kHz.....	59
Figure 19: Relaxation rate $f_p$ for the $\beta$ -relaxation versus inverse temperature for cPAA18 and cPAA45. The lines are fits of the Arrhenius equation to the corresponding data. The inset (a) gives the dielectric loss $\epsilon''$ vs. frequency for the $\beta$ -relaxation of the sample cPAA18 at different temperature. The lines are fits of the HN-equation to the corresponding data. Inset (b) gives the dielectric strength $\Delta\epsilon_\beta$ of the $\beta$ -relaxation of the sample cPAA18 versus inverse temperature.....	60

Figure 20: Dielectric loss $\epsilon''$ for the sample PAA05 vs. frequency and temperature during cooling in a 3D representation .....	62
Figure 21: Relaxation rate of the $\beta$ -process for plasma deposited PAA versus inverse temperature for different DC. The lines are fits of the Arrhenius equation to the data. The inset gives the dielectric loss versus frequency for the plasma deposited sample PAA01 at $T=229.1$ K during cooling. The solid line corresponds to the whole fit-function consisting of a HN-function and a high frequency tail. The dashed and the dashed dotted lines are the contributions of the relaxation process and the low frequency wing of the electrode peak.....	63
Figure 22: Activation energy for the $\beta$ -process vs. DC for plasma deposited PAA on heating process compared to conventional PAA18 .....	64
Figure 23: Dielectric loss vs. temperature at a fixed frequency of 1 kHz of the plasma deposited sample PAA05 on different thermal histories. The inset compares the dielectric loss of the plasma deposited sample PAA05 (first heating) with that for cPAA45 vs. temperature at a fixed frequency of 1 kHz.....	65
Figure 24: Relaxation rate of the $\beta$ -process versus inverse temperature for 1 <sup>st</sup> heating, cooling and 2 <sup>nd</sup> heating for PAA at DC=0.5 compared to cPAA. The lines are fits of the Arrhenius equation to the data .....	66
Figure 25: gives relaxation rate of electrode polarization $f_{EP}$ vs. $1/T$ for the sample PAA05 for 1 <sup>st</sup> heating, cooling and 2 <sup>nd</sup> heating .....	67
Figure 26: Thickness of plasma deposited PAAI layers versus deposition time for the different values of DC (a). Deposition rate R versus DC for AAI and n-propanol (b).....	71
Figure 27: Deposition rate normalized by the DC versus DC for AAI and n-propanol.....	71
Figure 28: High resolution XPS spectra of the sample PAAI05. The solid line represents the experimental data. The dotted line is a fit of a sum of four components to the data. The dashed	

lines represent the individual contributions. The inset gives the high resolution XPS spectra of pure PE .....	72
Figure 29: High resolution XPS spectra of the sample PAAI05 after derivatization with TFAA. The solid line represents the experimental data. The dotted line is a fit of a sum of five components to the data. The dashed lines represent the individual contributions .....	73
Figure 30: Concentration of hydroxyl groups per 100 carbon atoms versus DC. The dotted line indicates the maximal possible concentration of hydroxyl groups .....	74
Figure 31: FTIR spectra of PAAI deposited on Al substrate for different values of DC in comparison to the allyl alcohol monomer as blank. The different curves are y-shifted for sake of clearness. The inset enlarges the wavenumber region for the hydroxyl and for both the asymmetric and symmetric $-\text{CH}_2$ stretching vibrations of PAAI deposited on the aluminium substrate at DC= 0.1. The spectra are analysed by fitting three Gaussians to the data.....	75
Figure 32: Concentration of OH groups as estimated by $A_{\text{OH}}/A_{\text{CH}_2}$ for PAAI versus DC with aluminium and Glass substrates. The inset gives $A_{\text{OH}}/A_{\text{CH}_2}$ versus the concentration of OH groups estimated from the XPS measurements with aluminium and glass substrates.....	76
Figure 33: Concentration of the OH groups estimated from $A_{\text{OH}}/A_{\text{CH}_2}$ for plasma deposited PAAI versus DC with PE and PP substrates. The inset gives $A_{\text{OH}}/A_{\text{CH}_2}$ versus the concentration of OH estimated from the XPS measurements with PE and PP substrates .....	77
Figure 34: FTIR spectra of plasma deposited PAAI in the wavenumber range of the OH-stretching vibration deposited on different substrates with DC=0.5 compared to the allyl alcohol monomer.....	78
Figure 35: Dielectric loss $\epsilon''$ of the sample PAAI05 vs. frequency and temperature during cooling in a 3D representation .....	80
Figure 36: Dielectric loss versus frequency of the sample PAAI02 at T=261.1 K. The solid line corresponds to the whole fit-function consisting of a HN-function, a high frequency tail and a conductivity contribution at low frequencies. The dashed and the dotted lines are the	

contributions of the relaxation process and the low frequency wing of the electrode peak. The dotted line indicates the conductivity contribution .....	81
Figure 37: The relaxation rate for the $\beta$ -process for plasma deposited PAAI versus inverse temperature for the different values of DC for the first heating run. The lines are fits of the Arrhenius equation to the corresponding data.....	82
Figure 38: Activation energy for the $\beta$ -process vs. DC for plasma deposited PAAI on the first heating run.....	83
Figure 39: Dielectric loss vs. temperature at a fixed frequency of 1 kHz of the sample PAAI05 in the temperature range of the $\beta$ -relaxation for different thermal histories .....	83
Figure 40: Dielectric strength $\Delta\epsilon_\beta$ of PAAI vs. inverse temperature for $\beta$ -relaxation with respect to DC for the first heating. The inset displays dielectric strength $\Delta\epsilon_\beta$ of PAAI vs. DC at 265 K .....	84
Figure 41: $A_{OH}/A_{CH_2}$ calculated from FTIR versus the dielectric strength estimated from the DRS measurements of the plasma PAAI deposited on Al substrate at 265 K .....	85
Figure 42: Relaxation rate of the electrode polarization $f_{EP}$ for plasma deposited PAAI vs. inverse temperature for different values of DC for the 1 <sup>st</sup> heating process. The inset Fig. displays $T_g^{Diel}$ of PAAI vs. DC.....	86
Figure 43: Relaxation rate of the electrode polarization $f_{EP}$ vs. inverse temperature of the sample PAAI05 on different thermal histories .....	87
Figure 44: Waterfall presentation of XPS survey scans of O <sub>2</sub> , Ar plasmas and UV irradiation treated spin coated PS in comparison to pulse plasma deposited PS and commercial PS as blank .....	90
Figure 45: High resolution XPS C1s spectra of plasma-polymerized PS (plasma power =100 W, DC =0.5, pressure=10 Pa and flow rate of the monomer 10 g/h). The solid line represents the experimental data. The dashed lines represent the individual contributions.....	90



Figure 46: Concentration of the oxygen atoms per 100 carbon atoms for O <sub>2</sub> and Ar plasmas and UV irradiation treated spin coated PS, plasma deposited PS and commercial PS as blank .....	91
Figure 47: FTIR-ATR spectra of O <sub>2</sub> and Ar plasma and UV irradiation treated spin coated PS, plasma deposited PS films and a reference PS film .....	92
Figure 48: Water contact angle of O <sub>2</sub> , Ar plasma and UV irradiation treated spin coated PS, plasma deposited PS films and a reference PS film .....	95
Figure 49: Surface energy, disperse and polar part of O <sub>2</sub> and Ar plasma and UV irradiation treated spin coated PS, plasma deposited PS films and a reference PS film.....	95
Figure 50: The dielectric loss $\epsilon''$ of O <sub>2</sub> and Ar plasma and UV irradiation treated spin coated PS, plasma deposited PS films and a reference PS film prepared by spin coating on glass substrate a, b, c, d and e respectively on heating in 3D.....	97
Figure 51: The dielectric loss versus frequency for the plasma deposited PS polymer with DC=0.5 at T=325.17 K during heating. The solid line corresponds to the whole fit-function consisting of the conductivity, a HN-function and a high frequency tail. The dashed, dashed dotted and dotted lines are the contributions of the relaxation process, conductivity and the low frequency wing of the electrode peak respectively .....	97
Figure 52: Relaxation rate of the $\alpha$ -relaxation versus inverse temperature of PS thin films for: Ar, UV irradiation, and O <sub>2</sub> plasma, plasma deposited PS, cPS. Insert: dynamic glass transition for different processes .....	98
Figure 53: Relaxation strength of the $\alpha$ -relaxation versus inverse temperature of PS thin films for Ar and O <sub>2</sub> plasma UV irradiation, plasma deposited PS, and cPS as blank.....	99
Figure 54: Dielectric loss $\epsilon''$ for plasma-produced PS versus temperature at frequency of 1 kHz for: 1 <sup>st</sup> heating, cooling and 2 <sup>nd</sup> heating.....	101

Figure 55: Relaxation rate of $\alpha$ -process vs. inverse temperature for plasma deposited PS sample: 1 <sup>st</sup> heating, cooling, 2 <sup>nd</sup> heating and cPS. The inset shows the dynamic glass transition for different processes .....	101
Figure 56: Deposition rates of plasma deposited PAA, PS homopolymers and AA/S copolymer in dependence on DC .....	104
Figure 57: Normalized deposition rate vs. DC for plasma deposited: PAA, PS homopolymers and AA/S copolymer .....	106
Figure 58: High resolution XPS spectra of the sample with DC=0.5: (a)- before derivatization and (b)-after TFE-derivatization. The solid line represents the experimental data. The dashed lines represent the individual contributions .....	107
Figure 59: Dependence of COOH per 100 C atoms for plasma deposited: PAA homopolymers and AA/S copolymer on applied DC.....	109
Figure 60: Concentration of COOH groups for plasma deposited AA/S copolymer versus the concentration of COOH for plasma deposited PAA homopolymers with respect to DC. Both of them estimated from derivatization with TFE and the XPS measurements .....	110
Figure 61: FTIR spectra of plasma deposited PAA, PS homopolymers and AA/S 1:1 copolymer (with DC=0.5) compared to conventional cPAA.....	110
Figure 62: Gaussian fits of C=O band of a plasma-polymerized PAA film (DC=0.5). The solid line represents the experimental data. The dashed line is a fit of a sum of three Gaussians to the data. The dotted lines represent the individual contributions.....	111
Figure 63: Gaussian fits of C=O band of plasma-polymerized from 1:1 molar ratio of AA/S copolymers (DC=0.5). The solid line represents the experimental data. The dashed line is a fit of a sum of three Gaussians to the data. The dotted lines represent the individual contributions .....	112
Figure 64: $\frac{A_{1706}}{A_{1732}}$ vs. DC for plasma deposited: PAA homopolymers and AA/S copolymer	112

Figure 65: Correlation between XPS-measured COOH groups (TFE-derivatization) and FTIR-measured $\frac{A_{1706}}{A_{1732}}$ for plasma deposited AA/S copolymer with respect to DC.....	113
Figure 66: Heat flow of plasma-polymerized AA/S copolymers in dependence on temperature for the labeled DC values (2 <sup>nd</sup> heating run) (a): $T_g$ versus DC for plasma deposited: AA/S copolymer, PAA and PS homopolymers (b).....	115
Figure 67: Dependence of dielectric loss $\epsilon''$ versus frequency and temperature for plasma deposited (a)- PAA, (b)- PS homopolymers and (c)- AA/S copolymer at DC=0.1 for the first heating cycle.....	116
Figure 68: Dielectric loss $\epsilon''$ versus temperature at a frequency of 1 kHz for the plasma deposited copolymer of AA/S for different values of DC for the heating cycle.....	117
Figure 69: The dielectric loss versus frequency for the plasma deposited sample AA/S copolymer with DC=0.1 at $T=353.15$ K during heating. The solid line corresponds to the whole fit-function consisting of the conductivity, a HN-function and a high frequency tail. The dashed, dashed dotted and dotted lines are the contributions of the relaxation process, conductivity and the low frequency wing of the electrode peak respectively .....	118
Figure 70: Relaxation rate of the $\alpha$ -process versus inverse temperature for plasma deposited PAA, PS homopolymers and AA/S copolymer (DC=0.5).....	118
Figure 71: Relaxation rate of the $\alpha$ -process versus inverse temperature for plasma deposited AA/S copolymer for different values of DC. Insert: dynamic glass transition for different values of DC.....	119
Figure 72: Dielectric strength of the $\alpha$ -process versus inverse temperature of the plasma deposited AA/S copolymer for different values of DC.....	120
Figure 73: Dielectric strength $\Delta\epsilon_\alpha$ of plasma deposited AA/S copolymer vs. DC at $T=343$ K .....	121

Figure 74: Dielectric loss $\varepsilon''$ versus temperature at frequency of 1 kHz for pulsed plasma copolymer for heating and cooling runs (DC=0.1) .....	122
Figure 75: Thickness of the plasma (co)polymerized layer vs. deposition time for various comonomer ratios (a). The deposition rate of plasma deposited AA/S copolymers versus PMR [%] of acrylic acid (b) .....	123
Figure 76: Normalized deposition rate vs. PMR [%] of acrylic acid for plasma deposited AA/S copolymer.....	124
Figure 77: Concentration of the carboxylic groups per 100 C atoms after derivatization versus the comonomer ratio for plasma deposited AA/S copolymers (results from C1s peak deconvolution) compared to plasma deposited PAA homopolymers .....	125
Figure 78: $\pi$ - $\pi^*$ in plasma deposited AA/S copolymer films in dependence on the ratio of the comonomers from C1s deconvolution .....	125
Figure 79: Stretching vibration of the carbonyl group (C=O) for: (a) commercial PAA, (b) plasma deposited PAA homopolymers, and (c) plasma deposited AA/S copolymer with PMR [%] of 66.6 acrylic acid deconvoluted into three components.....	127
Figure 80: Concentration of COOH groups estimated from FTIR areas ratio $A_{1706} / A_{2917}$ for plasma deposited AA/S copolymer films in dependence on the PMR [%] of acrylic acid....	128
Figure 81: $\frac{A_{1706}}{A_{2917}}$ versus the concentration of COOH per 100 C atoms estimated from the XPS measurements for plasma deposited AA/S copolymers.....	129
Figure 82: Area % for different components of C=O bands (fit results) of AA/S plasma deposited copolymer films in dependence on PMR [%] of acrylic acid.....	130
Figure 83: Measure concentration of C=C groups estimated from FTIR areas ratio $A_{1493} / A_{2917}$ of AA/S plasma deposited copolymer films in dependence on the PMR [%] of styrene. The inset gives $A_{1493} / A_{2917}$ versus the concentration of $\pi$ - $\pi^*$ estimated from the XPS measurements .....	130

Figure 84: Heat flow of plasma deposited AA/S copolymers in dependence on the temperature for the labeled PMR [%] of acrylic acid values (2 <sup>nd</sup> heating run) (a). T <sub>g</sub> values versus PMR [%] of acrylic acid on 2 <sup>nd</sup> heating process (b) .....	132
Figure 85: Dielectric loss vs. temperature at a fixed frequency of 1 kHz of the plasma deposited sample AA/S copolymer in dependence on the PMR [%] of acrylic on heating...	133
Figure 86: Relaxation rate of the $\alpha$ -process versus inverse temperature for plasma deposited AA/S copolymers for different PMR [%] of acrylic acid for 1 <sup>st</sup> heating process (a). Dynamic glass transition temperature T <sub>g</sub> <sup>Diel</sup> versus PMR [%] of acrylic acid (b) .....	134
Figure 87 Dielectric strength of the $\alpha$ -process versus relative PMR [%] of acrylic acid at T=344 K (a). A <sub>1493</sub> /A <sub>2917</sub> and A <sub>1706</sub> /A <sub>2917</sub> calculated from FTIR versus the dielectric strength estimated from the DRS measurements for the AA/S copolymer deposited on Al substrate at 344 K (b) and (c) respectively .....	135
Figure 88: Dielectric loss $\epsilon''$ versus temperature at a frequency of 1 kHz for pulsed plasma copolymer with 50 % PMR of acrylic acid on different thermal histories .....	137
Figure 89: Relaxation rate of the electrode polarization f <sub>EP</sub> vs. inverse temperature dependence on the comonomer ratio for the heating process. The inset gives f <sub>EP</sub> vs. 1/T for the sample 50 % PMR of acrylic acid for 1 <sup>st</sup> heating, cooling and 2 <sup>nd</sup> heating .....	138

## List of Tables

Table 1: Bond energies of formation of the free radicals.....	6
Table 2: Physical properties of acrylic acid, styrene, and allyl alcohol <sup>[..]</sup> .....	39
Table 3: Analysis of the C1s peak for the non-derivatized and derivatized surface of plasma deposited PAA.....	52
Table 4: Activation energy for plasma deposited PAA05 sample for different thermal histories compared to cPAA .....	66
Table 5: Dynamic glass transition for plasma PAA on 1 <sup>st</sup> heating, cooling and 2 <sup>nd</sup> heating compared to T <sub>g</sub> of cPAA .....	68
Table 6: Gives the inspection of the C1s peak analysis of the non-derivatized and derivatized surface for plasma deposited PAAI.....	73
Table 7: Position of the maximum of the $\nu$ OH stretching vibration for PAAI deposited on different substrates with DC=0.5 as example.....	79
Table 8: gives the inspection of the C1s peak analysis of the non derivatized and derivatized surface for AA/S copolymer.....	107

## List of Schemes

Scheme 1: Derivatization reaction of COOH-groups with trifluoroethanol (TFE) in presence of di-tertbutyl-carbodiimide .....	44
Scheme 2: The derivatization reaction of OH groups for plasma deposited PAAI by TFAA .	46

# Chapter 1

## Introduction

### 1. Background and basics

#### *1.1. Plasma state*

Broadly speaking the plasma state <sup>[1-3]</sup> can be considered to be a gaseous mixture of oppositely-charged particles with a roughly zero net electrical charge.

Plasma is an ionized gas comprising a dynamic mix of electrons, ions, neutrons photons, free radicals, meta-stable excited species, neutral atoms and molecules, also called as fourth state of matter. <sup>[4]</sup> More than 90% of all matter in the universe exists in this plasma state. <sup>[5]</sup> Under the action of an electromagnetic field high energy species were produced by collisions (or radiative processes). They were accelerated under the influence of the electromagnetic field, collide with other species and loose its energy and transfer it to the other particle or to the wall. Elastic collisions of equiponderate particles equilibrate the energy within the plasma system and inelastic collisions of light electrons with heavy particle produce excitation, ionization, dissociation, recharging, charge transfer, recombination radiation etc. <sup>[6]</sup> The energy from the electromagnetic field is mainly acquired by plasma electrons because of its swift spur within the electrical field.

Their inelastic collisions of electrons with gas atoms or molecules leading to ionization and the appearance of the ion avalanche as the basic process of ignition and sustaining the plasma. Recombination and quenching at the walls limit the ion avalanche and produce a steady state of the plasma. Electrons and ions generate the plasma conductivity. The broad distribution of energy over all species in the plasma is reflected in the electron energy distribution function. In ordinary gas plasmas (glow discharges) under low-pressure the range of

energetic species also involves components with energies much higher than those of chemical bonds in polymers. It must be considered, that the supply of (electrical) energy is continuous. The transfer of energy leads to a variety of new species which are chemically active and thus can serve as precursor for the new stable compounds. Thus, by an elaborated choice of the precursor the resulting functional group can be roughly predetermined but restrained by decay or rearrangement in the plasma. However, numerous by-products and side-products are also formed. The plasma produced energy-rich species and their collision with the other neutrals initiates a new chemical processes giving rise to a phenomenon known as plasma chemistry. Using the oxygen ( $O_2$ ) plasma gas typically of  $O^+$ ,  $O^-$ ,  $O_2^+$  and  $O_3^+$  ions for example. The plasma particles are extremely unstable and their energetic states cause them to be highly reactive with particles or the surfaces that they contact. Chemists have always been fascinated by the various electric discharges, which they have observed in nature and into experimental studies. Their expectation was to possess a new convenient, clean, waste-free, one step, powerful universal chemical tool. As and when these techniques were available for producing discharges in the laboratory, they attempted to use them for chemical synthesis. One of the basic plasma experiments was this of Miller and Urey, who simulate the genesis of basic amino acids in the primitive Earth atmosphere by the action of spark discharges.<sup>[7,8]</sup> There are several reported attempts to manoeuvre the organic chemical reaction for the synthetic purpose using the plasma as a tool.<sup>[9-13]</sup> Chemist's perspective provides that plasma is a new way of transferring energy to molecules.

This phenomenon is very successfully manoeuvred into atmosphere, vacuum as well as into the water phases depending upon the utility and the feasibility of the techniques.<sup>[14]</sup>



## ***1.2. Classification of plasmas***

Plasma states can be divided in two main categories: Hot plasmas and cold plasmas. Hot plasmas are characterized by very high temperatures of electrons and heavy particles, both charged and neutral, and they are close to maximal degrees of ionization (100%). Cold plasmas are composed of low temperature particles (charged and neutral molecular and atomic species) and relatively high temperature electrons and they are associated with low degrees of ionization ( $10^{-4}$ –10%). Cold plasmas include low-pressure and atmospheric pressure.

### ***1.2.1. Cold plasmas***

#### ***1.2.1.1. Low-pressure***

Low-pressure cold plasmas <sup>[15]</sup> are initiated and sustained by dc, RF, or microwave (MW) power transferred to a low-pressure gas environment, with or without an additional electric or magnetic field. Ultimately, all these discharges are initiated and sustained through electron collision processes under the action of the specific electric or electromagnetic fields. Their special character as “cold” plasma is caused by the strong differences in (high) electron and (low) ion and gas temperature ( $T_{el} \gg T_{ion} \approx T_{neutr}$ ). As described before very light electrons cannot transfer their kinetic energy to heavy ions or neutrals efficiently by elastic collision because of the momentum and energy conservation law. Accelerated electrons (energetic electrons) induce ionization, excitation and molecular fragmentation processes leading to a complex mixture of active species, which will undergo, depending on the specific plasma mode (e.g. direct or remote plasma environments). The poly-recombination mechanisms are very different from reaction mechanisms known from conventional chemical processes. If electrons with broadly distributed kinetic energy, described by specific energy distribution functions initiate and control all the processes in glow discharges it might appear obvious that similar electron energy distribution environments created using different power sources (dc,

RF, MW, etc.) should initiate similar chemistries; and consequently, the type of the plasma would be of less importance for the generation of specific processes. Therefore, proper selection and control of plasma parameters are necessary for production of high quality layers.

RF discharges have advantages in comparison to dc discharges: (a) they can operate at lower pressures (the impedance of the discharge decreases with the increase of the frequency), (b) their ionization mechanism is more efficient (the electrons can gain energy during the whole cycle), (c) they can also be sustained in depositing (e.g. dielectric layers) discharge environments, (d) they are more uniform spatially. These characteristics make RF-plasmas the most common choice for the microelectronic industry. A schematic diagram of a capacitively coupled RF-plasma reactor, and the interaction of plasma species with the substrate are presented in Fig. 1. Adapted from ref. [16].

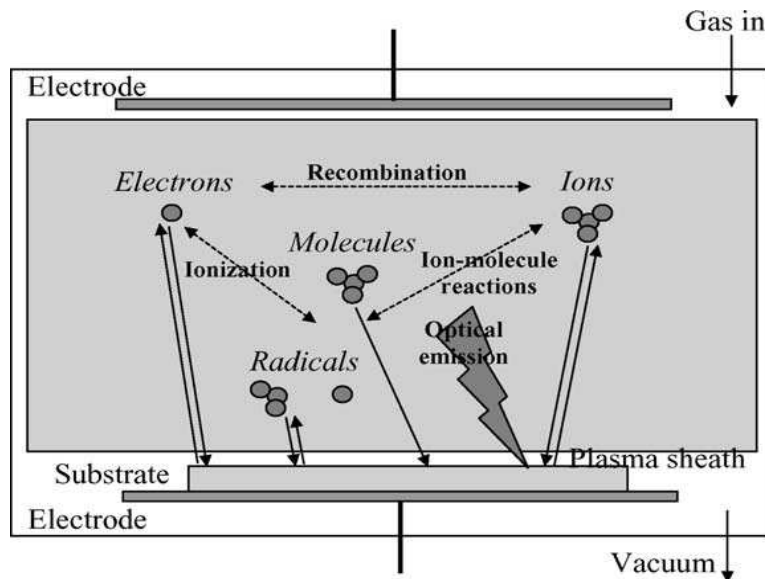
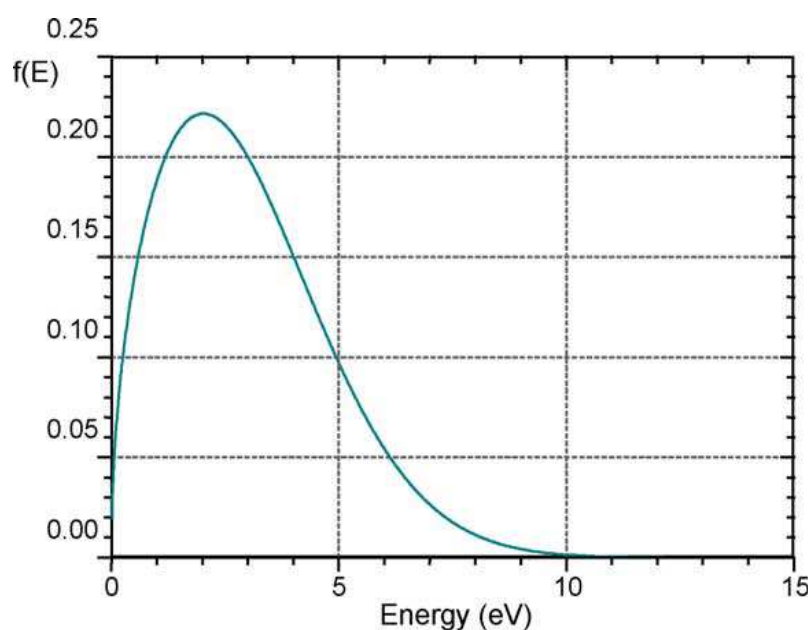


Figure 1: Interactions of plasma-generated species with the substrate

Plasma temperature is defined as the mean translational energy of particles in the discharge. As a result of the substantial mass difference existent between the electrons and heavy species, these particle populations can often be considered as two systems in their own ‘thermal equilibrium’. A plasma would be in thermodynamic equilibrium if temperatures of the electrons and neutral species, including the ionization, excitation, dissociation and radiation temperatures, were all equal. The “cold” plasma in contrary shows as before mentioned unbalance between electron and ion/gas temperature. Therefore, it is also called non-isothermal

plasma. The presence of a constant energy loss at the plasma boundaries (mainly by convection or radiation), complete thermodynamic equilibrium cannot be achieved.

The electron energy distribution of a low-pressure plasmas can be often described by the Druyvesteyn approximation (Fig. 2), where the temperature of electrons is considered much higher than that of ions, and when it is assumed that the only ‘energy losses’ are by elastic collisions (the electric field strength in the plasma is sufficiently low to neglect inelastic collisions). However, at higher degrees of ionization the influence of electron density on the energy distribution can be significant. <sup>[17,18]</sup> It can be observed that a small number of electrons have relatively high energies (5–15 eV) while the bulk of electrons belongs to the low-energy electron range (0.5–5 eV). Since, the ionization potentials of atoms of common organic structures (e.g.  $C^+ = 11.26$  eV;  $H^+ = 13.6$  eV;  $O^+ = 13.6$  eV;  $N^+ = 14.53$  eV, etc.) belong to the tail region of the electron energy distribution, low degrees of ionization of cold plasmas appear obvious. However, this argument is somewhat circular since the inelastic process of ionization is in large part what determines the electron temperature needed to sustain the discharge.



*Figure 2: Druyvesteyn electron energy distribution of the cold plasma (average electron energy: 3 eV) adapted from Ref. [16]*

It is extremely important to note that the energy range of most of electrons (2–5 eV) is intense enough to dissociate almost all chemical bonds involved in organic structures (Table

1), and organic structures containing main group elements, and to create free radical species capable of reorganizing into macromolecular structures. As a consequence, the structures of all volatile compounds can be altered and/ or converted into high molecular weight compounds, even if they do not have the functionalities which are present in common monomer structures. Higher energies are usually required for the dissociation of unsaturated linkages and the formation of multiple free radicals. Accordingly, initial or plasma-generated unsaturated bonds will have a better ‘survival rate’ under plasma conditions, in comparison to the  $\sigma$  linkages. Thus, it can be understood why plasma generated macromolecular structures are usually characterized by unsaturated, branched and crosslinked architecture.

Table 1: Bond energies of formation of the free radicals

Bond energies	
Species	Energy (eV)
<i>Diatomic molecules</i>	
C–H	3.7
C–N	3.1
C–F	5.7
C=O	7.7
C–C	3.5
<i>Polyatomic molecules</i>	
C=C	6.4
CH <sub>3</sub> -H	4.5
C <sub>2</sub> H <sub>5</sub> -H	4.3
CH <sub>2</sub> CH-H	4.8

Source: reference [16]

The plasma-synthesized macromolecular networks generated by plasma-state processes, directly from the recombination of plasma species on the surfaces, do not retain the structural characteristics of the starting materials. They are not based on repeating units and consequently, the term ‘plasma-polymers’, which is often used, is inappropriate for describing these structures.

In contrast, plasma-induced reactions involve plasma generated active sites (e.g. free radicals and charged functionalities) located on plasma-exposed substrate surfaces, which initiate conventional polymerization processes from conversion of monomers in the absence of a plasma (e.g. remote plasma zones and pulsed plasma environments). Besides the recombination mechanisms developed on surfaces, which confine a plasma, the active species of the discharge interact and continuously tailor the artificially exposed (reactor walls, various substrates, etc.) and self-generated (e.g. plasma synthesized macromolecular structures) surface layers. The competition between the recombination deposition processes and the ‘destructive’ interaction of plasma species with the nascent macromolecular structures will control the intensities and the predominance of ablation, surface functionalization and macromolecular-film-formation reactions.

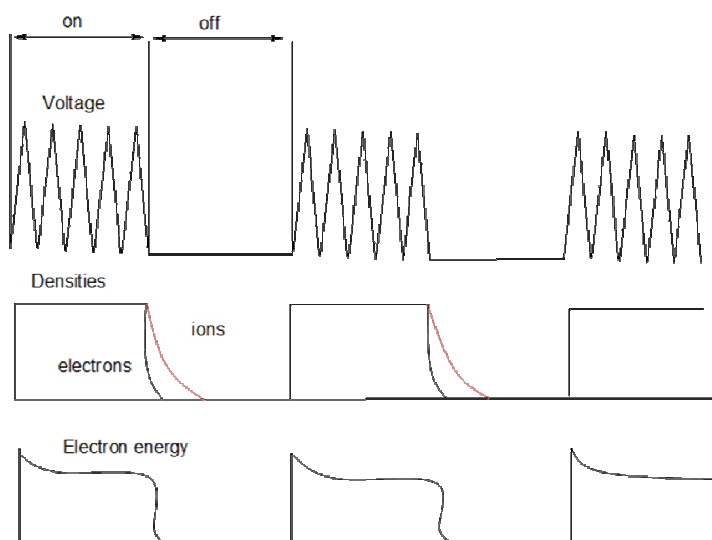


*Figure 3: Evolution of main parameters of pulsed plasma*

Modulated discharges (pulsed plasma) are created by using an RF carrier, switched on and off at a low frequency (longer period time). Pulsing is a repeating variation of a radio-frequency voltage or current from zero potential to ignition and then maintaining voltage and zero potential. Normally, radio-frequency discharge is continuously burning (continuous-wave=cw) with 13.56 MHz. The main parameters that characterize modulated discharges are: the pulse period (the time it takes to complete a pulse cycle) and the duty cycle (measures on period, as a percentage of total period-on and off) are given by:

$$\text{Period} = t_{on} + t_{off} \quad \text{and} \quad \text{Duty cycle} = t_{on} * 100 / [t_{on} + t_{off}]$$

### ***1.2.1.2. Atmospheric pressure***

Most previous research related to the plasma enhanced synthesis and surface modification of materials (deposition, surface functionalization, and etching) has been performed under low-pressure RF plasma environments, owing to the high efficiency of RF- discharges. <sup>[16]</sup> Dielectric-barrier discharges (DBD) and corona discharge are examples for atmospheric pressure and come more in the fore because of more industrial relevance. <sup>[16]</sup>

### ***1.2.1.3. Low-pressure high-density plasmas***

These plasmas <sup>[15]</sup> are usually operated at much lower pressures  $[(7.5\text{--}150) \times 10^{-5} \text{ Pa}]$ , and generate higher power densities and ionization degrees ( $>10\%$ ) in comparison to conventional RF discharges. Electron cyclotron resonance (ECR) plasmas and microwave plasmas are examples for low-pressure high-density plasmas. However, such plasma was not considered here.

## ***1.3. Applications of plasma low-pressure***

### ***1.3.1. Functionalization of organic and inorganic polymeric surfaces***

Plasma contains activated species able to initiate reactions at the solid surface of samples. It can be used in two ways depending on the gas employed. One use of it is the surface modification of polymers. This process is the alteration of the surface properties and surface morphology of the polymers through etching reactions, implantation of atoms and radical

generation. These reactions are achieved by the use of non-polymer forming plasma composed of inorganic gases such as  $N_2$  and  $O_2$ . This process of the surface modification by plasma is called as plasma treatment.

Another use of plasma is the deposition of thin polymeric films on solid substrates. When plasma is generated and organic vapors are introduced, plasma polymers are formed and all surfaces of substrates in the plasma zone are coated with these plasma polymers. This process of polymer-like layer formation by plasma is called as plasma polymerization. Plasma processes provide a cost effective and environmentally friendly alternative to many important industrial processes, because the method produces no undesired waste products.

Plasma promotes adhesion for metals, inorganic and polymers for example by increasing the effective surface area of polymers by etching. This roughening in turn promotes more intimate molecular contact between the metal and the adhesive allowing stronger bonds between them. <sup>[19]</sup> The highly reactive ions found in plasma make the processing a valuable tool in surface cleaning. Additionally plasma etching is a tool used in the semiconductor industry to create tunnels on surfaces. Goal of all surface functionalization is to form functional groups at substrate surface, which are able to link chemically with the coating. It is generally believed that covalent bonds across the composite interface produce maximal and long-lasting adhesion.

### ***1.3.2. Plasma deposition of biocompatible layers***

Deposition of macromolecular structures on biomaterial surfaces under cold-plasma conditions is another approach to obtain control of biological performance including, cell adhesion and growth characteristics, hemo-compatibility, anti-fouling behavior (prevention of protein adsorption), etc. of surfaces exposed to in vivo environments. Proteins naturally ad-

sorb at foreign surfaces and significantly alter the biocompatibility characteristics of medical implants and devices, biosensors, industrial bioprocesses, etc.

### ***1.3.3. Etching of polymer surfaces***

Most polymers are carbon- or carbon and heteroatom- based structures, which undergo intensive structural modifications in the presence of charged or neutral plasma-species by generating of volatile compounds at the surface. This includes mono- and multiple-free radical structures, ions of either polarity or molecular fragments bearing charged functionalities. Depending on the intensity of the production of low molecular weight, volatile structures, a more or less significant ablation process will accompany the surface-functionalization and deposition mechanisms.

### ***1.3. Surface functionalization***

Functionalization means the introduction of functional groups onto the polymer surface of substrates. The process which introduces chemically different types of functional groups a term of unspecific functionalization is used. Specific functionalization stands for monosort functional groups, e.g. only one type of functional groups exists. Usual functional groups are OH, COOH, NH<sub>2</sub> etc.

#### ***1.3.1. Plasma treatment***

Until recently, the plasma treatment of polymers was considered to be a process related only to variation in their surface properties. Structural and chemical transformations occurred on the surface and in a thin near-surface layer and did not affect the bulk properties of



polymeric materials. However, it is known that plasma UV radiation can penetrate into the depth of a polymer. The penetration depth and absorption of the radiation depend to a significant extent on the structure and properties of the modified material. In the late 1990s, it was found that the plasma treatment of polypropylene (PP) leads to substantial changes in its structure as well, involving the whole of the polymer volume simultaneously with its surface modification. <sup>[20-22]</sup>

*Plasma treatment* is the most often used and very viable method for polymer surface activation. <sup>[23]</sup> A method with a maximum power and versatility, which can be used for cleaning or etching of polymer surfaces by removing some of its topmost surface layers, introducing functional groups as well as depositing a thin polymer coatings on the polymer substrate. However, modification is a generic term used for all chemical and physical changes that are introduced to the surfaces of organic and inorganic materials. It can be roughening, coating, oxidizing etc.

Using the low-pressure oxygen plasma treatment the surface was functionalized within ca. 2 s followed by oxidation of carbon atoms below the top most carbon layer but within the information depth of the photoelectron spectroscopy method (XPS). After about 20 s a steady state of formation, further oxidation and splitting off the functional groups and forming gaseous degradation products ( $\text{CO}_2$ ,  $\text{CO}$ ,  $\text{H}_2\text{O}$ ) occurs. <sup>[24]</sup> Most often unspecific functionalization dominates, i.e. different types of functional groups are formed simultaneously as singly, doubly and triply bonded oxygen to carbon. The monotype functionalization is achieved by polymerization or copolymerization of monomers bearing functional groups. Thus, the resulting polymer also carries the same functional group as the monomer and forms a top-coating at the surface of the substrate.

### ***1.3.2. Plasma polymerization***

#### ***1.3.2.1. Basics of plasma polymerization***

Plasma polymerization is a thin film forming process, where thin films were deposited directly onto the surfaces of substrates. In this process, low-molecular weight molecules, e.g. monomers are converted into high molecular weight molecules, called as plasma polymers, with the assistance of energetic plasma particles, which are electrons, ions and radicals. In a chemical sense, plasma polymerization is different from conventional polymerization such as radical or ionic polymerization mechanisms.<sup>[25]</sup> In any case, polymers formed by plasma polymerization show a distinguished chemical composition, as well as chemical and physical properties from those formed by conventional polymerization, even if the same monomer is used. Plasma derived polymers are irregularly composed and structured, are generally unsaturated, and branched and/or cross-linked due to high electron temperatures ( $T_e$ ) of impinging particles and plasma-emitted UV radiation. This is illustrated by the structure of a styrene plasma polymer shown in Fig. 4. The high degree of crosslinking causes plasma polymers to be insoluble in most organic solvents. Also functional groups that are not present in styrene monomer and low molecular weight products often exist in plasma polymer structures acting there as lubricants and adulterate thermal properties. In addition, they may contain a large number of radicals available for post plasma reactions.<sup>[26, 27]</sup>

Plasma polymerization has been studied intensively since the 1950ies<sup>[28, 29]</sup> and especially in the 60ies.<sup>[30, 31]</sup>

So-called carbonaceous films were prepared by König and co-workers<sup>[28,32]</sup> in a glow discharge in benzene vapour using a parallel-plate electrode arrangement powered by singly rectified 50 Hz.

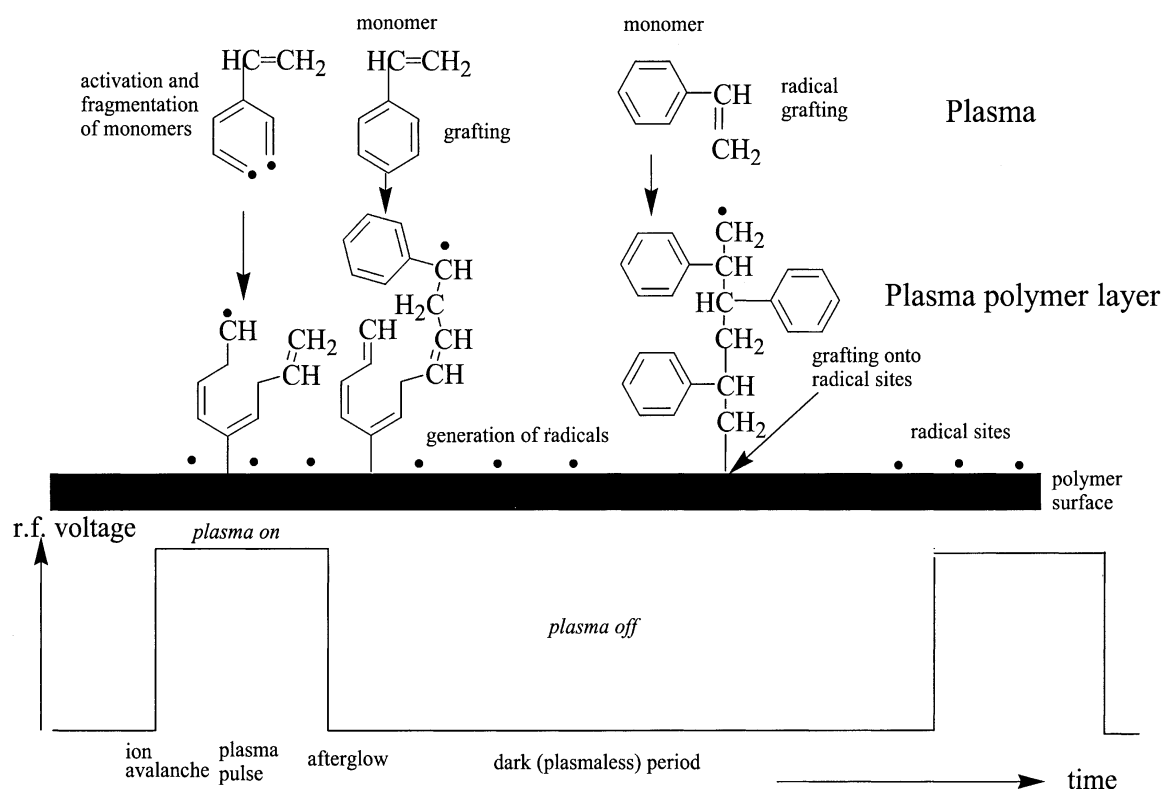


Figure 4: Model of a plasma deposited styrene film, as proposed by Friedrich et al. <sup>[27]</sup>

The deposition rate of a plasma polymer is determined by the following parameters: the geometry of the system, the reactivity of the starting monomer and its flow rate, the working gas pressure, the power and frequency of the excitation signal, the position of the substrate and, finally, the temperature of the substrate. <sup>[33]</sup>

However, surface modification of polymers has been widely studied due to its interest for industry regarding several applications involving adhesion, packaging and metallization, among others.

Plasma polymerization of volatile organic compounds is an industrially utilized way to produce thin pinhole-free and uniform films. While in the past the interest was focused primarily on inert films exhibiting protective properties against environmental influences as well as on coatings with anti-scratch properties or barrier properties for separation of gases and liquids now the need for production of thin films with monotype functional groups at the surface comes to the fore. <sup>[34]</sup>

Plasma polymerization technique became a popular approach for synthesis of functional polymers. Plasma polymers with desired structures and controlled density of a specific chemical group found many applications in different fields like adhesion and biomaterial science. <sup>[35]</sup> However, control of the chemical composition of plasma polymers is not straightforward.

### ***1.3.2.2. External plasma parameters***

Activation and fragmentation of the monomer molecules in the plasma are the first steps of the plasma polymerization process. Recombination of these fragments and subsequently re-activation and re-fragmentation of the recombined molecules by the plasma are the film-forming step. All these reactions, which affect the structure of the deposited films, depend on the internal plasma parameters, e.g., plasma (charge carrier) density  $n$ , temperature of electrons ( $\approx$ kinetic energy)  $T_e$  and ions (near gas temperature)  $T_i$ . Therefore, it is possible to alter and control some chemical aspects of the plasma polymerized films by an appropriate choice of the external plasma parameters. These are the magnitude of the plasma input power, the flow rate of the monomers introduced into the plasma, temperature and positioning of the substrates and the pressure in the reaction chamber. <sup>[36]</sup> Additionally, hydrodynamic factors e.g., reactor type <sup>[37]</sup>, reactor geometry <sup>[38]</sup>, electrode-less or with internal electrodes, type and geometry of electrodes, electrode gap, bias voltage, sample position (floating potential, electrode and mass), the inlet and the outlet of the monomer flow and its distribution in the reactor <sup>[26]</sup> have a great influence on the product of plasma polymerization. However, all the hydrodynamic factors were kept constant in this work; their effect will not be further discussed.

Plasma power is a parameter which directly affects the important internal plasma parameters. When the plasma power is increased primarily the density of charge carriers is increased but most often associated with increasing of the electrons ( $E_e$ ) is increased. This result

in an increase in the plasma density ( $n$ ), and temperature of electrons ( $T_e$ ) and ions ( $T_i$ ). Additionally, the mean free path of the plasma particles decreases and their collision cross-section increases. All these variations cause more energetic plasma, where the fragmentation and re-arrangement of the monomer molecules is pronounced. This generally ends in a more irregular, unsaturated, and branched and/or cross-linked plasma polymers.

When the monomer flow rate is decreased, the retention time of the monomer molecules in the plasma chamber increased. Thus monomer molecules are subjected to more collisions, which results in more fragmentation and re-arrangement in the plasma.

Yasuda combined these two parameters and proposed a controlling parameter,  $W/FM$ , where  $W$  is the plasma power [J/s],  $F$  is the monomer flow rate [mol/s], and  $M$  is the molecular weight of the monomer [kg/mol].<sup>[26]</sup> The  $W/FM$  parameter is an apparent input energy per monomer molecule [J/kg]. Magnitude of the  $W/FM$  parameter is considered to be proportional to the concentration of activated species in plasma. These variations in the polymer deposition rate with the  $W/FM$  parameter show that plasma initiates polymer forming and polymer degrading processes.

The polymer deposition rate increases with increasing  $W/FM$  parameter. The power supplied to monomer molecules is relatively low, so that the monomer molecules are subjected to less fragmentation. Plasma polymers with less rearrangement and loss of the functional groups i.e., with a certain level of the structural retention, are formed.

On the other hand, in the monomer-deficient region, the ablation process dominates and the polymer deposition rate decreases with increasing  $W/FM$  parameter due to low concentration of the monomer molecules. The power transferred to monomer molecules is rather high and the monomer molecules are subjected to extensive fragmentation. Irregularly structured plasma polymers with high re-arrangement of the monomer structure and low structural retention are formed.

Usually plasma polymerization is operated in the monomer-sufficient region. <sup>[26]</sup> It should be recognized that the chemical composition of the formed plasma polymers is strongly influenced by the magnitude of the plasma power and the monomer flow rate.

Additionally, continuous wave (CW) plasma polymerization is the traditional technique for the deposition of thin films. The power is supplied to the system continuously. Plasma polymers produced by CW plasmas are characterized by a considerable loss of functional groups preformed in the monomer, as well as irregular and cross-linked structures. <sup>[39]</sup> This is due to continuous fragmentation of monomers in the plasma and a random poly-recombination of fragments and atoms.

The main parameters that characterize pulsed plasmas are the pulse period and the duty cycle. The duty cycle (DC) values are calculated from the following equation:

$$DC = \frac{t_{pulse-on}}{t_{pulse-on} + t_{pulse-off}} \quad (1)$$

$t_{pulse-on}$  and  $t_{pulse-off}$  are the time intervals where the plasma power is on and off, respectively.

Additionally, the duty cycle is an effective external plasma parameter to control the power given to the plasma.

The effective energy  $W_{eff}$  provided by pulsed plasma can be estimated from the duty cycle values by using the following formula.

$$W_{eff} = W \times \frac{t_{pulse-on}}{t_{pulse-on} + t_{pulse-off}} \quad (2)$$

Where  $W$  is the power in wattage.

It has been often reported that pulsed plasma polymerization offers a good compromise to efficiently produce polymer structures with a minimum of irregularities and maximum retention of the functional groups preformed in the monomer. <sup>[40-44]</sup> The differences between the CW and the pulsed plasma deposited films were attributed to partially different reaction mechanisms when one or the other regime is used. During a CW plasma deposition, the competing

deposition and etching reactions of the excited species in the plasma lead to a different polymer structure when pulsed plasma is used. It appears that the “plasma off” periods in the pulsed experiments play a very important role in the deposition process, allowing polymerization reactions to take place, which could not normally occur under CW conditions. During the “plasma off” phase it is believed that some of the longer living radicals will continuously enable polymerization reactions, leading finally to a more conventional polymer structure.

The classic radical chain propagation is called chain growth polymerization. It forms normally regularly structured polymers most often with linear structure and high molar mass. However, under low-pressure conditions the chain propagation at radical sites is strongly hindered by the seldom transport of monomer molecules to the radical sites. Therefore, low chain growth and many terminations occur. Chain transfer, recombination and disproportionation hinder the formation of linear chains. Only the repeating pulses re-initiate continuously the chain growth mechanism.

#### ***1.3.2.3. Radicals generation and polymerization***

The freshly deposited plasma polymers typically contain radicals. This is because the radicals are the most relevant species in growth mechanism of plasma polymerization, which is productive for the formation of deposits. Additionally, ultraviolet light generated by the plasma (recombination radiation, line radiation) and ion as well as electron bombardment are also sources for formation of radicals in the deposits.

The quantity of these radicals in the deposited layer depends on the chemical nature of the monomer as well as on the external plasma parameters. <sup>[26]</sup>

The most obvious effect of radicals is that the freshly deposited plasma polymers rapidly react with in-diffusing oxygen when they are exposed to ambient air. The addition of oxygen to radicals produces peroxy radicals that are converted to peroxides and hydroperox-

ides. These peroxides and hydroperoxides are metastable and may decay into various reactive products and secondary radicals. This process is well-known as “auto-oxidation” process. <sup>[45, 46]</sup>

Plasma modified organics can be divided into two steps. <sup>[46]</sup> The primary ageing reaction is that molecular oxygen reacts with C-radical sites. This results in the formation of peroxy radicals (C-O-O $\cdot$ ). Decay of these peroxy radicals and formation of different oxygen functionalities are the secondary reaction step in the ageing process. In the case of plasma deposited films made from hydrocarbon monomers, e.g., ethylene and styrene, these peroxy radicals are mainly converted into hydroperoxides (C-O-OH) by the abstraction of hydrogen from adjacent C-H bonds. <sup>[45]</sup> The auto-oxidation process leads to the formation of different oxygen functionalities like C-O, C=O and COO as it was observed by XPS studies.

## 2. Review of literatures related to plasma (co)polymerization

Plasma polymerized layers are important for many different industrial applications and technologies. <sup>[47]</sup> This includes also high tech applications in sensor technologies and life science <sup>[48]</sup> where functionalized surfaces are required. The introduction of functional groups onto substrate surfaces for different applications by plasma treatment has a long tradition. Oxygen plasma and/or corona treatment in an air atmosphere produces a broad variety of different oxygen-containing functional groups. This versatile distribution of oxygen-containing units is sufficient for promoting printing or adhering processes. One method to produce functionalized surfaces is the plasma deposition of functional-group carrying monomers like acrylic acid, allyl alcohol, allyl amine or others on substrates. This includes also the copolymerization with other monomers like ethylene, butadiene, acetylene etc. Moreover, plasma polymerization has unique practical advantages which include (i) good adhesion to the substrate material, and (ii) chemically stable and physically durable nature of polymers. <sup>[49]</sup>



## **2.1. Homopolymerization**

As found in literature the characterisation of physicochemical properties for the thin organic plasma polymerized layers focuses on films, which are used as scratch protection finishing or on polymers which can replace brittle metallic or ceramic components in electronic circuits. <sup>[50-52]</sup> For instance Cech et al. <sup>[51, 53, 54]</sup> measured the mechanical (elastic modulus and hardness) and optical properties of plasma polymerized silane layers (tetravinylsilane and vinyltriethoxysilane) in dependence on the effective power of the plasma. Besides the mechanical properties of plasma polymerized films its electrical and dielectric properties are of greater importance. Investigations on electrical characterization of plasma polymerized materials were pioneered by Bradley and Hammes. <sup>[55]</sup> They polymerized approximately 40 potential monomers by plasma techniques and studied their dielectric and semiconducting properties. In general conventional plasma polymerization results in highly cross-linked and insulating coatings which can be applied as dielectric layers. <sup>[56]</sup> Nowadays there is also a considerable interest to enhance the conductivity of plasma polymerized films by thermal treatment or doping. <sup>[57]</sup> Chowdhury and Bhuiyan <sup>[58]</sup> employed dielectric relaxation spectroscopy to investigate virgin and thermal treated plasma-polymerized diphenyl thin films sandwiched between aluminium electrodes over a wide range of frequency and temperatures. Plasma polymerized decahydronaphthalene thin layers were investigated by Yang et al. <sup>[59]</sup> with the objective to replace the chemical vapour deposited SiO<sub>2</sub> as interlayer dielectric material. With increasing plasma power, the dielectric permittivity increases from 2.65 to 3.12. The films with the higher dielectric permittivity show smaller thickness reduction during annealing at 400 °C. Zhao et al. <sup>[60]</sup> reported the influence of the plasma deposition conditions on the dielectric properties of 1-cyanoisoquinoline films. Also in that case, the dielectric permittivity increases with increasing power of the plasma. Recently, an analogous study was carried out for plasma polymerized films using benzene and octafluorocyclobutane as monomers. <sup>[61]</sup>

As well as mono-type functionalized plasma polymers have been used for sensors or were produced in view of their interaction with biological materials such as peptides, proteins, or living cells, enzymes, antibodies, DNA and so on. In this context, the plasma polymerization of functional groups carrying monomers as well as copolymerization with 'neutral' monomers becomes interesting in terms of tailoring the surface functionality and its density as the basis for chemical coupling of sensor molecules. In this connection the introduction of COOH groups into the polymer surface opens an interesting field for creation of specific interactions. It is known from own works that carboxylic groups exhibit strong interactions to aluminium which gives rise to excellent adhesion in PP-Al composites. <sup>[34]</sup>

The simplest way to the surface modification of the substrate with COOH groups is presented by Badyal and Poncin-Epaillard. <sup>[62, 63]</sup> They postulate that carbon dioxide can form carboxylic groups by the following sum process:  $\text{C-H} + \text{CO}_2 \rightarrow \text{C-OOH}$ .

Allyl alcohol (AAI) is often favoured to create (more or less complete retention of all OH groups) monosort hydroxyl functionalized surfaces by the plasma deposition. It has a suited boiling point, has sufficient high deposition rates and its deposition leads to well adherent layers with a high concentration of functional groups. This is especially true, when it is deposited by a pulsed plasma technique. The structure of allyl alcohol radicals is stabilized by a mesomerism effect which is responsible for the fact that AAI cannot be polymerized to high molecular weight by a conventional radical mechanism. <sup>[64]</sup>

First experiments to plasma polymerize AAI were carried out by Denaro et al. <sup>[65]</sup>. They investigated the glow discharge polymerization of different organic vapours. There is evidence that the propagation step involves the reaction of radicals with monomer adsorbed on the electrodes. Fally et al. <sup>[66]</sup> studied plasma deposited AAI films by XPS and high resolution electron energy loss spectroscopy. They concluded that oxygen-rich polymers can be obtained from the unsaturated monomers at a low power. In the reactor at high power, fragmentation of the monomer leads to the elimination of oxygen fragments and to ablation reactions

during the polymerization processes. Allyl alcohol leads to the formation of polymers with a relatively low degree of crosslinking and high retention of hydroxyl content (53-72%) under soft conditions; however, Friedrich et al. found it with high retention content (95%).<sup>[67]</sup>

Yoshimura et al.<sup>[68]</sup> investigated nine oxygen-containing monomers by plasma polymerization processes. Highly hydrophilic films can be obtained by propargyl alcohol and AAl, the former was emphasized for hydrophilic finishing of surfaces with OH groups under low power so that oxygen atoms could be preserved in the resultant polymers in the forms of oxygen-containing functional groups. O'Toole and Short<sup>[69]</sup> polymerized allyl alcohol at a low electrical power. They found an inverse relationship between the concentration of OH groups of the deposited film and the power supplied by the plasma. Rinsch et al.<sup>[41]</sup> applied variable duty cycles (DC) for pulsed plasma deposition and obtained the highest OH-functionalization for the lowest value of DC. The application of a gradient layering technique was suited for both enhancing the adhesion and tailoring the functionality. Gombotz and Hoffman<sup>[70]</sup> developed a derivatization technique with trifluoroacetic anhydride (TFAA) and subsequent XPS analysis for the characterization of the functionality of hydroxyl-containing layers. The cross linking of AAl plasma deposited polymers and the mobility of the functional groups were studied by Ameen et al.<sup>[71]</sup> by applying washing tests with water and heating in an argon atmosphere, respectively.

The characterization of the AAl plasma homo- and copolymers by Fourier Transform Infrared FTIR, X-ray Photoelectron Spectroscopy (XPS) and Size Exclusion Chromatography (SEC) was reported by Mix et al.<sup>[34]</sup> In the soluble fractions of the AAl polymers, molecular masses in the range from 800 to 4000 Da were found depending on DC. The lowest masses were measured for the highest values of DC compared to the lowest one. Extensive studies of the ageing of plasma AAl polymers by Static Secondary Ion Mass Spectrometry were published by Unger et al.<sup>[72]</sup> Both, the crosslinking density and the unsaturated character of the allyl alcohol films increases with the ratio of the plasma power to the flow of the monomer

(P/F). The known highest concentration of OH groups in the deposited polymers were found for the lowest values of DC or the ratio P/F <sup>[73]</sup> estimated by Time-of-Flight Static Secondary Ion Mass Spectrometry measurements.

Plasma treatments include cleaning of the substrate by chemical and/or physical etching, polymerization of a thin layer at the surface and functionalization of the surface by the formation of new chemical species. <sup>[74]</sup> By introducing polar functionalities, the surface energy of the topmost layer of the surface is increased; therefore this process can be used for very specific applications, such as introducing of wettability, printability, adhesion and biocompatibility. <sup>[75-77]</sup>

Moreover, plasma treatment is a rapid, clean and non-solvent process that can be used to introduce a specific element or functional group onto the surface of a polymer by selecting a suitable gas. <sup>[78]</sup> Nitrogen-containing plasmas can introduce nitrogen functions such as amine, <sup>[79]</sup> mostly primary amine (NH<sub>2</sub>), imine (>C=NH), azomethine (>C=N-R), cyano or nitrile (–C≡N). <sup>[80]</sup> On the other hand, oxygen-containing plasmas are generally employed to degrade the surface of polymers. <sup>[81]</sup> They can also cause surface functionalization due to the incorporation of oxygen-containing components such as C–O, C=O, O–C=O and O=C–O–O onto the surface of the substrate. <sup>[82,83]</sup> For plasma treatments applied on polystyrene, various types of gases have been found in the literature: oxygen, <sup>[84]</sup> nitrogen <sup>[85]</sup> or argon. <sup>[86]</sup>

However, polymers have been widely used as biomaterials due to durability and low production cost. Among them polystyrene (PS) has commonly been used as a disposable culture dish because, besides these properties, it is optically transparent in visible range, and is non-toxic.

To produce polymer layers with the highest degree of retained functional groups as well as chemically well-defined composition and structure of the polymer backbone plasma polymerization is used. In general, this is impossible using the glow discharge plasma because of the excess of energy in comparison to energies necessary to start and propagate the pure

chemical formation of polymers. However, this comparison shows that the plasmas, in general, and the cw plasma, in particular, are not suited for producing well-defined polymer structures. Using styrene as the prototype for a vinyl monomer, since styrene is best suited for radical chain propagation, only  $\approx 1$  eV is needed to activate the vinyl bond. Using a radical initiator such as N, N'-azobisisobutyronitrile (AIBN) 1.4 eV are necessary to initiate the free radical polymerization. The rate of such a polymerization is directly proportional to the monomer concentration and to the square root of the initiator concentration. <sup>[87]</sup>

Moreover, the radical chain propagation is exothermic and, therefore, needs no additional energy except for initiation. For a pure chemical polymerization of styrene leading to polystyrene of a molecular mass of 100 kDa energy of 0.0015 eV is consumed per styrene molecule for initiation. The activation energy needed to initiate chain growth polymerization of vinyl monomers is  $\Delta G \approx +120$  kJ/mol (ca. 1 eV). <sup>[86,87]</sup> Since 5000-20000 additions/s occur at atmospheric pressure, each with ca.  $\Delta G \approx -20$  kJ/mol, this reaction is strongly exothermic. Comparing this energy with the average electron energy in the CW plasma ( $\varepsilon = 1-10$  eV) a considerable difference is obvious. However, all energy transferred to the monomer molecule by inelastic collisions with electrons during residence in the plasma zone ranges from 10 to 1000 eV. <sup>[88, 89]</sup> The excess energy leads to a large number of side reactions, because all chemical bonds in the monomer molecule can be broken. As a result, irregular structures are formed with an extremely broad molecular mass distribution, with high concentrations of trapped radicals and other defects. Thus, the mechanical and chemical properties are inadequate for many applications. Especially the long-term stability of such polymers is strongly limited by post-plasma oxidation. Therefore, it is obvious that the direct plasma exposure should be minimized as much as possible in order to produce highly chemically defined polymers. In contrast, the CW plasma is the worst case for plasma polymerization, much worse than the high energetic radiation chemical polymerization as reported by Westwood. <sup>[89]</sup>

Oran et al. <sup>[90]</sup> studied pulsed plasma deposited styrene and ethylene films by Time of Flight Static Secondary Ion Mass Spectrometry before and after exposure to ambient air. As well as the influence of the external plasma parameters on the secondary ion mass spectra of plasma deposited films was investigated. Concluded that, when the plasma polymers are exposed to air oxygen incorporation occurs. The oxygen uptake is high at the beginning and then it levels off. However, harder plasma conditions, which could be obtained by applying higher plasma power or lower monomer flow rate, result in higher oxygen uptake and vice versa. All plasma deposited films are unsaturated, branched and/or cross-linked to some extent. These properties of the films are found to depend on fragmentation and re-arrangement of the monomer molecules in plasma, which could be controlled by external plasma parameters.

## **2.2. Copolymerization**

Plasma copolymerized organic films are of growing interest and have been studied by a number of groups. The interest in plasma copolymers is driven by relevant technological applications in different fields starting from a conversion of harmful chlorofluoro carbons <sup>[91]</sup> to the improvement in cell immobilization on substrates. <sup>[92, 93]</sup> One overall objective of plasma copolymerization studies is to tailor technologically requested film properties. <sup>[94-97]</sup>

Plasma copolymerization has been often studied in terms of:

- (1) Determination of the density of functional groups at the surface of deposited films vs. variation of feed gas composition <sup>[67, 98]</sup> and,
- (2) Interaction, e.g. recombination reactions, between different monomers in the plasma environment. <sup>[99-101]</sup>

Copolymerization is a method used for creating (co)polymers with variable properties depending on type and ratio of copolymers. Many chemical copolymerizations are based on

free radical processes. One difference to plasma-assisted polymerization, however, is their retention of the regular structure. If monomers A and B are copolymerized, the resulting copolymers can show random (-AA-B-AB-AAA-B-...), alternating (-A-B-A-B-...), or block (-AAA-BB-AAAA-BBB-...) or graft (-AAAA (BBB)-AAAA (BBB)-) structure. <sup>[102]</sup>

Different models were developed for mathematical characterization of radical copolymerization process.

Friedrich et al. <sup>[103]</sup> reported on the tuning of the density of functional groups at surface of plasma polymers by copolymerization of functional-groups bearing monomers with neutral chain-extending comonomer. They investigated plasma copolymerized films of ethylene or styrene with allyl amine or allyl alcohol by FTIR and XPS and reported that the density of functional groups varies non-linear with respect to the feed gas composition. Dawson et al. <sup>[104]</sup> found an almost linear correlation between functional group concentration and the feed gas compositions for acrylic acid - 1,7-octadiene mixed plasma copolymerization as analyzed by XPS. However, the deviation from linearity might be due to the fragmentation and polymer recombination. Swaraj et al. investigated pulsed-plasma deposited styrene-allyl alcohol and ethylene-allyl alcohol copolymer films produced under conditions optimized for monomer structure retention and analyzed (“*in situ*”) by XPS, NEXAFS (Near Edge X-ray Absorption Fine Structure) and ToF-SSIMS (Time-of-Flight Static Secondary Ion Mass Spectrometry). <sup>[105]</sup> They confirmed the non-linear variations of  $O_{total}$  and -OH concentration vs. variation of the feed gas composition for both monomer combinations.

Mix et al. <sup>[34]</sup> studied pulsed plasma deposited allyl alcohol-styrene copolymers in dependence on DC, energy and precursor composition. SEC characterization of soluble copolymer fractions showed molecular masses of a few hundred up to five thousands g/mol. This concerns also a more regular structure of the copolymers.

Numerous applications of plasma deposition processes require an optimization to provide a high degree of retention of the monomer’s chemical functionality. It has been reported

in the literature <sup>[39-41]</sup> that a pulse plasma polymerization offers a better option to produce plasma polymers with minimized irregularities and a high degree of functionality retention. The effective power can be lowered in the case of pulse plasma polymerization to get a plasma environment that prevents excessive monomer fragmentation and reduces the plasma-induced damage of the deposited polymer layer. The percentage of chemically produced products can be also increased by plasma-less chain propagation within plasma off period. Such chemically produced polymers have less defects and irregularities. The next plasma pulse re-starts the chain growth process again. Such so called “mild” plasma conditions are obtained by using low duty cycles or low plasma power, resulting in sufficient surface concentrations of selected functionalities. Any increase in a duty cycle or plasma power will reduce the retention of the respective monomer functionalities by monomer fragmentation, resulting in wider and, of course, objectionable chemical variability of functionalities in the plasma deposited films. Duty cycle and plasma power additionally affect branching and crosslinking of the plasma polymers. <sup>[106,107]</sup> Consequently, the process parameters ‘plasma power’ and ‘duty cycle’ the only way variables to control the functional group concentrations at plasma deposited polymer films. One interesting way to adjust the concentration of the functional groups is the plasma-assisted copolymerization of functional groups bearing monomers with neutral monomers as reported by Friedrich et al. <sup>[108,109]</sup> who applied plasma copolymers to investigate the dependence of adhesion of Al-PP composites on type and concentration of different functional groups.

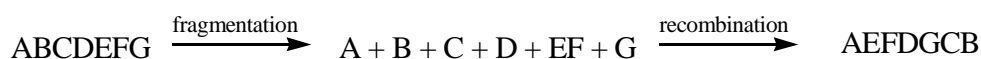
For a plasma copolymerization processes an additional variable process parameter is available to control functional group retention: the respective concentrations of the monomers in the feed gas mixture. These can be adjusted, e.g., by partial flow rates. When all other plasma parameters are constrained to plasma conditions providing high structure retention of monomers a variation of the concentration of monomers in the feed gas will enable film deposition with a controlled concentration of a selected functionality.



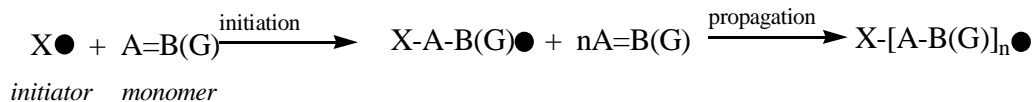
Many of details of the plasma polymerization with one or more precursors remain unclear, so defining relationships among process parameters, structure, and properties remains a key objective in studies of plasma polymerization films. Hirotsu et al. <sup>[95]</sup> found that plasma power is the key parameter in controlling chemical composition and morphology of copolymer films from acrylic acid and hexamethyldisilazane. Copolymer films produced at lower plasma power were hydrophilic, while those produced at higher plasma power were hydrophobic. Beck et al. <sup>[97]</sup> used plasma copolymerization of allyl amine with 1,7-octadiene and acrylic acid with hexane to generate new surfaces with controlled properties by varying plasma power and monomer flow rate. Other studies in the area of plasma copolymerization <sup>[91, 92, 110-113]</sup> have focused on the incorporation of different chemical functionalities into the final film and the impact of this incorporation on surface characteristics. However, little work has been done on the physical characteristics of the interfaces in these systems. In this contribution, the details of the structure with depth of copolymer films were reported. Recently, the effect of the duty cycle on thin plasma poly(acrylic acid) films was studied by Fahmy et al. <sup>[106, 107]</sup> using a combination of dielectric relaxation spectroscopy, XPS and FTIR.

Only limited reports on the mechanism of plasma copolymerization have been published due to the complicated plasma environment. <sup>[114]</sup> Enclosed the different possibilities of polymerization, copolymerization or homopolymerization are listed.

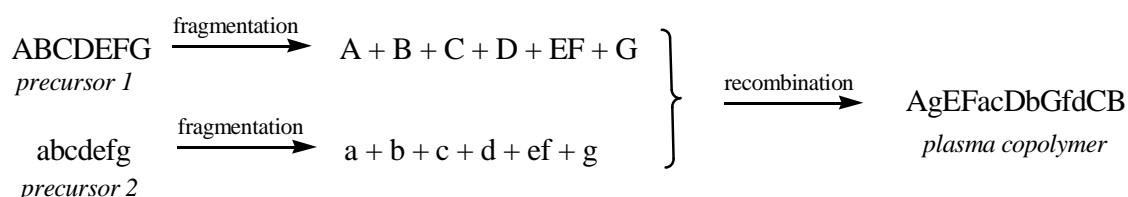
**plasma polymerization (fragmentation-polyrecombination)**



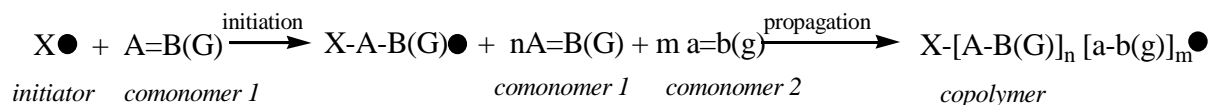
## plasma-initiated radical chain growth polymerization



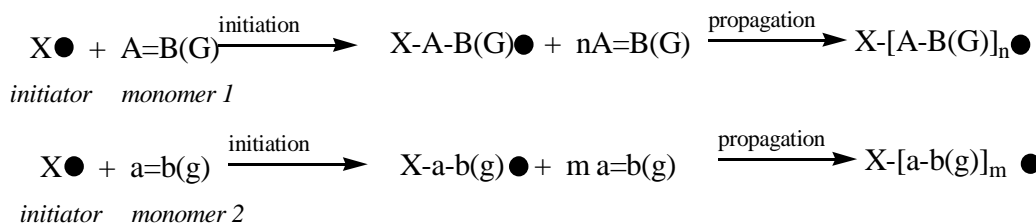
### plasma copolymerization (fragmentation-polyrecombination)



**plasma-initiated chemical copolymerization**



**homopolymerization instead of copolymerization to a "blend"**



**alternating copolymer**



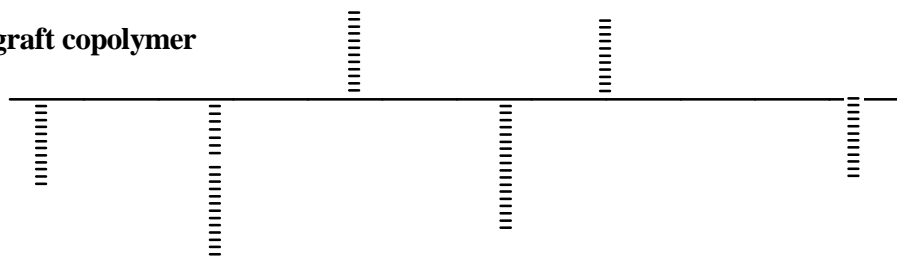
**block copolymer**



**random copolymer**



**graft copolymer**



### 3. Motivation

#### 3.1. Plasma polymerization

The literature survey indicates that till date the mechanism of plasma polymerization is poorly understood. Fragmentation and poly-recombination reactions take place within the plasma, where the contribution of these reactions to polymer formation is not clear. The most important problem of plasma exposure to polymers is the excess of energy delivered by the plasma. The energy is consumed by the particle bombardment and the UV-irradiation.

These two processes provoke random chain scissions, H abstraction, C-radical formation, unsaturations, auto oxidation, degradation, crosslinking etc. in polymers.<sup>[45,115,116]</sup> For attaching plasma atoms or fragments as (plasma gas-specific) functional groups onto polymer surfaces only a small amount of energy is useful for replacing hydrogen atoms by plasma fragments (functional groups). The replacement of hydrogen from the C atom may be possible either by nucleophilic substitution or by radical-radical recombination. Substitution reactions are more selective, however, implausible. Recombination reactions are probable because of the high rate of radical formation but this process is not selective and proceeds more or less randomly. The very high chemical activity of such plasmas (continuous flow of energy and enthalpy) alter the surface energy and the chemistry on polymer materials surface. It is believed that the substrate surface firstly arriving monomer fragments and atoms are attached by radical recombination to the polymer surface, thus forming covalent bonds between substrate and growing plasma polymer layer. Generally measured high peel strength of such plasma polymer layers confirms this assumption.

Acrylic acid, allyl alcohol and styrene are used as monomers to prepare plasma polymerized films on different substrates (organic and inorganic) using a pulsed and continuous plasma technique. Acrylic acid and allyl alcohol were chosen for this study because it is known that these plasma polymers can form adhesion-promoting interlayer for instance in fiber/epoxy composites and can also serve as a biocompatible interface.<sup>[117-119]</sup> Moreover, from

a more scientific point of view acrylic acid can be easily polymerized by conventional polymerization processes. For that reason the properties of plasma deposited poly(acrylic acid) can be compared with that of poly(acrylic acid) polymerized by radical polymerization. The polystyrene (PS) has commonly been used as a disposable culture dish because, besides these properties, it is optically transparent in visible range, and non-toxic.

Therefore, as an experimental parameter the duty cycle of the pulsed plasma is varied over a broad range of values. The properties of the obtained materials are investigated by a combination of surface and volume sensitive techniques. Concerning the latter point, in addition to FTIR, dielectric spectroscopy is employed in a broad range of frequencies and temperatures using molecular mobility as a probe for the structure.

While the chemical characterization of functionalized plasma polymer films is well developed using various spectroscopic techniques, the investigation of other properties like mechanical, electrical or thermal (physicochemical properties) is scarce in the literature. Therefore, the study of the surface and bulk properties in relation to both the chemical structure of the films and the plasma conditions is required for the preparation of tailor-made plasma polymerized layers.

Volatile organic compounds may be used to deposit ultra-thin, pinhole-free films. These films are commonly referred to as plasma polymers or plasma deposits. The approach is attractive as it affords control over film chemistry and thickness, and film deposition is uniform and takes place within a clean environment, i.e., without any use of solvents. Plasma treatment provides an important and powerful technique for altering the surface chemistry of materials without changing their bulk properties. Therefore they have been used for a wide variety of applications ranging from electrical devices to medical implants.

In many cases, polymers formed by plasma polymerization are different in chemical composition, and structure as well as physical properties e.g., conductivity, from those formed by classic polymerization, even if the same monomer is used. The structure of plasma poly-

mers are rather complex. They are to some extent unsaturated, branched and crosslinked. In a plasma polymerization process the chemical structure of the plasma polymer can be altered by a selection of external plasma parameters, e.g. duty cycle and plasma power or W/FM (Yasuda) factor respectively. The characterization of plasma polymers and the investigation of their structural dependence on the external plasma parameters require a multi-method approach. An improved understanding of the composition/structure-property relationships is required to optimize the design and film fabrication for various applications.

Organic thin films with defined chemistry and properties are required for various applications in fields concerning, e.g. electronics, biology, medicine and optics. The thin polymeric layers have to be well defined with surfaces and bulk properties such as topography, surface tension, glass transition, density and distribution of chemical groups and surface charges. So the advanced characterization methods are applied on thin films.

Here, investigation of the surface functionalization and bulk properties of the plasma deposited thin films are in the focus. Films were studied with respect to DC.

For the first time the dielectric dynamics of spin-coated polystyrene exposed to O<sub>2</sub> and Ar plasma and plasma-emitted UV irradiation as well as to pulsed plasma polystyrene over a broad range of frequency and temperature was investigated. Sense of plasma or UV exposure of commercial polystyrene was to identify secondary changes of plasma polymers during deposition by irradiation and particle bombardment.

### ***3.2. Plasma copolymerization***

Copolymerized products are of special interest because it is obvious that technologically requested film properties may be “tailored”. Monomers to be used are simple organic molecules with a polymerizeable C=C bond, such as acrylic, vinyl or with limitations allyl.

Chemical properties of interest are the unsaturated, branched and crosslinked character of the films, as well as the retention of the respective monomer functionality.

*Copolymerization consists* coupling two or more comonomer units by covalent linking in different arrangements as shown before. For adhesion promotion or biocompatible or bio-active surface the tuning of the density of functional groups is of importance. Thus, hyphenating of monomer forming an inert polymer segment and a monomer carrying functional groups by attachment of monomer molecule may be used for adjusting the number of functional groups by varying the comonomer ratio. Several types of copolymers of inert and reactive units can be formed as graft, block, random or alternating copolymer as shown before.

Here, the production and characterization of acrylic acid (AA)/styrene (S) deposited copolymers is reported in comparison to pure plasma poly (acrylic acid) (PAA) and poly (styrene) (PS) (homo-) polymers deposited under the same experimental conditions. The aim was to find the percentage of comonomer in the precursor mixture, which allowed depositing of copolymer layers with chemically defined and adjustable structures and physical properties without or at least with only a small number of defects using the pulsed plasma technique to know more information about plasma copolymers (alternative or branching or random).

### ***3.3. Organic and inorganic substrates***

Polyethylene and polypropylene have very good recycling abilities within the existing commercial engineering plastics remained a prominent object of intense studies for improvement of their interactions to other solids and liquids. <sup>[120]</sup> The majority of its technical applications are connected with a highly adherent bonding to other materials. Diverse new applications for engineering polymers have therefore made polymer surface modification methods to a subject of intense research.

However, polypropylene and polyethylene are widely used in many technological fields due to their suitable bulk properties, easy workability and low manufacturing costs. While maintaining the bulk properties of polymers, the plasma modification of their surface properties can tailor polymers for specific use. Thus, for many applications it is necessary to modify their surface chemically, in order to enhance, e.g. paint adhesion or metal–polymer bonding [121] polymer–polymer bonding or to generate bio functional surfaces. [118] Vascular grafts, heart valves, catheters, intraocular lenses and contact lenses are only a few examples of various applications in the biomedical field. As a first step, for example a reproducible functionalization with carboxylic groups is required. [122]

Plasma copolymer layers may be coated onto different target materials. Interesting applications are known in the fields of metal-polymer or glass-polymer composites such as dry Al-polymer condensers or coated plane glass in buildings. Aluminum is a suitable substrate electrode for the deposition of a variety of electro-active films including conducting polymers. [123]

However, the glass substrate is the most common commercial glass with low cost. It possesses a large variety of applications in optic devices and optical communications when doped with other elements or compounds. For example, rare-earth doped soda-lime glass can be used in medical diagnostics, laser glasses, undersea optical communication, integrated-optical devices and optical data storage [124, 125] where periodical nano-structures on glass substrate are necessary to obtain required optical properties. It is, however, a high challenge for glass processing to get nano-structures due to its hard, brittle, non-conductive and other inert properties. Recently, there is a growing interest in developing nano-processing to fabricate nano scale structures on glass substrate. [126] It leads to many investigations on the sophisticated fabrication methods, such as nano imprinting, [127] electron beam lithography [128] and chemical etching.

#### 4. Enrichment of functional groups at substrate surfaces

For specific applications such as medical engineering, biotechnology, optimized adhesion and for any post-plasma chemical processing (grafting) homo-functionalized polymer surfaces are required as discussed in the introduction.

The first goal was to initiate a plasma polymerization of unsaturated organic compounds containing polymerizable double bonds such as acrylic acid (COOH), allyl alcohol (OH), allylamin (NH<sub>2</sub>) and styrene (aryl). Thus, plasma copolymerization of the acrylic acid-styrene was performed.

The nature of the polymers should be analyzed for retention of functional groups in the corresponding polymer, branching, crosslinking or other deviations from the classic structure of unsaturated polymers. Nevertheless, the partial crosslinking, characteristic for each plasma process, should help to deposit a coating.

For this coating process the most important questions were: what are the most important functional groups, how much of the functional groups has retained the polymerization process, what is the resulting of the functional group density and its effect on the wettability of the surface and how are the bulk properties such as thermal stability, dynamic mobility and conductivity of the deposited thin films. These can be checked roughly by C1s peak fitting for identification of basic structural elements occurring in XPS (X-ray Photoelectron Spectroscopy) spectra, in combination with FTIR, CAM (contact angle measurements), DSC (differential scanning calorimetry) and DRS (Dielectric Relaxation Spectroscopy). It was not in the focus of this work to identify the exact structure of copolymers and the sequence of monomer units and therefore of functional groups. Working hypothesis was the formation of an alternate copolymer consisting of [AB]<sub>n</sub> comonomer units. Block, graft or random structure as well as (partial) co-existence of two homopolymers as “blend” may also occur. The identification of structure needs further investigations by chromatography if dissoluble or NMR.



## 5. Approach and perspective of the work

The functionalization of the outermost surface with O containing groups involves OH, C-O-C, epoxy, C-O-OH, CHO,  $R_1R_2C=O$ , COOH, COOR, CO-O-OH,  $CO_3$ , C=C etc. These functional groups are capable of improving strongly the adhesion properties of polymers to metals, other polymers, fibers or adhesives because of acid-base interactions, hydrogen bonds or even chemical bonds etc. at the interface of composite materials. For advanced future applications and basic research on the polymerization mechanism it is desirable to know the structure of the thin films and properties of it for better tuning the properties by optimizing plasma conditions. A future way is also combining the plasma-chemical with chemical processing, thus producing maximal activation of inert surface of solids and modifying them by selective chemical graft or coating processes.

With regard to biomedical applications OH, COOH, CHO, epoxy, SH and  $NH_2$  groups are of special interest. These polar groups are reactive and can be used as the starting and anchoring-point for subsequent highly selective chemical graft reactions. Biochemically modified polymer surfaces are important in new fields like nucleotide synthesis, DNA chips, and tissue engineering.

### 5.1. Brief overview of proposed work

This work will focus on:

1. Surface coating of inorganic materials and polymers, in particular polyolefins and polyolefine-like polymers, with plasma polymers.
2. The influence of the plasma parameter variation on the introduction of functional groups to substrate surfaces was experimentally verified.

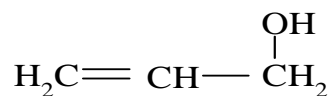
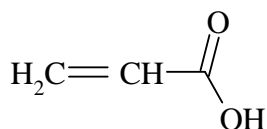
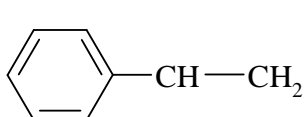
3. Variation of deposition parameters and characterization of produced plasma polymer films in comparison to conventional polymers.
4. Measuring the dielectric properties of the plasma (co)polymer films as fairly new and comprehensive characterization method of ultra-thin polymer-like films and referring them to the surface composition in dependence of:
  - 4.1. Influence of the plasma parameter (duty cycle)
  - 4.2. Agency of the comonomer ratio
5. Effect of O<sub>2</sub>, Ar, and UV-C plasma exposure resp. irradiation on spin coated films in comparison to analogous plasma deposited polymer films and virgin conventional spin coated polymer film.
6. Tests of thermal stability for different plasma thin polymer films with respect to plasma conditions and materials were performed.

## Chapter 2

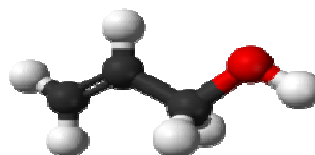
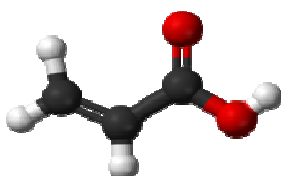
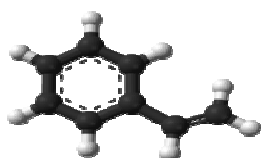
### Experimental

#### 1. Chemical structures

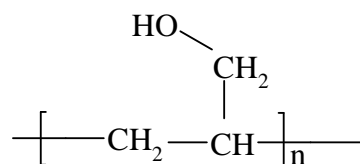
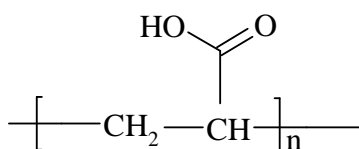
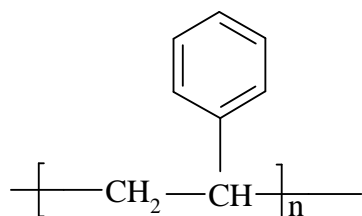
(a)



(b)



(c)



(d)

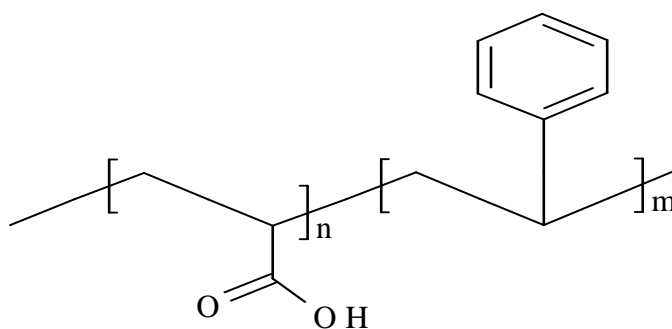


Figure 5: (a) Chemical structure of styrene (S), acrylic acid (AA) and allyl alcohol (AAl), (b) It is in 3D, (c) homopolymers of it and (d) acrylic acid styrene tentative copolymer (AA/S)

## 2. Materials

Aluminium (Al) deposited onto glass by thermal evaporation (ca. 100 nm), uncoated glass, polyethylene (PE) and polypropylene (PP) were used as substrates.

With purity of 99.95% and diameter 0.5 mm Al wires were obtained from Goodfellow. As glass substrate carefully cleaned (see below) microscope slides were used. The polyethylene (thickness 40  $\mu\text{m}$ ) and polypropylene (thickness 0.1 mm) foils were supplied by Alkor Folien GmbH, Germany.

The monomers acrylic acid and styrene (purity >>99% grade) were obtained from Fluka. They were distilled before use also to remove stabilizers. To compare the plasma polymerized materials with conventionally synthesised polymers two samples of poly(acrylic acid) with two different molecular weights (1800 g/mol and 450 000 g/mol) were purchased from Sigma-Aldrich. These samples are denoted as cPAA18 and cPAA45 and their corresponding glass transition temperatures  $T_g$  (DSC, 10 K/min, second heating run) are 370 K and 403.4 K, respectively.

To compare the plasma polymerized materials with conventionally synthesised polymers one sample of polystyrene with molecular weights (50,000 g/mol) were purchased from Polysciences Inc. Warrington, PA.

Trifluoroethanol (TFE), pyridine (with purity >99% MERCK, Germany) and N, N'-di-tertbutylcarbodiimide (Fluka) were used as received for derivatizing the COOH groups. Propionic acid ( $\text{CH}_3\text{CH}_2\text{COOH}$ ) was obtained from MERCK, (Germany) with 99 % purity.

Allyl alcohol, trifluoroacetic anhydride (TFAA; needed for derivatization of OH groups) were used as well as n-propanol ( $\text{CH}_3\text{CH}_2\text{CH}_2\text{OH}$ ) from MERCK (Germany) with 99.5 % purity.

Fig. 5 gives the chemical structure of the monomers, polymers and regular copolymer as it can be obtained by conventional polymerization.

Table 2 shows physical and chemical properties of acrylic acid, styrene and allyl alcohol monomers.

Table 2: Physical properties of acrylic acid, styrene, and allyl alcohol <sup>[129,130,131]</sup>

Property	Acrylic acid (CH <sub>2</sub> =CHCOOH) MW=72.07	Styrene (C <sub>6</sub> H <sub>5</sub> CH=CH <sub>2</sub> ) MW=104.2	Allyl alcohol (CH <sub>2</sub> =CHCH <sub>2</sub> OH) MW= 58.1
Colour	Colourless	Colourless to yellow	Colourless
B. p.	141 °C	145 °C	97 °C
M. p.	14 °C	-30.6 °C	-12.9 °C
R. Density (water=1)	1.05	0.91	0.9
Solubility in water at 20 °C	miscible	0.03 g/100 ml	miscible
Vapour pressure, kPa at 20 °C	413	0.67	2.5
R. vapour density (air=1)	2.5	3.6	2.0
Auto-ignition temperature	360 °C	490 °C	378 °C
Viscosity (20 °C)	1.3 cSt	0.8 cSt	1.3 cSt
T <sub>g</sub>	134°C	100 °C	75°C

### 3. Sample preparation

#### 3.1. Plasma deposited thin films

##### 3.1.1. Plasma deposited thin polymer films

The deposition experiments were accomplished in a stainless steel reactor made by Ilmvac, Germany with a volume of 50 dm<sup>3</sup>. The reactor was equipped with a pulsable radio-frequency (r.f. 13.56 MHz) generator with an automatic matching unit and a flat r.f. electrode (5 cm x 35 cm). A cylinder with a diameter of 10 cm served as a rotating ground electrode (12 revs/min). It was mounted at a distance of 2.5 cm with respect to the hot (r.f. powered) electrode. The substrate was fixed on the ground electrode (see Fig. 6). The monomer was dosed

by a mass flow controller for liquids (Liquid-Flow®, Bronkhorst) adjusted to the desired the flow rate.

The media was introduced by a heatable gas/liquid distributor consisting of perforated metallic tubes kept at 75 °C. The pressure was kept constant at 10 Pa by varying the speed of the turbomolecular pump and/or the orifice of an automatic butterfly valve (V.A.T.). A quartz microbalance was used for monitoring the deposition rate. As the densities of ultra thin layers are difficult to measure, a density of 1 g/cm<sup>3</sup> was assumed to calculate the film thickness. This means that the absolute values of the thicknesses can have some deviations, but this potential error was the same for all the discussed cases. Knickmeyer et al. and Friedrich et al. have published recently density values also for polyolefin-like plasma polymers. [88] Therefore, relative changes can be discussed. Moreover, one can argue that the density of the deposited layers can depend on the plasma conditions like the duty cycle. This might be the case but the expected differences in the density values are argued to be small (< 5%) and negligible as compared to other effects. Additionally, each sample was scratched and the thickness was measured by Atomic Force Microscopy AFM. It was about 135 nm for all samples with an error of 10 %. There was no significant dependence of DC.

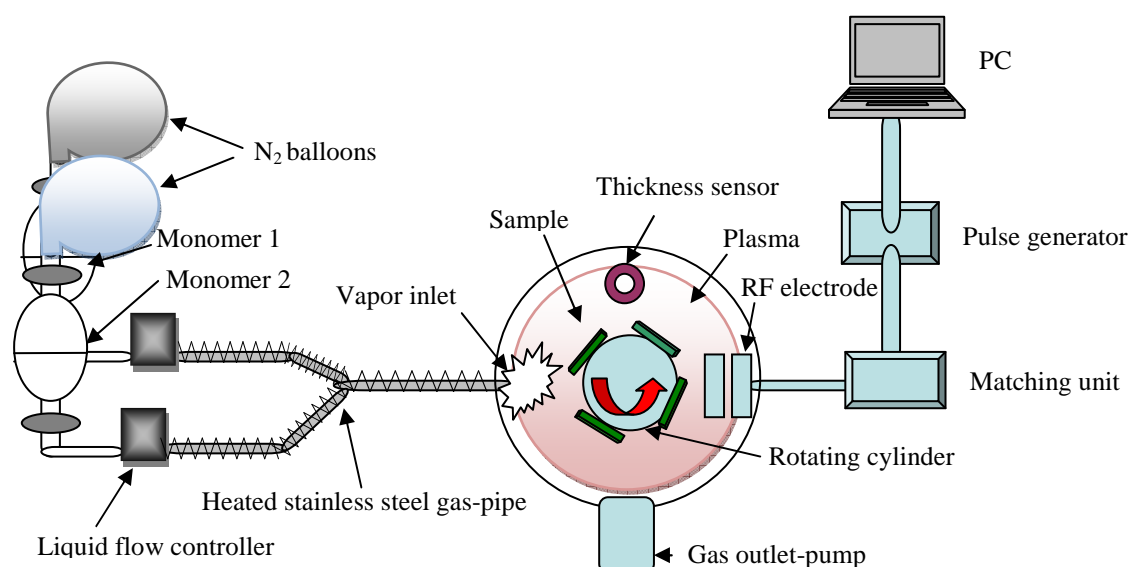


Figure 6: Plasma reactor

Continuous wave as well as pulsed r.f. plasma modes (pulse frequency 1000 Hz) were applied. The duty cycle (DC) characterizes the pulse period as was showed in [Equation \(1\)](#).

DC was varied between 0.1 and 1. The effective power  $W_{eff}$  depends on DC according to [Equation \(2\)](#). The maximal power  $W$  was adjusted to 100 W which corresponds to DC=1.

The nomenclature of the plasma polymerised products used in the following:

PS<sub>xx</sub>, PAA<sub>xx</sub>, PAA<sub>lxx</sub> and AA/S(x:y) are for polystyrene, poly(acrylic acid), poly(allyl alcohol) and acrylic acid-styrene copolymer plasma where xx is the duty cycle and (x:y) molar ratio.

Before use the PE foils were ultrasonically cleaned in diethylether for 15 min. After that a polymer layer with a thickness of 150 nm was deposited in the most cases. For the dielectric investigations the samples must be electrically contacted. Therefore the polymer was sandwiched between two aluminium electrodes as described in ref. [\[132\]](#). Glass substrates were cleaned during a first step in an ultrasonic alkaline bath at 333 K for 15 min followed by a second ultrasonic bath with ultra-high purified water (Millipore, resistivity > 18 MΩ/cm). Then the glass plates were first rinsed in acetone and then in chloroform, which were distilled before used. After this cleaning procedure the substrates were dried by a nitrogen flow and an aluminium electrode was deposited onto the glass substrate by thermal evaporation in vacuum of  $1.3 \times 10^{-4}$  Pa. After the evaporation of this first electrode the plates were rinsed again in acetone. Subsequently a film with a thickness of 150 nm was plasma deposited. The sample preparation was finished by the evaporation of the counter electrode on the top of the polymer film, which was oriented perpendicular to the first one. To minimize the diffusion of metal atoms into the film and to avoid damages of the polymer a so-called flash evaporation was applied. This means the evaporation time was kept as short as possible (<2 s). It is known that under these conditions a sharp and smooth metal/polymer interface is obtained. [\[133\]](#)

The crossing area of the perpendicularly oriented metal stripes defines the capacitor for the measurement (see Fig. 7).

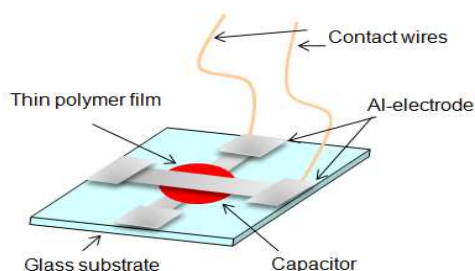


Figure 7: Shows the dielectric relaxation's sample

For FTIR spectroscopy the sample was prepared on a thin Al layer on a glass target as described for dielectric spectroscopy. Additionally, the plasma polymerized layers were deposited on a glass cylinder (thickness 500 nm) and scratched off to investigate thermal properties by differential scanning calorimetry using scratched flakes.

### 3.1.2. Plasma deposited thin copolymer films

Two monomers were introduced via a heated stainless steel gas-pipes kept at 75 °C as described before. The total flow rate was kept constant but the partial flow rates of the monomer were varied to prepare plasma copolymers at different feed gas compositions. All other external plasma parameters were kept constant in the experiments.

### 3.2. Spin coated thin films

Commercial polystyrene particles were dissolved in toluene to 25 wt % and then spin-coated (spin speed = 5000 rev min<sup>-1</sup> for 50 s) onto glass and aluminum substrates to obtain thin films with ca. 150 nm thickness as measured by AFM. The samples were kept in a vacuum oven at 130°C for 16 h to evaporate the solvent (annealing process).



Then the samples placed on the ground electrode in the plasma chamber. One of the samples was masked by quartz glass to study the effect of plasma UV irradiation with a cut-off wavelength of about 180 nm on the sample only and the second one was exposed directly to the plasma without any window.

Oxygen and argon were then introduced into the chamber with gas flow rate 25 sccm. Plasma parameters kept constant like in plasma polymerization (power =100 W, duty cycle (DC) =0.5, pressure 10 Pa and the exposure time is 1 sec. see Fig. 8).

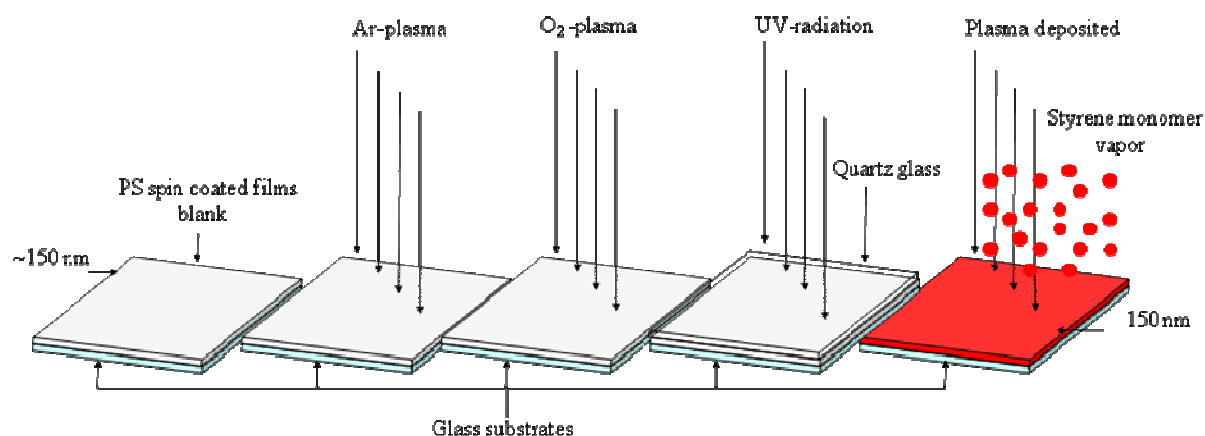


Figure 8: Presentation of the different samples for  $O_2$ , Ar plasmas and UV irradiation treated spin coated PS in comparison to plasma PS and commercial PS as a blank

## 4. Characterization methods

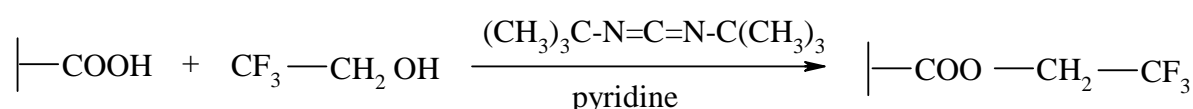
### 4.1. Surface functionality

The surface composition of the deposited film were analyzed by XPS by monitoring the C1s, O1s, N1s and F1s peaks using a SAGE 150 (Specs, Berlin, Germany) spectrometer equipped with a hemispherical analyzer Phoibos 100 MCD-5. Non-monochromatic Mg  $K_{\alpha}$  radiation with 11 kV and a power 220 W was employed at a pressure  $ca. 10^{-7}$  Pa in the analysis chamber. The angle between the axis of X-ray source and the analyzer lenses was  $54.9^{\circ}$ .

The analyzer was mounted at 18° to the surface normal. XPS spectra were acquired in the constant analyser energy (CAE) mode. The analyzed surface area was about 3 x 4 mm. The measured elemental concentrations were referenced to 100 C atoms. The information depth of XPS measurements is between 5 and 7 nm.

#### 4.1.1. Derivatization of functional groups for improved XPS analysis

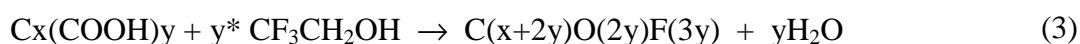
##### 4.1.1.1. Carboxylic group derivatization



*Scheme 1: Derivatization reaction of COOH-groups with trifluoroethanol (TFE) in presence of di-tertbutylcarbodiimide*

To distinguish between carboxylic acid and ester group formation on substrates surface in context with the scheme of gas phase derivatization presented in [Scheme 1](#), the chemical derivatization of COOH groups with trifluoroethanol (TFE) was applied. <sup>[134]</sup> Derivatization proves chemically the presence of –COOH functionalities contributing to the C1s subpeak at 289.1 eV binding energy). The reaction is carried out at room temperature in the gas phase. However, this region of binding energy region is also attributed to the ester group-COOR bonded carbon. Unambiguous specific identification of -COOH groups needs the derivatization of COOH group by 2, 2, 2-trifluoroethanol (TFE) in presence of a carbodiimide (used as scavenger for produced water) and measuring thus the introduced fluorine concentration by means of XPS. <sup>[135]</sup>

From these data the concentration of the carboxylic groups per 100 carbon atoms  $c(\text{COOH})$  can be calculated based on the following reaction scheme:



where  $y$  denotes the fraction of the carbonyl bonds and  $x$  the fraction of carbon in other functional groups, which cannot be converted by TFE.  $x$  and  $y$  can be estimated from the concentration of carbon  $[C]$  and fluorine  $[F]$  of the derivatized sample measured by XPS elemental analysis by

$$y = \frac{[F]}{3} \quad \text{and} \quad x = [C] - \frac{2[F]}{3} \quad (4a)$$

The concentration of carbonyl groups per 100 carbon  $c(\text{COOH})$  atoms is calculated as:

$$c(\text{COOH}) = 100 \frac{y}{x} = 100 \frac{[F]}{3[C] - 2[F]} \quad (4b)$$

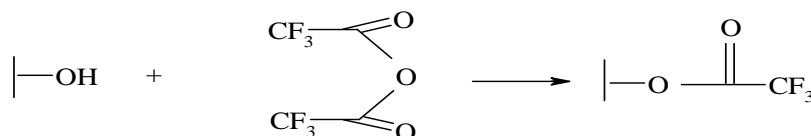
This calculation implies the homogeneous distribution of COOH groups within the sampling depth of the XPS method (5-7 nm).

Simultaneously, the deposited crosslinked polymer layer may be further modified by the plasma exposure. The thus produced functionalities or those which are rearranged during the deposition process maybe hydroxyl, ether, epoxy, ketone, aldehyde, acids, esters, peroxy acids and carbonates. The XPS measurement was used to identify such functional groups as hydroxyl, ether, epoxy (286.3 eV), ketone, aldehyde (287.5 eV), acid and ester (289.1 eV). The data obtained after X-ray photoelectron spectroscopic analysis was processed using the software CASA-XPS. It was expected that  $-\text{COOH}$  groups may not completely survive the polymerization process because of decarbonylation and decarboxylation reactions.

Nevertheless, a large fraction of the survived  $-\text{COOH}$  groups were esterified and then detected. The total oxygen percentage (all oxygen containing groups) may also reflect the process of  $-\text{COOH}$  group destruction because the decarboxylation as well as the decarbonylation decreases the total bonded oxygen percentage. On the other hand the simultaneous surface oxidation increases the oxygen content.

#### 4.1.1.2. Hydroxyl group derivatization

The derivatization of OH groups was selective in high yield by using trifluoroacetic anhydride TFAA in the vapor phase. <sup>[136]</sup> The TFAA derivatization of hydroxyl functional group for improved XPS analysis was highly selective in the absence of any amino groups, and showed a high yield by using it in the vapor phase. Scheme 2 represents this gas phase reaction.



*Scheme 2: The derivatization reaction of OH groups for plasma deposited PAAl by TFAA*

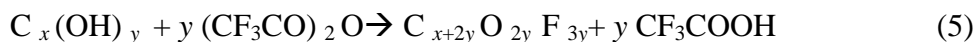
The principle of this method is the reaction of a functional group at the surface with a substance containing one or better more hetero atoms which are not present in the deposited layer. The requirements of such substances and reactions are summarized in ref. <sup>[137]</sup>.

TFAA was used as a reagent to estimate the concentration of the hydroxyl groups at the polymer surfaces. The reaction converts the OH groups into trifluoroacetates (see Scheme 2). Using the fluorine signal in the XPS spectra a quantification of the OH groups is possible. Precondition is that the functional groups are homogeneously distributed within the XPS sampling depth. TFAA reacts rapidly with the hydroxyl groups but it does not react or only very slowly with alkenes, ethers, ketone and esters. <sup>[138]</sup>

The plasma polymerized samples were exposed to a saturated TFAA vapour for 15 min, rinsed after that treatment extensively with isopropyl ether, and dried under vacuum prior to the XPS measurement because one mole trifluoroacetic acid is also formed simultaneously.

The F1s peaks were used for quantifying the presence of –OH groups among all other singly oxygen to carbon bonded (C-O) species (C-OH-alcohols, C-O-C-ethers, COC epoxides and hydroperoxides-CO-OH), by derivatizing them with TFAA.

From these data the concentration of hydroxyl groups per 100 carbon atoms  $c_{\text{(OH)}}$  can be calculated using the following reaction scheme (see also [Scheme 2](#)):



Here  $y$  denotes the fraction of the hydroxyl groups and  $x$  the fraction of carbon in other functional units which cannot be converted by TFAA. Both,  $x$  and  $y$  can be estimated from the concentration of carbon [C] and fluorine [F] obtained from the XPS spectra of the derivatized sample according to [Equation \(4a\)](#).

#### ***4.2. Contact angle measurements (CAM)***

To estimate the surface energy of samples, contact angle measurements were carried out. Diiodomethane, ethylene glycol, formamide and water have been used as test liquids. The measurements were carried out using the automated contact angle system G2 (Krüss, Germany) by the sessile drop method. For analysis, the method after Owens-Wendt-Rabel and Kaelble was selected as given by the Krüss software. All chemicals were purchased from Aldrich and used as received, unless stated otherwise. Solvents were at least analytical-grade quality.

#### ***4.3. Chemical composition estimated by FTIR***

FTIR spectra were recorded from 4000 to 550  $\text{cm}^{-1}$  accumulating 64 scans at a resolution of 4  $\text{cm}^{-1}$  using a Nicolet Nexus 8700 FTIR spectrometer (Nicolet, USA) in the ATR mode (Diamond Golden Gate, Nicolet, USA). All spectra were subjected to diamond ATR and baseline corrections. Peak areas were estimated by applying the OMNIC software.

Additional the spectra were analysed by deconvolution (fitting Gaussians to special bands). In difference to XPS, a sample thickness up to 2.500 nm is analyzed by FTIR-ATR.

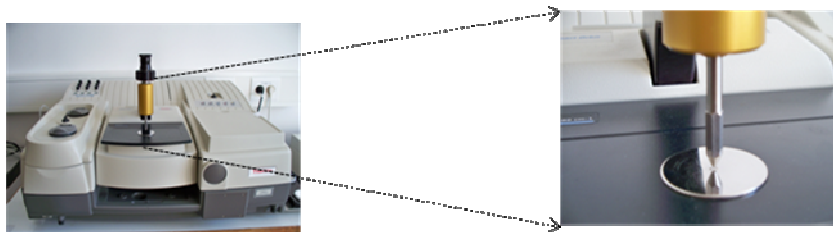


*Figure 9: Diamond golden gate apparatus (FTIR)*

#### ***4.4. Thermal measurements***

The thermal analysis was carried out by differential scanning calorimetry (DSC, Seiko<sup>®</sup> instruments). N<sub>2</sub> is used as inert gas. The samples were measured in the temperature range from 173 K to 460 K with a heating rate of 10 K/min for 1<sup>st</sup> heating, cooling and 2<sup>nd</sup> heating run. The glass transition temperature T<sub>g</sub> was taken as the inflection point of the heat flow of the second heating run.

#### ***4.5. Dynamic mobility and dielectric properties***

Broadband Dielectric Relaxation Spectroscopy (B-DRS) is very sensitive towards structural changes in the polymer bulk and in this work also in that of ultra-thin layers. It detects the molecular mobility in the plasma polymerised layers, such as molecular fluctuations of dipoles (including radicals). For polymers these fluctuations are related to the molecular mobility of groups, segments or the whole polymer chain as well. For details see ref. [139].

A high resolution alpha analyzer (Novocontrol<sup>®</sup>) is used to measure the complex dielectric function  $\varepsilon^*(f) = \varepsilon'(f) - i\varepsilon''(f)$  ( $f$ - frequency,  $\varepsilon'$  and  $\varepsilon''$ -real and imaginary part of the complex dielectric function,  $i = \sqrt{-1}$ ) in the frequency range from  $10^{-1}$  to  $10^7$  Hz and temperature ( $T$ ) from 173 to 453 K. The temperature was controlled by a Quatro Novocontrol<sup>®</sup> cryo-system with temperature stability better than 0.1 K. For more details see ref. [140].

## Chapter 3

### Results and discussion

#### 1. Acrylic acid plasma deposited thin polymer films

##### *1.1. Kinetics of polymer deposition*

Inset of Fig. 10 displays the thickness of the layer versus the deposition time for the various duty cycles. For each value of DC, the data can be well described by a straight line. From its slope the deposition rate  $R$  can be deduced (Fig. 10) for acrylic acid. The deposition rate increases with increasing DC. It is worth mentioning that the found dependence is non-linear as might be expected. To understand this non-linear behaviour one has to consider which processes can take place during the plasma deposition. There are two main processes. Both of them are due to the high energy density of the plasma. Firstly, the double bond of the acrylic acid can be activated leading to radicals, which can undergo a normal chain growth polymerization process under low pressure conditions. This process takes place with a rate  $R_{\text{Chain}}$  and will lead to regular structures similar to that obtained by a conventional polymerization process. Secondly, due to the high energy density of the plasma a fragmentation of the monomer takes place followed by a poly-recombination which leads in general to irregular, unsaturated or branched structures. The rate of the latter process is denoted as  $R_{\text{Frag}}$  where the overall deposition rate is given by  $R = R_{\text{Chain}} + R_{\text{Frag}}$ . In addition to these processes, the possibility of depolymerisation and a partial removal of the deposited layer cannot be neglected.

To differentiate between these two main processes, the plasma deposition of acrylic acid can be compared with that of a molecule having a similar chemical structure without any double bonds. An appropriate candidate is propionic acid ( $\text{CH}_3\text{-CH}_2\text{-COOH}$ ). Fig. 10 shows that the deposition rate of propionic acid is low in comparison to acrylic acid and independent of DC. The comparison of the deposition rates of acrylic acid and propionic acid shows that in



the former case in addition to fragmentation preferred chain growth polymerization occurs due to the presence of the double bond.

Chain growth polymerization due to the double bond takes place during both the time intervals of deposition, i.e.  $t_{\text{pulse-on}}$  and  $t_{\text{pulse-off}}$ . In order to compare the deposition rates and the contribution of chain growth polymerization during the plasma  $t_{\text{pulse-off}}$  time for the different DC directly, the deposition rates are normalized to the time where the plasma was on ( $t_{\text{pulse-on}}$ ). Equivalently the deposition rate can be divided by DC (see Fig. 11). In such a presentation, the value of the normalized deposition rate at the highest duty cycle (DC=1) is an estimate for the contribution of chain growth polymerization to R during the plasma  $t_{\text{pulse-on}}$  time, because the rate of fragmentation is constant for all values of DC (see results obtained for propionic acid, Fig. 10).

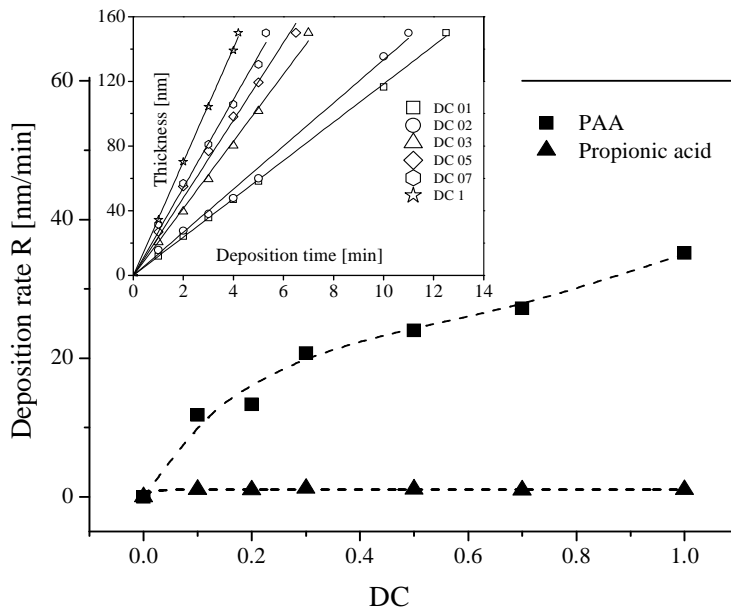


Figure 10: Deposition rate for AA and propionic acid versus DC. The error of the data is smaller than the size of the symbols. The inset gives thickness of the plasma polymerised layer versus deposition time for various DC

Fig 11 shows that the normalized deposition rate is maximal for the lowest duty cycle. This means that the rate of the chain growth process during the plasma  $t_{\text{pulse-off}}$  time is essentially higher for low values of DC. This might also imply that for low values of DC a more regular structure is formed.

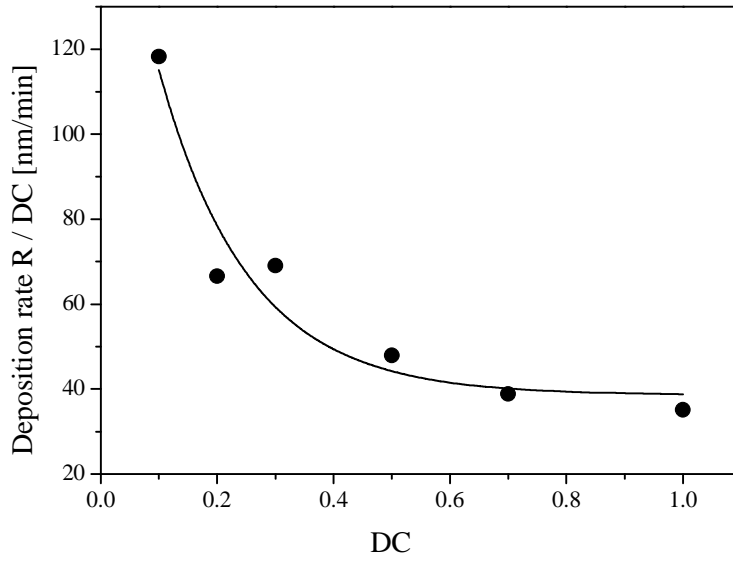


Figure 11: Deposition rate of PAA normalised to the duty cycle versus DC

### 1.2. Estimation of the surface functionality by derivatization and XPS

XPS is used to estimate the overall composition of the deposited layer. According to the Equation 2 the effective power of the plasma increases with growing of DC and therefore influences the fragmentation of the monomers per time unit.

Table 3: Analysis of the C1s peak for the non-derivatized and derivatized surface of plasma deposited PAA

DC	As synthesized	Derivatized
	O/C	CF <sub>3</sub> [Atom-%]
Theoretically	0.670	33.3
0.1	0.430	18.3
0.2	0.479	14.7
0.3	0.418	11.0
0.5	0.407	10.1
0.7	0.401	11.5
1.0	0.362	08.5

In Table 3 the concentrations of carbon and oxygen are summarized for the different DC values. The concentration of C atoms grows with increasing DC slightly and that of oxygen decreases correspondingly.

More information about the concentration of functional groups gives the inspection of the C1s peak and especially the analysis of the derivatized surface. Fig. 12 gives the high resolution XPS spectra in the energy range of the C1s peak for acrylic acid plasma polymerized at a DC=0.5 and derivatized with TFE. All XPS spectra were normalized to C-C/C-H at 285 eV. Further on the following carbon-containing functionalities in the C1s peak were assigned to the following bonding energies: C-O at 286.3 eV, C=O at 287.5 eV; COOH or COOR at 289.1 eV and CF<sub>3</sub> at 293 eV.

The concentration of carboxylic groups per 100 carbon  $c(\text{COOH})$  atoms is calculated and plotted versus DC in Fig. 13 according to Equation (4b).

Firstly, the concentration of the carboxylic groups is much smaller than expected from the chemical structure of poly(acrylic acid). Secondly,  $c(\text{COOH})$  decreases with increasing DC. Both effects are due to the fragmentation of the monomer in the plasma. The effective power increases with increasing DC and, therefore, the degree of fragmentation and rearrangement of the monomer, resulting in a lower concentration of carboxylic groups and a higher concentration of radicals. [141]

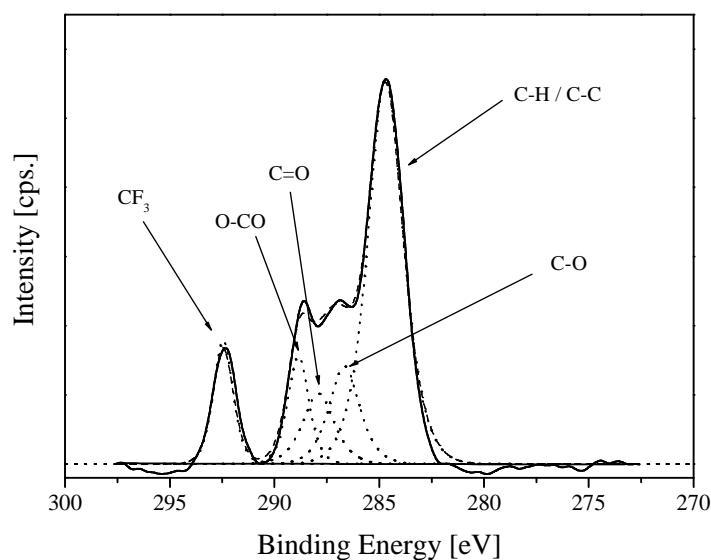


Figure 12: High resolution XPS spectra of the sample PAA01 after derivatization with TEF. The solid line represents the experimental data. The dashed line is a fit of a sum of five Lorentz/Gauss functions (Lorentz fraction 72 %) to the data. The dotted lines represent the individual contributions

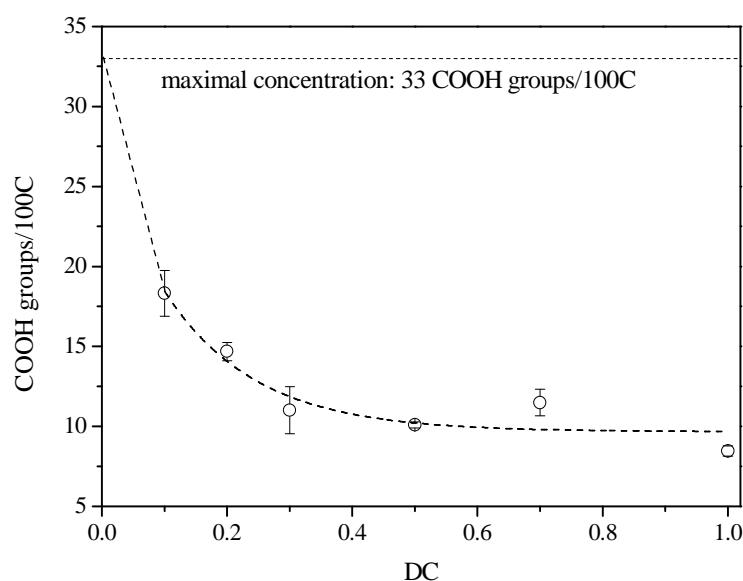


Figure 13: Concentration of the carboxylic groups per 100 carbon atoms for PAA versus DC. The error bars results from three different measurements at the same sample. The dotted line indicates the maximal possible concentration of carboxylic groups

### 1.3. Investigation of the chemical composition by FTIR

In difference to XPS, FTIR spectroscopy can be employed to investigate the chemical structure across the whole film. Fig. 14 compares the FTIR spectra of cPAA18 with that of plasma polymerised acrylic acid deposited on a thin aluminium layer. Both spectra are quite similar. The broad band in the wavenumber range from  $3000\text{ cm}^{-1}$  to  $2500\text{ cm}^{-1}$  is related to stretching vibrations of the OH group of the COOH unit and to vibrations of the  $\text{CH}_2$  unit. [122] The absorptions at wavenumber below  $1450\text{ cm}^{-1}$  are due to bending vibration of the CH ( $1451\text{ cm}^{-1}$  -  $1412\text{ cm}^{-1}$ ) and the C-O-H group ( $1234\text{ cm}^{-1}$  -  $1167\text{ cm}^{-1}$ ). Most important for the following discussion is the stretching vibration of the carbonyl group ( $\text{C}=\text{O}$ ). The inset of Fig. 14 shows the enlarged view in the wavenumber range of the  $\text{C}=\text{O}$  vibration from  $1850\text{ cm}^{-1}$  to  $1550\text{ cm}^{-1}$  for cPAA18. A detailed examination reveals that this band is quite complex and consists at least of two different contributions. The main component at  $1703\text{ cm}^{-1}$  is attributed to the carbonyl stretching vibration ( $\text{C}=\text{O}$ ) of carboxylic groups. The second contribution with a shoulder at  $1651\text{ cm}^{-1}$  is related to the vibration of another structural unit. According to the literature this band is due to dimers formed by the  $\text{C}=\text{O}$  group [142] or  $\text{C}=\text{C}$  double bonds. [102] For quantitative analysis two Gaussians are fitted to the data (see inset Fig. 14).

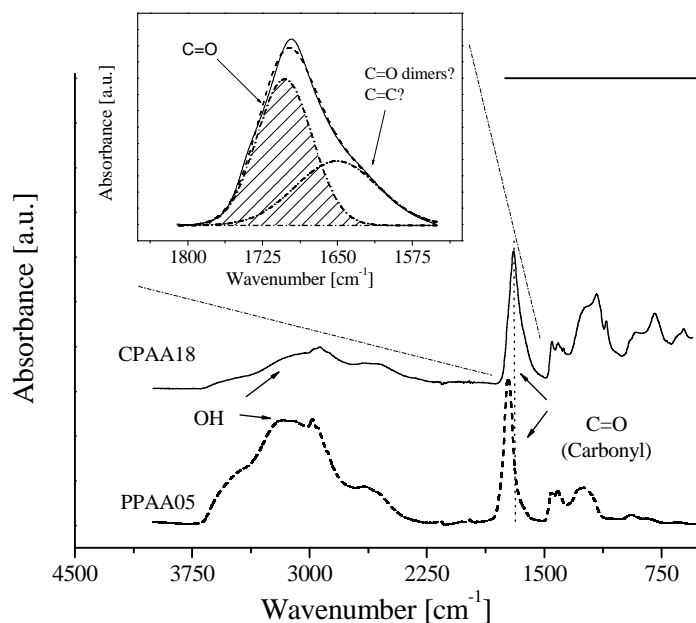


Figure 14: FTIR spectra for the plasma PAA deposited with a duty cycle of 0.5 in comparison to conventional PAA. The inset enlarges the wavenumber region for the carbonyl stretching vibration. The dashed line is a fit of two Gaussians to the data where the dashed-dotted lines are the individual contributions

Fig. 15 gives the FTIR spectra for plasma PAA deposited with a duty cycle of 0.2. Compared to cPAA the main peak of the C=O stretch is shifted from  $1703\text{ cm}^{-1}$  to  $1735\text{ cm}^{-1}$ . This indicates the formation of other bonds in addition to those expected for PAA (COOH) like ketones or ester groups. <sup>[143]</sup> The following procedure is employed to analyse the spectra quantitatively where three Gaussians were fitted to the data. One Gaussian is located at  $1735\text{ cm}^{-1}$  to describe the main part of the peak. From the XPS measurements it is known that O-C=O groups are formed. To model this in the FTIR spectra a Gaussian is placed at  $1703\text{ cm}^{-1}$ . Finally, to describe the contribution of dimers formed by the C=O group a third Gaussian is located at  $1651\text{ cm}^{-1}$  similar to conventional PAA. To reduce the number of the free fitting parameters and to stabilize the fit, the maximum positions of the Gaussians are kept constant during this analysis. Fig. 15 gives an example for this procedure. For all the cases, the regression coefficient is better than 0.99.

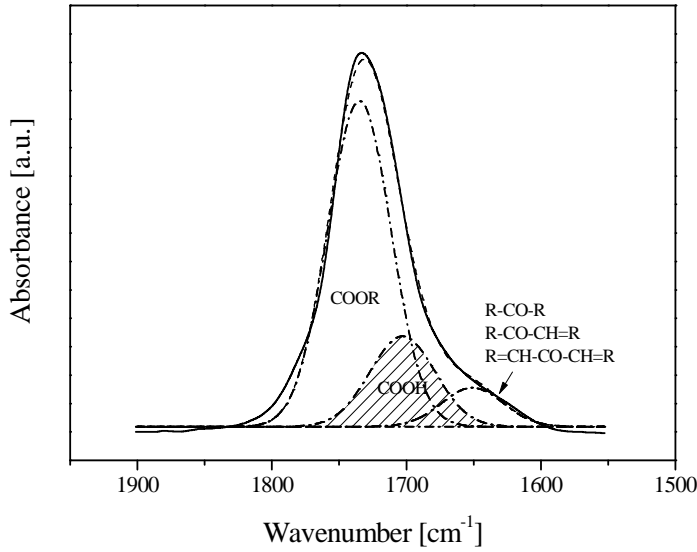


Figure 15: FTIR spectra for the plasma PAA deposited with a duty cycle of 0.2 (sample PAA02, solid line) in the wavenumber region for the carbonyl stretching vibration. The dashed line is a fit of three Gaussians to the data where the dashed-dotted lines are the individual contributions

From these fits the areas of the Gaussians at  $1703\text{ cm}^{-1}$  ( $A_{1703}$ ) and  $1735\text{ cm}^{-1}$  ( $A_{1735}$ ) are taken and their ratio  $\frac{A_{1703}}{A_{1735}}$  is calculated as a measure for the concentration of COOH groups estimated from FTIR. In Fig. 16,  $\frac{A_{1703}}{A_{1735}}$  is plotted versus DC. This figure resembles a close similarity to the concentration dependence of the COOH groups estimated from XPS measurements (see Fig. 13). In principle XPS and FTIR should provide the same information about the concentration of the COOH groups. Therefore, in inset of Fig. 16  $\frac{A_{1703}}{A_{1735}}$  is displayed versus the concentration of COOH groups estimated from XPS measurements which should be a constant. However, this graph shows an approximately linear dependence between both concentrations. To discuss this fact the different analytical depths of the two methods has to be considered. XPS is sensitive to a layer of 5 to 7 nm where as FTIR provides information across the whole sample thickness. The amount of energy increases with increasing DC in the form of electrons, ions radiation etc. is introduced into the system. In addition to that UV radiation which can penetrate deeply into the sample volume is of great importance. This energy input in its different forms will damage PAA at larger distance from the surface which is

already polymerized. That is not the case at the surface where polymerization takes place at a higher rate in addition to defragmentation and depolymerisation. For that reason the ratio of the COOH groups estimated by FTIR (whole sample) and XPS (only surface) decreases with increasing DC (see inset of Fig. 16).

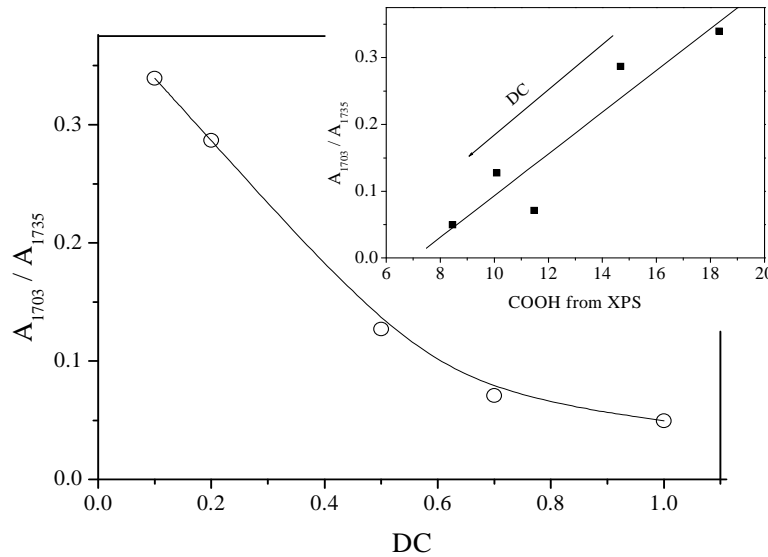


Figure 16: Measure concentration of COOH groups of PAA

from FTIR  $\frac{A_{1703}}{A_{1735}}$  versus DC.

The inset gives  $\frac{A_{1703}}{A_{1735}}$  versus the concentration of COOH estimated from the XPS measurements

#### 1.4. Thermal properties

The inset of Fig. 17 compares the DSC curves for cPAA45 and plasma PAA deposited with a DC of 0.1 and 0.7. For each material a step-like change in the heat flow is observed which indicates the glass transition. The glass transition temperature  $T_g$  is estimated from the inflection point of the heat flow and plotted versus DC in Fig. 17.

For all plasma deposited PAA samples the values of the glass transition temperatures are lower than those for cPAA and decreases with increasing DC. From this dependence two can conclude. All of them depend on the mechanism of polymerization process. Firstly, during the plasma polymerization a highly branched structure with many dangling ends is produced which may act as an internal plasticizer yielding. The number of these dangling ends increases with increasing values of DC which lead to a decreased  $T_g$ . The extrapolation of this

dependence to  $DC=0$  meets the value of  $T_g$  of cPAA18. If this is observed just by change or bears fundamental information requires additional investigations. Secondly, a fragmentation of the monomer followed by poly-recombination increases with increasing DC. A product with low MW probably was formed with growing DC.

So,  $T_g$  decreases from high MW to lower one in cPAA and the lowest one is the plasma deposited PAA.

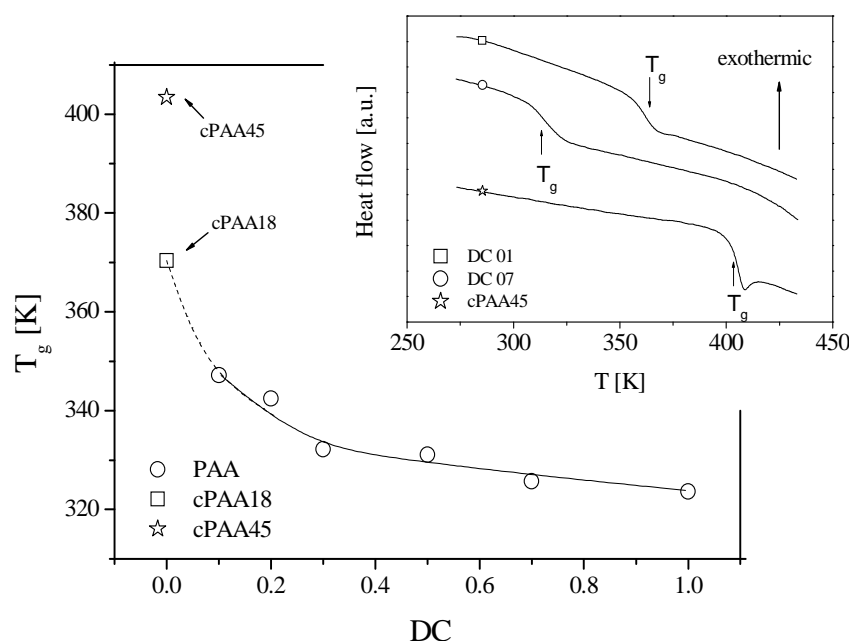


Figure 17: Glass transition temperature  $T_g$  versus DC for conventionally and plasma deposited PAA. The dashed line is the extrapolation of the dependence obtained for plasma deposited PAA to cPAA18. The inset gives the heat flow versus temperature for conventional and plasma deposited PAA for the second heating run at a rate of 10 K/min

### 1.5. Dynamic mobility and thermal stability

Dielectric relaxation spectroscopy (DRS) was used for measuring the molecular dynamics of thin plasma-polymerized polymer films. Molecular dynamics means the possibilities of macromolecules to make movements, oscillations or rotations by absorbing energy from an applied high-frequency field. These movements are strongly related to the structure of polymers. Polar groups (dipoles), radicals, crosslinking etc. change strongly the energy absorption.



Moreover, the temperature influences the thawing or freezing of many fluctuations of macromolecules. The existence and if possible the estimation of glass transition temperature ( $T_g$ ) should be checked as well as oxidative and thermal stability by means of the DRS method.

A general overview about the dielectric relaxation behaviour of polymers can be found in textbooks.<sup>[144]</sup> Before the dielectric behaviour of the plasma deposited PAA is discussed in detail, the dielectric properties of the conventional products are considered.

In the frame of the linear response theory the real and loss part of the complex dielectric function is related to each other by the Kramers-Kronig relationships. Therefore both quantities contain the same information and here only the  $\epsilon''$  is discussed.

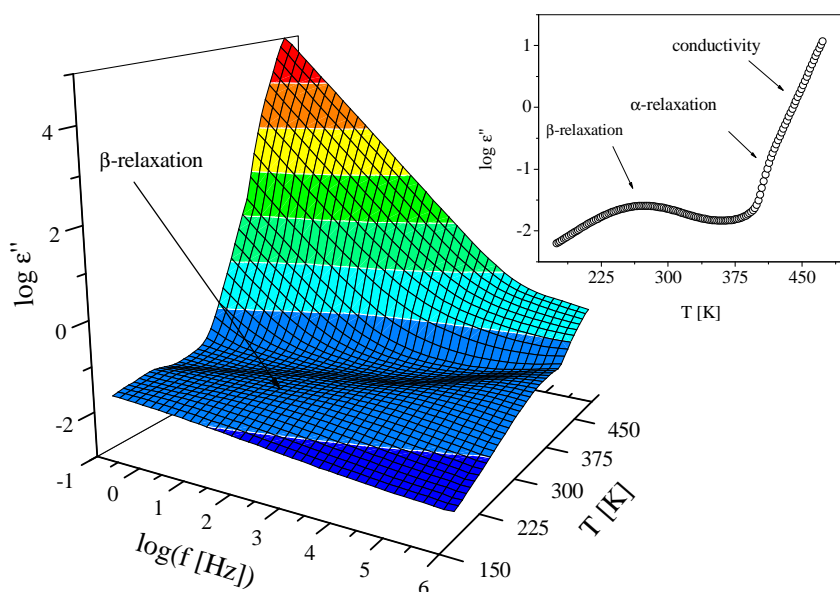


*Figure 18: Dielectric loss  $\epsilon''$  for the sample cPAA45 vs. frequency and temperature in a 3D representation. The inset gives the dielectric loss for cPAA45 vs. temperature at a fixed frequency of 1 kHz*

Fig. 18 gives the dielectric loss for cPAA with the molecular weight of 450,000 g/mol versus frequency and temperature in a 3D representation. One relaxation process, indicated by a peak in the dielectric loss is observed at low temperatures which are called as  $\beta$ -relaxation. As expected it shifts to higher frequencies with increasing temperature. For higher temperatures the dielectric loss increases with frequency and temperature without clear indication of a further relaxation process. That increase of the dielectric loss is related to conduction phe-

nomena corresponding to the drift motion of charge carriers. The carboxylic group is able to separate a proton, for instance in the presence of water, so poly(acrylic acid) is a polyelectrolyte.

In the inset of Fig. 18 the dielectric loss is plotted versus temperature at a fixed frequency. Again at low temperatures the  $\beta$ -relaxation is observed. At higher temperatures, in the range of the glass transition measured by DSC an ill-defined shoulder is visible which might correspond to the dynamic glass transition ( $\alpha$ -relaxation) overlaid by the strong conductivity contribution.

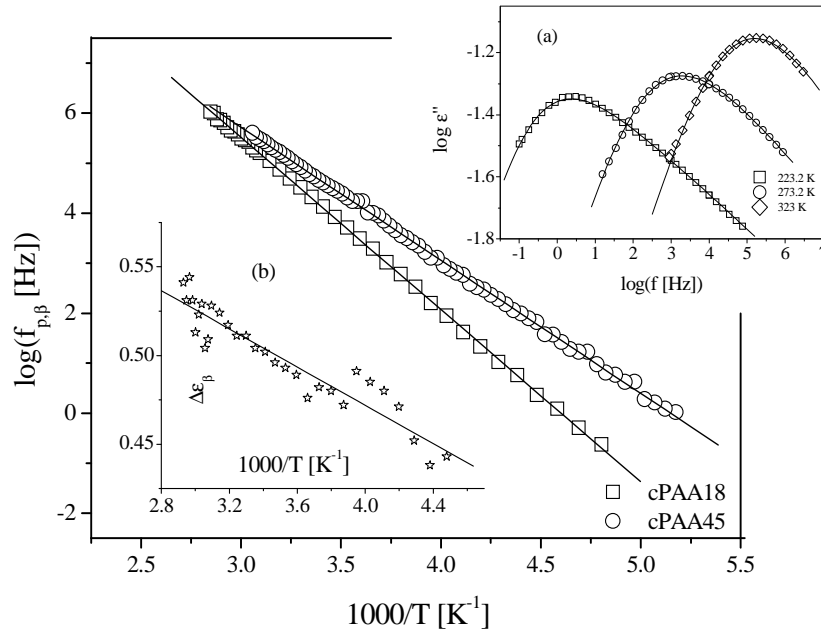


Figure 19: Relaxation rate  $f_p$  for the  $\beta$ -relaxation versus inverse temperature for cPAA18 and cPAA45. The lines are fits of the Arrhenius equation to the corresponding data. The inset (a) gives the dielectric loss  $\epsilon''$  vs. frequency for the  $\beta$ -relaxation of the sample cPAA18 at different temperature. The lines are fits of the HN-equation to the corresponding data. Inset (b) gives the dielectric strength  $\Delta \epsilon_\beta$  of the  $\beta$ -relaxation of the sample cPAA18 versus inverse temperature

The model-function of Havriliak-Negami (HN-function) <sup>[145]</sup> was employed to analyze the  $\beta$ -relaxation. The HN-function reads

$$\varepsilon^*(f) - \varepsilon_\infty = \frac{\Delta\varepsilon}{(1 + (if/f_0)^\beta)^\gamma} \quad (6)$$

$f_0$  is a characteristic frequency related to the frequency of maximal loss  $f_p$  (relaxation rate,)<sup>[146]</sup>  $\beta$  and  $\gamma$  are fractional parameters ( $0 < \beta \leq 1$  and  $0 < \gamma \leq 1$ ) characterizing the shape of the relaxation time spectra.  $\Delta\varepsilon$  denotes the dielectric strength of each process.  $\varepsilon_\infty$  gives  $\varepsilon'$  for  $f \rightarrow \infty$ . The relevant details can be found in ref. [146]. Examples of this procedure are given in the inset (a) of Fig. 19. From the fit, the relaxation rate  $f_p$  and the dielectric strength  $\Delta\varepsilon$  are deduced in their temperature dependences (see Fig. 19).

The temperature dependence of the relaxation rate  $f_{p,\beta}$  of the  $\beta$ -relaxation is linear versus inverse temperature and can be described by the Arrhenius equation

$$f_{p,\beta} = f_\infty \exp\left(-\frac{E_{a,\beta}}{k_B T}\right) \quad (7)$$

where  $E_a$  is the activation energy and  $f_\infty$  the pre-exponential factor and  $k_B$  the Boltzmann constant. The estimated values of the activation energy are 65.8 kJ/mol ( $\log(f_\infty [\text{Hz}]) = 15.8$ ) and 50.9 kJ/mol ( $\log(f_\infty [\text{Hz}]) = 13.7$ ) for cPAA18 and cPAA45 respectively. The values are in the order of magnitude of localized processes where the activation energy for cPAA18 is essentially higher than that of cPAA45. The reason for the different behaviour is not clear up to now and requires additional investigations.

The Debye theory of dielectric relaxation generalized by Kirkwood and Fröhlich<sup>[147]</sup> predicts for the temperature dependence of the dielectric relaxation strength

$$\Delta\varepsilon = \frac{1}{3\varepsilon_0} g \frac{\mu^2}{k_B T} \frac{N}{V} \quad (8)$$

where  $\mu$  is the mean dipole moment of the process under consideration and  $N/V$  is the number density of dipoles involved.  $g$  is the so-called Kirkwood/Fröhlich correlation factor, which describes static correlation between the dipoles. The Onsager factor is omitted for the sake of

simplicity. The inset (b) of Fig. 19 gives the relaxation strength  $\Delta\epsilon_\beta$  for the  $\beta$ -relaxation of cPAA18 versus inverse temperature. It is well known for localized fluctuations  $\Delta\epsilon_\beta$  increases with increasing temperature. This increase of  $\Delta\epsilon_\beta$  is probably due to an increase of the fraction of fluctuation dipoles which contribute to the  $\beta$ -process.

Fig. 20 gives the dielectric loss of a plasma PAA (DC=0.5, sample PAA05) versus frequency and temperature in a 3D representation during cooling. The plasma polymerized samples are measured as thin films sandwiched between aluminium electrodes as described in detail before. For the thin film capacitors the resistance  $r$  of the Al electrodes cannot be neglected. This resistance leads to an artificial loss contributions (electrode peak) on the high-frequency side of the spectra with a time constant  $\tau_{\text{Res}} = r * C'$  ( $C'$  - sample capacity). At least two further processes are detected which will be discussed latter.

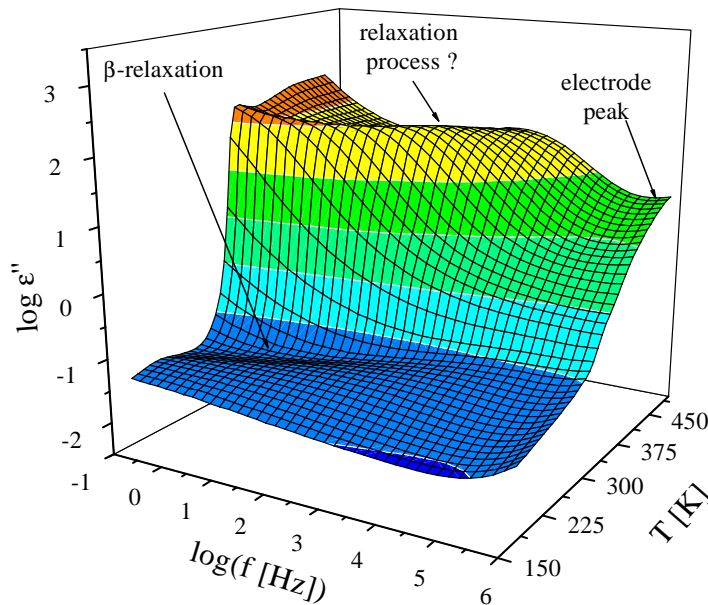


Figure 20: Dielectric loss  $\epsilon''$  for the sample PAA05 vs. frequency and temperature during cooling in a 3D representation

To draw a first conclusion one has to state that the dielectric behaviour of the plasma deposited PAA is different from that of cPAA (compare Fig. 18 and Fig. 20).

To analyze the relaxation process found in plasma deposited PAA the HN-function is used again to analyze the data. The electrode peak is taken into consideration by a Debye function as described in ref. [132]. Here, the frequency position of the electrode peak is out-

side the experimental used frequency window (see Fig. 20) and it can be approximated by its low frequency tail. Therefore the whole fit function reads as

$$\varepsilon''(f) = \text{Im}\left\{ \frac{\Delta\varepsilon}{(1 + (if/f_0)^\beta)^\gamma} \right\} + A * f \quad (9)$$

where A is a fitting parameter. An illustration for that procedure is given in the inset of Fig. 21.

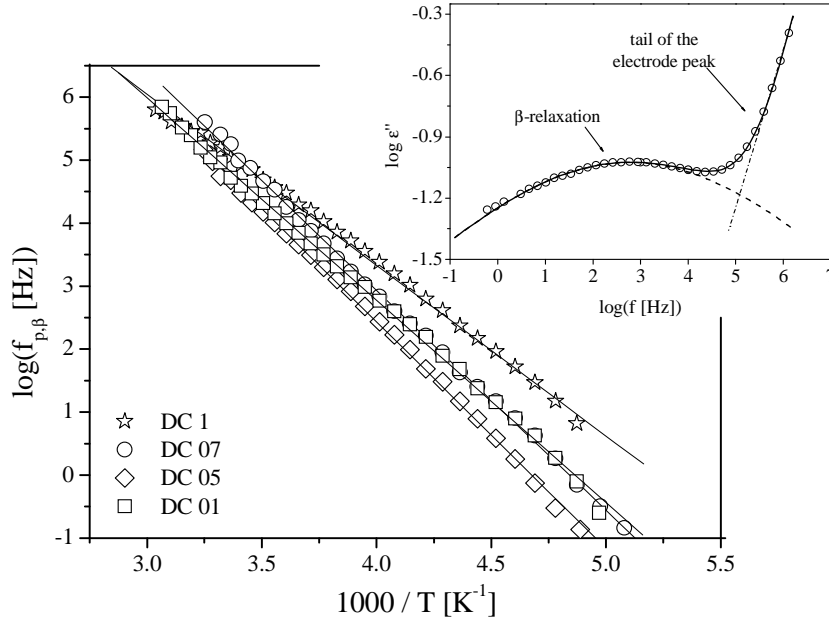
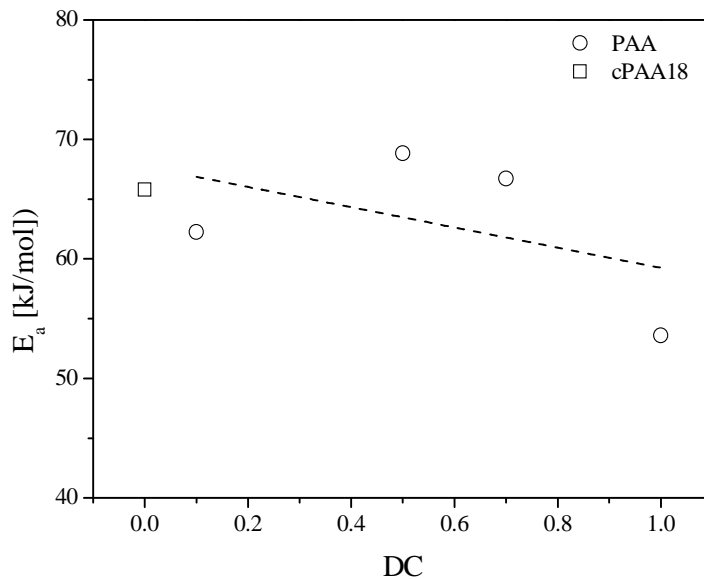


Figure 21: Relaxation rate of the  $\beta$ -process for plasma deposited PAA versus inverse temperature for different DC. The lines are fits of the Arrhenius equation to the data. The inset gives the dielectric loss versus frequency for the plasma deposited sample PAA01 at  $T=229.1$  K during cooling. The solid line corresponds to the whole fit-function consisting of a HN-function and a high frequency tail. The dashed and the dashed dotted lines are the contributions of the relaxation process and the low frequency wing of the electrode peak

Fig. 21 displays the relaxation rates for the  $\beta$ -process versus inverse temperature in the Arrhenius diagram for different DC for the first heating process. Like for cPAA for each value of DC the data can be described by the Arrhenius equation (Equation 7) and the activation energy  $E_a$  can be extracted. Even from the raw data given in Fig. 21 one can conclude that for the first heating run the activation energy of the  $\beta$ -process depends on the duty cycle.

Therefore, in Fig. 22 the activation energy for the  $\beta$ -process is plotted versus DC on heating.  $E_a$  decreases with increasing DC. Generally the  $\beta$ -relaxation in polymers is due to localized

fluctuations of more or less polar groups. For poly(acrylic acid) this process should be related to the carboxylic groups. <sup>[148]</sup> The activation energy of the  $\beta$ -relaxation depends on the local structure of the polymer including the interaction of these different groups. As discussed above with increasing DC the amount of energy introduced to the system increases. For that reason with increasing DC the irregularity of the plasma polymerized structures increases which can have an increasing amount of dangling ends. These dangling ends will increase the local free volume which will lead to a decrease of the activation energy. Moreover, the COOH-groups can form intermolecular hydrogen bonds. The concentration of carboxylic groups decreases with increasing duty cycle and therefore its intermolecular interaction decreases. This effect will also lead to a decreased value of the activation energy as observed.



*Figure 22: Activation energy for the  $\beta$ -process vs. DC for plasma deposited PAA on heating process compared to conventional PAA18*

To discuss the dielectric behaviour in more detail [Fig. 23](#) gives the dielectric loss versus temperature at a fixed frequency (isochronal plot) for different thermal histories for the sample PAA05. The first run is a heating measurement of the as prepared sample from low to high temperatures. The second run is the subsequent cooling from high to low temperatures. A pronounced hysteresis is observed between these two runs. The third heating run is more or less similar to the cooling cycle. For all runs at low temperatures the  $\beta$ -relaxation is observed

as a well defined peak in the spectra. For the first heating run a shoulder is observed at higher temperatures than that of the  $\beta$ -relaxation. At the first glance it seems similar to the behaviour observed for conventional PAA (see insets of Fig. 18 and Fig. 20). However, a closer inspection shows that this shoulder is probably due to the glass transition and is shifted to lower temperatures for the plasma deposited PAA (see inset of Fig. 23).

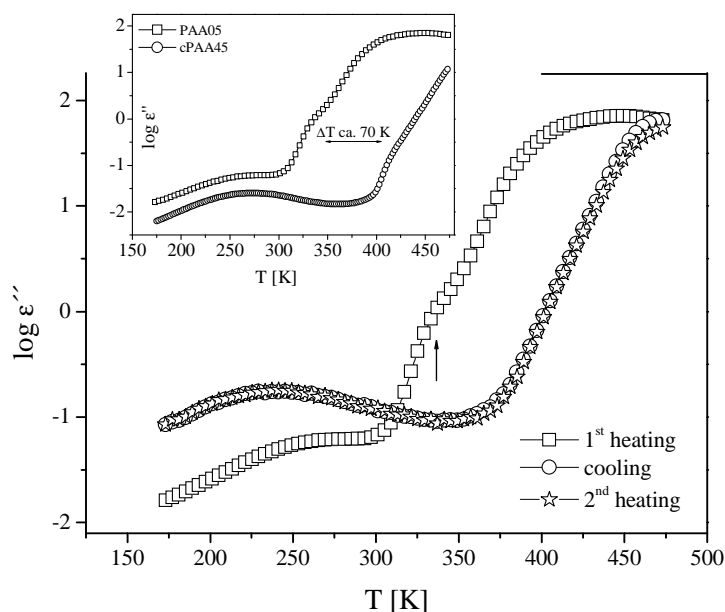


Figure 23: Dielectric loss vs. temperature at a fixed frequency of 1 kHz of the plasma deposited sample PAA05 on different thermal histories. The inset compares the dielectric loss of the plasma deposited sample PAA05 (first heating) with that for cPAA45 vs. temperature at a fixed frequency of 1 kHz

The hysteresis between the first heating and the cooling run can be explained by the following consideration. As discussed above during the plasma deposition of acrylic acid a highly branched product with many free radicals is formed. These free radicals were able to react with each other to form a more crosslinked network during heating. After this heat treatment a thermally stable product is formed. The thermal stability is evidenced by the fact that there is no difference in the dielectric spectra between the first cooling and the second heating run. This will be discussed in more detail later on.

Fig. 24 gives the relaxation rates for the  $\beta$ -process versus inverse temperature in the Arrhenius diagram for different thermal histories for the plasma deposited PAA sample at DC=0.5 in comparison to cPAA. The data can be described by the Arrhenius equation (Equation 7) and the activation energy  $E_a$  can be calculated.

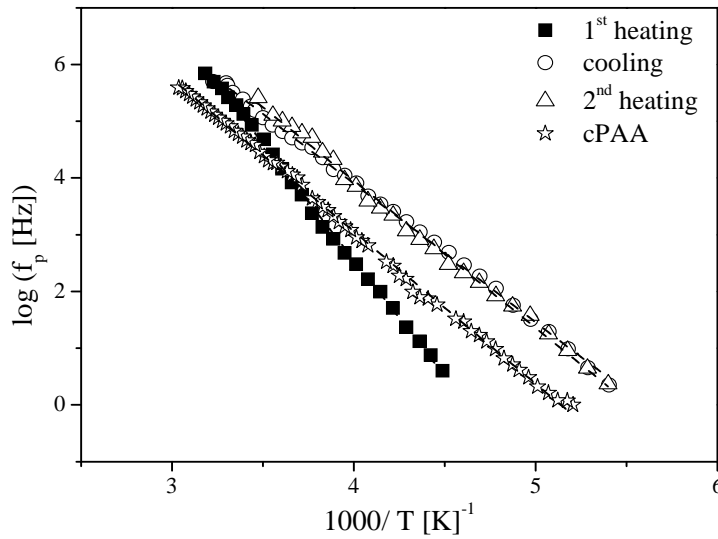


Figure 24: Relaxation rate of the  $\beta$ -process versus inverse temperature for 1<sup>st</sup> heating, cooling and 2<sup>nd</sup> heating for PAA at DC=0.5 compared to cPAA. The lines are fits of the Arrhenius equation to the data

Table 4: Activation energy for plasma deposited PAA05 sample for different thermal histories compared to cPAA

<i>Process</i>	<i>E<sub>a</sub></i>
<i>1<sup>st</sup> heating</i>	78.6
<i>cooling</i>	46.8
<i>2<sup>nd</sup> heating</i>	49.6
<i>cPAA</i>	51.4

The activation energy is decreased from ca. 79 kJ/mol (first heating) to ca. 47 kJ/mol (cooling). After the first heating run thermal stability is evidenced by the fact that there is no difference in the activation energy between cooling and the second heating run (Fig. 24 and Table 4). Homogenised samples were obtained after first heating run and are much closed to cPAA. The plasma deposition of poly(acrylic acid) forms a highly branched product with many free radicals. These free radicals were able to hinder the localized fluctuation of func-



tional groups, because it can be form some kinds of linkage with COOH. These free radicals or charges were able to react with each other to form a more crosslinked network during heating and COOH will become free. So, the activation energy is decreased after heat treatment and a thermally stable product is formed.

The process observed at higher temperatures than that of the  $\beta$ -relaxation has a quite high intensity. There seems to be no dipole moments in the sample which can cause a dielectric relaxation process such a high dielectric strength. For that reason and considering the fact that also the plasma deposited PAA has a high conductivity, this process is assigned to electrode polarization. Electrode polarization is due to the blocking of charge carriers at electrodes. In the considered experiments, aluminium is evaporated as electrodes. It is well known that the blocking of the charge carriers at electrodes can be described by an electrical double layer with an effective spacing characterized by its Debye length  $L_D$ . This double layer represents an additional capacitance  $C_{DL}$  in the system. The time constant ( $\tau_{EP}$ ) for electrode polarization is related to the conductivity  $\sigma$  of the system. Although an interfacial polarization is not a relaxation process it can be also analyzed by fitting the HN-function to the data and the rate for electrode polarization  $f_{EP} \sim 1/\tau_{EP} \sim 1/\sigma$  can be estimated in its temperature dependence.

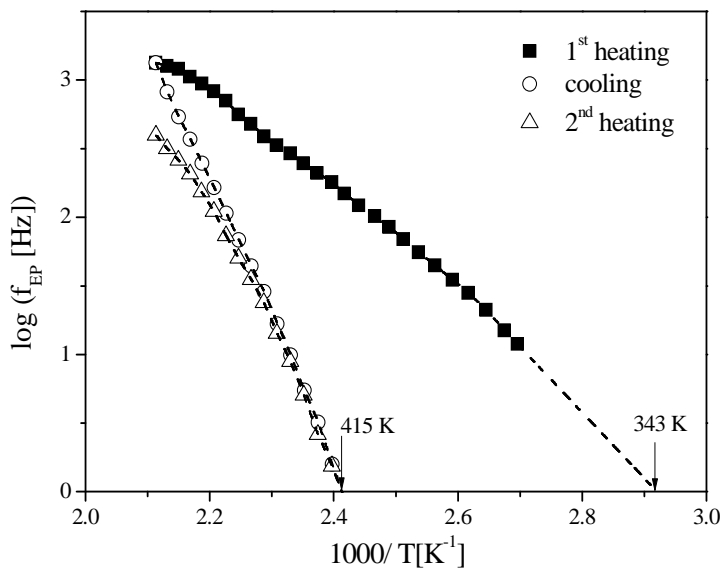


Figure 25: gives relaxation rate of electrode polarization  $f_{EP}$  vs.  $1/T$  for the sample PAA05 for 1<sup>st</sup> heating, cooling and 2<sup>nd</sup> heating

Fig. 25 gives the temperature of the rate of electrode polarization  $f_{EP}$  in the Arrhenius diagram for the sample PAA05 for 1<sup>st</sup> heating, cooling and 2<sup>nd</sup> heating run. Firstly, as expected from Fig. 23 there is a strong hysteresis between heating and cooling which is due to chemical reaction processes within the sample.

Secondly, a detailed inspection of the temperature dependence of  $f_{EP}$  obtained for heating reveals that this dependence is non-monotonous and carries some structure. This structure is related to the kinetics of the chemical reaction that takes place during the heating process. Thirdly, the temperatures dependence measured for  $f_{EP}$  during cooling is shifted to higher temperatures compared to the dependence measured for the 1<sup>st</sup> heating. The temperature of  $f_{EP}$  is related to the mobility of the charge carriers which is connected to segmental mobility. The shift to higher temperatures for the cooling run therefore indicates a lower segmental mobility and higher glass transition temperature of plasma deposited PAA layer obtained during heating. These results points to a crosslinked structure.

Table 5: Dynamic glass transition for plasma PAA on 1<sup>st</sup> heating, cooling and 2<sup>nd</sup> heating compared to  $T_g$  of cPAA

Polymer	Process	$T_g$ [K]
cPAA*		407
	1 <sup>st</sup> heating	343
Plasma PAA	cooling	415
	2 <sup>nd</sup> heating	415

\*[129]

The dependence  $f_{EP}$  on temperature are curved when plotted versus  $1/T$  and might be analyzed by the Vogel/Fulcher/Tammann (VFT-) formula <sup>[144]</sup> which reads:

$$f_{(p,\alpha)} = f_{\infty,\alpha} \exp \frac{A}{T - T_0} \quad (10)$$

( $\log f_{\infty}$ ,  $A$  are constants).  $T_0$  is the so-called Vogel or ideal glass transition temperature. [Fig. 25](#) shows that the data sets seem to be described by the VFT formula. For conventional polymeric systems  $T_0$  is found to be 50 K to 70 K below the glass transition temperature  $T_g$ .

## 2. Allyl alcohol plasma deposited thin polymer films

### 2.1. Kinetics of polymer deposition

Fig. 26a displays the thickness of the deposited layer versus the deposition time for the different values of DC. For each value of DC, the data can be described by a straight line. From its slope the deposition rate  $R$  is obtained. The deposition rate increases with increasing DC for low values of DC. For higher values of DC,  $R$  is approximately constant or even decreases (see Fig. 26b). This means that the dependence of  $R$  versus DC is non-linear as might be expected. To understand this non-linear behaviour one has to consider the different processes which can take place during the plasma deposition as discussed in plasma deposited PAA. There are two main processes. Both of them are due to the high energy density of the plasma. Firstly, the double bond of the allyl alcohol can be activated leading to radicals which can undergo a normal chain grow polymerization process and will lead to regular structures. Secondly, fragmentation of monomers takes place followed by a poly-recombination reaction which will lead in general to irregular structures. Otherwise, the possibility of depolymerisation and a partial removal of the deposited layer cannot be neglected as mentioned before.

To differentiate between these two processes, the deposition rate of AAl can be compared with that of a molecule having a similar chemical structure but without any (polymerizable) double bond. An appropriate candidate is n-propanol ( $\text{CH}_3\text{-CH}_2\text{-CH}_2\text{OH}$ ). Fig. 26b shows that the deposition rate of n-propanol is low in comparison to that of allyl alcohol and is more or less independent of the DC. The comparison of the deposition rates of allyl alcohol and n-propanol shows that in the former case in addition to fragmentation chain growths polymerization occurs due to the presence of the double bond in the monomer.

Chain growth polymerization due to the double bond takes place during both the time intervals of deposition, i.e.  $t_{\text{pulse-on}}$  and  $t_{\text{pulse-off}}$ . In order to compare the deposition rates and the contribution of chain growth polymerization during the plasma  $t_{\text{pulse-off}}$  time for the different

duty cycles directly, the deposition rates are normalized by the time where the plasma was on ( $t_{\text{pulse-on}}$ ). Equivalently the deposition rate can be divided by DC (see Fig. 27).

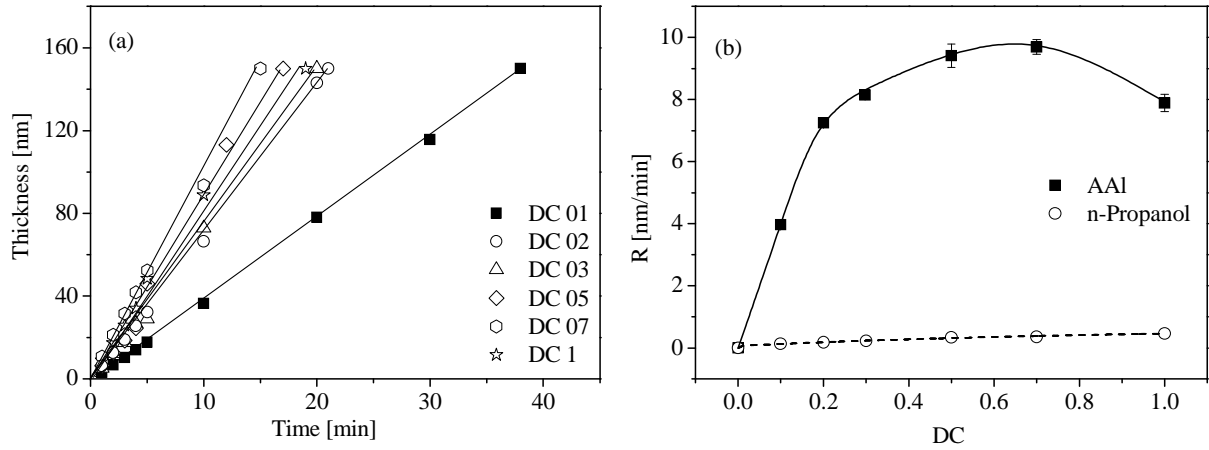


Figure 26: Thickness of plasma deposited PAAl layers versus deposition time for the different values of DC (a). Deposition rate  $R$  versus DC for AAl and  $n$ -propanol (b)

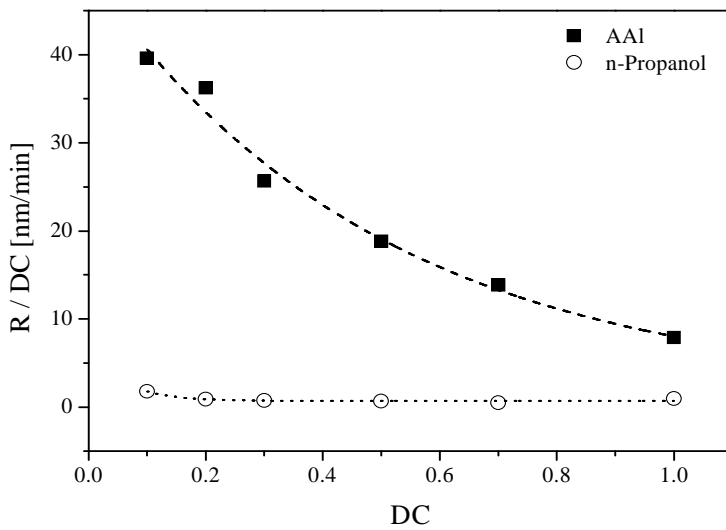


Figure 27: Deposition rate normalized by the DC versus DC for AAl and  $n$ -propanol

In such a representation, the value of the normalized deposition rate at the highest value of the duty cycle ( $DC=1$ ), is a hint to the contribution of chain growth polymerization to  $R$  during the plasma  $t_{\text{pulse-on}}$  time. The rate of fragmentation is constant for all values of DC (see results obtained for propionic acid and  $n$ -propanol, Figs. 10 and 26b). Fig. 27 shows further that the normalized deposition rate of PAAl is maximal for the lowest value of DC. This means that

the rate of the chain growth process during the plasma  $t_{\text{pulse-off}}$  time is essentially higher for low values of DC. This might also imply that for low values of DC a more regular structure is formed.

## 2.2. Estimation of the surface functionality by derivatization and XPS

The estimation of functional groups on the surfaces can be done by derivatization and subsequent XPS measurements.

The inset Fig. 28 shows the binding energy in the range of the C1s peak of the XPS spectra for pure PE (without a deposited film). C-C/C-H and C-O bonds are observed, the C-O bond might be due to oxygen adsorption processes.

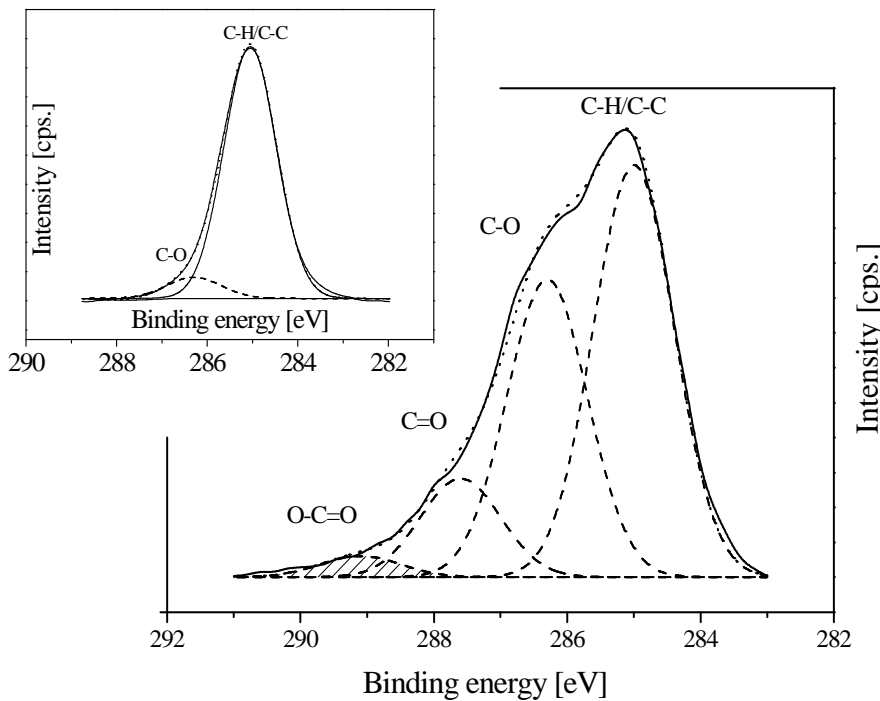


Figure 28: High resolution XPS spectra of the sample PAAI05. The solid line represents the experimental data. The dotted line is a fit of a sum of four components to the data. The dashed lines represent the individual contributions. The inset gives the high resolution XPS spectra of pure PE

Figs. 28 and 29 show the C1s spectra of a deposited plasma PAAI films before and after derivatization with TFSA of a sample prepared at a DC value of 0.5. The deconvolution of the C1s peak of plasma deposited PAAI (Fig. 28) was done assuming four components assigned to the following bonds: C-C/C-H: 285.0 eV, C-O: 286.3 eV, C=O: 287.5 eV and

COO: 289.1 eV. The corresponding fractions of the components were estimated by fitting Gauss-Lorenz to the data.

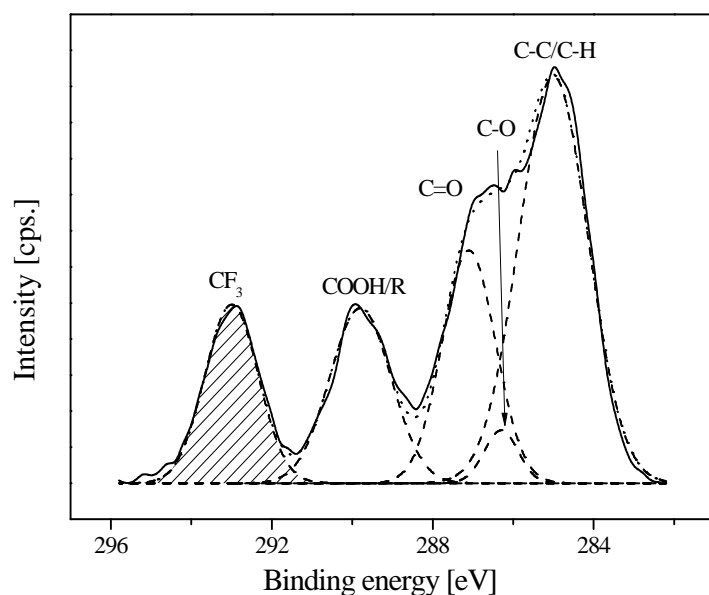


Figure 29: High resolution XPS spectra of the sample PAAI05 after derivatization with TFAA. The solid line represents the experimental data. The dotted line is a fit of a sum of five components to the data. The dashed lines represent the individual contributions

Table 6: Gives the inspection of the C1s peak analysis of the non-derivatized and derivatized surface for plasma deposited PAAI

	C-C/C-H %	C-O %	C=O %	COO %	CF <sub>3</sub> %
	285.0 eV	286.3 eV	287.5 eV	289.1 eV	293 eV
<b>non-derivatized</b>	56.43	36.13	05.84	01.60	-
<b>derivatized</b>	35.49	14.17	17.70	16.60	16.03

C=O and COO groups were also observed (see Table 6). The fragmentation of the monomer and poly-recombination followed by post-plasma oxidation as well is the reason for these groups formed. In addition to radical polymerization (regular structure) of poly(allyl alcohol), hydrogen abstraction might be occur and allylic radicals were formed.

In the presence of allylic radicals and enol resonance structures, this can tautomerize to produce aldehyde. The allylic radicals formed in the abstraction reaction are relatively unreactive to other allyl monomers because of its resonance stabilization. <sup>[149]</sup>

The C1s spectrum of the derivatized PAAI05 layer was deconvoluted into five peaks, including an additional component at 293.0 eV for the  $\text{CF}_3$  bond. The values are obtained for the concentration showed in Table 6.

The comparison of Figs. 28 and 29 reveals that the contribution of the C-O bond to the spectra is reduced but not completely eliminated by the TFAA derivatization. This means that some C-O bonds have to be assigned to ether-type linkages rather than to hydroxyl groups, which do not participate in the derivatization reaction and remain therefore unchanged.

Equation (4b) can be used to calculate the concentration of hydroxyl groups per 100 carbon atoms  $c(\text{OH})$  and plotted versus DC in Fig. 30.

Firstly, the concentration of hydroxyl groups is much smaller than the value expected from the regular chemical structure of PAAI. Secondly,  $c(\text{OH})$  decreases with increasing DC. Both effects are due to the fragmentation of the monomer in the plasma. The energy input increases with increasing DC according to Equation (2) and therefore, also the degree of fragmentation and rearrangement of the monomer resulting in a lower concentration of hydroxyl groups and a higher concentration of radicals. <sup>[141]</sup>

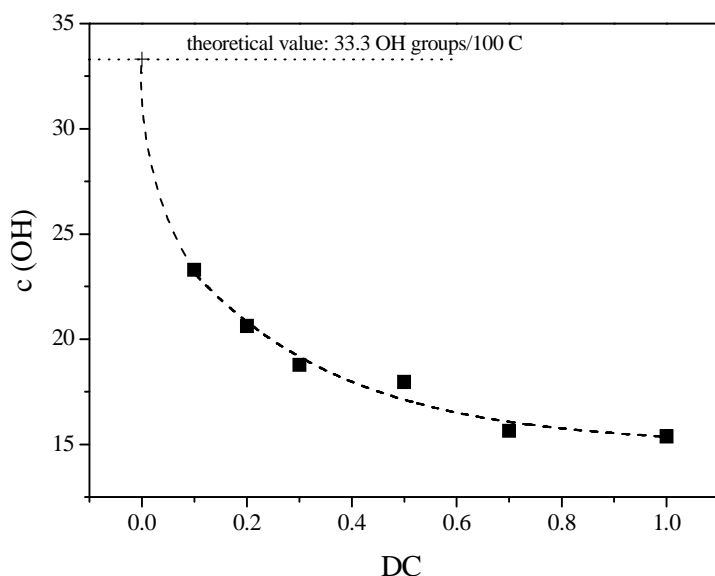


Figure 30: Concentration of hydroxyl groups per 100 carbon atoms versus DC. The dotted line indicates the maximal possible concentration of hydroxyl groups



### 2.3. Investigation of the functionality of films on different substrates by FTIR

ATR-FTIR gives information about the structure of a sample across the whole thickness of the film while XPS is sensitive to a layer of 5 to 7 nm as pointed out sometimes before. In this section, PE and PP as organic and aluminium and glass as inorganic substrates are used. Fig. 31 shows the FTIR spectra of plasma PAAI deposited on an Al substrate for different values of DC.

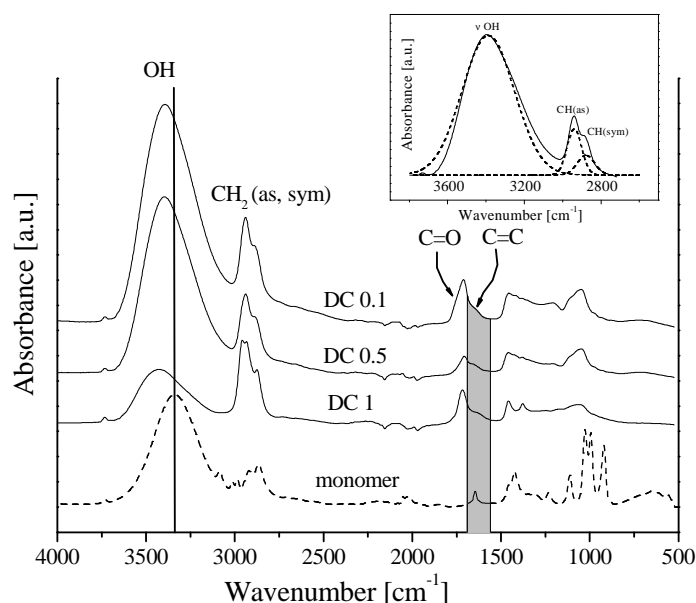


Figure 31: FTIR spectra of PAAI deposited on Al substrate for different values of DC in comparison to the allyl alcohol monomer as blank. The different curves are y-shifted for sake of clearness. The inset enlarges the wavenumber region for the hydroxyl and for both the asymmetric and symmetric  $\text{CH}_2$  stretching vibrations of PAAI deposited on the aluminium substrate at  $\text{DC} = 0.1$ . The spectra are analysed by fitting three Gaussians to the data

Firstly, all spectra exhibit the stretching vibrations which are characteristic for poly(allyl alcohol): the  $\nu$  OH stretching vibration at  $\sim 3400 \text{ cm}^{-1}$  associated with  $\text{CH}_2(\text{as})$  at  $\sim 2940 \text{ cm}^{-1}$  and the  $\text{CH}_2(\text{sym})$  vibrations at  $\sim 2880 \text{ cm}^{-1}$  are observed together with the corresponding  $\nu$  C–O vibration at  $\sim 1047 \text{ cm}^{-1}$ . After the abstraction of the allylic hydrogen by radicals, chain ends with vinyl groups and aldehyde groups can be obtained.<sup>[150]</sup> Therefore, the C=O stretching vibration characteristic for carbonyl bonds near  $1700 \text{ cm}^{-1}$  is also found associated with  $\nu$  C=C at  $\sim 1660 \text{ cm}^{-1}$ . However, the most important for the following discussion is the stretching vibration of the hydroxyl group (OH).

The following procedure is employed to analyse the spectra quantitatively where three Gaussians were fitted to the data. One Gaussian is located at  $\sim 3400 \text{ cm}^{-1}$  to describe the  $\nu$  OH

stretching vibration. The contribution of  $\text{CH}_2(\text{as})$  vibrations at  $\sim 2940\text{ cm}^{-1}$  and  $\text{CH}_2(\text{sym})$  vibrations at  $\sim 2880\text{ cm}^{-1}$  due to the  $-\text{CH}_2-$  groups were described by two further Gaussians. To reduce the number of the free fitting parameters and to stabilize the fit, the maximum positions of the Gaussians are kept constant during this analysis. The inset Fig. 31 gives an example for this procedure.

From these fits the areas of the Gaussians at  $3400\text{ cm}^{-1}$  ( $A_{\text{OH}}$ ) and  $2940\text{ cm}^{-1}$  ( $A_{\text{CH}_2(\text{as})}$ ) are taken and their ratio  $\frac{A_{\text{OH}}}{A_{\text{CH}_2}}$  is calculated as a measure for the concentration of the OH groups estimated from FTIR. The reference to the  $\text{CH}_2$  vibration is an approximation which is only exactly valid if the concentration of the  $\text{CH}_2$  groups does not depend on DC due to fragmentation. The discussion of the dependence of the deposition rate on DC shows that the deposition of n-propanol due to fragmentation is quite low and does not depend on the DC. The same can be assumed for allyl alcohol. Moreover other side reactions ( $\text{C}=\text{O}$ ) are marginal. This means that mainly  $\text{CH}_2$  main chain structures are formed in the plasma polymerization process and therefore the choice of  $\text{CH}_2(\text{as})$  reference is an acceptable approximation.

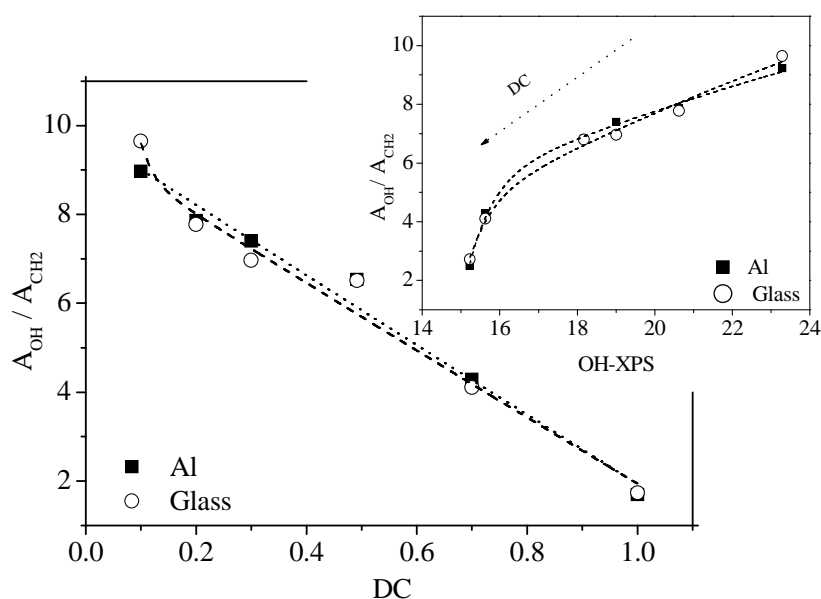


Figure 32: Concentration of OH groups as estimated by  $A_{\text{OH}}/A_{\text{CH}_2}$  for PAAI versus DC with aluminium and Glass substrates. The inset gives  $A_{\text{OH}}/A_{\text{CH}_2}$  versus the concentration of OH groups estimated from the XPS measurements with aluminium and glass substrates

The concentration of OH groups estimated by XPS and FTIR-ATR of plasma PAAI decreases with increasing DC (see Figs. 30, 32 and 33). Based on the assumption that the deposition rate

( $R = R_{\text{Chain}} + R_{\text{Frag}}$ ) is much higher than the depolymerisation and a partial removal of the deposited layer the ratio of the concentration of OH groups estimated by XPS versus that obtained by FTIR should be constant value independent on DC.

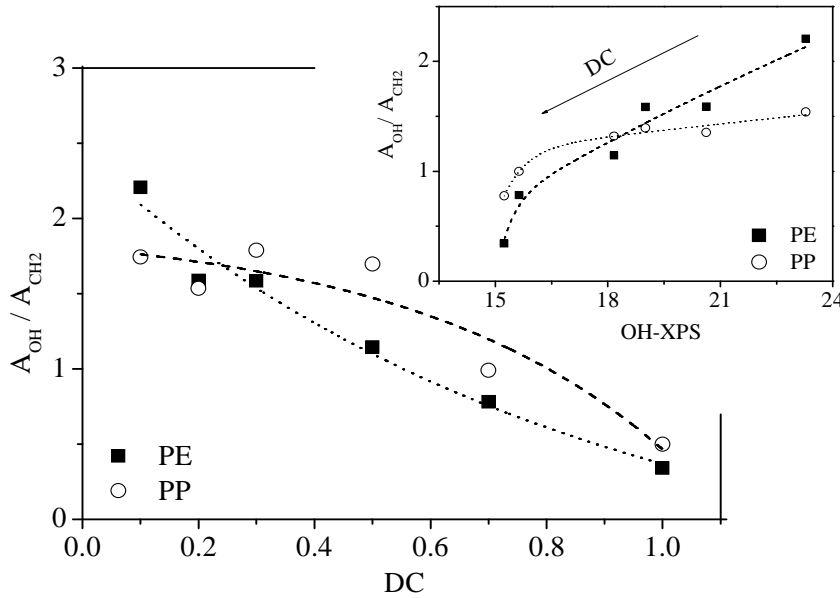


Figure 33: Concentration of the OH groups estimated from  $A_{OH}/A_{CH_2}$  for plasma deposited PAAI versus DC with PE and PP substrates. The inset gives  $A_{OH}/A_{CH_2}$  versus the concentration of OH estimated from the XPS measurements with PE and PP substrates

Therefore, in inset of Figures 32 and 33  $\frac{A_{OH}}{A_{CH_2}}$  is displayed versus the concentration of OH groups estimated from XPS measurements. As a result with increasing DC the concentration of OH-groups estimated from FTIR is smaller than expected from XPS measurements.

To discuss this result the different analytical depth of both methods has to be considered again. XPS is sensitive to a layer with a thickness of 5 to 7 nm whereas FTIR provides information across the whole sample thickness as discussed before in plasma PAAI. The amount of energy increases in form of electrons, ions radiation etc. with increasing DC is introduced into the system. In addition to that UV radiation which can penetrate deeply into the sample volume is of great importance. This energy input in its different forms will damage PAAI at larger distance from the surface which is already polymerized. That is not the case at the surface where polymerization takes place at a higher rate in addition to defragmentation and depolymerisation. For that reason the ratio of the OH groups estimated by FTIR (whole

sample thickness) and XPS (only surface) decreases in different manner with increasing DC (see inset of Fig. 32).

In case of PE and PP substrates like for Al and glass substrates, the  $\nu$  OH stretching vibration at  $\sim 3370\text{ cm}^{-1}$  and the corresponding  $\nu$  C–O vibration at  $\sim 1042\text{ cm}^{-1}$  were observed. The characteristic  $\text{CH}_2(\text{as})$  and  $\text{CH}_2(\text{sym})$  vibrations at  $\sim 2915\text{ cm}^{-1}$  and  $\sim 2850\text{ cm}^{-1}$  are related to both plasma deposited PAAI films and to the substrate, which is detected through the 150 nm thick plasma polymer layer. This means the sum  $A_{\text{CH}_2} = A_{\text{CH}_2(\text{PAAI})} + A_{\text{CH}_2(\text{PE})}$  is measured. The thickness of substrates is constant for all the duty cycles. Therefore, the same procedure to determine the concentration of the OH groups like for the Al and glass substrates can be applied.

The concentrations of OH groups of plasma PAAI deposited on PE and PP substrates have the same dependence on DC like for the Al or glass substrates (see Fig. 33). The absolute values of the ratio  $\frac{A_{\text{OH}}}{A_{\text{CH}_2}}$  are reduced in comparison to the data estimated for Al and glass substrates because of the contribution of the substrate to  $A_{\text{CH}_2}$ . From these results it is to conclude that the different substrates do not influence the concentration of OH groups for the deposited layers.

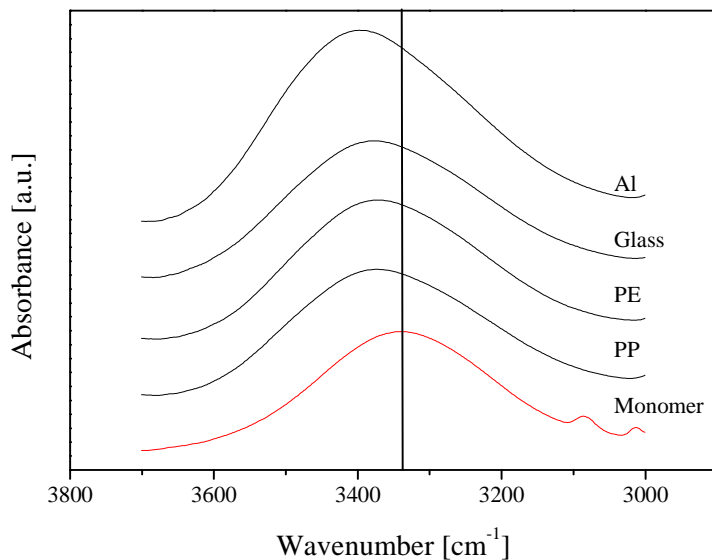


*Figure 34: FTIR spectra of plasma deposited PAAI in the wavenumber range of the OH-stretching vibration deposited on different substrates with DC=0.5 compared to the allyl alcohol monomer*

An intense inspection of the stretching vibration of OH groups shows that the maximum peak position is shifted to higher wavenumbers by ca.  $30\text{ cm}^{-1}$  in case of PE and PP substrates in comparison to the allyl alcohol monomer. The reason is the plasma energy attacks the surfaces of substrates in the very early stage of the deposition and might generate some radicals and oxygen groups (hydroxyl, carbonyl, ether and epoxy groups) on the substrate. Hydrogen bonds can be formed between the hydroxyl groups of plasma deposited PAAI and the hydroxyl groups which are created on the substrate surface. This will shift the OH vibration to higher wavenumbers.

The maximum position of the OH stretching vibration of plasma PAAI deposited on a glass substrate is more or less shifted to the same wavenumbers as observed for PE or PP. The glass surface carries hydroxyl group which can form also hydrogen bonds to the hydroxyl groups of the plasma deposited PAAI in a similar way as found for polymeric substrates.

The peak position of hydroxyl groups are shifted to essential higher wavenumbers ( $60\text{ cm}^{-1}$ ) compared to the monomer in case of the Al substrate. This large shift is probably due to the lone pair of electrons of oxygen for the OH group. It can react with Al and form a coordination bond (see Fig. 34 and Table 7).

*Table 7: Position of the maximum of the  $\nu$  OH stretching vibration for PAAI deposited on different substrates with DC=0.5 as example*

Substrates	Wavenumber ( $\text{cm}^{-1}$ )
	at maximum band of $\nu$ OH vibration
Aluminium (Al)	3398
Glass	3378
Polyethylene (PE)	3373
Polypropylene (PP)	3373
Allyl alcohol monomer as blank	3341

A similar behaviour is observed for all other values of DC.

## 2.4. Dynamic mobility and thermal stability

For investigating the molecular dynamics of the thin polymer films, dielectric spectroscopy as probe for its structure is employed. It is proven that, DRS is a powerful tool to investigate the molecular mobility and the structure of polymers.<sup>[151]</sup> This is especially true for the investigation of thin and ultra thin polymeric films or layers because the sensitivity of DRS increases with decreasing thickness of the capacitor.<sup>[152]</sup>

Fig. 35 gives the dielectric loss for plasma deposited PAAI05 versus frequency and temperature in a 3D representation during cooling. At least one relaxation process indicated by a peak in the dielectric loss is observed at low temperatures which is called  $\beta$ -relaxation. This relaxation process corresponds to localized fluctuations. As expected the peak shifts to higher frequency with increasing temperature. For higher temperature than those of the  $\beta$ -relaxation a further process is observed which is assigned to electrode polarization. As argued before the electrode polarization is related to the drift motion of charge carriers, which are blocked at electrodes which do not behave completely Ohmic. This causes an additional capacitance in the system which is charged /discharged in the electric AC-field.

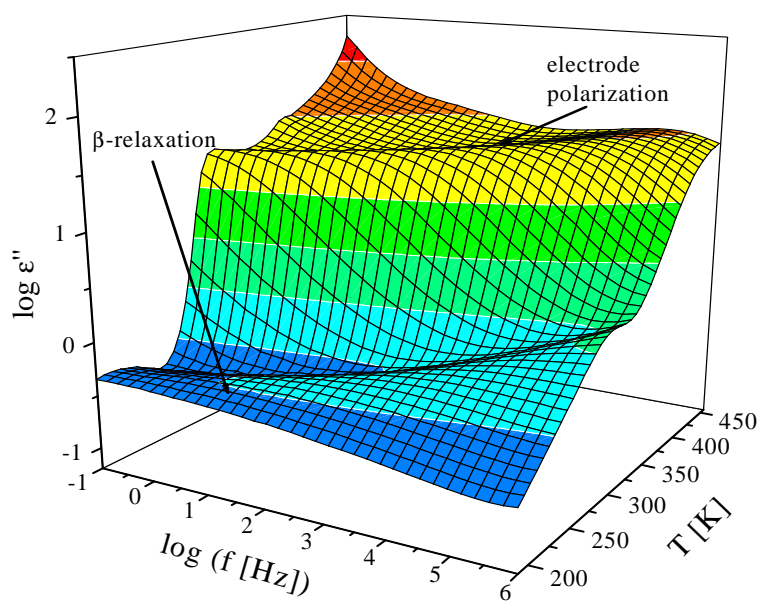


Figure 35: Dielectric loss  $\epsilon''$  of the sample PAAI05 vs. frequency and temperature during cooling in a 3D representation

The HN-function (9) is used to analyze the data. The electrode peak is taken into consideration as Debye function as described in ref. [139]. An illustration for that procedure is given in Fig. 36.

Conduction effects were treated in the usual way by adding a conductivity contribution  $\sigma_0 / \epsilon_0 (2\pi f)^x$  to the dielectric loss.  $\sigma_0$  is a fitting parameter related to the dc conductivity of the sample and  $\epsilon_0$  is the dielectric permittivity of vacuum. The parameter  $x$  ( $0 < x \leq 1$ ) describes for  $x < 1$  non-Ohmic effects in the conductivity. An illustration for that procedure is given in the Fig. 36.

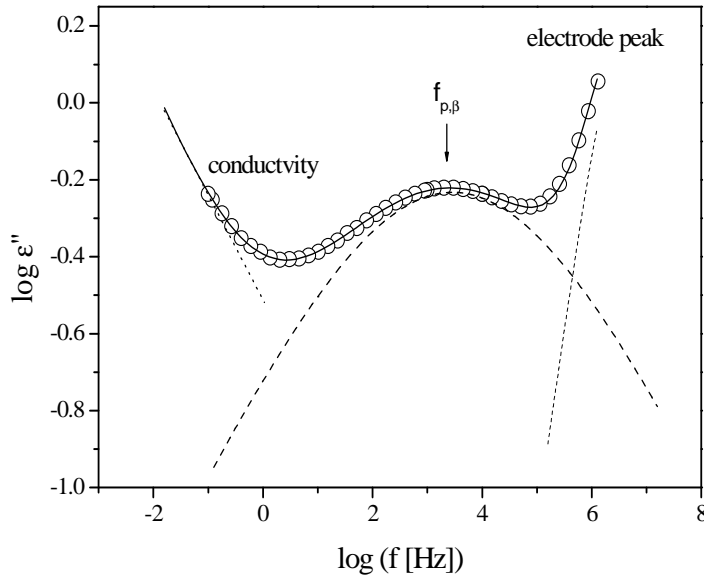


Figure 36: Dielectric loss versus frequency of the sample PAA102 at  $T=261.1$  K. The solid line corresponds to the whole fit-function consisting of a HN-function, a high frequency tail and a conductivity contribution at low frequencies. The dashed and the dotted lines are the contributions of the relaxation process and the low frequency wing of the electrode peak. The dotted line indicates the conductivity contribution

Fig. 37 displays the relaxation rates for the  $\beta$ -process versus inverse temperature in the Arrhenius diagram for different DC for the first heating run. For each value of DC the data can be described by the Arrhenius Equation (7).

Even from the raw data given in Fig. 37 one can conclude that for the first heating run the activation energy of the  $\beta$ -process depends on DC. Therefore, as shown in Fig. 38 the activation energy for the  $\beta$ -process is plotted versus DC.

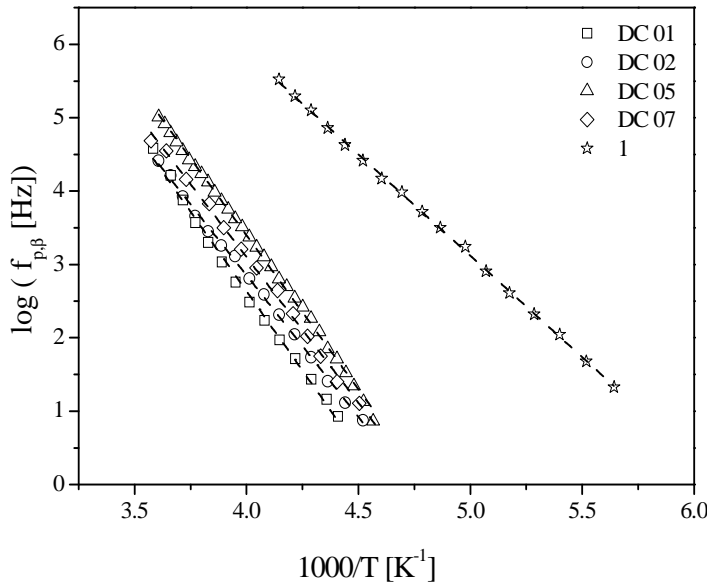


Figure 37: The relaxation rate for the  $\beta$ -process for plasma deposited PAAI versus inverse temperature for the different values of DC for the first heating run. The lines are fits of the Arrhenius equation to the corresponding data

$E_a$  decreases with increasing DC. Generally, as discussed before the  $\beta$ -relaxation in polymers is due to localized fluctuations. For poly(ally alcohol) this process should be related to the hydroxyl groups. <sup>[148]</sup> The activation energy of the  $\beta$ -relaxation depends on the local structure of the polymer including the interaction of these different groups. As discussed above with increasing DC the amount of energy introduced to the system increases. For that reason with increasing DC the irregularity of the plasma polymerized structures increases which can have an increasing amount of dangling ends. These dangling ends will increase the local free volume which will lead to a decrease of the activation energy. Moreover the OH-groups can form intermolecular hydrogen bonds. The concentration of hydroxyl groups decreases with increasing duty cycle and therefore, its intermolecular interaction. This effect will also lead to a decreased value of the activation energy as observed.

It is interesting to note that the activation energy for the  $\beta$ -relaxation of conventional PAAI obtained by mechanical measurements is 73 kJ/mol. This value is close to the data obtained for low duty cycles. The addition of only 6 wt-% of a polar solvent decreases the activation energy to 68 kJ/mol. This result is in the line of the argumentation given above.



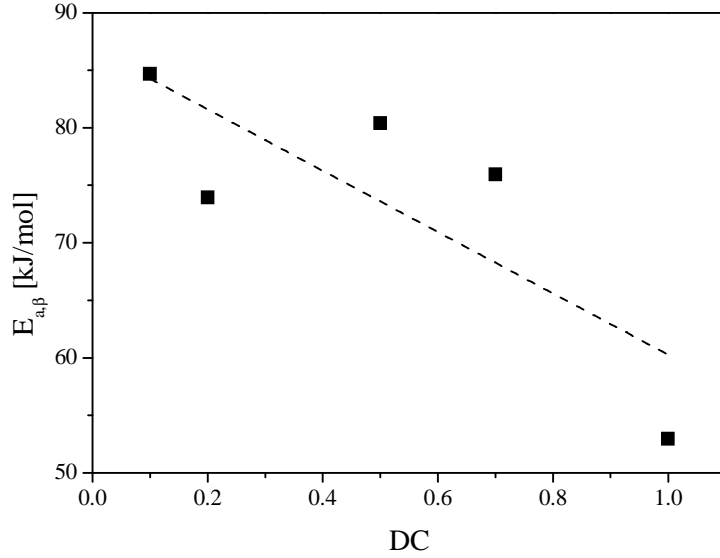


Figure 38: Activation energy for the  $\beta$ -process vs. DC for plasma deposited PAAI on the first heating run

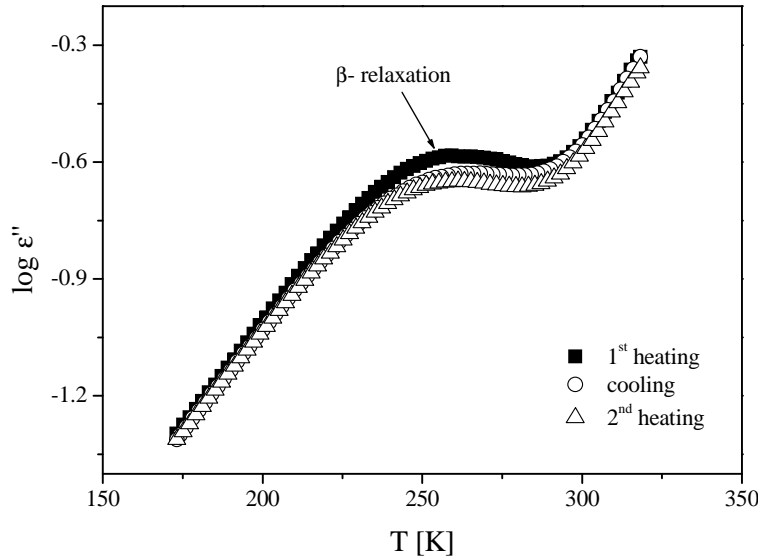


Figure 39: Dielectric loss vs. temperature at a fixed frequency of 1 kHz of the sample PAAI05 in the temperature range of the  $\beta$ -relaxation for different thermal histories

To discuss the dielectric behaviour for the 1<sup>st</sup> heating, cooling and 2<sup>nd</sup> heating run in more detail Fig. 39 must be considered. It gives the dielectric loss versus temperature at a fixed frequency (isochronal plot) for the different thermal histories for the sample PAAI05 as an example.

In all cases at low temperatures the  $\beta$ -relaxation is observed as a well defined peak in the spectra. For the cooling run, the intensity of this relaxation process is decreased. The activation energy is decreased from ca. 84 kJ/mol (first heating) to ca. 72 kJ/mol (cooling). After the first heating run, the thermal stability is evidenced by the fact that there is no difference in the

dielectric spectra and the activation energy between the first cooling and the second heating run. This will be discussed in more detail later on.

Fig. 40 presents the dielectric strength  $\Delta\epsilon_\beta$  for the  $\beta$ -relaxation of PAAI the different DC versus inverse temperature. It is well known for localized fluctuations that,  $\Delta\epsilon_\beta$  increases with increasing temperature. This increase of  $\Delta\epsilon_\beta$  is probably due to an increase of the fraction of fluctuating dipoles which contribute to the  $\beta$ -process. Generally  $\Delta\epsilon_\beta$  decreases with increasing DC (see also the inset Fig. 40).

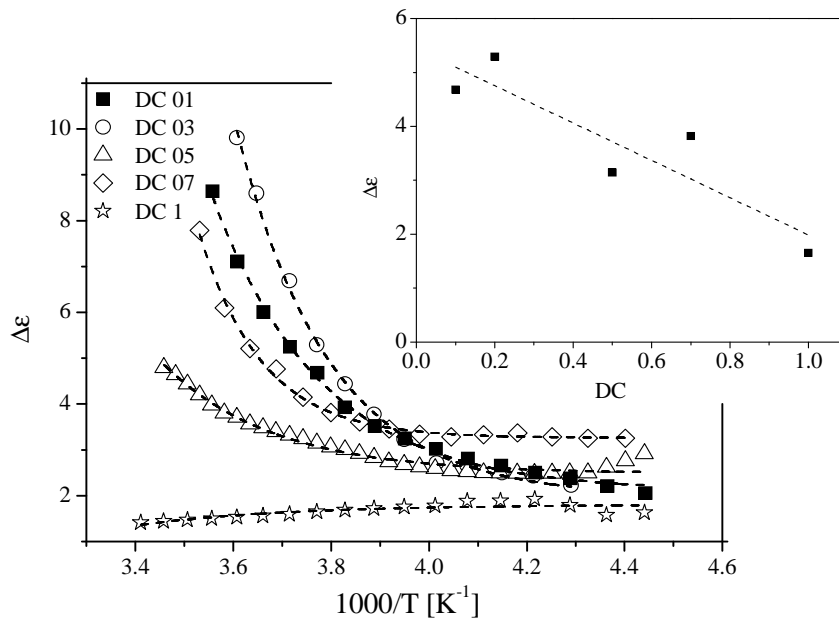


Figure 40: Dielectric strength  $\Delta\epsilon_\beta$  of PAAI vs. inverse temperature for  $\beta$ -relaxation with respect to DC for the first heating. The inset displays dielectric strength  $\Delta\epsilon_\beta$  of PAAI vs. DC at 265 K

Conforming to Equation (8), this implies that the number density of dipoles decreases with increasing DC. This is in agreement with the FTIR experiments. These experiments show that the number of hydroxyl groups which are involved in dielectric  $\beta$ -relaxation decreases with increasing DC. Note that also the temperature dependence of dielectric strength changes with DC. At low values of DC the temperature dependence of  $\Delta\epsilon_\beta$  are more pronounced than for higher values of it.

Assuming that, the hydroxyl groups are mainly responsible for the  $\beta$ -relaxation according to Equation (8). Dielectric spectroscopy and FTIR should provide similar information about the concentration of OH groups. Therefore, Fig. 41 displays  $\frac{A_{OH}}{A_{CH_2}}$  of plasma PAAI deposited on Al substrates versus the dielectric strength estimated from DRS measurements at 265 K. For the case that the dielectric  $\beta$ -relaxation is only due to hydroxyl groups a constant value should be observed. This graph shows that an approximately linear dependence between both quantities is observed. To discuss this result the different sensitivity of both methods has to be considered.

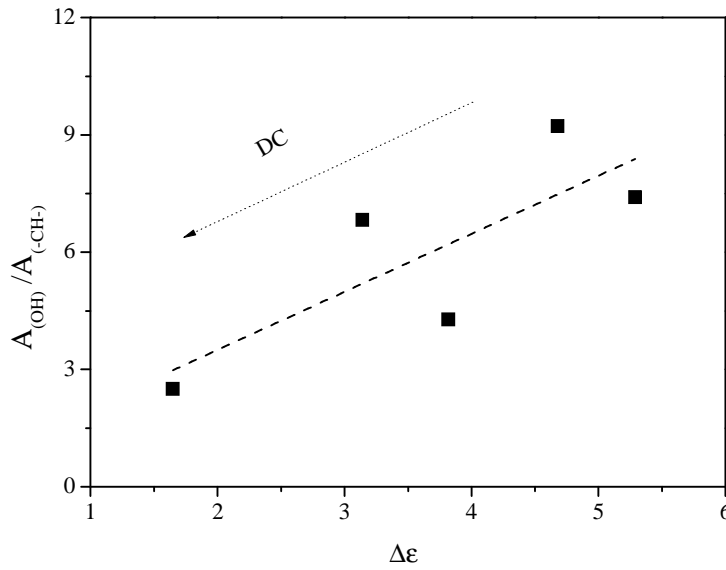


Figure 41:  $A_{OH}/A_{CH_2}$  calculated from FTIR versus the dielectric strength estimated from the DRS measurements of the plasma PAAI deposited on Al substrate at 265 K

The analysis of FTIR measurements as discussed above provides information only about the concentration of OH groups. Dielectric spectroscopy measures an effective dipole moment which can include other functional groups like C=O, C-O-C, etc. which can be created during the plasma polymerization process. The results show that  $\frac{A_{OH}}{A_{CH_2}}$  decreases with decreasing  $\Delta\epsilon_\beta$  (this means with increasing DC) is an expression of the fact that with increasing DC more

and more irregular structures are formed which can contain other functional groups like carbonyl, ester or ketone groups (see section FTIR measurements).

The process observed at higher temperature than that is characteristic for the  $\beta$ -relaxation has a quite high intensity. There seems to be no molecular dipole moment in the sample which can cause a dielectric relaxation process with such a high dielectric strength. For that reason and considering the fact that plasma deposited PAAI has a given conductivity, this process is assigned to the electrode polarization. Although an interfacial polarization is not a relaxation process it can be also analyzed by fitting the HN-function to the data and the rate for electrode polarization  $f_{EP} \sim 1/\tau_{EP} \sim 1/\sigma$  can be estimated in its temperature dependence as discussed before.

Fig. 42 compares the temperature dependence of the rate of electrode polarization for different values of DC for the first heating. Firstly, with increasing DC the rate of the electrode polarization shifts to higher values of the temperature. The conductivity which dominates  $f_{EP}$  is directly related to the segmental mobility which is responsible for glassy dynamic in polymeric systems. A crude estimation of a dielectric glass transition temperature can be estimated by  $T_g^{Diel} = T(f_{EP}=1 \text{ Hz})$ .

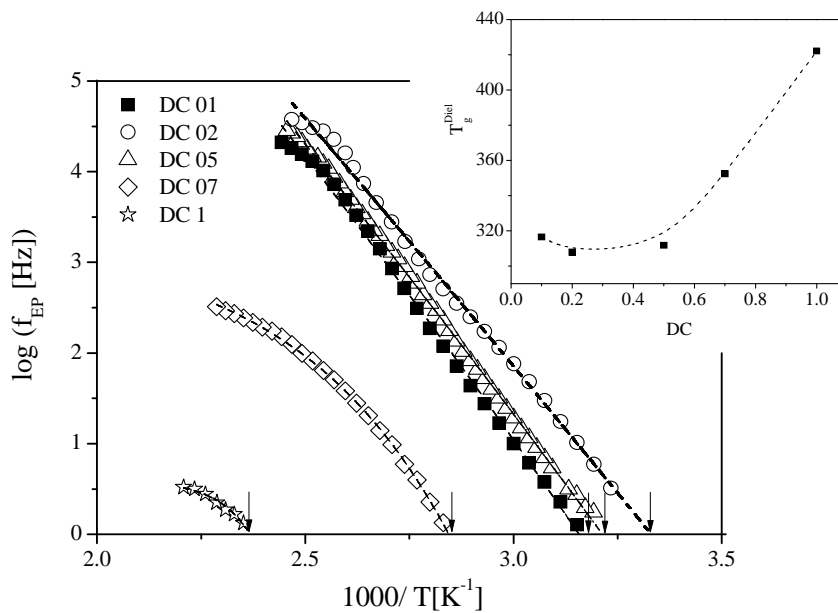


Figure 42: Relaxation rate of the electrode polarization  $f_{EP}$  for plasma deposited PAAI vs. inverse temperature for different values of DC for the 1<sup>st</sup> heating process. The inset Fig. displays  $T_g^{Diel}$  of PAAI vs. DC

$T_g^{\text{Diel}}$  is plotted versus DC in the inset of Fig. 42. As already seen from the raw data shift of the rate of electrode polarization to higher temperatures with increasing DC indicates an increase of the glass transition with increasing DC.

Moreover, it is worth to note that the glass transition temperature of conventional polymerized poly(allyl alcohol) ( $T_g=348$  K) <sup>[130]</sup> is quite close to  $T_g^{\text{Diel}}$  estimated for low duty cycles. This is a further indication that plasma PAAI deposited at low duty cycles has a similar structure than conventional PAAI.

Secondly, for segmental dynamics the temperature dependence of the corresponding rate should follow the Vogel-Fulcher-Tammann (VFT-) formula. <sup>[153-155]</sup> The fact that the segmental mobility is related to the temperature dependence of  $f_{EP}$  should also follow the VFT- Equation (10) as discussed above.

Fig. 42 shows that the functional form of  $f_{EP}(T)$  depends on DC.

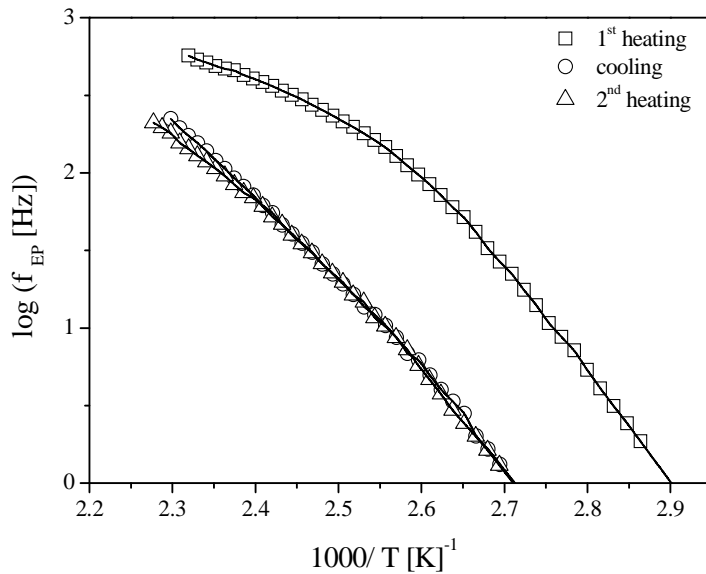


Figure 43: Relaxation rate of the electrode polarization  $f_{EP}$  vs. inverse temperature of the sample PAAI05 on different thermal histories

Fig. 43 gives the temperature dependence of the rate of electrode polarization for the different thermal histories for the sample PAAI05 as an example. The rate of the electrode polarization shifts to higher values of the temperature for the cooling and the second heating

process. The dynamic glass transition is increased from ca. 345 K (first heating) to ca. 370 K (cooling and 2<sup>nd</sup> heating). If this shift is due to physical or chemical changes in the sample it needs further investigations. After the first heating run thermal stability is evidenced by the fact that there is no difference in the rate of electrode polarization and the dynamic glass transition between the first cooling and the second heating run. The increase of the estimated glass transition temperature points to crosslinking reactions.

### 3. Plasma deposited and spin coated thin polystyrene films

The obtained results are grouped and discussed in two parts: The first one focuses on the surface properties of the film, on their chemical modifications and wettability occurring on the first tens of nanometer below the surface. The second one focuses on the dynamic mobility of the whole films (bulk properties).

Plasma treatment of polymers could be expressed as first cleaning and secondly functionalization followed by thirdly etching. However, the processes on the surface correspond to different types of reactions (i.e. radical formation, crosslinking, degradation and functionalization). The degradation, crosslinking, radicals and functionalization are the most important ones for any adhesion or printing application and are examined in detail for O<sub>2</sub>, Ar plasma treated and UV-irradiated PS spin coated films in comparison to the plasma-deposited PS and commercial (reference) PS.

#### 3.1. Functionalization

Surface functionalization was characterized firstly by XPS analysis for the surface chemical identification then by Attenuated Total Reflectance-Fourier Transmission Infrared (ATR-FTIR) for quantification and finally, by contact angle and surface energy measurements for the upper most monolayer.

A XPS survey scan of the conventional polystyrene film (Figs. 44 and 46) shows that, it is really free of oxygen, i.e., the O surface concentration is below the detection limit of XPS (<0.5 %).<sup>[156,157]</sup> Also, the overall XPS spectra of the UV irradiated samples present a few (2 %) oxygen atoms.

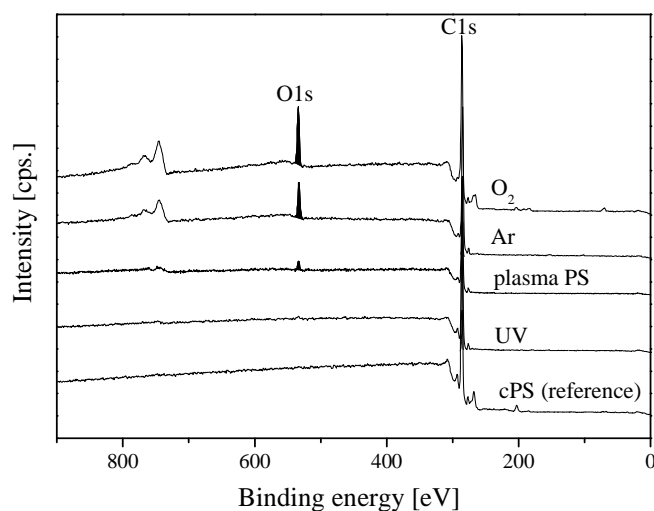


Figure 44: Waterfall presentation of XPS survey scans of  $O_2$ , Ar plasmas and UV irradiation treated spin coated PS in comparison to pulse plasma deposited PS and commercial PS as blank

Styrene is a vinyl monomer and therefore it is easily to polymerize by a radical mechanism using plasma as a source of radicals. The predominant chemical polymerization during plasma exposure may be the reason for the low concentration of radicals and therefore oxygen introduction. The post-plasma oxygen introduction by the reaction of C-radical sites with molecular oxygen from air did not exceed  $\sim 4$  oxygen atoms per 100 C atoms (Figs. 45 and 46).

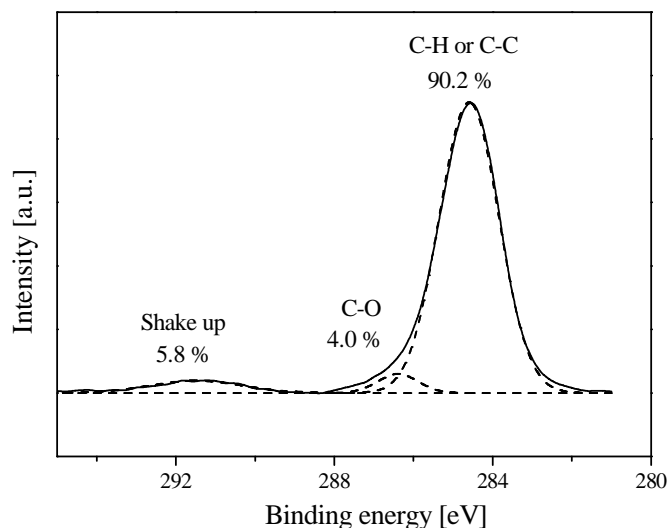
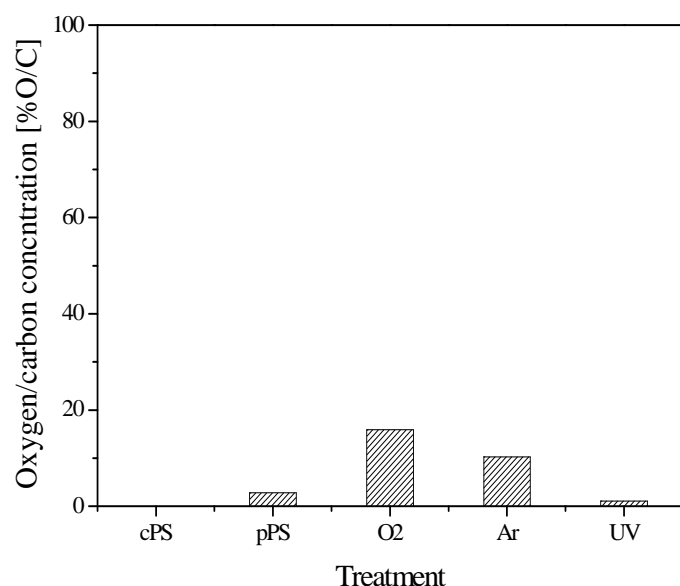


Figure 45: High resolution XPS  $C1s$  spectra of plasma-polymerized PS (plasma power =100 W, DC =0.5, pressure=10 Pa and flow rate of the monomer 10 g/h). The solid line represents the experimental data. The dashed lines represent the individual contributions

The high-resolution  $C1s$  peak of the spectrum for the polystyrene control (reference) sample shows the typical composition of polystyrene, which can be represented by carbon–carbon single and double bonds (aliphatic and aromatic) with respective proportions 1: 3 and



the characteristic  $\pi - \pi^*$  shake-up satellite binding appears at 291.5 eV due to resonance of the aromatic rings of polystyrene. <sup>[158]</sup> The overall spectrum of plasma deposited polystyrene shows that the oxygen content is ca. 4% (see Fig. 45). Plasma polymerized styrene does not show much differences to the commercial reference polystyrene in the XPS spectrum (Fig. 46). <sup>[159]</sup>



*Figure 46: Concentration of the oxygen atoms per 100 carbon atoms for O<sub>2</sub> and Ar plasmas and UV irradiation treated spin coated PS, plasma deposited PS and commercial PS as blank*

When decomposing the high-resolution C1s peak of the spectrum of O<sub>2</sub>, Ar plasma-treated and UV-irradiated (<180 nm) polystyrene and pulsed plasma deposited polymer films. The results show that the newly formed functions are C-C or C-H (284.6 eV), C-O bond (286.3 eV) in addition, the  $\pi - \pi^*$  shake-up satellite binding shows appears at (291.5 eV). <sup>[158]</sup>

Figure 46 shows that the oxygen concentration was ca. 4% in plasma deposited polystyrene, in spin coated commercial polystyrene treated with O<sub>2</sub>, Ar and UV irradiation ( $\lambda > 180$  nm), the oxygen concentration were 15, 10 and 2% respectively after only 1 s of treatment. Oxygen incorporation seems to be more rapid with O<sub>2</sub> plasma than with Ar plasma exposure or plasma polymerization and UV irradiation, respectively.

### 3.2. Chemical composition of the films

Plasma surface modifications due to interactions with plasma particles are confined only to a few nanometers below the surface. <sup>[160]</sup>

FTIR and XPS spectra obtained from O<sub>2</sub>, Ar plasma treated and UV irradiated PS, plasma polymerized and reference PS film are presented in Figs. 44 and 47. Fig. 48 verifies that all these PS films show very similar IR spectra. The main finger-printing IR bands of plasma deposited PS are unequivocally found: Both bands of the mono-substituted aromatic ring at 700 cm<sup>-1</sup> and 758 cm<sup>-1</sup>, which are assigned to out-of-plane deformation bending, the ‘five aromatic finger’ bands between 1665 and 2000 cm<sup>-1</sup> and the two bands at 1449 cm<sup>-1</sup> and 1493 cm<sup>-1</sup> due to  $\delta$  CH and  $\nu$  C=C aromatic vibrations. Furthermore, the bands related to aromatic and aliphatic (asymmetric and symmetric) CH<sub>2</sub> stretching take place in the region from 3000 to 3100 and 2927 and 2872 cm<sup>-1</sup>, respectively. Another band appears exclusively in the spectra of plasma polymers at 2962 cm<sup>-1</sup> that is due to asymmetric  $\nu$ CH<sub>3</sub> stretching vibrations. Plasma polymer samples were exposed to the atmosphere after deposition and readily adsorb oxygen. Also the moisture that is present in the environment indicated by the broad band range from 3600 cm<sup>-1</sup> to 3100 cm<sup>-1</sup>. <sup>[161-163]</sup>

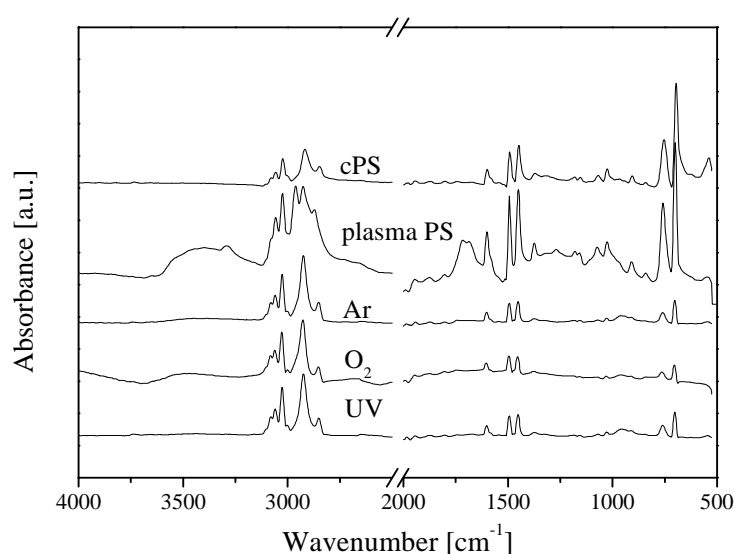


Figure 47: FTIR-ATR spectra of O<sub>2</sub> and Ar plasma and UV irradiation treated spin coated PS, plasma deposited PS films and a reference PS film

The most intense band in the region of aliphatic  $\nu$  CH<sub>2</sub> vibrations in the spectrum of the reference polymer sample occurs at 2918 and 2848 cm<sup>-1</sup>. These bands originate from asymmetric and symmetric CH<sub>2</sub> stretching vibrations of the backbone. They are substantially reduced in the spectra of plasma polymers. It can be concluded that a non-linear backbone was formed but a cross-linked and branched structure evidenced by the strong appearance of methyl end-groups. Considering the XPS results, C1s core level (including its  $\pi - \pi^*$  shake-up feature) and valence band spectra (Fig. 47), a rather good agreement between the data of the pulsed-plasma deposited film and the spin coated reference was found as also detected by Retzko et al. [159]

The surface of the spin-coated virgin commercial (reference) PS films is treated with Ar plasma and is exposed to the atmosphere. The plasma-activated surface readily adsorbs or bonds oxygen and moisture those are present in the environment which is indicated by two components,  $\nu$ OH stretching vibration and oxygen as  $\nu$ C=O at the broad band range from 3600 cm<sup>-1</sup> to 3100 cm<sup>-1</sup>. The explanation is that the very short exposure (1 s) of the PS film to the Ar plasma is sufficient to abstract hydrogen and make C-C scissions. Thus, free radicals at or near the surface are formed, which then interact to form the crosslinking, unsaturated groups, peroxides and crosslinking. The plasma also removes the low molecular-weight materials produced by plasma or at commercial PS or converts them to a high-molecular weight by crosslinking reactions. [164] The irradiation of PS films with 1 s of the plasma-UV ( $\lambda_{\text{cutoff}} < 180$  nm  $\approx$  8 eV) produces only a few changes. Therefore, it is close to the commercial PS in comparison to the argon-plasma treated sample. This means the effects of the UV-C radiation on PS is minimal. It can be assumed that the radiation flux is low. Moreover, the quantum yield for PS and  $\lambda = 253$  nm radiation is also low ( $5 \cdot 10^{-4}$ ). [165]

On the other hand, the 1s-exposure of PS to the O<sub>2</sub> plasma has a comparatively stronger effect, also in comparison to argon-plasma treated sample. In addition to the activation of the polymer surface, functionalization of polymer occurs due to the chemically active nature

of the O<sub>2</sub> plasma (Fig. 47). The broad OH-stretching band ranges from 3600 cm<sup>-1</sup> to 3100 cm<sup>-1</sup> was observed. It indicates that, the surface is not simply activated but it is also modified with O-containing groups among them are also OH groups. This effect is responsible for the decrease in the contact angle than the argon treated PS surface. It must be noted that, OH-groups can only be formed by an indirect way because oxygen plasma has no hydrogen. Hydrogen may be released from the PS molecule or it is adsorbed at the walls of the plasma reactor.

### 3.3. *Contact angle measurement (CAM)*

Many polymer films and fibers have a low surface energy, are poorly wettable by solvents, show low tack, and exhibit low adhesion to deposited metal layers. One of the most promising and advanced polymer modification techniques is the low-temperature plasma treatment. This technique allows modifying the surface properties over a wide range and the field of application of polymeric materials can be considerably extended. <sup>[166]</sup>

Water contact angles of PS exposed to the plasma UV (<180 nm) and those of plasma-polymerized PS are close to that of commercial reference PS. They contrast strongly to those of strongly lowered oxygen and argon-plasma treated samples, which are significantly. This means the effect of low-energy UV (<8 eV) on the structure of PS was limited. This weak answer for irradiation is surprising because the  $\sigma \rightarrow \sigma^*$  transition of C-H, C-C and C-C<sub>arom</sub> bond scissions are in the range of 3.7 to 6.5 eV. <sup>[167]</sup> The surface of plasma deposited polymer films has more or less similar properties as the conventional (reference) PS. However, the water CAM of Ar and O<sub>2</sub> plasma treated PS films were strongly reduced. O<sub>2</sub> and Ar plasma change the PS surface from hydrophobic to hydrophilic character see Fig. 48.

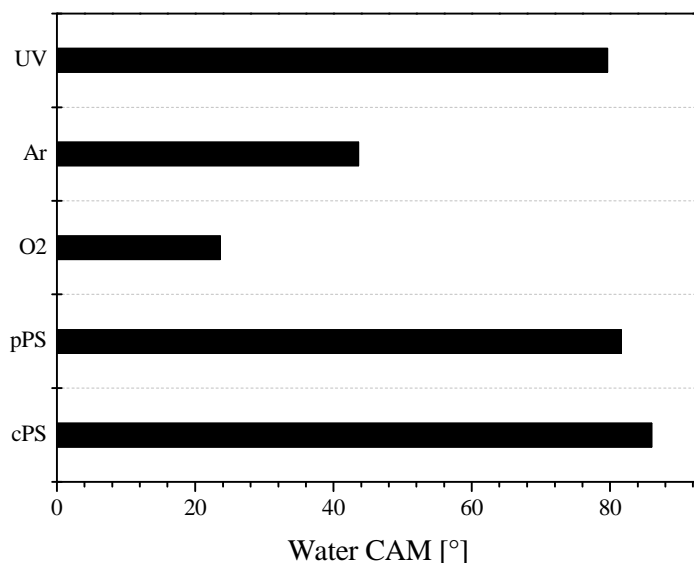


Figure 48: Water contact angle of O<sub>2</sub>, Ar plasma and UV irradiation treated spin coated PS, plasma deposited PS films and a reference PS film

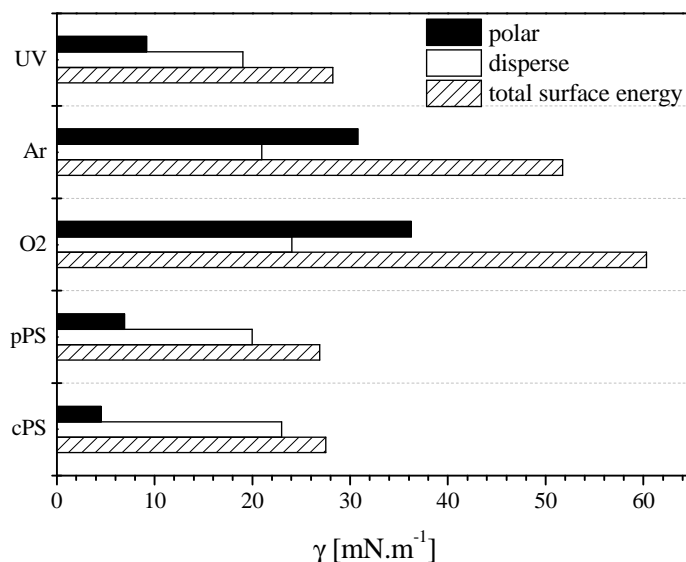


Figure 49: Surface energy, disperse and polar part of O<sub>2</sub> and Ar plasma and UV irradiation treated spin coated PS, plasma deposited PS films and a reference PS film

The total surface energy ( $\gamma$ ) of PS increases adequately within 1 s Ar and O<sub>2</sub> plasma treatment caused by considerable increase in the polar contribution due to the newly incorporated O-functional groups into the PS surface (Fig. 49).

### 3.4. Dynamic mobility and thermal stability

Fig. 50 shows the comparison of the dielectric loss versus temperature ( $T$ ) and frequency ( $f$ ) for spin-coated PS treated by O<sub>2</sub>, Ar plasma and irradiated by UV (>180 nm) and

the comparison to pulsed-plasma produced PS as well as to conventional reference PS in terms of a 3D plot.

Firstly, at higher temperatures, in the range of the glass transition temperature as measured by DSC (Differential Scanning Calorimetry) an ill-defined shoulder is visible, i.e. a peak, which might correspond to the dynamic glass transition ( $\alpha$ -relaxation) was observed.

Secondly, it should be remembered that the samples are measured as thin films sandwiched between aluminium electrodes. So, for the thin film capacitors, the resistance of the Al electrodes leads to an artificial loss contributions (electrode peak) on the high-frequency side of the spectra.

HN-function (9) is used to analyze the data. The electrode peak is taken into consideration by a Debye function. An illustration for that procedure is given in Fig. 51.

For higher temperature the dielectric loss increases with frequency and temperature by presenting clear indication of another relaxation process after  $\alpha$ -relaxation in case of plasma deposited PS, which is the several times before observed, electrode polarization. Electrode polarization is due to free radicals and post-plasma oxidation in the bulk of the polymer.

The spectra reveal strong differences between the totally plasma-synthesized polymer and the only plasma-modified commercial polystyrene samples on the other hand. It is also known that the properties of polystyrene depend strongly on the microstructure of the chain.<sup>[168]</sup> For instance, a strong dependence of the glass transition temperature and the dielectric strength on the vinyl content of statistical polystyrene was observed.

Results depicted in Fig. 50 indicate that the microstructure of reference PS and those treated by O<sub>2</sub>, Ar plasma and UV irradiation is quite different. However, the microstructure of the product obtained by the pulsed-plasma polymerization is very different in comparison to cPS. It is likely that, a highly cross-linked structure is obtained because the plasma process

can activate the double bonds present as vinyl group, the C-C  $\sigma$ -bonds and the much stronger bonded aromatic double bonds in the benzene ring.

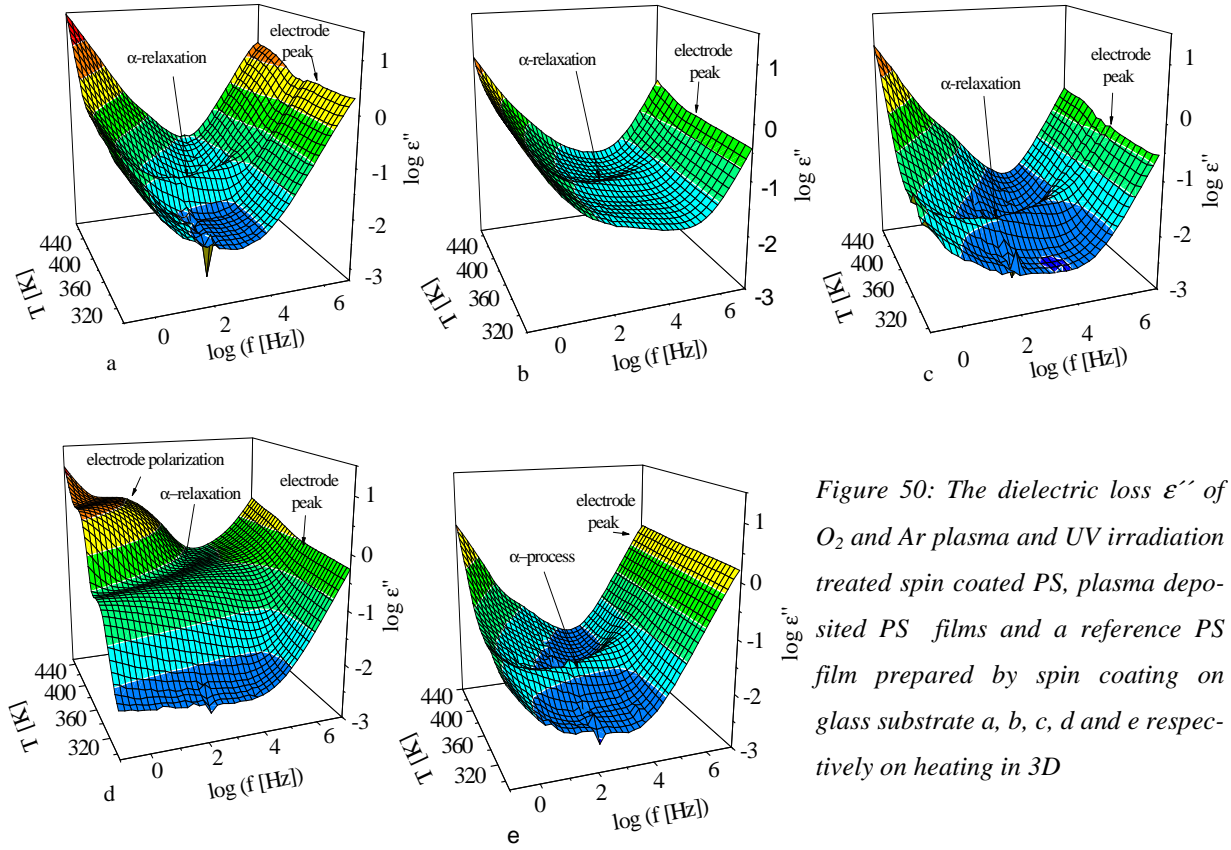


Figure 50: The dielectric loss  $\epsilon''$  of  $O_2$  and Ar plasma and UV irradiation treated spin coated PS, plasma deposited PS films and a reference PS film prepared by spin coating on glass substrate a, b, c, d and e respectively on heating in 3D

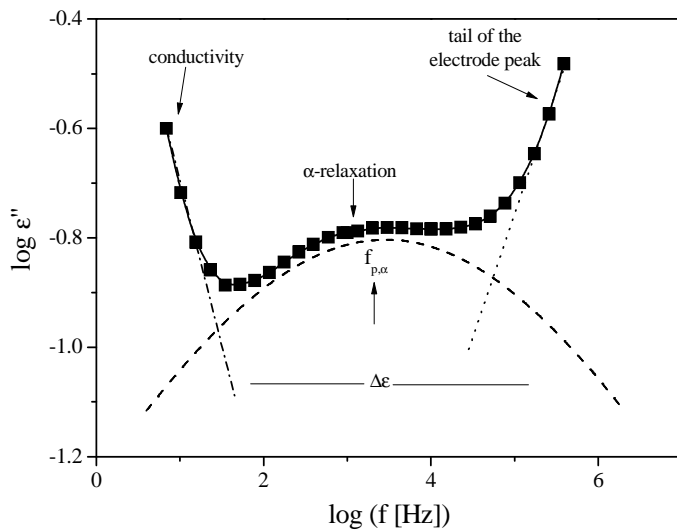


Figure 51: The dielectric loss versus frequency for the plasma deposited PS polymer with  $DC=0.5$  at  $T=325.17$  K during heating. The solid line corresponds to the whole fit-function consisting of the conductivity, a HN-function and a high frequency tail. The dashed, dashed dotted and dotted lines are the contributions of the relaxation process, conductivity and the low frequency wing of the electrode peak respectively

The values of the  $T_g$  of plasma-polymerized PS films ( $T_g=322$  K measured by DSC method) were significantly lower than the  $T_g=373$  K<sup>[131]</sup> for conventional reference PS.

It can be concluded that the molecular mobility is higher in plasma polymers than in the reference polymers as might be expecting. During the plasma polymerization a highly branched structure with many dangling ends is produced which may act as an internal plasticizer yielding. These dangling ends lead to a decreased  $T_g$  as interpreted above. <sup>[106]</sup>

The temperature dependence of the relaxation rate of the  $\alpha$ -relaxation  $f_{(p, \alpha)}$  show a curved trace in the plot  $\log f_{p, \alpha}$  versus  $T^{-1}$ . This dependence can't be well described by the Vogel-Fulcher-Tamman-Hesse (VFT) <sup>[153]</sup> Equation (10).

This equation indicates that the  $\alpha$ -relaxation is a not-activated process. Hence, the  $\alpha$ -relaxation is related to  $T_g$ ,  $f_{p, \alpha}$  and it shows the same dependence on chain architecture as  $T_g$  (Fig. 52)

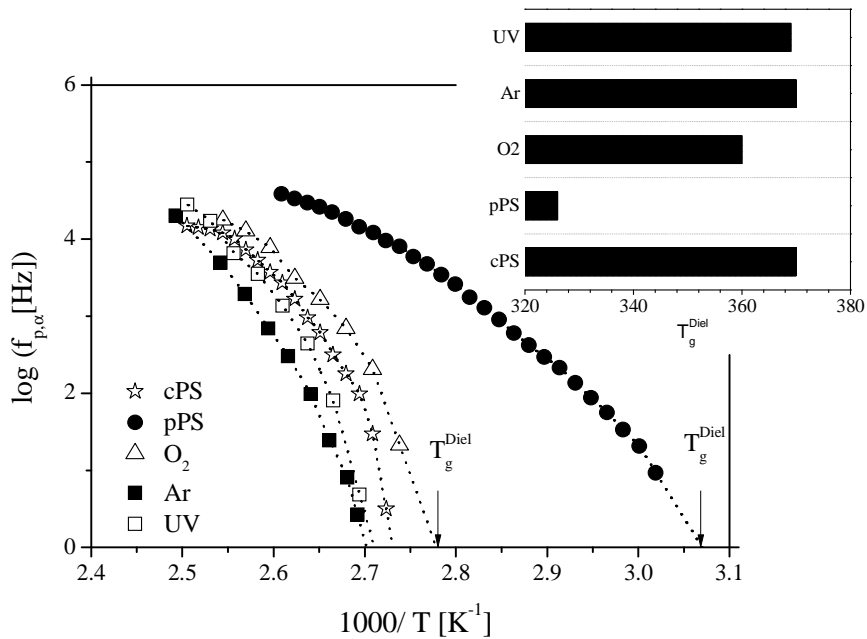


Figure 52: Relaxation rate of the  $\alpha$ -relaxation versus inverse temperature of PS thin films for: Ar, UV irradiation, and O<sub>2</sub> plasma, plasma deposited PS, cPS. Insert: dynamic glass transition for different processes

Fig. 52 compares the temperature dependence of the rate of  $\alpha$ -relaxation for different processes and for the first heating of plasma deposited PS. Firstly, for plasma-produced PS the rate of  $\alpha$ -relaxation shifts more to lower temperature. On the other hand, the rate of  $\alpha$ -relaxation for O<sub>2</sub> plasma exposure shifts to lower temperature compared to cPS. Ar plasma



and UV irradiated samples show that the rate of  $\alpha$ -relaxation has more or less similar temperature values as cPS. This means the plasma-produced PS structure is different in compared to cPS.

A crude estimation of a dielectric glass transition temperature can be estimated by  $T_g^{\text{Diel}} = T(f_{EP}=1 \text{ Hz})$ .  $T_g^{\text{Diel}}$  is plotted versus the different processes in the inset of Fig. 52. From the raw data, the rate of  $\alpha$ -relaxation shifts to lower temperatures for plasma-produced PS then  $O_2$  plasma. It has a small shift to lower temperature indicating a decrease of the glass transition temperature for both methods. The  $\alpha$ -relaxation is related to the  $T_g$  of the system and for that reason this process is called dynamic glass transition.  $\alpha$ -relaxation characterizes the segmental motion of the chain. It is likely that, a decreased  $T_g$  due to the dangling ends which is produced during the plasma polymerization or plasma treatments. Therefore, the segmental motion is increased and leads to decrease of dynamic glass transition.

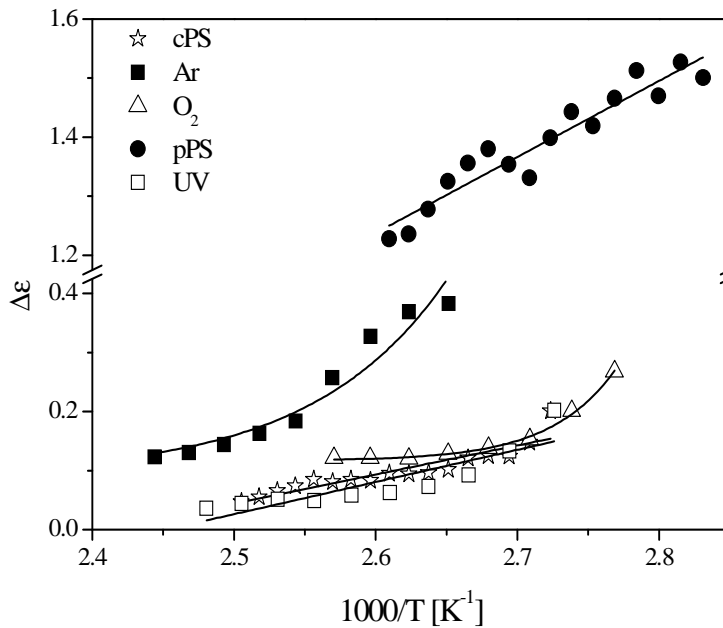


Figure 53: Relaxation strength of the  $\alpha$ -relaxation versus inverse temperature of PS thin films for Ar and  $O_2$  plasma UV irradiation, plasma deposited PS, and cPS as blank

Moreover, it is worth noting that, the dynamic glass transition temperature  $T_g^{\text{Diel}}$  of spin-coated PS treated by Ar plasma, UV-irradiation and cPS are quite close together. That means the effect of Ar plasma and Ar plasma UV irradiation on the surface and bulk of thin films is very limited within 1 s of exposure.

According to the Kirkwood and Fröhlich [Function \(8\)](#), the dependence of the dielectric strength ( $\Delta\epsilon$ ) on the temperature is plotted in the [Fig. 53](#).  $\Delta\epsilon$  is proportional to the mean squared dipole moment  $\mu^2$ , number density of the dipoles and therefore, to the mobility of dipoles.  $\Delta\epsilon$  of plasma deposited PS was a high value reference to cPS.

At a first glance, this is expected because the dipole moment of plasma-polymerized PS should be higher than that of cPS. Therefore, it is concluded that the increasing concentration of oxygen groups like hydroxyl and carbonyl groups increases also the number density of dipoles and therefore, also the dipole moment. On the other hand,  $\Delta\epsilon$  of PS treated by  $O_2$  plasma shows an increase which was expected in comparison to PS treated by Ar plasma and UV irradiation as well as plasma-deposited PS and cPS, which is interpreted as an increase of the dipole moment  $\mu$  at high concentrations of OH groups and so on. However, it is shown that  $\Delta\epsilon$  of the plasma deposited PS is very high compared to others. The dielectric spectroscopy is a 'bulk method' and therefore this result points to a homogeneous composition of the layers.

According to the above discussion, the plasma process produces a number of unsaturated free radicals but trapped radicals on the surface and in the bulk of plasma-generated PS.

This line of argumentation leads to the hypothesis that the plasma-synthesized products are not thermally stable because the free radicals can recombine at elevated temperatures. This is demonstrated in [Fig. 54](#) for discussing the dielectric loss behaviour for the 1<sup>st</sup> heating, cooling and 2<sup>nd</sup> heating run in more detail. [Fig. 54](#) presents the dielectric loss versus temperature at a fixed frequency (1 kHz) (isochronal plot) for the different thermal histories for the sample. In all cases the  $\alpha$ -relaxation is observed as a well defined peak in the three spectra. For the cooling run the intensity of this relaxation process is shifted to higher temperature because the (polar) radicals are converted into less polar groups indicating also a change in structure. After the first heating run thermal stability is evidenced by the fact that there is no difference in the dielectric spectra between cooling and 2<sup>nd</sup> heating run.

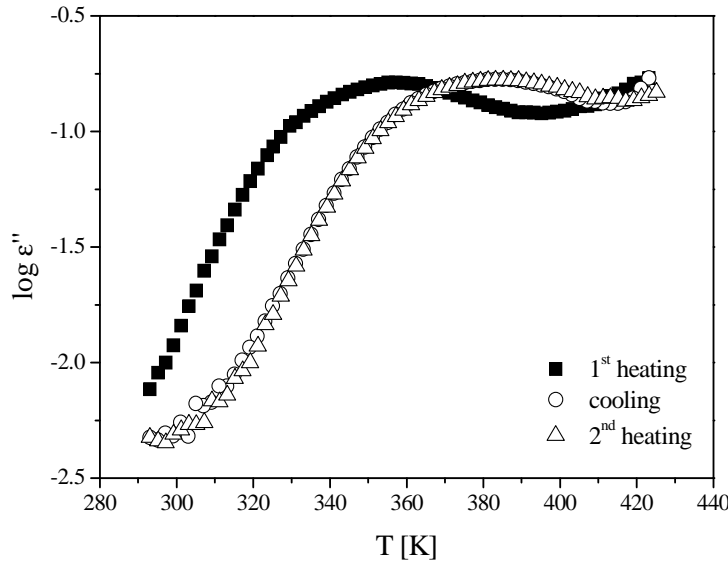


Figure 54: Dielectric loss  $\epsilon''$  for plasma-produced PS versus temperature at frequency of 1 kHz for: 1<sup>st</sup> heating, cooling and 2<sup>nd</sup> heating

For segmental dynamics the functional form of the temperature dependence of the corresponding rate should follow the Vogel/Fulcher/Tammann (VFT-) formula.

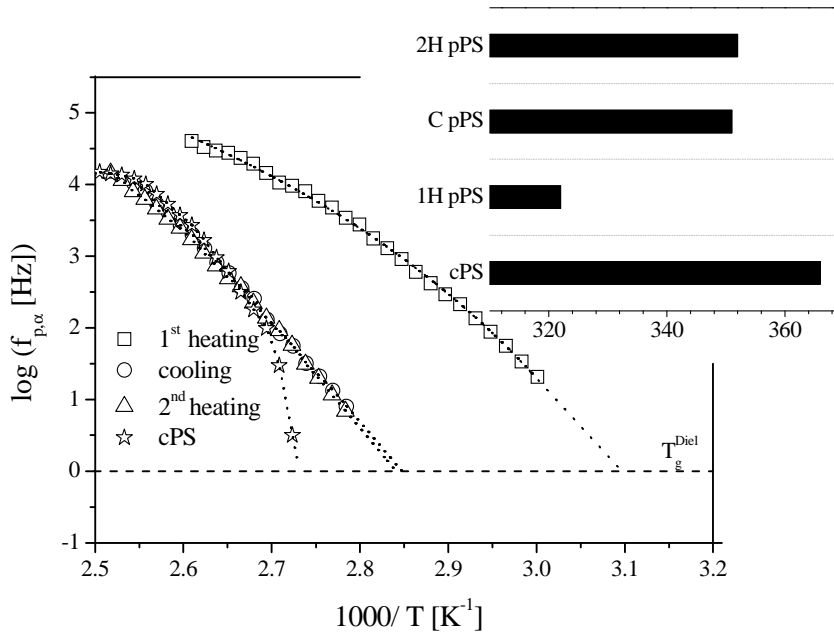


Figure 55: Relaxation rate of  $\alpha$ -process vs. inverse temperature for plasma deposited PS sample: 1<sup>st</sup> heating, cooling, 2<sup>nd</sup> heating and cPS. The inset shows the dynamic glass transition for different processes

Therefore, Fig. 55 shows the temperature dependence of the rate of  $\alpha$ -relaxation for the different thermal histories of the plasma-polymerized PS sample. The rate of the  $\alpha$ -relaxation shifts

to higher values of the temperature for the cooling and second heating processes. The inset in [Fig. 55](#) displays that the dynamic glass transition is increased from ca. 322 K (first heating) to ca. 352 K (cooling and second heating). It may be caused by C-C recombination. After the first heating run a thermal stable products were obtained. It is evidenced by the fact that there is no difference in the rate of  $\alpha$ -relaxation and the dynamic glass transition between the first cooling and the second heating run. Additionally, after first heating the dynamic glass transition is close to that of cPS. This behaviour is limited for Ar, O<sub>2</sub> plasma and UV irradiation in compared to plasma PS films.

#### **4. Acrylic acid-styrene plasma deposited thin copolymer films**

Assuming a random poly-recombination of small fragments and atoms formed from the comonomers in the plasma. The resulting ‘‘copolymer’’ films should be preferentially characterized by a linear correlation between feed gas composition and film chemistry for the measured properties mentioned above. The fact that in this study definitely non-linear correlations are obtained points to effective chemical copolymerization processes during film deposition. Therefore, an attempt can be made to understand the observed non-linear correlations in terms of approaches which have been developed for classic radical copolymerization processes (reviewed for instance in ref. [87]). The plasma polymerization mechanism is not expected to be a completely free radical mechanism.

The final conclusion is that the structures of the plasma deposited copolymer films can't be easily anticipated from the structure of the respective plasma homopolymers. This behavior is due to interactions and/or recombination reactions between monomer molecules during their respective plasma copolymerization process.

Through a careful selection of the feed gas composition, plasma copolymerization can be used to control the concentration of surface functional groups in plasma deposited films. The chemical structure of the plasma deposited copolymer films are partially different from the structure of the respective plasma homopolymers, i.e., the nature of plasma copolymers might not be straightforwardly predicted by a detailed knowledge of the structure of these homopolymers. These results can be explained by the chemical interactions and recombination reactions taking place between monomer molecules in the plasma and/or during the deposition process.

## 4.1. Influence of the Duty Cycle

### 4.1.1. Kinetics of the copolymer deposition

Monomers are difficult to plasma polymerize in the plasma under complete retention of the monomer structure in comparison to commercial polymerization. <sup>[106]</sup> Plasma polymers are characterized by an irregular polymer structure as demonstrated by FTIR and DRS and often large concentration of C-radical sites responsible for extensive post-plasma oxidation. Using pulsed plasma technique this situation could be considerably improved. <sup>[169]</sup>

Styrene is a vinyl comonomer and acrylic acid belongs to the acrylic comonomers and they are easily to activate and therefore to polymerize by a radical mechanism. The copolymerization parameters determine reflects the reactivity and compatibility as well as the chance of forming homo or copolymers. More details of chemical copolymerization can be found in ref. <sup>[170]</sup>. Also under exposure to low-pressure plasma both acrylic acid and styrene have a high tendency of simultaneous homopolymerization or copolymerization as shown by high deposition rates in Fig. 56. In detail the deposition rate of AA/S is close to that of pure acrylic acid (AA) (see Fig. 56).

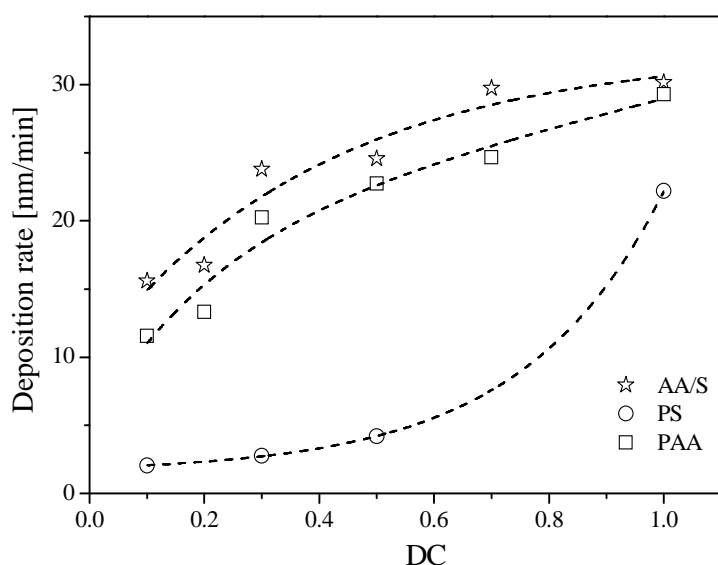


Figure 56: Deposition rates of plasma deposited PAA, PS homopolymers and AA/S copolymer in dependence on DC

For styrene the deposition rate increases strongly for higher values of the DC. This can be interpreted as dominance of fragmentation followed by a poly-recombination mechanism.

As discussed in detail in ref [106] the deposition rate of acrylic acid shows a non-linear behaviour. This behaviour depends on the mechanism of the film formation corresponding to high energy density of the plasma.

As discussed before, during the plasma deposition there are two main processes. Firstly, the double bond can be scission to a C-C single bond by only 1 eV energy input ( $R-CH=CH_2 + plasma \rightarrow R-CH\bullet-CH_2\bullet$ ) and a normal chain-growths polymerization (chain propagation) process can be started under low-pressure conditions maybe as a biradical process:  $R-CH\bullet-CH_2\bullet + 2 R-CH=CH_2 \rightarrow \bullet CHR-CH_2-CHR-CH_2-CHR-CH_2\bullet$ . Another variant is the attachment of a H atom or a radical to the double bond:  $R-CH=CH_2 + H\bullet \rightarrow R-CH_2-CH_2\bullet$ . This process takes place with a rate  $R_{Chain}$  and will lead to regular structures similar to that obtained by a conventional polymerization process. Secondly, due to high energy density of the plasma a fragmentation of the monomer takes place followed by a poly-recombination, maybe as only one example:  $R-CH=CH_2 + plasma \rightarrow uC\bullet + vCH\bullet + w\bullet CH_2 + xCH_3\bullet + zH\bullet \rightarrow randomly\ composed\ and\ structured\ polymer$ , with irregular, unsaturated radicals, branched or crosslinked structures. The rate of the latter process is denoted as  $R_{Frag}$  where the overall deposition rate is approximately given by  $R = R_{Chain} + R_{Frag}$ . In addition to these processes a depolymerisation and a partly removal of the deposited layer have to be consider.

To compare the deposition rates for the different DC directly, the deposition rate has to be normalized by the time where the plasma was on ( $t_{on}$ ). Equivalently the deposition rate can be divided by the DC (Fig. 57).

This Figure shows that the normalized deposition rate of plasma (co) polymer is maximal for the lowest DC. This means that the rate for the chain propagation process is essentially higher for low DC. This might also imply that for low DC a more regular structure is formed. The marked increase in deposition rate for AA/S compared to both monomers is not clearly additive, i.e. the sum of normalized deposition rates of the comonomers did not give exactly the

normalized deposition rate of the comonomer mixture. The plasma chamber consists of acrylic acid and styrene as monomers vapour before plasma inlet. Additionally, an interaction between acrylic acid, an electron accepting monomer and styrene, an electron donating monomer can take place.<sup>[171]</sup> So, the deposition rate of AA/S copolymer contains deposition rate of three compounds.

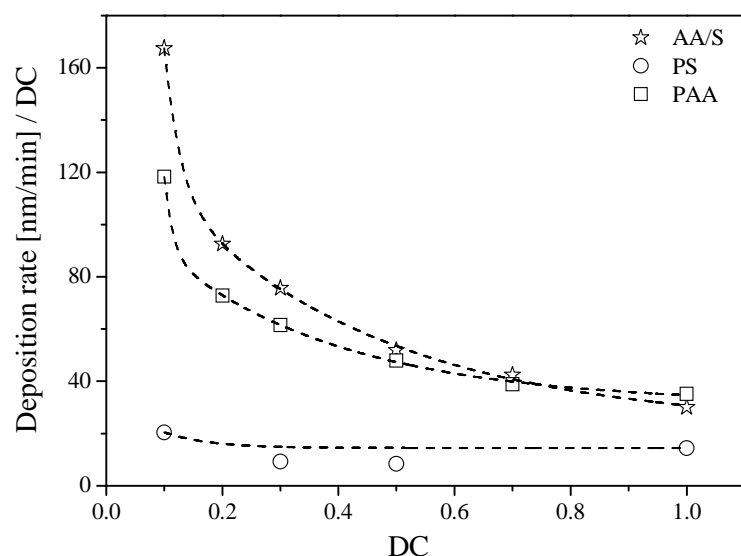


Figure 57: Normalized deposition rate vs. DC for plasma deposited: PAA, PS homopolymers and AA/S copolymer

#### 4.1.2. Retention of functional groups during copolymerization

The estimation of the concentration of functional groups on the surface is based on the reaction of these groups with a substance containing at least one hetero element in its structure and followed by a XPS-measurement of the derivatized surface. The concentration of carboxylic groups at acrylic acid and acrylic acid-styrene copolymers with respect to DC was analyzed according to Scheme 1.

Fahmy et al.<sup>[106]</sup> discussed the composition of the C1s peak of plasma deposited PAA at DC=0.5 and the one derivatized with TFE.

Fig. 58a and b show the C1s spectra of a deposited AA/S copolymer films before and after derivatization with TFE of a sample prepared at a DC value of 0.5. The deconvolution of



the C1s peak of AA/S before derivatization (Fig. 58a) was done assuming five components assigned to: C-C/C-H: 285.0 eV, C-O: 286.3 eV, C=O: 287.5 eV,  $\Sigma$ COOH + COOR: 289.1 eV and the shake up satellite caused by  $\pi \rightarrow \pi^*$  interaction at (291.5 eV) was observed hinting to aromatic (or other unsaturated or conjugated) structures. At derivatized samples an additional component at 293.0 eV for the CF<sub>3</sub> bond was considered (Fig. 58b).

Table 8: gives the inspection of the C1s peak analysis of the non derivatized and derivatized surface for AA/S copolymer

	C-C/C-H %	C-O %	C=O %	COO %	$\pi$ - $\pi^*$ %	CF <sub>3</sub> %
	285.0 eV	286.3 eV	287.5 eV	289.1 eV	291.5 eV	293 eV
<b>non-derivatized</b>	83.0	7.9	1.9	3.8	3.5	-
<b>derivatized</b>	78.4	9.3	4.5	4.2	1.9	1.6

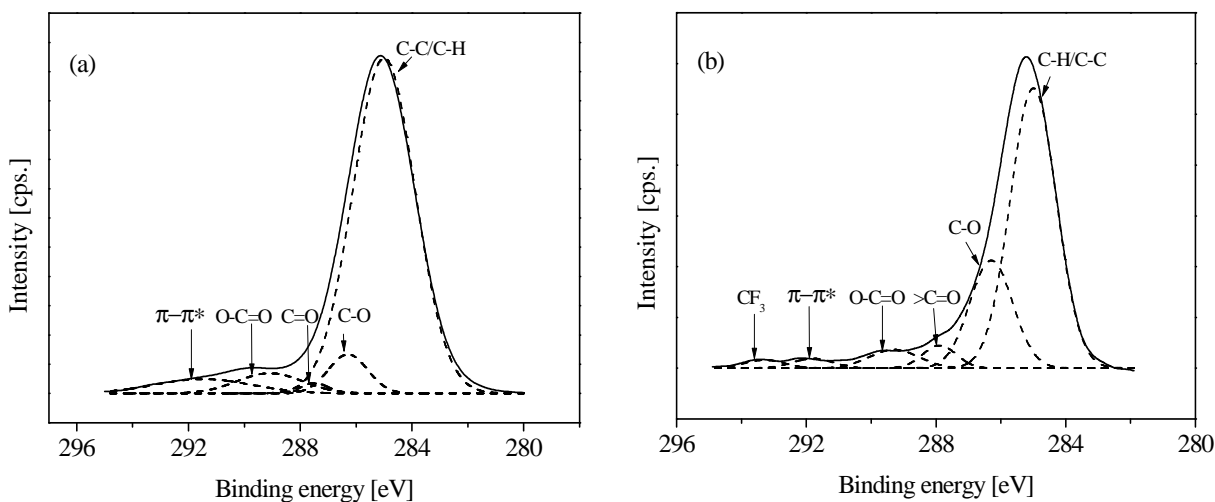


Figure 58: High resolution XPS spectra of the sample with DC=0.5: (a)- before derivatization and (b)-after TFE-derivatization. The solid line represents the experimental data. The dashed lines represent the individual contributions

The comparison of Figs. 58a and b reveals that the contribution of the CF<sub>3</sub> group, which is related to the TFE-derivatized COOH groups, is equal to 1.6 %. Therefore, the concentration of COOR defines as:  $C_{\text{COOR}} = C_{\text{COO}} - C_{\text{COOH}} = (3.79 - 1.6) \% = 2.19 \%$ . This means

that some COO bonds have to be rather assigned to ester-type linkages than carboxylic groups, which do not participate in the derivatization reaction and remain, therefore, unchanged. Table 8 shows the inspection of the C1s peak analysis of the non-derivatized and derivatized surface.

Increasing DC produces a decrease in COOH functions. This behaviour is probably due to a fragmentation of monomers and decarboxylation of acrylic acid (see Fig. 59).<sup>[172-174]</sup> A strong difference in COOH-group retention between pure acrylic acid homopolymer and acrylic acid-styrene copolymers is obvious (Fig. 59).

For conventional radical copolymerization of styrene and acrylic acid for a feed composition of 1:1 the corresponding copolymer has approximately also a 1:1: composition.<sup>[170]</sup> Therefore, an acrylic acid/styrene copolymer (molecular ratio of both monomers = 1:1) contains 9 COOH groups per 100C-atoms theoretically. The low number of COOH groups is a consequence of a high carbon content introduced by the styrene monomer. For comparison: a 1:1 copolymer of acrylic acid/ethylene theoretically contains 20 COOH groups per 100 C-atoms. For the plasma deposited 1:1 copolymer the number of detected COOH groups was found to be in the order of 1-2 COOH groups hinting to the fact that other processes are going on plasma polymerization.<sup>[174]</sup> Also by FTIR it was found that the plasma polymerization of pure acrylic acid leads in a decreased C=O-band with increasing DC. The same behavior was observed for the thermal degradation of poly(acrylic acid) in argon atmosphere.<sup>[175]</sup>

Figure 59 shows that the concentration of carboxylic groups decreases with increasing DC. This is similar to the plasma deposition of pure acrylic acid but the dependence on DC is different for both systems. To investigate this in more detail the concentration of COOH groups in the copolymer is plotted versus that of the homopolymers in Fig. 60. A constant trend in dependent on DC should be observed if the acrylic acid is deposited for the copolymer in a similar manner for homopolymers. Figure 60 shows that for higher values of the duty

cycle a smaller amount of COOH groups is found than that expected from the structure of the plasma deposited homopolymer. This can be discussed in two directions:

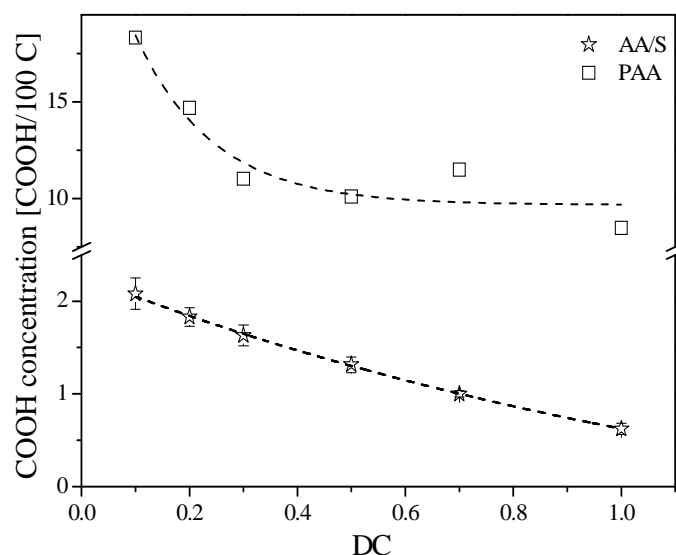


*Figure 59: Dependence of COOH per 100 C atoms for plasma deposited: PAA homopolymers and AA/S copolymer on applied DC*

Figure 56 shows that the deposition rate of styrene increases strongly for the highest values of the duty cycle. This might indicate that for high values of DC the introduction of styrene is favored and lower concentrations of acrylic acid units are obtained than expected from the corresponding homopolymers.

The second direction of the discussion is related to the monomer fragmentation. The energy input increases with increasing DC, and therefore, the degree of fragmentation of the monomer. For higher values of DC a higher concentration of styrene radicals (or styrene-like) is formed than for lower DC. The styrene radicals can interfere with the acrylic acid and modify its structure before deposition. This may result in the formation of other oxygen-containing groups than the COOH group. Unfortunately, one cannot discriminate between both explanations in the moment.

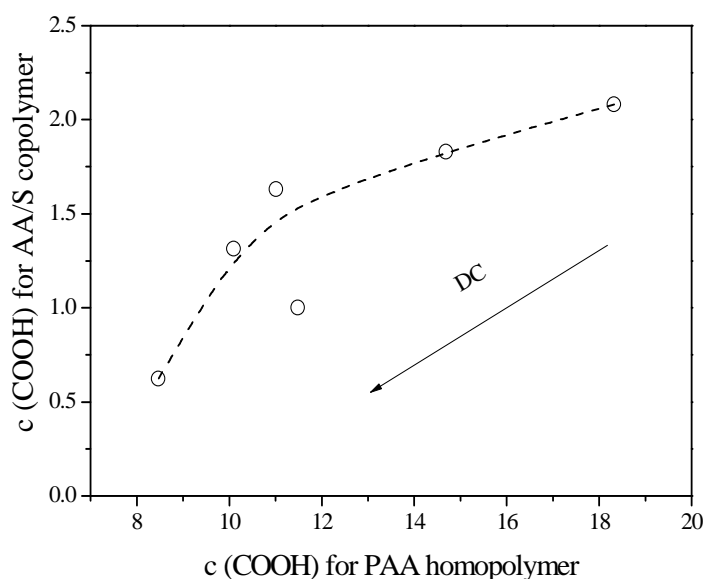


Figure 60: Concentration of COOH groups for plasma deposited AA/S copolymer versus the concentration of COOH for plasma deposited PAA homopolymers with respect to DC. Both of them estimated from derivatization with TFE and the XPS measurements

#### 4.1.3. Investigation of the chemical composition by FTIR

FTIR spectra of plasma-polymerized S, AA/S and AA are shown in Fig. 61. All spectra exhibit stretching vibrations of the polymer backbone consisting of the  $\nu$  CH<sub>2</sub> (as/sym) in the wavenumber range from 2916 to 2844 cm<sup>-1</sup> and associated with the C=O stretching near 1700 cm<sup>-1</sup>. With regard to the PS segments at 700/760 cm<sup>-1</sup> the aromatic C–C stretching, at 1494/1601 cm<sup>-1</sup> the aromatic C=C stretching is observed and the aromatic  $\delta$  C–H takes place at 3080/3060/3020 cm<sup>-1</sup>. [161-163]

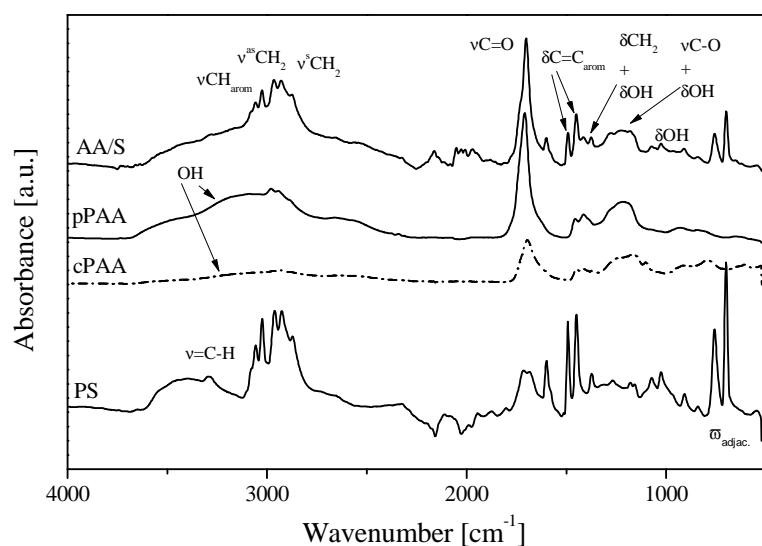


Figure 61: FTIR spectra of plasma deposited PAA, PS homopolymers and AA/S 1:1 copolymer (with DC=0.5) compared to conventional cPAA

The most important fact for the following discussion is the C=O stretching vibration which is described by three components (Gaussians) at: 1737, 1712 and 1680  $\text{cm}^{-1}$ . As example for that analysis see Fig. 62 for plasma deposited PAA05 sample. Wang et al. [176] discussed three components with maxima positioned at 1749, 1715 and 1685  $\text{cm}^{-1}$  measured for conventional polymerized poly(acrylic acid) and copolymers of acrylic acid with styrene. The band at 1680  $\text{cm}^{-1}$  is assigned to the C=O stretching of dimers show also this structure also dangling bonds etc. as well as intermolecular hydrogen bonding or C=C double bonds. [161] The main component at 1712  $\text{cm}^{-1}$  is attributed to the stretching vibration (C=O) of carboxylic groups. To describe the contribution of ester [143] formed by COOR groups a third Gaussian is located at 1737  $\text{cm}^{-1}$ . The ester groups may be formed by self condensation of  $n\text{CH}_2=\text{CH}-\text{COOH} \rightarrow \sim\text{CH}_2-\text{CH}_2-\text{CO}-\text{O}\sim$  [102] or due to a fragmentation of the monomer followed by poly-recombination.

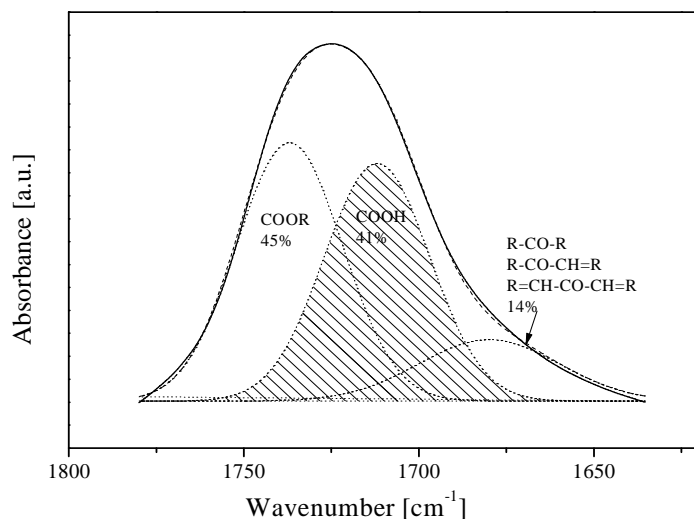


Figure 62: Gaussian fits of C=O band of a plasma-polymerized PAA film (DC=0.5). The solid line represents the experimental data. The dashed line is a fit of a sum of three Gaussians to the data. The dotted lines represent the individual contributions

Fig. 63 gives the FTIR spectra for plasma polymerized AA/S copolymer deposited with a duty cycle of 0.5 compared to plasma deposited PAA homopolymers the main peak of the C=O stretch is shifted from 1712  $\text{cm}^{-1}$  to 1706  $\text{cm}^{-1}$ . The peak located at 1737 shifted to 1732  $\text{cm}^{-1}$  which describes the contribution of ester units formed by the COO group. A third

Gaussian is located at  $1680\text{ cm}^{-1}$  similar to that observed for plasma deposited PAA homopolymers. This indicates a change of the structure compared to those expected from plasma deposited PAA (COOH). From the XPS measurements it is known that C=O, COOH and COOR groups are formed.

From the fits the areas of the peaks at  $1706\text{ cm}^{-1}$   $A_{1706}$  and  $1732\text{ cm}^{-1}$   $A_{1732}$  are taken and its ratio is calculated as a measure for the concentrations of the COOH to COOR groups estimated by FTIR:  $\frac{A_{1706}}{A_{1732}}$  is plotted versus DC (Fig. 64) to discuss regularity of the carboxylic group for AA/S copolymers compared to PAA plasma deposited homopolymers.

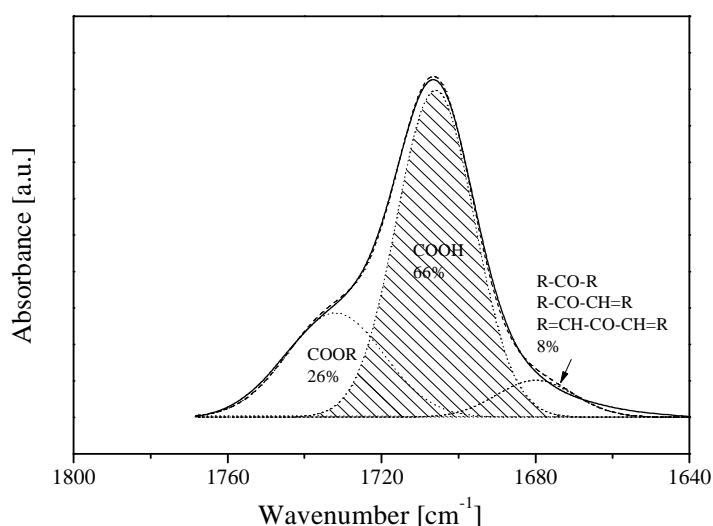


Figure 63: Gaussian fits of C=O band of plasma-polymerized from 1:1 molar ratio of AA/S copolymers (DC=0.5). The solid line represents the experimental data. The dashed line is a fit of a sum of three Gaussians to the data. The dotted lines represent the individual contributions

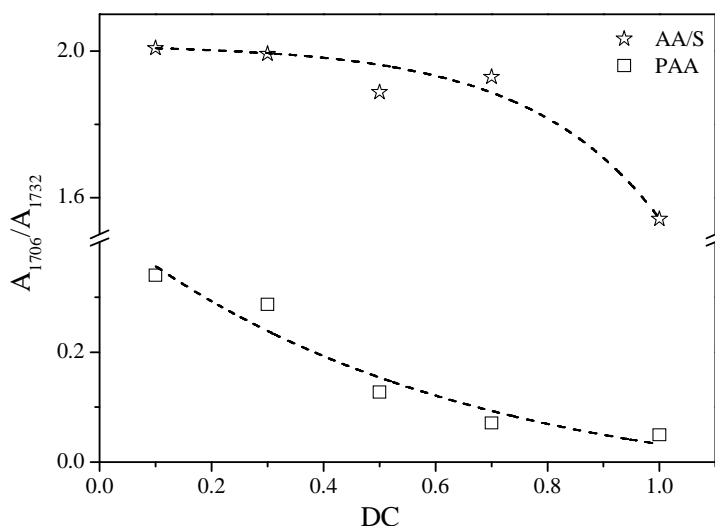


Figure 64:  $\frac{A_{1706}}{A_{1732}}$  vs. DC for plasma deposited: PAA homopolymers and AA/S copolymer

This graph shows firstly that the concentrations of COOH groups decrease with increasing DC for both PAA and copolymer and secondly that there is a strong difference between the homopolymers and copolymers. Additionally decarbonylation and dehydrogenation may produce  $\alpha$ ,  $\beta$ -unsaturated ketone as found by the FTIR analysis.

This dependence affirms that for low values of DC more COOH groups are present in AA/S copolymers. Moreover, for copolymers the dependence of the concentration of carboxylic groups obtained by FTIR on DC is much stronger than that for the plasma deposited homopolymers. This behaviour is similar to the results obtained by XPS.

XPS and FTIR should provide the same information about the concentration of the COOH groups. Therefore, Fig. 65 displays  $\frac{A_{1706}}{A_{1732}}$  versus the concentration of COOH groups per 100 C atoms estimated from the XPS measurements. This Figure shows that the concentration of COOH groups per 100 C atoms decrease with increasing DC.

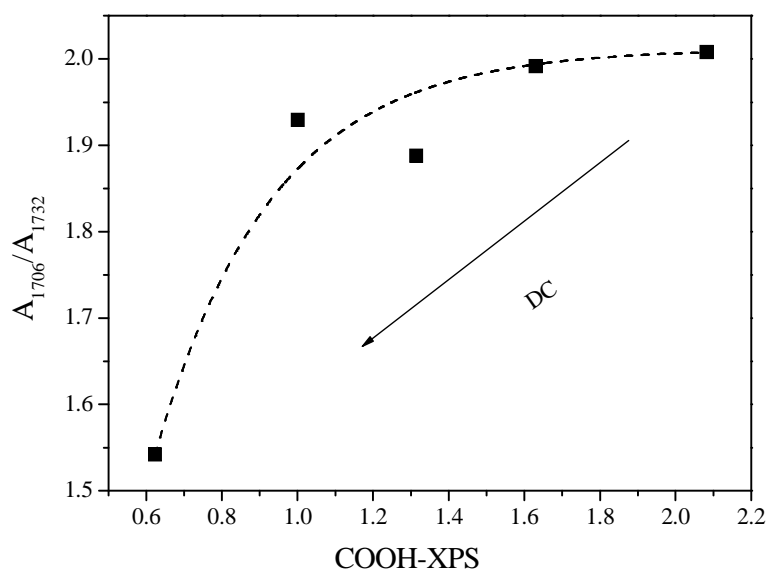


Figure 65: Correlation between XPS-measured COOH groups (TFE-derivatization) and FTIR-measured  $\frac{A_{1706}}{A_{1732}}$  for plasma deposited AA/S copolymer with respect to DC

From the theoretical point of view a constant value should be obtained. As discussed above for plasma deposited PAA and PAAI this result, the different analytical depth of both methods has to be considered. However, for pulse plasma the values of the concentration of carboxylic

groups on the surface is proportional to that calculated in the whole thickness sample was observed. For the continuous wave the concentration of it on the surface was very low compared to that estimated by FTIR. This behaviour is corresponding to the high energy of the plasma.

#### 4.1.4. Thermal analysis

Fig. 66a gives the DSC curves for AA/S copolymers deposited for different values of DC. For each material a step-like change is observed in the heat flow which indicates the glass transition. The glass transition temperature  $T_g$  is estimated from the inflection point of the heat flow of the second heating run and plotted versus duty cycle in Fig. 66b. These data are compared to the values obtained for plasma deposited PAA homopolymers.

Firstly, for all plasma deposited PAA, PS homopolymers and the AA/S copolymers samples the  $T_g$  values are lower than those measured for conventional PAA (379) <sup>[177]</sup> and polystyrene (373 K) <sup>[131]</sup>. It can be concluded that plasma polymerization technique results in products with a lower molecular weight and probably with a highly branched structure compared to the conventional polymerized materials. <sup>[178,179]</sup> In the latter case the dangling ends of the branched structures act as internal plasticizer like for conventional poly(n-alkyl methacrylates).

Secondly, the glass transition temperatures for the plasma deposited copolymers are also lower than those of plasma deposited PAA (see Fig. 66a). Probably, the introduction of the bulky styrene units increases the free volume and also avoids the formation of hydrogen bonds. Both effects will lead to a reduction of the glass transition temperature.

For the copolymers  $T_g$  decreases for low values of DC up to DC=0.5. A similar dependence was observed for the plasma deposited PAA homopolymers (see Fig. 66b). Then the  $T_g$  increases with increasing DC in difference to the PAA homopolymers. This behaviour confirms the results obtained by monitoring the deposition rate, XPS and FTIR measure-



ments. As argued for the deposition rate, the rate for the chain propagation process is essentially higher for low DC. However, the energy input increases with increasing DC, and therefore the degree of fragmentation of the monomers. The latter leads to decrease of the concentration of COOH groups as well as in an increase of crosslinking. Especially the crosslinking increases with increasing values of DC which lead to an increased  $T_g$ .

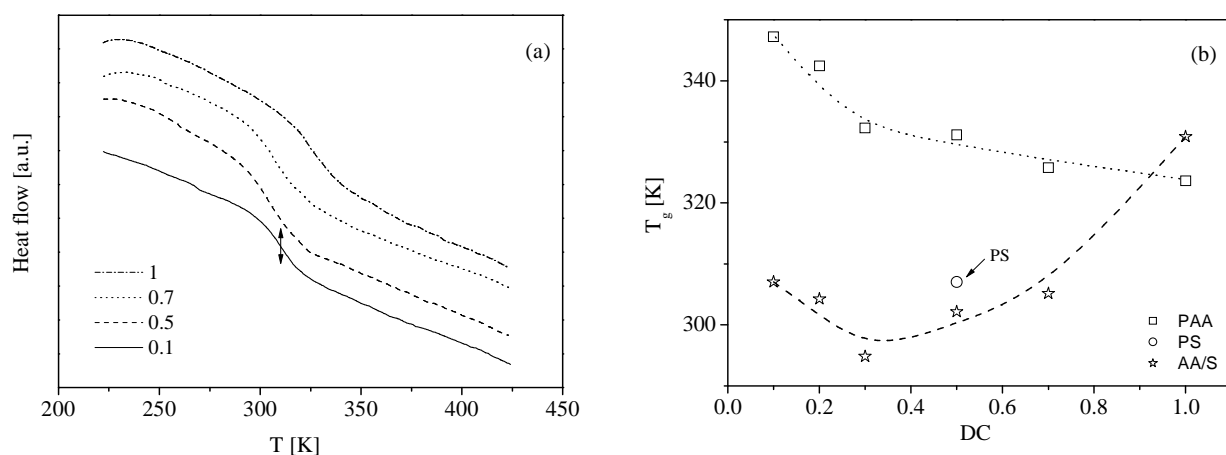


Figure 66: Heat flow of plasma-polymerized AA/S copolymers in dependence on temperature for the labeled DC values (2<sup>nd</sup> heating run) (a):  $T_g$  versus DC for plasma deposited: AA/S copolymer, PAA and PS homopolymers (b)

#### 4.1.5. Dynamic mobility and thermal stability

In detail, glassy dynamics is investigated as well as oxidative and thermal stability. Therefore, the sample is cooled down to 173K and after the dielectric properties are measured during heating. This means the appropriate temperature is selected, the samples equilibrated at this temperature and the dielectric loss is measured in a frequency scan isothermally. Then the next higher temperature is selected till 453 K (heating cycle). Then, the same procedure is applied by subsequently lowering the temperature down to 173K (cooling cycle).

Before the dielectric properties of the plasma AA/S copolymer are discussed, the dielectric loss versus frequency ( $f$ ) and temperature ( $T$ ) for plasma-polymerized PAA and PS homopolymers should be considered (Fig. 67).

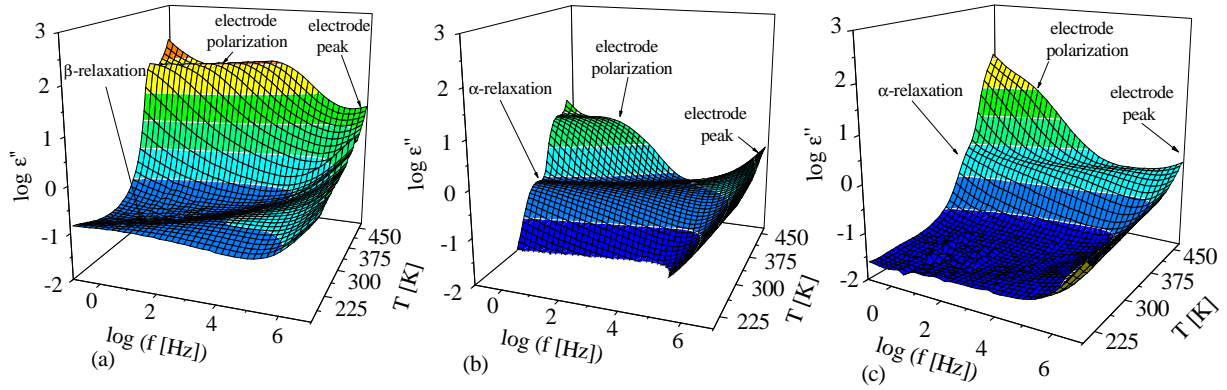


Figure 67: Dependence of dielectric loss  $\epsilon''$  versus frequency and temperature for plasma deposited (a)- PAA, (b)- PS homopolymers and (c)- AA/S copolymer at DC=0.1 for the first heating cycle

The dielectric relaxation behavior of plasma deposited poly(acrylic) acid is discussed in detail above [106]. A relaxation process indicated by a peak in the dielectric loss is observed at low temperature for this material (Fig. 67a), which is assigned to the  $\beta$ -relaxation. The  $\beta$ -relaxation corresponds to localized fluctuation of the dipoles related to the carboxylic groups. At even higher temperatures a clear indication of a further process is visible called electrode polarization.

In case of plasma deposited PS, it is argued in details above in section [Plasma deposited and spin coated thin polystyrene films]. The electrode peak and the electrode polarization were also observed like for plasma-polymerized PAA. In the range of glass transition measured by DSC, a relaxation process takes place, which corresponds to the dynamic glass transition temperature due to segmental dynamics ( $\alpha$ -relaxation). A more detailed discussion of plasma deposited polystyrene including a comparison with conventional synthesized polystyrene was discussed above.

For the AA/S copolymer, similar to PAA and PS plasma deposited homopolymers an electrode peak (higher frequencies) and the electrode polarization (higher temperatures) are observed. In difference to plasma deposited PAA homopolymers no unambiguous  $\beta$ -relaxation is observed for the copolymer deposited with DC=0.5 (see Fig. 67c) because the

dielectric loss covers a wide range. Therefore, the dielectric loss in the temperature range of the  $\beta$ -process is plotted versus temperature at a frequency of 1 kHz for different values of the DC in Figure 68 for the heating cycle. For DC=0.1 a well defined  $\beta$ -relaxation is observed which decreases in its intensity with increasing DC. For DC=0.5 this relaxation process disappears completely. In reference [106] the  $\beta$ -relaxation is assigned to the localized fluctuations of the carboxylic groups. Therefore, the decrease of the intensity of the  $\beta$ -process with increasing value of DC has to be attributed to a decrease of the number density of carboxylic groups. This line of argumentation is in complete agreement with the results of XPS and FTIR investigations.

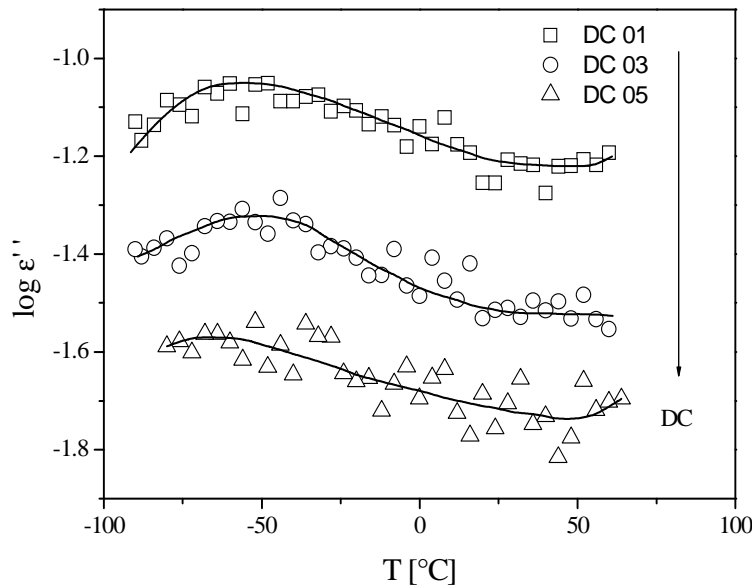


Figure 68: Dielectric loss  $\varepsilon''$  versus temperature at a frequency of 1 kHz for the plasma deposited copolymer of AA/S for different values of DC for the heating cycle

In the temperature range, where the  $\alpha$ -relaxation is observed for plasma deposited polystyrene, this process is detected also for the copolymer.

The dielectric spectra are analyzed fitting the model function of Havriliak and Negami (HN-function) to the data, which serves for calculating the relaxation rate  $f_p$  at maximal dielectric loss and the dielectric relaxation strength  $\Delta\varepsilon$ .

The electrode peak is taken into consideration by a Debye function as described in plasma deposited PAA, PAAI and PS homopolymers thin films. For cases where the frequency posi-

tion of the electrode peak is outside of the experimental accessible frequency window the Debye function is approximated by its low frequency tail. An illustration for that procedure is given in Fig. 69.

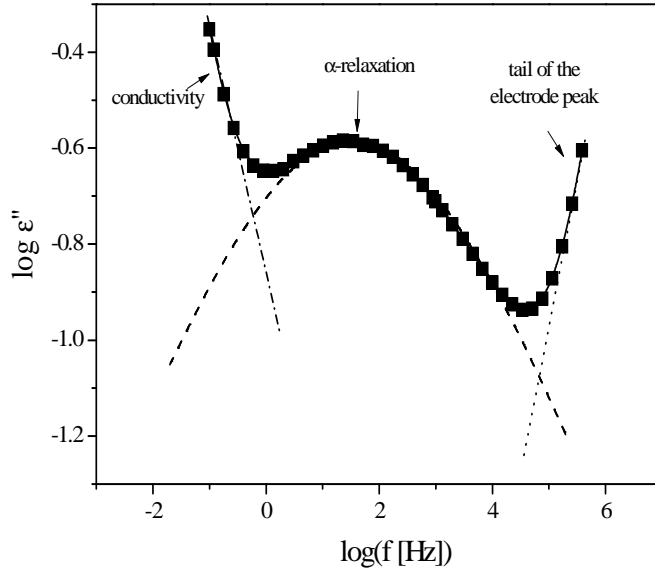


Figure 69: The dielectric loss versus frequency for the plasma deposited sample AA/S copolymer with  $DC=0.1$  at  $T=353.15$  K during heating. The solid line corresponds to the whole fit-function consisting of the conductivity, a HN-function and a high frequency tail. The dashed, dashed dotted and dotted lines are the contributions of the relaxation process, conductivity and the low frequency wing of the electrode peak respectively

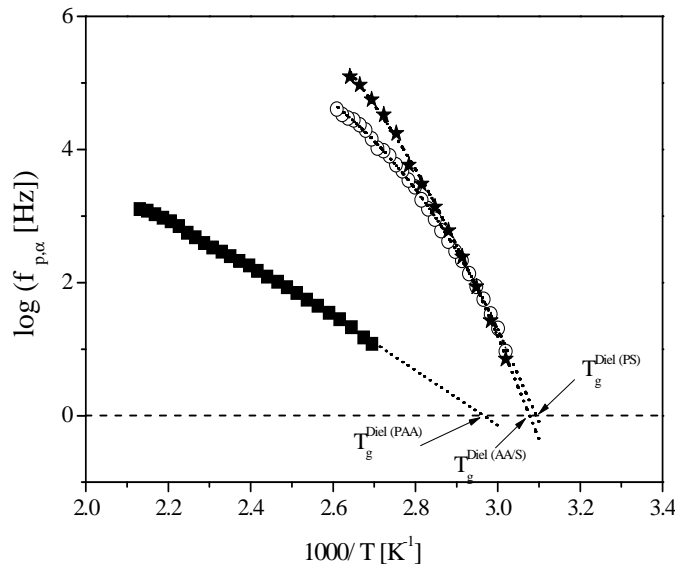


Figure 70: Relaxation rate of the  $\alpha$ -process versus inverse temperature for plasma deposited PAA, PS homopolymers and AA/S copolymer ( $DC=0.5$ )

Fig. 70 compares the temperature dependence of the relaxation rate of the  $\alpha$ -relaxation  $f_{(p, \alpha)}$  versus  $T^{-1}$  for the plasma deposited polystyrene and the corresponding copolymer for  $DC=0.5$ . Considering the fact that the rate for the electrode polarisation  $f_{EP}$  is related to  $f_{p, \alpha}$  (see [106,107])  $f_{EP}$  for plasma-polymerized PAA is added as well. At the first glance the

temperature dependence of the relaxation rate of the plasma deposited copolymer is similar to that of polystyrene. This might be due to the fact that for poly(acrylic acid) the segmental dynamics is strongly influenced by the formation of hydrogen bonds. The possibility of the formation of hydrogen bonds is strongly reduced for the copolymer. For chemically stable polymers the temperature dependencies of relaxation rates might be described by the Vogel-Fulcher-Tamman-Hesse (VFT) Equation (10).

Generally, it is believed that the dependence according to Eq. (10) is a signature of glassy dynamics. For DC=0.5 the temperature dependence of relaxation rates seems to follow the VFT-equation. A dielectric glass transition temperature can be estimated by  $T_g^{\text{Diel}} = T(f_p=1 \text{ Hz})$  (see Fig. 70).  $T_g^{\text{Diel}}$  for the AA/S copolymer is ca. 325 K and it is closed to  $T_g^{\text{Diel}}$  of PS (323 K) while  $T_g^{\text{Diel}}$  for PAA is ca. 338 K.

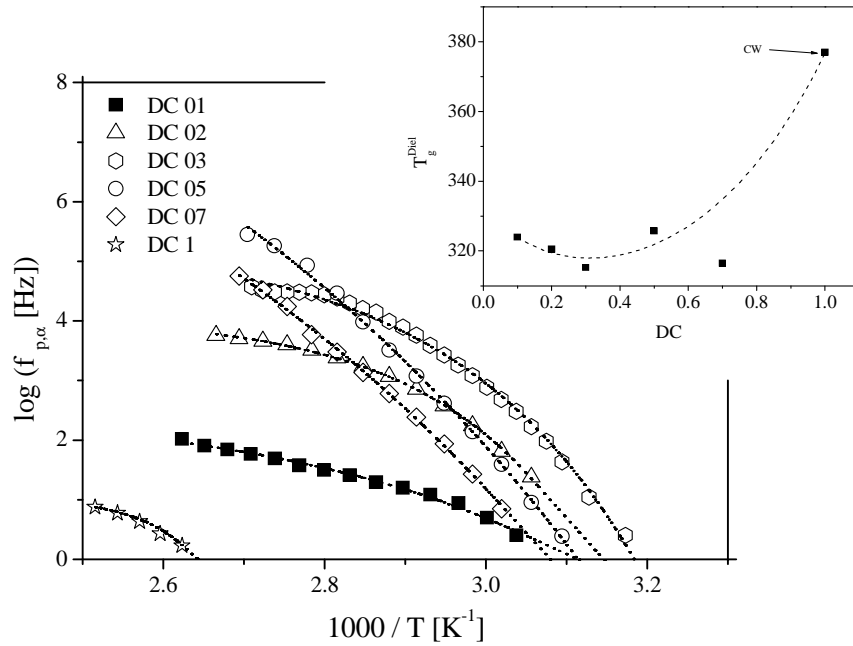


Figure 71: Relaxation rate of the  $\alpha$ -process versus inverse temperature for plasma deposited AA/S copolymer for different values of DC. Insert: dynamic glass transition for different values of DC

Fig. 71 compares the temperature dependence of the relaxation rate of the  $\alpha$ -relaxation for different values of DC on heating. Firstly, with increasing DC the rate of  $\alpha$ -relaxation

more or less shifts to higher temperatures. Secondly it becomes clear from Fig. 71 that the temperature dependence of  $f_{p,\alpha}$  cannot be described in the whole temperature range by the VFT-equation. This dependence is non-monotonous and carries some structure (see for instance data for DC=0.1 or DC=0.7). To discuss this behaviour one has to bear in mind that during the plasma polymerization a large number of radicals are formed which do not react completely during the deposition process. After deposition these radicals are quenched and the deposited layer is in a metastable but non-equilibrium state. By heating up the segments become mobile at the glass transition temperature, and these radical undergo a post-plasma reaction. Therefore this structure in the temperature dependence is related to the kinetics of the chemical reaction that takes place during the heating process.

Nevertheless, a  $T_g^{\text{Diel}}$  can be estimated and plotted versus DC in the inset Fig. 71.  $T_g^{\text{Diel}}$  decreases firstly with the duty cycle up to a DC value of 0.5 then the  $T_g$  increases with growing DC. This behaviour is similar to that obtained by DSC. Firstly, the dielectric spectroscopy measures the glass transition temperature in these systems. Secondly, this behaviour can be discussed in the same way as the DSC measurements and the results that obtained by monitoring the deposition rate, XPS, FTIR and DSC measurements are consistent.

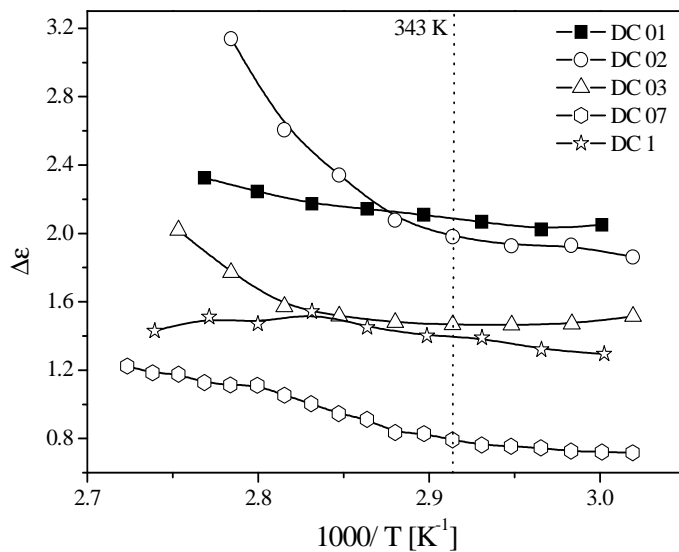


Figure 72: Dielectric strength of the  $\alpha$ -process versus inverse temperature of the plasma deposited AA/S copolymer for different values of DC

Fig. 72 presents the dielectric strength  $\Delta\epsilon_\alpha$  for the  $\alpha$ -process of plasma deposited AA/S copolymer for the different values of DC versus inverses temperature according to the Kirkwood and Fröhlich function (8). With rising temperature,  $\Delta\epsilon_\alpha$  increases slightly. This increase of  $\Delta\epsilon$  is probably due to an increase of the number density of dipoles, which contributes to  $\alpha$ -process and which might be related to the chemical reaction discussed above.

$\Delta\epsilon$  decreases with increasing duty cycle. Therefore, in Fig. 73,  $\Delta\epsilon$  is taken at  $T=343$  K and plotted versus DC. According to Equation (8) this implies that the number density of dipoles decreases with increasing DC at 343 K (Fig. 73). This is in agreement with the FTIR and XPS experiments. These experiments show that the number of carboxylic groups which are involved in dielectric  $\alpha$ -relaxation decreases with increasing DC. It is noteworthy that also the temperature dependence of the dielectric strength changes with the DC. At low value of the DC the temperature dependence of  $\Delta\epsilon_\alpha$  is more pronounced than for higher values of it.

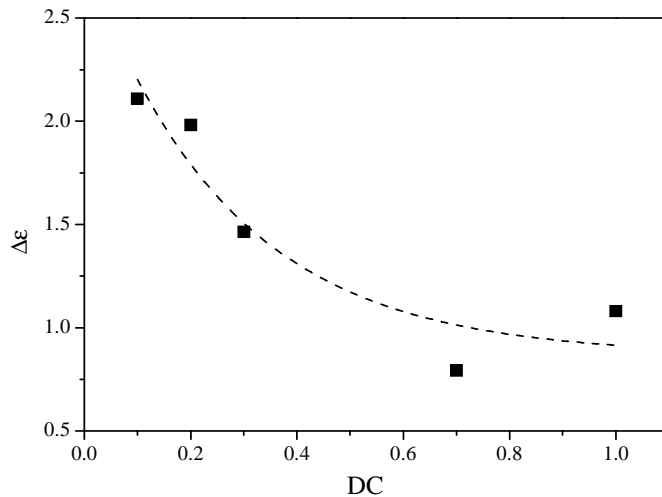


Figure 73: Dielectric strength  $\Delta\epsilon_\alpha$  of plasma deposited AA/S copolymer vs. DC at  $T=343$  K

To discuss the dielectric behaviour for the heating and cooling run in more detail Fig. 74 is presenting the dielectric loss versus temperature at a fixed frequency (isochronal plot) for heating and cooling run for the sample plasma AA/S deposited copolymer with  $DC=0.1$  as an example. For both cases at low temperatures the  $\beta$ -relaxation is observed as a well de-

defined peak in the spectra. For the first heating run a shoulder is observed at higher temperatures than that of the  $\beta$ -relaxation which corresponds to the  $\alpha$ -relaxation.

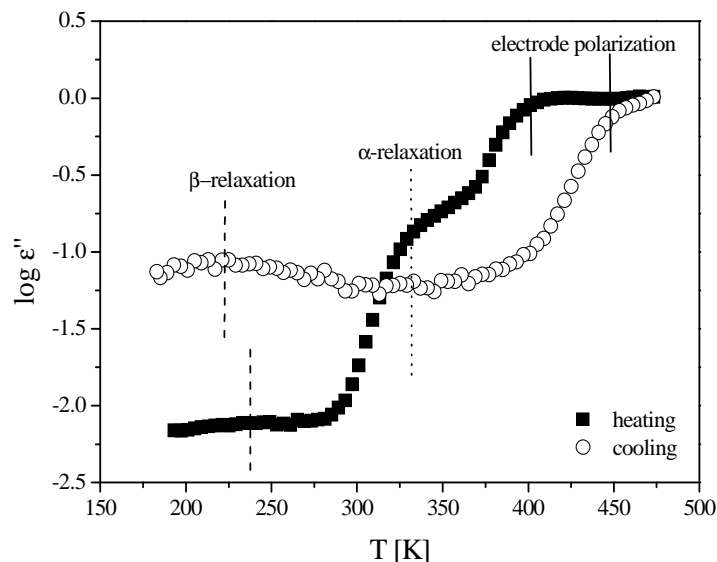


Figure 74: Dielectric loss  $\epsilon''$  versus temperature at frequency of 1 kHz for pulsed plasma copolymer for heating and cooling runs ( $DC=0.1$ )

Fig. 74 reveals that the dielectric loss is dramatically reduced in the range of  $\alpha$ -relaxation and electrode polarization. The hysteresis between the first heating and the cooling run can be explained by the following consideration. As discussed above during the plasma deposition of polymer a highly branched product with many free radicals is formed. [106,107] These free radicals were able to react with each other to form a more crosslinked network during heating. So, the  $\alpha$ -relaxation process seems to disappear and maximum peak of the electrode polarization shifted to high temperature indicating also a change in structure. Otherwise, the dielectric loss is dramatically increased in the range of  $\beta$ -relaxation.  $\beta$ -relaxation is assigned to the localized fluctuations of the carboxylic groups. The radicals which are generated during plasma polymerization process probably form some kind of bonds with COOH groups. So, it employs an important role to hinder localized fluctuation of COOH groups. Therefore the increase of the intensity of the  $\beta$ -process after heating run has to be attributed to increase the number density of free carboxylic groups.



## 4.2. Influence of the comonomer ratio

### 4.2.1. Kinetics of the copolymer deposition

To study the effect of the comonomer ratio on film deposition rate, duty cycle, pressure, power, and temperature were held constant.

The deposition rates were calculated from diagrams showing film thickness vs. deposition time, which lasted between 4 and 35 min, (see Fig. 75a). Acrylic acid deposited faster than styrene. As discussed above the double bond can be broken by only a 1 eV energy input ( $\text{R-CH=CH}_2 + \text{plasma} \rightarrow \text{R-CH}\cdot\text{-CH}_2\cdot$  or  $\text{R-CH=CH}_2 + \text{H}\cdot \rightarrow \text{R-CH}_2\text{-CH}_2\cdot$ ) and a normal chain-growth polymerization (chain propagation) process can be started maybe as a biradical process:  $\text{R-CH}\cdot\text{-CH}_2\cdot + 2 \text{R-CH=CH}_2 \rightarrow \cdot\text{CHR-CH}_2\text{—CHR-CH}_2\text{-CHR-CH}_2\cdot$ . However, the resonance of the benzene ring plays an important role for the stability of the vinyl group and therefore, it needs high energy to be activated. So, the deposition rate of PS was lower than that of PAA. <sup>[106]</sup> The copolymer deposition rate was found in the order of pure acrylic acid (Fig. 75b).

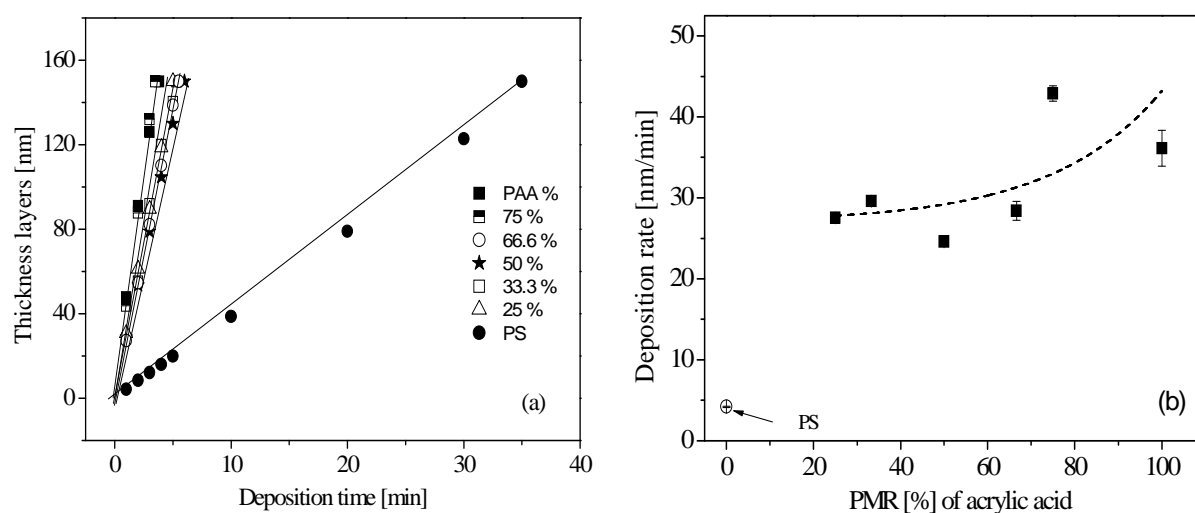
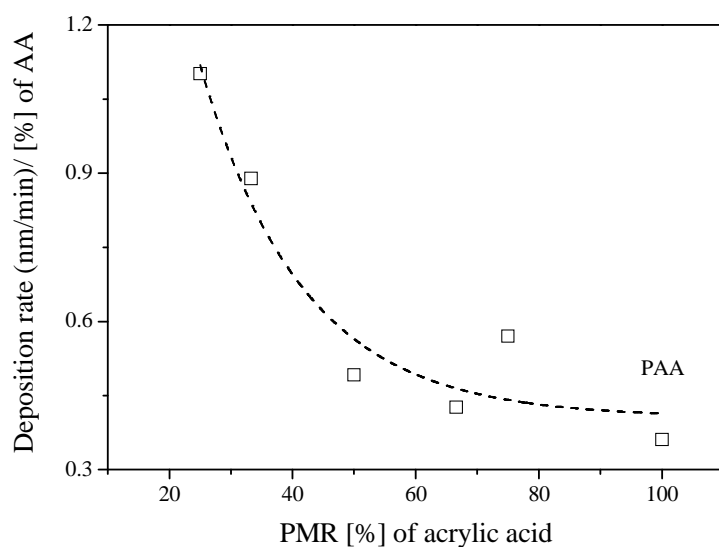


Figure 75: Thickness of the plasma (co)polymerized layer vs. deposition time for various comonomer ratios (a). The deposition rate of plasma deposited AA/S copolymers versus PMR [%] of acrylic acid (b)

The marked increase in the deposition rate for AA/S compared to the both monomers. The plasma chamber consists of acrylic acid and styrene as monomers vapour before plasma inlet. Additionally, an interaction between acrylic acid, an electron accepting monomer and styrene, an electron donating monomer can takes place.<sup>[180]</sup> So, the deposition rate of AA/S copolymer contains deposition rate for three compounds as discussed before.

To compare the deposition rates for the different precursor mixture directly, the deposition rate can be normalized by divided by the comonomer ratio of AA (Fig. 76).

Figure 76 shows that the normalized deposition rate of plasma deposited AA/S copolymer is maximal for the lowest ratio of acrylic acid monomer. This means that the rate for the chain propagation process is essentially higher for low ratio of the acrylic acid monomer. This might also imply that for low ratio of the acrylic acid monomer a more regular structure is formed.<sup>[106,107]</sup>



*Figure 76: Normalized deposition rate vs. PMR [%] of acrylic acid for plasma deposited AA/S copolymer*

#### **4.2.2. Retention of functional groups during copolymerization**

The estimation of functional groups on the surfaces is possible by derivatization and XPS-measurement of introduced labels. According to Figs. 58a and b and Table 8 that is some COO band assigned to ester-type.

Fig. 77 shows that the COOH groups grow with increasing fraction of acrylic acid in the precursor as might be expected. More details were discussed in the section AA/S copolymer with influence of DC. However, it's very low in comparison to plasma-polymerized PAA.

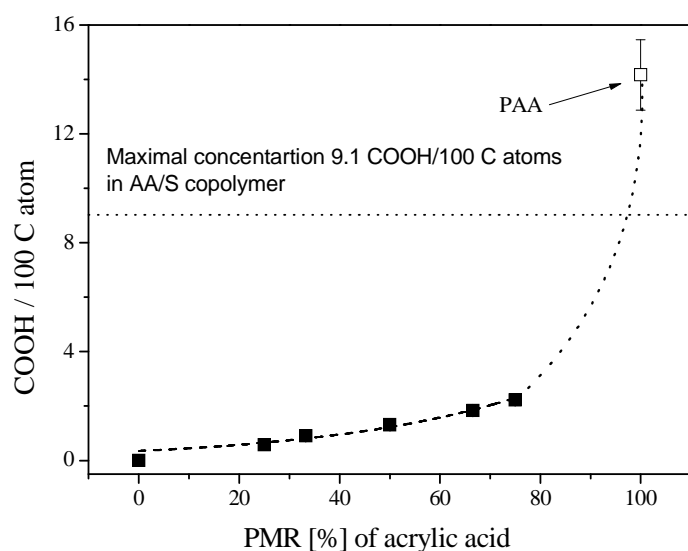


Figure 77: Concentration of the carboxylic groups per 100 C atoms after derivatization versus the comonomer ratio for plasma deposited AA/S copolymers (results from C1s peak deconvolution) compared to plasma deposited PAA homopolymers

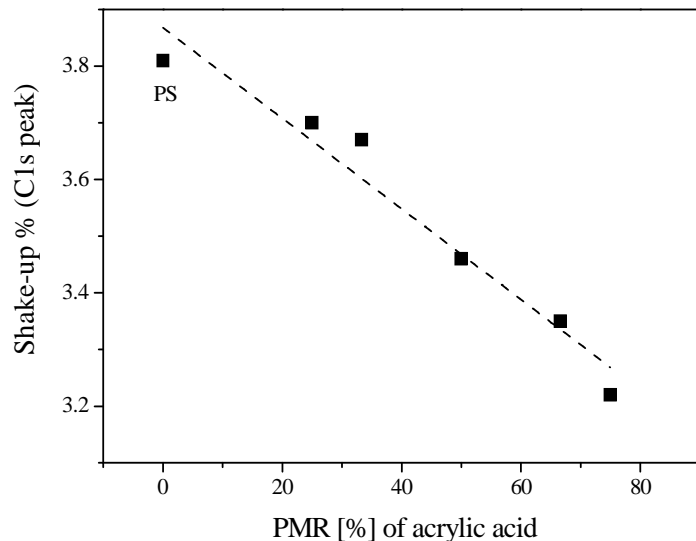


Figure 78:  $\pi$ - $\pi^*$  in plasma deposited AA/S copolymer films in dependence on the ratio of the comonomers from C1s deconvolution

For the plasma deposited copolymer, the number of detected COOH groups and benzene ring were found to be in the order of 1-2 COOH groups and 3-4 benzene rings (see Figs. 77 and 78). This point indicates to the fact that other processes are going on during plasma polymerization. However, the energy input leads to a fragmentation of the monomers fol-

lowed by poly-recombination as well as the concentration of the COOH groups and benzene rings are lower than that expected for the conventional copolymers.

However, the  $\pi \rightarrow \pi^*$  component increases due to growing parts of the aromatic rings on the surface as might be expected (Fig. 78).

#### 4.2.3. Investigation of the chemical composition by FTIR

Fig. 79 images the stretching vibration of the carbonyl group (C=O) in the region between  $1800\text{ cm}^{-1} - 1550\text{ cm}^{-1}$  for commercial poly(acrylic acid) PAA18 (MW 1800 g/mol) (Fig. 79a), plasma deposited PAA (Fig. 79b) and an AA/S plasma copolymer with PMR [%] of 66.6 acrylic acid (Fig. 79c).

A detailed examination reveals that this peak is quite complex and consists of two or more different contributions. Wang et al. [176] discussed three components with a maximum positioned at  $1685$ ,  $1715$  and  $1749\text{ cm}^{-1}$  measured in common poly(acrylic acid) and copolymers of acrylic acid with styrene as discussed above. The maximum position changed with respect to AA fraction in the copolymers. Dong et al. [181] inserted four components. The maxima observed at  $1686$ ,  $1705$ ,  $1725$  and  $1742\text{ cm}^{-1}$  were assigned to inner hydrogen bonded COOH groups of oligomeric COOH ( $1686\text{ cm}^{-1}$ ), C=O stretching of cyclic hydrogen bonded COOH (dimers;  $1742\text{ cm}^{-1}$ ), free COOH ( $1705\text{ cm}^{-1}$ ) and terminal groups COOH in oligomers ( $1725\text{ cm}^{-1}$ ).

Zhang et al. [182] observed the polymerization of acrylic acid on silicon oxide surfaces. The peaks at  $1636\text{ cm}^{-1}$  and  $1620\text{ cm}^{-1}$  were assigned to the C=C stretching vibration (of (unreacted) acrylic acid monomer) while the absorptions at  $1702$  and  $1730\text{ cm}^{-1}$  were assigned to the C=O stretching vibration of free and bonded COOH groups, respectively.

In accordance to Wang [176] three components were fitted to the data for common PAA. Fig. 79a shows the enlarged view in the wavenumber range of the C=O vibration for

cPAA. A detailed examination reveals that this band is quite complex and consists of three different contributions. The main component at  $1700\text{ cm}^{-1}$  is attributed to carbonyl stretching vibration ( $\text{C}=\text{O}$ ) of carboxylic groups. The second one with a shoulder at  $1664\text{ cm}^{-1}$  is related to the vibration of dimers formed by the  $\text{C}=\text{O}$  group. [142]

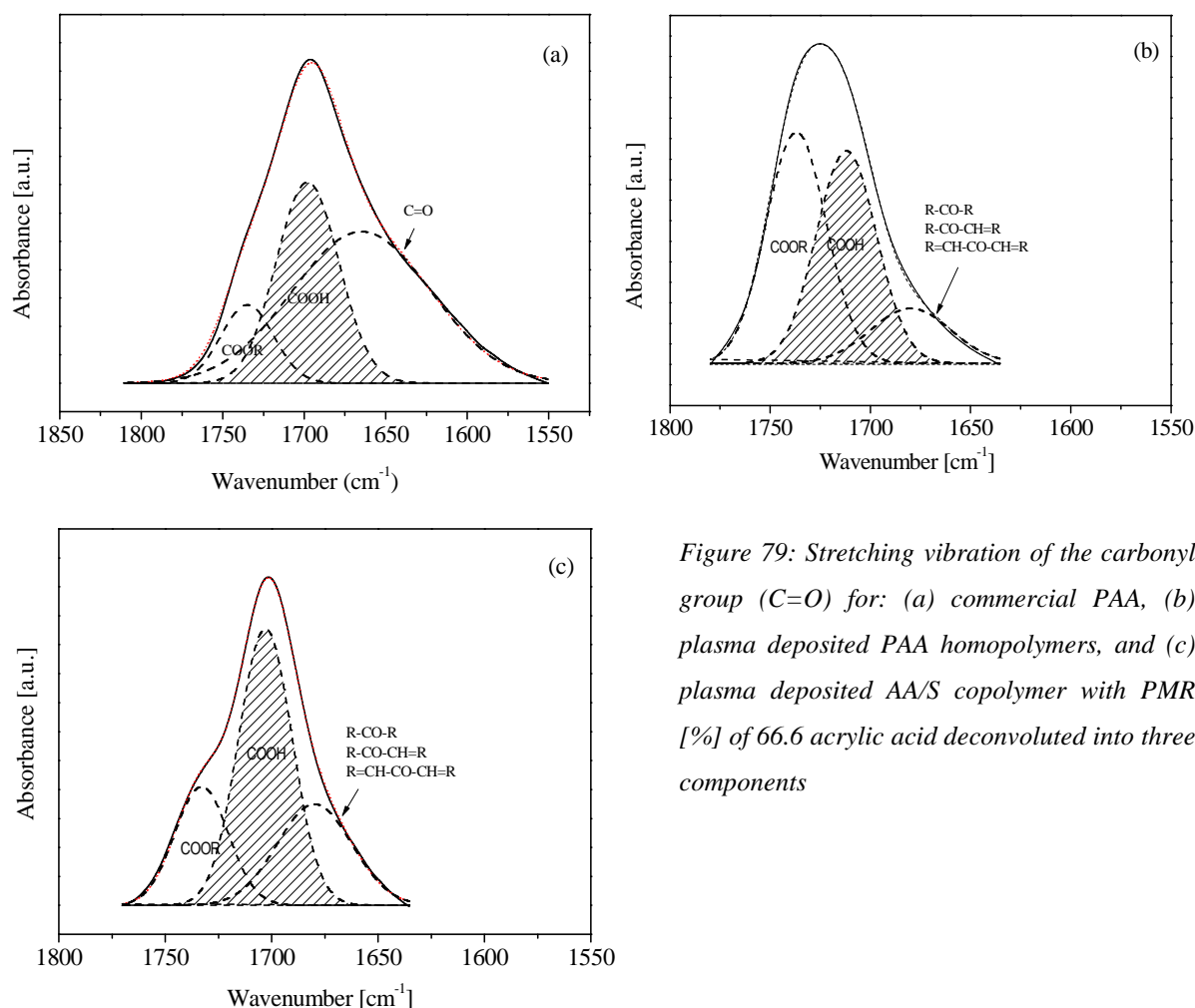


Figure 79: Stretching vibration of the carbonyl group ( $\text{C}=\text{O}$ ) for: (a) commercial PAA, (b) plasma deposited PAA homopolymers, and (c) plasma deposited AA/S copolymer with PMR [%] of 66.6 acrylic acid deconvoluted into three components

Finally, the band at  $1734\text{ cm}^{-1}$  is assigned to  $\text{C}=\text{O}$  stretching vibration of ester groups formed by self-condensation. [102] Fig. 79b shows the  $\text{C}=\text{O}$  region for plasma PAA compared to cPAA the main peak of the  $\nu(\text{C}=\text{O})$  is shifted from  $1700\text{ cm}^{-1}$  to  $1712\text{ cm}^{-1}$ . Furthermore, the band at  $\sim 1740\text{ cm}^{-1}$  indicates the formation of other bonds in addition to those expected for poly(acrylic acid) (COOH) like ketone or ester groups. [143] The band at  $1680\text{ cm}^{-1}$  is assigned to  $\nu(\text{C}=\text{O})$  from dimer,  $\text{C}=\text{C}$  as well as intermolecular hydrogen bonding.

The following procedure was employed to analyze the spectra quantitatively with three components fitted to the data. The maximum were appeared at  $1737\text{ cm}^{-1}$  (ester),  $1706\text{ cm}^{-1}$  ( $\text{C}=\text{O}$ ) corresponding to  $\text{COOH}$  group and  $1680\text{ cm}^{-1}$  (dimers) or  $\text{C}=\text{C}$  as well as inter-molecular hydrogen bond. From the XPS measurements it is known that  $\text{C}=\text{O}$ ,  $\text{COOH}$  and  $\text{COOR}$  groups are formed. In Fig. 79c the FTIR spectra of  $\text{C}=\text{O}$  for plasma-polymerized AA/S is displayed. Compared to plasma PAA the main peak of the  $\text{C}=\text{O}$  stretch is shifted from  $1712\text{ cm}^{-1}$  to  $1706\text{ cm}^{-1}$  and closed to cPAA. This indicates the change of the structure compared to those expected for plasma PAA ( $\text{COOH}$ ).

From the FTIR spectra the areas of  $\text{C}=\text{O}$  peaks at  $1706\text{ cm}^{-1}$   $A_{1706}$  and  $\text{CH}_2(\text{as})$  peaks at  $2917\text{ cm}^{-1}$   $A_{2917}$  were taken and the ratios were calculated as a measure for the concentration of the  $\text{COOH}$  groups estimated from FTIR.

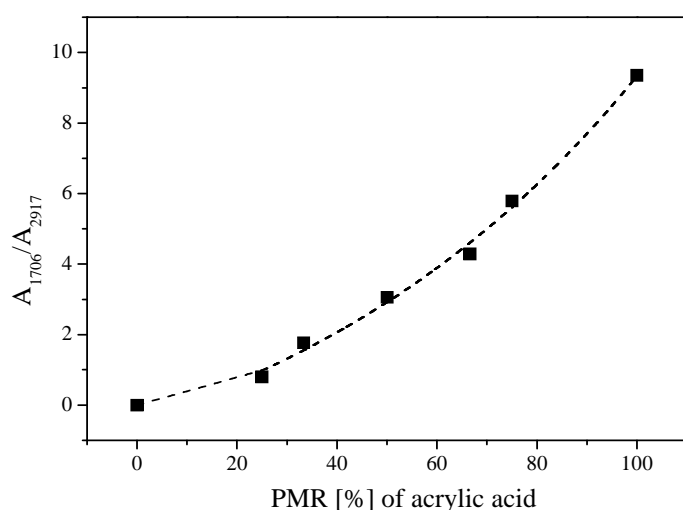


Figure 80: Concentration of  $\text{COOH}$  groups estimated from FTIR areas ratio  $A_{1706} / A_{2917}$  for plasma deposited AA/S copolymer films in dependence on the PMR [%] of acrylic acid

$\frac{A_{1706}}{A_{2917}}$  is plotted versus the ratio of the comonomers in Fig. 80. This Figure resembles a close similarity to the concentration dependence of  $\text{COOH}$  groups per 100 C atoms estimated from XPS measurements (Fig. 77). It shows that the concentration of  $\text{COOH}$  groups increases with increasing fraction of acrylic acid comonomer.

XPS und FTIR should provide analogue information about the concentration of COOH groups as contributed before. Therefore, Fig. 81 displays  $\frac{A_{1706}}{A_{2917}}$  as a concentration of COOH groups estimated from FTIR versus the concentration of COOH groups per 100 C atoms estimated from XPS measurements. It gives perfect a straight line.

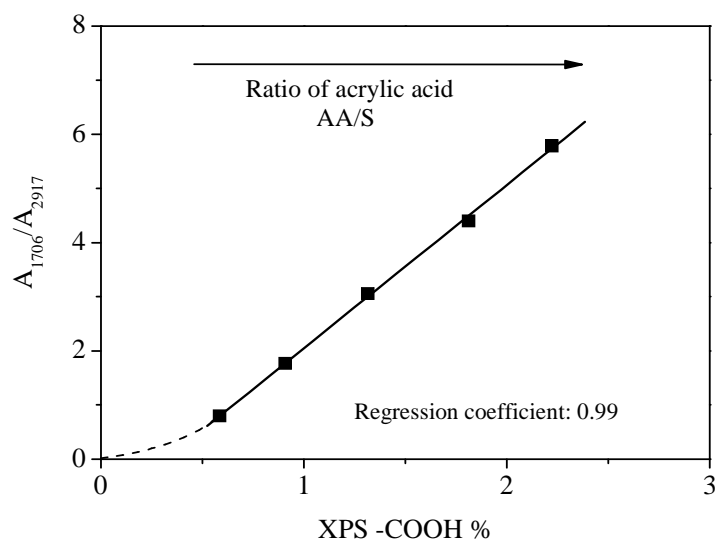


Figure 81:  $\frac{A_{1706}}{A_{2917}}$  versus the concentration of COOH per 100 C atoms estimated from the XPS measurements for plasma deposited AA/S copolymers

This means the concentration of COOH on the surface (XPS, 5-7 nm) and in the bulk (FTIR,  $\sim 2.5 \mu\text{m}$ ) is growing proportional with increasing fraction of acrylic acid in precursor.

Fig. 82 displays fractions of different C=O components with respect to the ratio of comonomer in precursor. It shows a constant level for all components until  $\sim 50\%$  PMR of acrylic acid. The free COOH component ( $\sim 1706 \text{ cm}^{-1}$ ) decreases and the COOR ( $1737 \text{ cm}^{-1}$ ) component increases with rising acrylic acid fractions, while the third component presenting R-CO-R/R-CO-CH=R/R=CH-CO-CH=R vibrations ( $1680 \text{ cm}^{-1}$ ) only slightly increases. This behaviour is possibly to explain with a lower concentration of styrene units in the copolymers approving stronger intermolecular hydrogen interactions (lower concentration of free COOH groups). Moreover, the styrene monomer maybe prevents fragmentation of the carboxylic groups of acrylic acid during the plasma polymerization process or vice versa. However, with

increasing ratio of styrene monomer the distance between the carboxylic groups isn't enough to develop intermolecular hydrogen bonds.

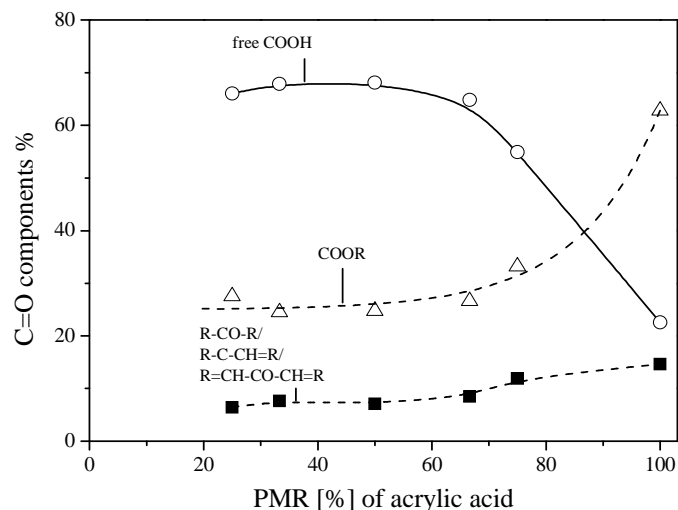


Figure 82: Area % for different components of C=O bands (fit results) of AA/S plasma deposited copolymer films in dependence on PMR [%] of acrylic acid

In Fig. 83  $\frac{A_{1493}}{A_{2917}}$  is plotted versus the ratio of the comonomer.

This graph shows that the concentrations of  $C=C_{arom}$  groups at  $1493\text{ cm}^{-1}$  increase with increasing the ratio of styrene comonomer in relation to the concentration of  $CH_2$  (as) at  $2917\text{ cm}^{-1}$ , as expecting.

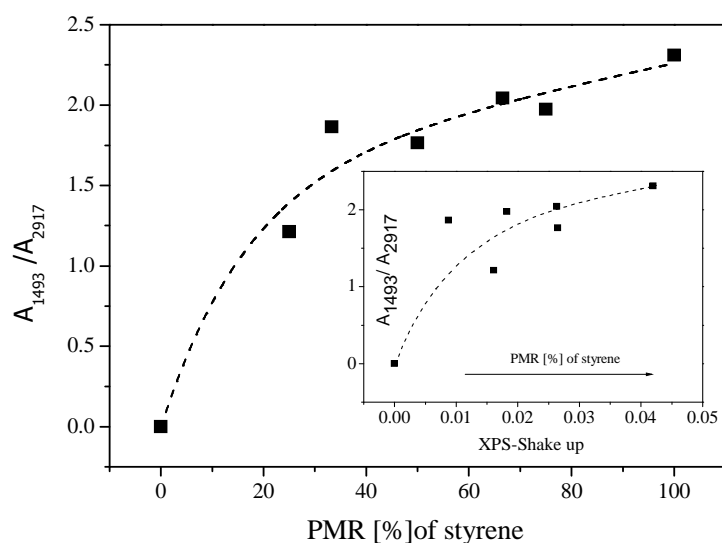


Figure 83: Measure concentration of C=C groups estimated from FTIR areas ratio  $A_{1493}/A_{2917}$  of AA/S plasma deposited copolymer films in dependence on the PMR [%] of styrene. The inset gives  $A_{1493}/A_{2917}$  versus the concentration of  $\pi-\pi^*$  estimated from the XPS measurements



As discussed above XPS and FTIR should provide the same information about the concentration of the  $C=C_{\text{arom}}$  groups. Therefore, the inset of [Figure 83](#) displays  $\frac{A_{1493}}{A_{2917}}$  versus the concentration of  $\pi-\pi^*$  related to  $C=C_{\text{arom}}$  groups estimated from the XPS measurements. From the theoretical point of view a constant value should be obtained. This graph shows that an approximately linear dependence between both concentrations is observed.

To discuss this result the different analytical depth of both methods has to be considered. XPS is sensitive to a layer with a thickness of 5 to 7 nm whereas FTIR provides information across the whole sample thickness. For a more extended discussion see refs. [\[106,107\]](#).

#### 4.2.4. Thermal analysis

[Fig. 84a](#) compares the DSC curves for plasma AA/S copolymer deposited with respect to the composition of the feed gas mixture. For each material a step-like change in the heat flow is observed which indicates the glass transition. The glass transition temperature  $T_g$  is estimated from the inflection point of the heat flow and plotted versus the PMR [%] of AA in [Fig. 84b](#).

Firstly, as argued above for all plasma deposited PAA, PS and AA/S (co) samples the  $T_g$  values are lower than those for conventional PAA and polystyrene. It is concluded that plasma polymerization technique results in products with a lower molecular weight as well as a highly branched structure with many dangling ends is formed. These dangling ends lead to a decreased  $T_g$ .

Secondly the glass transition temperature of the plasma deposited copolymer is also lower than that of PAA (see [Fig. 84b](#)). It is likely that, the introduction of the bulky styrene units increases the free volume and also avoids the formation of hydrogen bonds. Both effects will

lead to a reduction of the glass transition temperature. So,  $T_g$  of AA/S copolymer increases with increasing PMR [%] of AA monomer. This behaviour confirms the results that obtained by XPS and FTIR measurements.

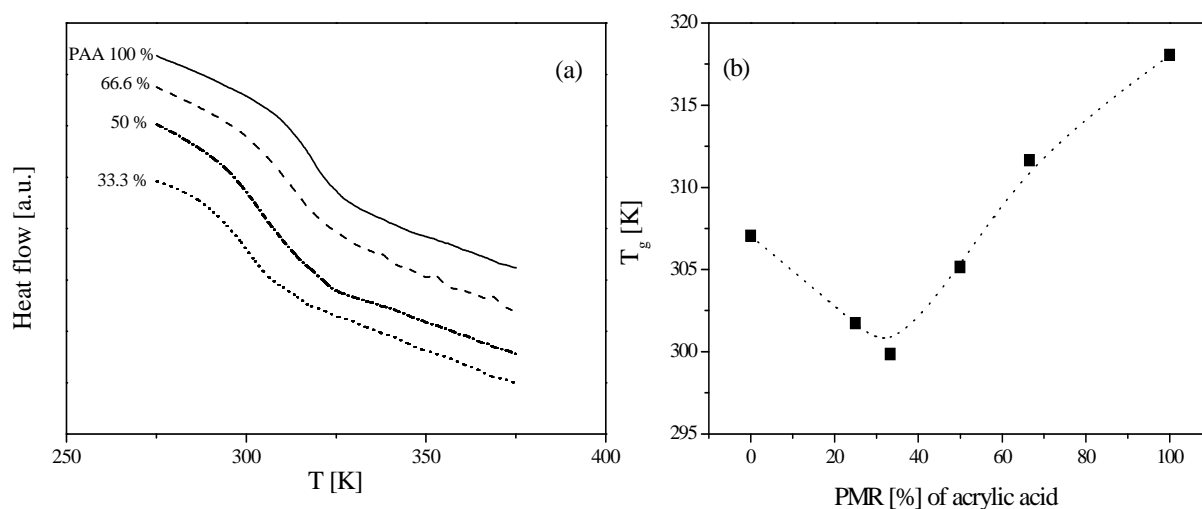


Figure 84: Heat flow of plasma deposited AA/S copolymers in dependence on the temperature for the labeled PMR [%] of acrylic acid values (2<sup>nd</sup> heating run) (a).  $T_g$  values versus PMR [%] of acrylic acid on 2<sup>nd</sup> heating process (b)

As argued for the deposition rate, the rate for the chain propagation process is essentially higher for low acrylic acid comonomer in precursor mixture. However, the increase of the COOH groups leads to increase of hydrogen bonds. The latter leads to decrease in the concentration of the free COOH groups as well as in an increase of crosslinking. Especially, the increase of the crosslinking leads to an increased  $T_g$ .

#### 4.2.5. Dynamic mobility and thermal stability

In previous sections XPS and FTIR the measured and the theoretically expected compositions, especially the number of functional groups of copolymers were found to be very similar. However, first the stability of copolymers was measured again using dielectric relaxation spectroscopy for measuring the molecular dynamics of thin polymer films and investigat-

ing of the polymer bulk to characterize the regular and irregular structures, estimation of the  $T_g$  and thermal stability.

The dielectric loss in the temperature range of the  $\beta$ -process is plotted versus temperature at a fixed frequency (1 kHz) for different values of the comonomer ratio in Fig. 85. In plasma deposited PAA homopolymers a well defined  $\beta$ -relaxation is observed which decreases an intensity with decreasing PMR [%] of AA monomer. For 50 % this relaxation process disappears practically completely. In plasma deposited PAA <sup>[106]</sup> the  $\beta$ -relaxation is assigned to the localized fluctuations of the carboxylic groups as argued before. Therefore, the decrease of the intensity of the  $\beta$ -process with decreasing value of PMR [%] of AA monomer has to be attributed to decrease the number density of carboxylic groups. This line of argumentation is in complete agreement with the XPS and FTIR investigations.

At higher temperatures, in the range of the glass transition measured by DSC an ill-defined shoulder is visible which corresponds to the dynamic glass transition ( $\alpha$ -relaxation) in polymers and copolymers on heating up.

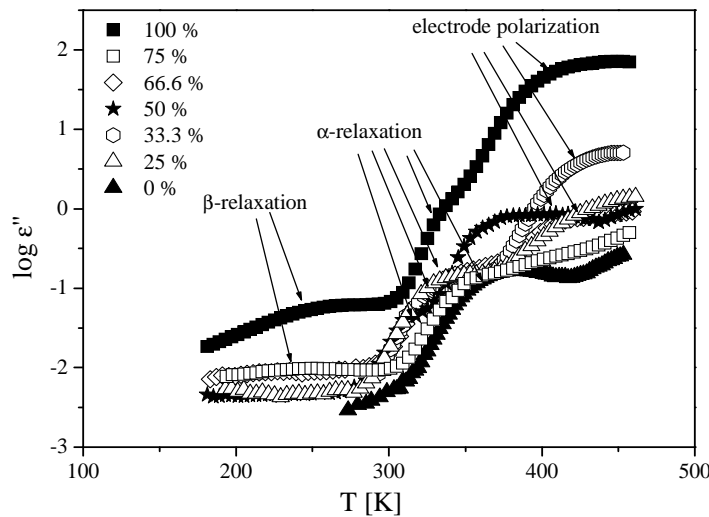


Figure 85: Dielectric loss vs. temperature at a fixed frequency of 1 kHz of the plasma deposited sample AA/S copolymer in dependence on the PMR [%] of acrylic on heating

The temperature dependence of the relaxation rate  $f_{p, \alpha}$  of the  $\alpha$ -relaxation is non-linear versus inverse temperature and can't be described by (VFT) Equations (10).

Fig. 86a shows the fit of relaxation rate  $f_{p,\alpha}$  is deduced in there temperature dependencies.

To discuss this behaviour one has to bear in mind that during the plasma polymerization a large number of radicals are formed which do not react completely during the deposition process. After deposition these radicals are quenched and the deposited layer is in a metastable but non-equilibrium state. By heating up the segments become mobile at the glass transition these radical undergo a post-plasma reaction. Therefore, this structure in the temperature dependence is related to the kinetics of the chemical reaction that takes place during the heating process. Fig. 86b displays the dynamic  $T_g$  decreases with increasing the ratio of styrene monomer.

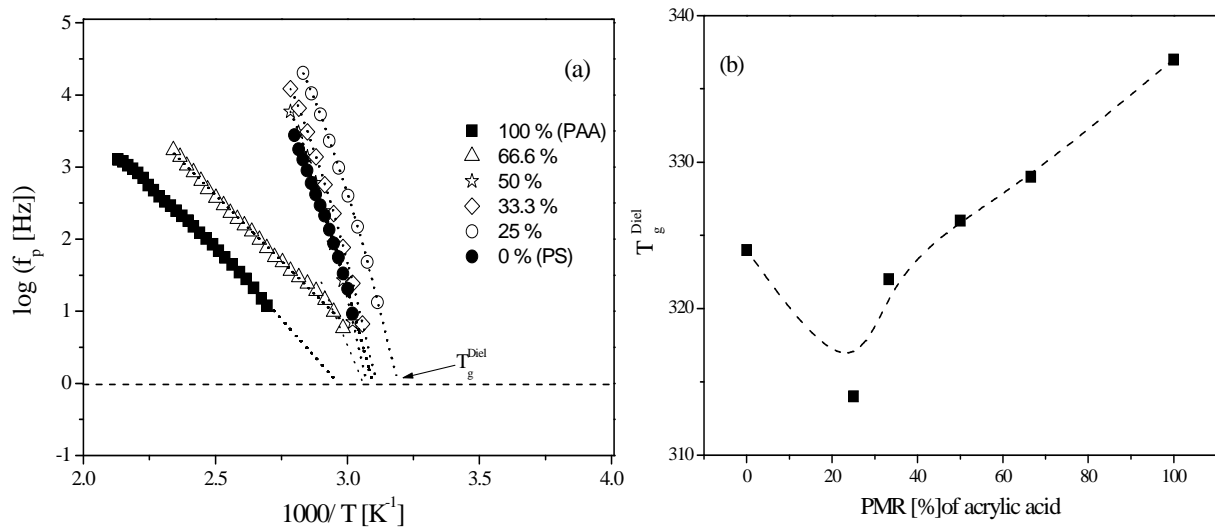


Figure 86: Relaxation rate of the  $\alpha$ -process versus inverse temperature for plasma deposited AA/S copolymers for different PMR [%] of acrylic acid for 1<sup>st</sup> heating process (a). Dynamic glass transition temperature  $T_g^{\text{Diel}}$  versus PMR [%] of acrylic acid (b)

This behaviour is similar to that obtained by DSC. Firstly, the dielectric spectroscopy measures the glass transition for these systems. Secondly, this behaviour can be discussed in the same way like for the DSC measurements and the results that obtained by monitoring the deposition rate, XPS, FTIR and DSC measurements are consistent. The possibility of the formation of hydrogen bonds is strongly reduced for the AA/S plasma deposited copolymers.

However, the distance between the chains increases due to the presence of the styrene repeat units. Therefore, the crosslinking decreases which leads to a decrease of the  $T_g^{\text{Diel}}$ .

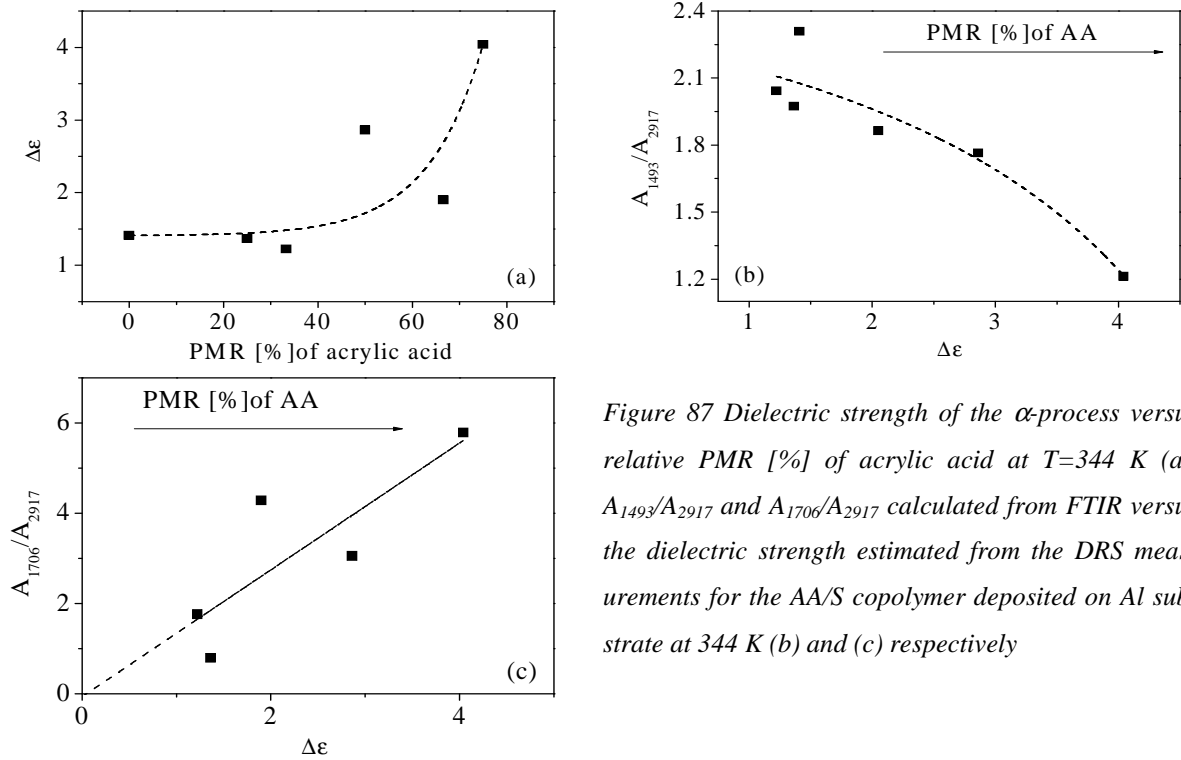


Figure 87 Dielectric strength of the  $\alpha$ -process versus relative PMR [%] of acrylic acid at  $T=344$  K (a).  $A_{1493}/A_{2917}$  and  $A_{1706}/A_{2917}$  calculated from FTIR versus the dielectric strength estimated from the DRS measurements for the AA/S copolymer deposited on Al substrate at 344 K (b) and (c) respectively

Fig. 87a gives the dielectric strength  $\Delta\epsilon$  for the  $\alpha$ -process versus of the PMR [%] of AA at 344 K. As it is well known for mobility of ions which related to the dielectric strength ( $\Delta\epsilon$ ),  $\Delta\epsilon$  increases with increasing the ratio of AA monomer. According to equation (8),  $\Delta\epsilon$  is related to the number density of the dipoles corresponding to COOH groups.

Dielectric spectroscopy and FTIR should provide similar information about the concentration of the functional groups. Therefore, Figs. 87b and c display  $\frac{A_{1493}}{A_{2917}}$  and  $\frac{A_{1706}}{A_{2917}}$  for the

AA/S copolymer deposited on Al substrates calculated from FTIR versus the dielectric strength estimated from DRS measurements at 344 K. The dielectric strength of  $\alpha$ -relaxation is due to the segmental motion of chain. Carbonyl groups and phenyl groups employ an important role for this behaviour.

Fig. 87b shows that an approximately curve dependence between both quantities is observed. The analysis of the FTIR measurements provides information only about the concentration of  $C=C_{\text{arom}}$  groups related to the benzene ring. The  $\frac{A_{1493}}{A_{2917}}$  decreases with increasing  $\Delta\epsilon$  (this means with decreasing the PMR [%] of styrene) are an expression of the fact that with increasing the PMR [%] of styrene, the number of dipoles corresponding to COOH groups is decreased.

On the other hand Fig. 87c shows that an approximately linear dependence between both quantities is observed. To discuss this result the different sensitivities of both methods have to be considered. The analysis of the FTIR measurements as discussed above provides information only about the concentration of COOH groups. Dielectric spectroscopy measures an effective dipole moment which can include other functional groups like C=O, C-O-C, COOR, COOH, phenyl etc. which can be created during the plasma polymerization process.

$\frac{A_{1706}}{A_{2917}}$  increases with increasing  $\Delta\epsilon$  proportionally for plasma deposited AA/S copolymer.

To discuss the dielectric behaviour for AA/S plasma deposited copolymers in more details, different thermal histories were studied. Fig. 88 gives the behaviour of AA/S (50 % PMR of acrylic acid as an example) in case of heating up, cooling down then followed by 2<sup>nd</sup> heating up. For all cases at low temperatures the  $\beta$ -relaxation isn't observed as a well defined peak in the spectra. For the first heating run a shoulder is observed at higher temperatures than that of the expecting for  $\beta$ -relaxation which corresponds to the  $\alpha$ -relaxation.

However, the dielectric loss is dramatically reduced in the range of  $\alpha$ -relaxation for the cooling run compared to the 1<sup>st</sup> heating run. Moreover, the electrode polarization is shifted to higher temperatures. This hysteresis between the first heating and the cooling run can be explained by the following consideration. As discussed above during the plasma deposition of polymer a highly branched product with many free radicals is formed. [106,107] These free radi-

cals were able to react with each other to form a more cross-linked network during heating. So, the  $\alpha$ -relaxation process seems to disappear and maximum peak of the electrode polarization shifted to high temperature indicating also a change in the structure. Otherwise, the dielectric loss is increased in the range of  $\beta$ -relaxation. As discussed above the  $\beta$ -relaxation is assigned to the localized fluctuations of carboxylic groups. Therefore, the increase of the intensity of the  $\beta$ -process after heating run has to be attributed to increase the number density of free carboxylic groups.

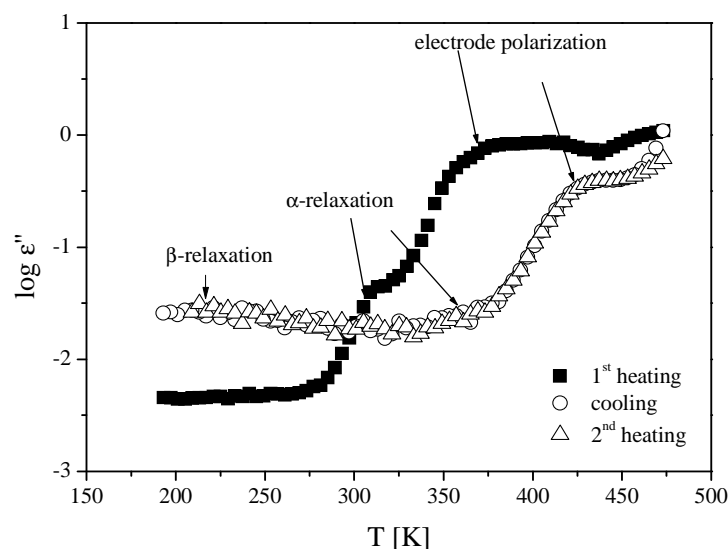


Figure 88: Dielectric loss  $\varepsilon''$  versus temperature at a frequency of 1 kHz for pulsed plasma copolymer with 50 % PMR of acrylic acid on different thermal histories

This line of argumentation leads to the hypothesis that the plasma-synthesized products are not thermally stable because the unsaturated radicals can react at high temperatures. [106] After the first heating run thermal stability is evidenced by the fact that there is no difference in the dielectric spectra.

The dielectric spectra are analyzed fitting the model function of Havriliak and Negami (HN-function (9)) to the data also in this case.

The process observed at higher temperatures than that of the  $\alpha$ -relaxation has a quite high intensity. There seems to be no dipole moments in the sample which can cause a dielectric re-

laxation process such a high dielectric strength. For that reason and considering the fact that also the plasma deposited AA/S copolymer has a high conductivity this process is assigned to electrode polarization.

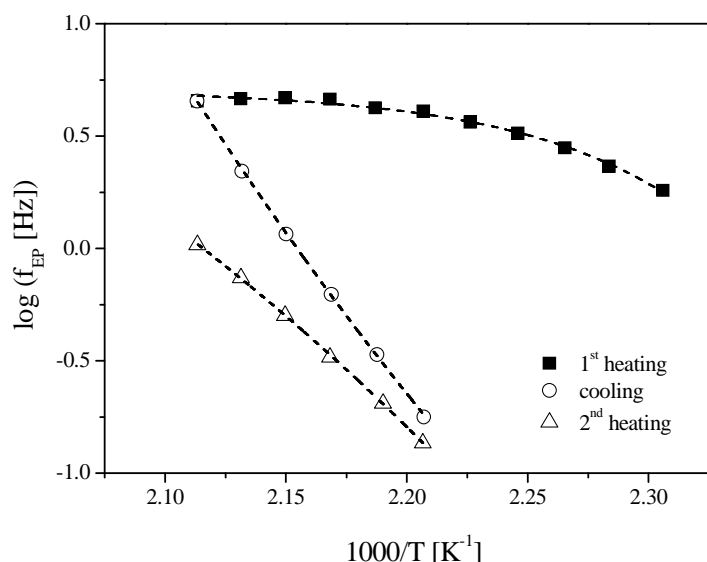


Figure 89: Relaxation rate of the electrode polarization  $f_{EP}$  vs. inverse temperature dependence on the comonomer ratio for the heating process. The inset gives  $f_{EP}$  vs.  $1/T$  for the sample 50 % PMR of acrylic acid for 1<sup>st</sup> heating, cooling and 2<sup>nd</sup> heating

Fig. 89 gives the temperature of the rate of electrode polarization  $f_{EP}$  in the Arrhenius diagram for the sample 50 % PMR of acrylic acid for 1<sup>st</sup> heating, cooling and 2<sup>nd</sup> heating. Firstly, as expected from Fig. 88 there is a strong hysteresis between heating and cooling which is due to chemical reaction processes within the sample. Secondly, a closer inspection of the temperature dependence of  $f_{EP}$  obtained for heating reveals that this dependence is monotonous and carries some structure. This structure is related to the kinetics of the chemical reaction that takes place during the heating process. Thirdly, the temperatures dependence measured for  $f_{EP}$  during cooling is shifted to higher temperatures compared to the dependence measured for heating. The temperature of  $f_{EP}$  is related to the mobility of the charge carriers which is connected to segmental mobility. The shift to higher temperatures for the cooling run therefore indicates a lower segmental mobility and higher glass transition temperature of the AA/S copolymer layer obtained during heating. These points related to a cross-linked structure.



## Chapter 4

### Conclusions

Poly(acrylic acid) were deposited by pulsed plasma polymerization as a thin films. The structure-property relationships of these samples were studied with respect to the duty cycle of the plasma by a broad combination of different techniques and probes.

The dependence of the deposition rate versus DC is non-linear. The deposition of the plasma polymer due to the activation of the double bond of acrylic acid as regular structures (radical polymerization under low pressure conditions). Additionally, a fragmentation of the monomer takes place followed by a poly-recombination which leads in general to irregular, unsaturated radicals or branched structures depending on duty cycle. Especially at low DC values, the chain growth polymerization (classic propagation) is the dominating step. In addition to these processes a depolymerisation and a partial detachment of the deposited layer can take place.

XPS measurements in combination with a derivatization technique are employed to estimate the concentration of carboxylic groups in dependence on the surface of films. These investigations show that only a part of the maximal possible number of COOH is detected. Moreover, the concentration of carboxylic groups decreases with increasing of DC. This result is discussed in the framework of an increasing fragmentation of the acrylic acid with increasing DC. To compare the concentration with that in the bulk, FTIR spectroscopy is employed by applying detailed band analysis. In general, FTIR spectroscopy gives the same dependence of the concentration of COOH groups on DC like XPS. The concentration of COOH groups in the volume decreases with increasing DC in comparison with that of the surface carboxylic groups. These observed differences are discussed considering the different analytical depths of both methods.

The combination of dielectric relaxation spectroscopy (DRS) and differential scanning calorimetry (DSC) give information about the bulk behaviour and thermal stability of the film with respect to DC. The dielectric measurements reveal that the structure of the plasma deposited polymers is different from that of the bulk material. These investigations indicate that, plasma deposited PAA has a highly branched structure with many dangling ends which may act as internal plasticizer. Poly(acrylic acid), which is already polymerized, might be more and more damaged with increasing DC at a farther distance from the surface. The number of these dangling ends increases, which leads to a decreased glass transition temperature. Therefore, the molecular mobility of PAA films deposited at low duty cycles is more related to conventional poly(acrylic acid) than for higher values of DC.

Moreover, the dielectric measurements show that the plasma deposited films are not thermally stable but undergo a post-plasma chemical reaction during heating where the reaction kinetics depends on DC. The chemical reaction is evidenced by the fact that there is a strong hysteresis in the dielectric spectra between the first heating and the subsequent cooling run. For the 2<sup>nd</sup> heating the data agree with the first cooling run which indicates a thermal stability after the chemical reaction.

Dielectric spectra show at high temperature a process with a quite high intensity considering the fact that also, the plasma deposited PAA has a high conductivity. This process is assigned to electrode polarization (EP). The temperature dependence measured for its characteristic rate  $f_{EP}$  is quantitatively analyzed. As  $f_{EP}$  is related to the mobility of charge carriers this analysis provides information about the reaction kinetics.

Thin PAAI films were deposited by pulsed plasma polymerization on different substrates (organic and inorganic). The structure-property relationships of allyl alcohol polymers were studied in dependence on DC by various techniques and probes. The dependence of the deposition rate on the DC was found to be non-linear.

XPS measurements were accomplished to analyse the chemical surface composition of the deposited films. A derivatization technique in combination with XPS measurements were used to get information about the hydroxyl group concentration of the plasma deposited PAAI. FTIR-ATR measurements were carried out to compare the OH concentrations at the surface and the bulk.

It was found that the concentration of hydroxyl groups on the surface decreases with increasing DC. A similar trend was found for the volume bulk. The depiction of the OH concentration measured by XPS and FTIR analysis of the area ratio of OH band/CH<sub>2</sub> band showed a negative slope with growing DC. The differences observed are discussed considering the different analytical depths of both methods. The results suggest a possible allyl alcohol polymerization in comparison to depolymerization of the deposited plasma polymer layer during the deposition process. The effective energy increases with increasing DC. PAAI might be damaged at a farther distance from the surface which is already polymerized due to this energy.

PAAI deposited on different substrates revealed a shift of the OH band maximum up to 60 cm<sup>-1</sup> to higher wavenumbers in the order AAI- monomer >PP>PE>glass>aluminium. The shift hints to a possible interaction between PAAI deposits and substrate.

The dielectric measurements reveal that the structure of the plasma deposited polymer is dependent on the DC. With increasing DC, the fragmentation and poly-recombination (free radicals cross-linking) was increased and leads to an increased T<sub>g</sub>.

Moreover, the dielectric measurements show that the plasma deposited PAAI films are also not thermally stable but undergo a post-plasma chemical reaction during heating where the reaction kinetics depends on the DC. The chemical reaction is evidenced by the fact that there is a strong hysteresis in the dielectric spectra between first heating subsequent cooling run. For 2<sup>nd</sup> heating the data agrees with cooling run which is indicated by thermal stability after the chemical reaction like that observed for PAA.

Dielectric investigations also show at higher temperature a process with a quite high intensity. By considering the fact PAAI has conductivity, this process is assigned to electrode polarization (EP). The temperature dependence measured for the characteristic rate  $f_{EP}$  related to the mobility of charge carriers is quantitatively analyzed and it provides information about the reaction kinetics.

O<sub>2</sub>, Ar plasma treatment and UV irradiation from Ar plasma filtered by a quartz window ( $\lambda < 180$  nm) are chosen to study the effects of short-time exposure (1 s) to plasma or UV on spin-coated and untreated commercial PS surfaces and bulk compared to plasma-produced thin films of PS and cPS. The effects of O<sub>2</sub>, Ar plasma and UV irradiation on polystyrene within 1 s were sufficient to modify surface and also surface-near layers. Thus, this study could be important to understand the effect of plasma on the different phases of plasma polymerization. Interactions between the surface and these reactive species (such as radicals, ions and metastable species) can modify the physicochemical properties of the surface. The effects of plasma treatments on the functionalization were compared.

In terms of the variation of the surface energy, the oxygen containing and Ar plasmas show identical effects evidencing the dominance of an oxidation process using oxygen plasma which is the same as for auto-oxidation after Ar plasma exposure. Both plasmas indicate that the upper monolayer of the polystyrene film can be functionalized rapidly. The surface energy and the surface functionalization of the spin-coated PS treated with the plasma Ar and UV as well as the plasma-synthesized PS are close to the commercial PS when they were compared in terms of oxygen introduction. The effect of the UV of a long wavelength was limited while the sufficient energy for any bond scission (8 eV in maximum) on structural modifications of PS. The surface of plasma PS films has more or less similar properties like that obtained by conventional PS. However, the water CAM of the treatment of PS with Ar and O<sub>2</sub> plasma were reduced significantly. O<sub>2</sub> and Ar plasma leads to the transformation of PS surface from hydrophobic to hydrophilic.

The dielectric strength  $\Delta\epsilon$  of plasma deposited PS was a high value reference to cPS. This is expected because the dipole moment of plasma-deposited PS should be higher than that of cPS. It is concluded that the increasing concentration of free radicals and oxygen-containing groups post-plasma introduced by auto-oxidation, leads to a decrease of the molecular mobility. It was speculated that hydrogen bonds and dipole-dipole interactions fix neighbored chains, which is often called “semi-crystallization”. On the other hand, for PS exposed to the O<sub>2</sub> plasma an increase in  $\Delta\epsilon$  was expected in comparison to PS treated by Ar plasma and UV irradiation, plasma-generated PS and cPS (from XPS and FTIR results), which is interpreted as an increase of the dipole moment  $\mu$  at high concentrations of OH groups and so on. But it showed that  $\Delta\epsilon$  of plasma PS is very high compared to others. The dielectric spectroscopy is a ‘bulk method’ and this result points to a homogeneous composition of the layers.

The plasma deposited PS film prepared at desired plasma conditions, except being branched and/or crosslinked, is chemically similar to the PS reference sample in terms of XPS and FTIR results. However, the dielectric measurements reveal that the structure of thin plasma polymer PS films is different in comparison to cPS. Moreover, the dielectric measurements show also that the plasma deposited films are not thermally stable and undergo a post-plasma chemical reaction during heating. The chemical reaction is evidenced by the fact that there is a strong hysteresis in the dielectric spectra between the first heating and the subsequent cooling run. For the 2<sup>nd</sup> heating the data agrees with the first cooling run which is indicated by thermal stability after the chemical reaction during first heating similar to that observed for PAA and PAAI plasma deposited. The conclusion may be drawn that annealing may be a proper method to improve the thermal stability of plasma polymers.

In general, the observations may be summarized as follows: The chemical structures of the plasma deposited films are different from the structure of the classic reference polymers. This is because all plasma deposited films are irregular, possessing unsaturated radicals,

double bonds, branched and/or cross-linked structure to some extent. These common trends are attributed to a higher degree of fragmentation and re-arrangement of the monomer molecules in the plasma.

AA/S (co)polymers were deposited by pulsed-plasma polymerization. The structure of these polymers was studied with respect to DC of the plasma.

In addition to the normal chain-growth polymerization (chain propagation) process also a fragmentation of comonomers takes place followed by a poly-recombination process, which leads to irregular, unsaturated radicals, formation of C=C double bonds, branched and/or crosslinked structures due to the plasma-initiated. It was shown that for low DC the chain growths polymerization is the dominating process. The deposition rate of AA/S copolymer contains deposition rates for three compounds. These compounds are acrylic acid and styrene as monomers vapour before plasma inlet. Additionally, an interaction between acrylic acid, an electron accepting monomer and styrene, an electron donating monomer can take place. Therefore, the deposition rate for AA/S copolymer is high compared to both monomers.

XPS in combination with derivatization technique was employed to estimate the concentration of carboxylic groups in plasma-polymerized AA/S copolymer. These investigations show that only a part of COOH groups present in the introduced acrylic acid is detected. As expected, the concentration of survived carboxylic groups decreases with DC. For acrylic acid and its polymer decarboxylation may be possible in plasma ( $R-COOH + plasma \rightarrow R-H + CO_2$ ), also decarbonylation (Norrish) and total fragmentation in case of high specific plasma energy. Styrene may react by cleavage of phenyl rings under plasma exposure. <sup>[183,184]</sup> To compare the COOH-concentration at the surface and in the surface-near layer XPS and FTIR results were compared. The concentration of COOH groups decreases as well on surface as in bulk with increasing DC.

It was found that, the concentration of carboxylic groups on the surface decreases with increasing DC. A similar trend was found for the volume. The depiction of the COOH concentration measured by XPS and FTIR analysis of the area ratio of COOH band/COOR band showed a negative slope with growing DC. The results suggest a possible AA/S copolymerization in comparison to depolymerization of the deposited plasma polymer layer during the deposition process. The effective energy increases with increasing DC. AA/S copolymers might be damaged at a farther distance from the surface which is already polymerized due to this energy. Therefore, the concentration of COOH groups for DC=1 is very low at the surface in comparison to that in the bulk.

The concentration of COOH groups in relation to that of COOR groups is higher in plasma deposited AA/S copolymer than in the plasma deposited PAA homopolymers. It is likely that, due to the longer distance between two neighbored COOH groups and therefore, a hampered self-condensation leads to the higher concentration of COOH groups in the copolymer.

DRS and DSC give information about the bulk behaviour and thermal stability of the film in dependence on DC. It was found that the crosslinking is lower for plasma AA/S copolymer in comparison to that of plasma PAA homopolymers. Furthermore,  $\alpha$ -relaxation in DRS results was observed which is related to the segmental fluctuations of the styrene repeat unit.

Moreover, the dielectric measurements show that the plasma deposited AA/S- copolymer films are not thermally stable but undergo a post-plasma chemical reaction during heating. Radical-radical recombination ( $R_1\bullet + \bullet R_2 \rightarrow R_1-R_2 + \Delta$ ) may occur or auto-oxidation ( $R\bullet + \bullet O-O\bullet \rightarrow R-O-O\bullet \rightarrow$  hydroperoxides  $\rightarrow$  oxidized products). The occurrence of chemical reactions is evidenced by a strong hysteresis in the dielectric spectra between heating and the subsequent cooling run.

Through a careful selection of the feed gas composition, plasma copolymerization can be used to control the concentration of surface functional groups in plasma deposited films. The chemical structure of the plasma deposited copolymer films are partially different from the structure of the respective plasma homopolymers, i.e., the nature of plasma copolymers might not be straightforwardly predicted by a detailed knowledge of the structure of these homopolymers. These results can be explained by the chemical interactions and recombination reactions taking place between monomer molecules in the plasma and/or during the deposition process.

The structure of acrylic acid-styrene (AA/S) plasma copolymers as thin films fortifies the continuing interest in achieving controlled surface functionalization. As well as volume sensitive methods (FTIR, dielectric spectroscopy, and differential scanning calorimetry) were combined with surface analytics by employing XPS.

The concentration of carboxylic groups increases (measured by the XPS) with increasing fraction of acrylic acid in the comonomer precursor mixture. This result is discussed in context with defragmentation of the acrylic acid. To compare the surface and bulk concentration of COOH groups detailed band analysis of the FTIR spectra was applied.



## Fields of Application

### 1. Thin films (micro...)

*Protective coatings:* Against mechanical stress (scratch and wear resistance, hardness)

Against chemical attack (corrosion and solvent resistance)

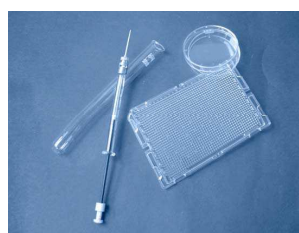
*Coatings with specified transport properties:*

- Optical transport (lenses, mirrors, waveguides, etc...)
- Electrical transport (conductive and dielectric layers, etc...)
- Material transport
- Material specific permeation (separation membranes)

*Material transport out of layer- systems:* Defined release (***in medicament as antibacterial agent***) dosage systems.


### 2. Ultra-thin films (nano...)

- Tailored surface energy (wettability water repellency) (solid-liquid-gaseous)
- Tailored contact between polymers and other phases:
- Static: solid-solid, (Adhesion)
- Dynamic: solid-(liquid)-solid (tribology)
- Interaction with biological systems (binding and adsorption of biomolecules, biocompatible or bioactive surfaces)
- Separation membranes and ion-exchange materials
- Basic research and analytical methods
- Thin plasma films deposited for diagnostics and therapy. It was replacement of glass in medicine and pharmacy.



## CURRICULUM VITAE

### 1) Personal Information

Name	Alaa Fahmy Mohamed	
Nationality	Egyptian	
Gender	Male	
Address	Werneuchener Str. 19 /13055 Berlin, Germany	
Phone no.	Office: (0049) 030-81044658 Fax: (0049) 030-8104 1637	
Email Address	<a href="mailto:alaa.mohamed@bam.de">alaa.mohamed@bam.de</a> , and <a href="mailto:al_fahmy@yahoo.com">al_fahmy@yahoo.com</a>	
Education	B.Sc. in Chemical Science (2001), Department of Chemistry, Faculty of Science, Al Azhar University, Cairo. Egypt.	
Grade	Excellent with honor degree	
Postgraduate	Studies two semesters ended on 2002	
Master Title	“Thermodynamic studies of formation of some important complexes in solutions” 2005	
MSc supervisors	Prof. Dr. Hassan A. Shehata, Prof. Dr. AbdAllah A. Mohammed (both of them Al Azhar University) and Prof. Dr. Fared I. Eldessouky (Canal Suez University)	
Registrations	PhD. student at Faculty of science, Al Azhar University, Cairo. Egypt 2006.	
Current Occupation	Assistant lecturer at Department of Chemistry, Faculty of science, Al Azhar Univer- sity. Cairo. Egypt.(from 8/2005 till now)	
Current Registrations	PhD. student at Faculty of science, Technical University Berlin, Germany	
PhD supervisors	Prof. Dr. Jörg F. Friedrich and Prof. Dr.-Ing. Manfred H. Wagner (BAM and TU Berlin)	
Language	Arabic (Native), English (Good) and Deutsch (average)	

### 2) Experiences

Ministry /Company/ Institute	Job	Time
The Egyptian Euro. Canada Company (for dyes), Menoufia, Egypt	Chemist	5 month (from 3/ 2002 to 7/ 2002)

<b>Ministry of the health, Menoufia, Egypt</b>	Chemist (chemical analysis Lab.)	1 year and 7 months (from 7/2003 to 2/2004)
<b>Ministry of the Scientific Research, Mubarak City for Scientific Research and Technology Applications, New Materials &amp; Advanced Technology Research Institute, Alexandria, Egypt</b>	Assistant Researcher	8 months (from 2/2004 to 10/2004)
<b>Ministry of the Higher Education, Faculty of science, Al Azhar University, Cairo, Egypt</b>	Administrator and Assistant Lecturer	from 11/2004 to 7/2005 and from 8/2005 till now
<b>Federal Institute for Materials Research and Testing, Berlin, Germany</b>	Researcher Assistant	from 10/2007 till now

## Publications from this work

### *Conferences and Seminars*

#### a. Conferences

- 1) 'Physical and Chemical Properties of Plasma Polymerized Acrylic Acid Thin Films' in :8<sup>th</sup> International Conference on Advanced Polymers via Macromolecular Engineering, (**Alaa Fahmy**, Renate Mix, Andreas Schönhals, Jörg Friedrich) Oct. 4 -7, **2009**, Dresden-Germany
- 2) 'Physical and Chemical Properties of Plasma Polymerized Allyl alcohol Thin Films' in 12<sup>th</sup> International Conference on Plasma Surface Engineering **PSE**, (**Alaa Fahmy**, Renate Mix, Andreas Schönhals, Jörg Friedrich) Sep. 13 -17, **2010**, Garmisch-Partenkirchen, Germany
- 3) 'Structure-Property Relationships of Thin Plasma Deposited Poly (acrylic acid) Films' in Deutsche Physikalische Gesellschaft e.V. DPG-Spring-Meeting, (**Alaa Fahmy**, Renate Mix, Andreas Schönhals, Jörg Friedrich) Mar. 13-18, **2011**, Dresden-Germany
- 4) 'Structure of Plasma-Deposited Copolymer Films Prepared from Acrylic Acid and Styrene in dependence on the precursor mixture' in 18<sup>th</sup> International Colloquium on Plasma Processes (CIP), (**Alaa Fahmy**, Renate Mix, Andreas Schönhals, Jörg Friedrich), Jul. 4-8, **2011**, Nantes, France

(The best student poster presentation)

- 5) 'Surface and Bulk Properties of Spin Coated Commercial and Plasma-Polymerized Polystyrene Thin Films' in dependence on the precursor mixture' in 18<sup>th</sup> International Colloquium on Plasma Processes (CIP), (**Alaa Fahmy**, Renate Mix, Andreas Schönhals, Jörg Friedrich), Jul. 4-8, **2011**, Nantes, France
- 6) 'Structure of Plasma-Deposited Copolymers Films Synthesized of the Two Chemically Well-Polymerizable Comonomer Acrylic Acid and Styrene' in dependence on the precursor mixture' in The 20<sup>th</sup> International Symposium on Plasma Chemistry (**Alaa Fahmy**, Renate Mix, Andreas Schönhals, Jörg Friedrich), Jul. 24-29, **2011**, Philadelphia, USA

**b. Workshop**

- 1) 'Surface and bulk of Thin Plasma Deposited Poly(acrylic acid) Films' in Fraunhofer-Institut für Angewandte Polymerforschung, Nov. **2009**, Golm, Germany

**c. Seminars**

- 1) 'Morphology and Properties of Plasma Deposited Poly(allyl alcohol) Nano Films' for Polymerwissenschaftliches Seminar in BAM, Oct. 7, **2010**, Berlin-Germany
- 2) 'Structure-Property Relationships of Thin Plasma Deposited Polymer Films' for Polymerwissenschaftliches Seminar in Technical University Berlin, Feb. 16, **2011**, Berlin, Germany
- 3) 'Plasma Deposition of Polymeric Thin Layer' for Doktorandenseminar – Polymerwissenschaften Seminar in BAM, Apr. 6, **2011**, Berlin, Germany

***Publications***

- 1) 'Structure of Plasma Deposited Poly (acrylic acid) Films' **Alaa Fahmy**, Renate Mix, Andreas Schönhals, Jörg Friedrich, Plasma Processes and Polymers, 8, 147, **2011**
- 2) 'Structure-Property Relationship of Thin Plasma Deposited Poly (allyl alcohol) Layers' **Alaa Fahmy**, Renate Mix, Andreas Schönhals, Jörg Friedrich, Plasma Chemistry and plasma processing, 31, 477, **2011**
- 3) 'Structure of Plasma-Deposited Copolymer Films Prepared from Acrylic Acid and Styrene' **Alaa Fahmy**, Renate Mix, Andreas Schönhals, Jörg Friedrich, accepted **2011**, ISPC 20; Plasma Chemistry and plasma processing

- 4) `Structure of Plasma-Deposited Copolymer Films Prepared from Acrylic Acid and Styrene: Part I Influence of the Duty Cycle´ Alaa Fahmy, Renate Mix, Andreas Schönhals, Jörg Friedrich, Accepted **2011**, Plasma Processes and Polymers
- 5) `Structure of Plasma-Deposited Copolymer Films Prepared from Acrylic Acid and Styrene with respect to the Comonomer Ratio´ Alaa Fahmy, Renate Mix, Andreas Schönhals, Jörg Friedrich, Submitted, **2011**, Plasma Processes and Polymers
- 6) `Bulk Structure Changes in Products From Spin Coated Thin Films under Surface Treatment with the impulse Plasma Ar, O<sub>2</sub>- and UV-Treated Plasma as well as Thin Plasma-Polymerized Polystyrene Films´ Alaa Fahmy, Renate Mix, Andreas Schönhals, Jörg Friedrich, To be submitted **2011**, Macromolecules

## Chapter 5

### References

- 
- [1] B. Eliasson , M. Hirth, U. Kogelschatz, J Phys D: Appl. Phys. **1987**, 20, 1421;
  - [2] B. Eliasson, W. Egli, U. Kogelschatz, Pure Appl. Chem. **1994**, 66, 1279;
  - [3] A. C. Gentile, M. J. Kushner, J. Appl. Phys. **1996**, 79, 3877;
  - [4] W. Crookes, Proceedings of the Royal Society of London, **1880**, 469;
  - [5] W. Crookes, Nature, **1879**, 20, 439;
  - [6] G. Hertz, R. Rompe, Academy Publisher, Berlin, **1973**;
  - [7] S. L. Miller, Science, **1953**, 117, 528;
  - [8] S. L. Miller, H. C. Urey, Science **1959**, 130, 245;
  - [9] P. L. Spedding, Nature, **1967**, 214, 124;
  - [10] H. Yasuda, J. Polym. Sci.: Macromolecular Reviews, **1981**, 16, 199;
  - [11] N. Na, Y. Xia, Z. Zhu, X. Zhang, R. Cooks, Angew. Chem. Int. Ed. **2009**, 48, 2017;
  - [12] E. Linder, A. Davis, J. Phys. Chem. **1931**, 35, 3649;
  - [13] Bondt, Deimann, P. van Trostwijk, Lauwerenburg, in: J. Fourcroy, Ann. Chem. **1796**, 21, 58;
  - [14] A. T. Bell in: Techniques and Applications of Plasma Chemistry, Edited by J. R. Hollahan, A. T. Bell, Chapter 1, John Wiley & sons New York, **1974**;
  - [15] J. L. Cecchi In: S. M. Rossnagel, J. J. Cuomo, W. D Westwood, Ed. In: plasma processing technology. Park Ridge, N. J: Noyes Publication; **1990**;
  - [16] F. S. Denes, S. Manolache, Prog. Polym. Sci. **2004**, 29, 815;
  - [17] H. Herman, Plasma-sprayed coatings. Sci Am. **1988**, 259,112;
  - [18] D. R. Mac Rae, Plasma Chem. Plasma Process. **1989**, 9, 85;
  - [19] P. Zhang, Macromolecules, **1999**, 32, 2149;

- 
- [20] L. Rishina, E. Visen, L. Sosnovskaya, T. Lodugina, L. Shibryaeva, A. Veretennikova, and A. Gilman, *J. Eur. Polym.* **1998**, 37, 1013;
- [21] L. A. Rishina, L. S. Shibryaeva, A. B. Gil'man, , N. P. Bessonova, T. A. Ladygina, D. P. Shashkin, *Vysokomol. Soedin. Ser. A*, **2000**, 42, 441;
- [22] J. Friedrich, I. Loeschcke, J. Gähde, K. Richter, *Acta Polymerica*, **1981**, 32, 337;
- [23] M. Ozdemir, C. Yurteri, H. Sadikoglu, *Critical Reviews in Food Science and Nutrition*, **1999**, 39, 457;
- [24] J. Friedrich, W. Unger, A. Lippitz, I. Koprinarov, St. Weidner, G. Kühn, L. Vogel, in: *Metallized Plastics 5 & 6: Fundamental and Applied Aspects*, K. Mittal, (ed.), VSP, Utrecht, **1998**, 271;
- [25] N. Inagaki (Editor); "Plasma Surface Modification and Plasma Polymerization", Technomic Publishing Inc. USA. **1996**;
- [26] H. Yasuda (Editor); "Plasma Polymerisation", Academic Press Inc. London, **1985**;
- [27] J. F. Friedrich, I. Retzko, G. Kühn, W. E. S. Unger, A. Lippitz, *Surf. Coat. Technol.* **2001**, 142, 460;
- [28] H. König, G. Helwig, *Y. Physik*, **1951**, 129, 491;
- [29] H. Schmellenmeier, *Exp. Techn. Phys.* **1953**, 1, 49;
- [30] J. Goodmann, *J. Polym. Sci.* **1960**, 44, 551;
- [31] L. V. Gregor, *IBM Journal*, **1968**, 140;
- [32] A. Brockes, H. König, *Y. Physik*, **1958**, 152, 75;
- [33] P. Favia, R. d'Agostino, *Surf. Coat. Technol.* **1998**, 98, 1102;
- [34] R. Mix, J. Falkenhagen, R.-D. Schulze, V. Gerstung, J. F. Friedrich, *Poly. surf. Modifi.* edited by K. L. Mittal, **2009**, 5, 317;
- [35] R. d'Agostino (Editor); "Plasma Deposition, Treatment, and Etching of Polymers", Academic Press, Inc. London, **1990**;

- 
- [36] H. Biederman, Y. Osada; Adv. Polymer Sci. **1990**, 95, 59;
- [37] Y. S. Yeh, I. N. Shyy, H. Yasuda; J. Appl. Polym. Sci., Appl. Polym. Symp. **1988**, 42, 1;
- [38] H. Y. Kim, H. K. Yasuda; J. Vac. Sci. Technol. A, **1997**, 15, 1837;
- [39] J. Friedrich, R. Mix, G. Kühn, I. Retzko, A. Schönhals, W. Unger; Composite Interfaces, **2003**, 10, 173;
- [40] A. M. Hynes, M. J. Shenton, M. J. Badyal; Macromolecules, **1996**, 29, 4220;
- [41] C. L. Rinsch, X. Chen, V. Panchalingam, R. C. Eberhart, J. H. Wang, R. B. Timmons; Langmuir, **1996**, 12, 2995;
- [42] J. H. Wang, J. J. Chen, R. B. Timmons; Chem. Mater. **1996**, 8, 2212;
- [43] L. M. Han, K. Rajeshwar, R. B. Timmons; Langmuir, **1997**, 13, 5941;
- [44] M. T. van Os, B. Menges, R. Foerch, G. J. Vansco, W. Knoll; Chem. Mater, **1999**, 11, 3252;
- [45] J. Friedrich, G. Kühn, J. Gähde, Acta Polymerica, **1979**, 30, 470;
- [46] T. R. Gengenbach, Z. R. Vasic, R. C. Chatelier, H. J. Griesser; J. Polym. Scien. A, **1994**, 32, 1399;
- [47] W. E. S. Unger, S. Swaraj, U. Oran, A. Lippitz, Surf. Interface Anal. **2006**, 38, 522;
- [48] A. Hiratsuka, I. Karube, Electroanalysis, **2000**, 12, 695;
- [49] H. Yasuda, M. Gazicki. Biomaterials, **1982**;
- [50] V. Cech, J. Studynka, N. Conte, V. Perina, Surf. Coat. Technol. **2007**, 201, 5512;
- [51] R. Prikryl, V. Cech, L. Zajickova, J. Vanek, S. Behzadi, F. R. Jones, Surf. Coat. Technol. **2005**, 200, 468;
- [52] D. S. Kumar, Y. Yoshida, Surf. Coat. Technol. **2003**, 169, 600;
- [53] J. Studynka, B. Cechalova, V. Cech. Surf. Coat. Technol. **2008**, 202, 5505;
- [54] V. Cech , J. Studynka , B. Cechalova , J. Mistrik , J. Zemek, Surf. Coat. Technol. **2008**, 202, 5572;



- 
- [55] A. P. Bradley, J. P. Hammes, J. Electrochem. Soc. **1963**, 110, 15;
- [56] H. Biederman, D. Slavinska, Surf. Coat. Technol. **2000**, 125, 371;
- [57] D. S. Kumar, J. Appl. Polym. Sci. **2000**, 75, 1176;
- [58] F. U. Z. Chowdhury, A. H. Bhuiyan, Thin Solid Films, **2000**, 370, 78;
- [59] J. Yang, C. Shim, D. Jung, Thin Films Chem. Vap. Dep. **2002**, 8, 35;
- [60] X.-Y. Zhao, M.-Z. Wang, Z. Wang, Plasma Processes. Polym. **2007**, 4, 840;
- [61] H. Jiang, L. Hong, N. Venkatasubramanian, J. T. Grant, K. Eyink, K. Wiacek, S. Fries-Carr, J. Enlow, T. J. Bunning, Thin Solid Films, **2007**, 515, 3513;
- [62] A. G. Shard, J. P. S. Badyal, J. Phys. Chem. **1991**, 95, 9438;
- [63] N. Medard, J.-C. Soutif, F. Poncin-Epaillard, Surf. Coat. Technol. **2002**, 160, 197;
- [64] S. J. Oh, D. R. Kinney, W. Wang, P. L. Rinaldi, Macromolecules, **2002**, 35, 2602;
- [65] A. R. Denaro, P. A. Owens, A. Crawshaw. Eur. Pol. J. **1970**, 6, 487;
- [66] F. Fally, I. Virlet, J. Riga, J. J. Verbist, J. Appl. Polym. Sci. **1996**, 59, 1569;
- [67] J. Friedrich, G. Kühn, R. Mix, W. Unger, Plasma Process. Polym. **2004**, 1, 28;
- [68] K. Yoshimura, K. Hozumi, T. Tatsuta, M. Sawai, O. Tsuji. J. Appl. Pol. Sci. **1996**, 59, 1033;
- [69] L. O'Toole, R. D. Short, J. Chem. Soc., Faraday Trans. **1997**, 93, 1141;
- [70] W. R. Gombotz, A. S. Hoffman. J. Appl. Pol. Sci. Symp. **1988**, 42, 285;
- [71] A. P. Ameen, R. D. Short, R. J. Ward; Polymer, **1994**, 35, 4382;
- [72] S. U. Oran, S. Swaraj, J. F. Friedrich, W. E. S. Unger. Plasma Processes. Pol. **2005**, 2, 563;
- [73] S. Candan, Turk, J. Chem. **2002**, 26, 783;
- [74] C.-M. Chan, T.-M. Ko, H. Hiraoka, Surf. Sci. Rep. **1996**, 24, 1;
- [75] C. C. Dupont-Gillain, Y. Adriaensen, S. Derclaye, P. G. Rouxhet, Langmuir, **2000**, 16, 8194;

- 
- [76] C. C. Dupont-Gillain, B. Nysten, V. Hlady, P. G. Rouxhet, J. Colloid Interface Sci. **1999**, 220, 163;
- [77] S. Wild, L. L. Kesmodel, J. Vac. Sci. Technol. A, **2001**, 19, 856;
- [78] S. C. Choi, W. K. Choi, HJ. Jung, B. C. Chung, Y. S. Yoo, S. K. Koh. J. Appl. Polym. Sci. **1999**, 73, 41;
- [79] J. Lub, FCBMV. Vroonjoven, E. Bruninx. Polymer, **1998**, 30, 40;
- [80] F. M. Petrat, D. W. Wolany, B. C. Schwede, L. Wiedmann, A. Benninghoven. Surf. Interface Anal. **1994**, 21, 274;
- [81] R. Foerch, NS. McIntyre. J. Polym. Sci. Polym. Chem. **1990**, 28, 193;
- [82] N. Inagaki, S. Tasaka, K. Hibi. Polym. Preprints, **1990**, 31, 380;
- [83] N. Shahidzadeh-Ahmadi, MM. Chehimi, F. Arefi-Khonsari, N. Foulon-Belkacemi, J. Amouroux, M. Delamar. Colloids Surf. Physicochem. Eng. Asp. **1995**, 105, 277;
- [84] E. Occhiello, M. Morra, P. Cinquina, F. Garbassi. Polymer, **1992**, 33, 3007;
- [85] A. Hollander, J. E. Klemberg-Sapieha, M. R. Wertheimer. J. Polym. Sci. Polym. Chem. **1995**, 33, 2013;
- [86] H. Miura, K. Sugiyama, M. Oshima, S. Kanagawa, T. Matsuda, T. Mitamura, O. Nomura. Communication, **1998**, 10, 656;
- [87] H.-G. Elias, An Introduction to Polymer Science. VCH, Weinheim, **1997**;
- [88] J. Friedrich, J. Gähde, H. Frommelt, H. Wittrich, Faserforsch. Textiltechn./Z. Polymerenforsch. **1976**, 27, 520;
- [89] A. R. Westwood, J. Eur. Polym. **1971**, 7, 363;
- [90] U. Oran, S. Swaraj, J. F. Friedrich, W. E. S. Unger, Surf. Coat. Technol. **2005**, 200, 463;
- [91] O. Tsuji, T. Minaguchi, H. Nakano, Thin Solid Films, **2001**, 390, 159;
- [92] R. Daw, T. O'Leary, J. Kelly, R. D. Short, M. Cambray-Daekin, A. J. Devlin, I. M. Brook, A. Scutt, S. Kothari, Plasmas Polym. **1999**, 4, 113;

- 
- [93] R. M. France, R. D. Short, E. Duval, F. R. Jones, *Chem. Mater.* **1998**, 10, 1176;
- [94] T. Hirotsu, Z. Hou, A. Partridge, *Plasmas Polym.* **1999**, 4, 1;
- [95] T. Hirotsu, C. Tagaki, A. Partridge, *Plasmas Polym.* **2002**, 7, 353;
- [96] M. R. Alexander, T. M. Duc, *Polymer*, **1999**, 40, 5479;
- [97] A. J. Beck, F. R. Jones, R. D. Short, *Polymer*, **1996**, 37, 5537;
- [98] T. Shirafiji, Y. Miyazaki, Y. Hayashi, S. Nishino, *Plasma Polym.* **1999**, 4, 57;
- [99] K. Yoshimura, T. Minaguchi, H. Nakano, T. Tatsuta, O. Tsuji, *J. Photopolym. Sci. Technol.* **2001**, 12, 73;
- [100] T. Shirafiji, Y. Miyazaki, Y. Nakagami, Y. Hayashi, S. Nishino, *Jpn. J. Appl. Phys.* **1999**, 38, 4520;
- [101] A. J. Beck, J. D. Whittle, N. A. Bullett, P. Eves, S. Mac Neil, S. L. McArthur, A. G. Shard, *Plasma Process. Polym.* **2005**, 2, 641;
- [102] H.-G. Elias, *Macromolecules*, Hüthig & Wepf, Basle, **1990**, 221;
- [103] J. Friedrich, R. Mix, G. Kühn, in: *Plasma Processing and Polymers*, R. d'Agostino, P. Favia, C. Oehr, M. R. Wertheimer, Wiley-VCH, Weinheim, S. **2005**, 3;
- [104] R. A. Dawson, R. D. Short. *Biomaterials*, **1998**, 19, 1717;
- [105] S. Swaraj, U. Oran, J. F. Friedrich, A. Lippitz, W. E. S. Unger. *Plasma Processes. Polym.* **2007**, 4, 376;
- [106] A. Fahmy, R. Mix, A. Schönhals, J. F. Friedrich *Plasma Process. Polym.* **2011**, 8, 147;
- [107] A. Fahmy, R. Mix, A. Schönhals, J. F. Friedrich, *Plasma Chem. Plasma Process.* **2011**, 31, 477;
- [108] J. Friedrich, G. Kühn, R. Mix, A. Fritz, A. Schönhals, *J. Adhesion Sci. Technol.* **2003**, 17, 1591;
- [109] J. F. Friedrich, R. Mix, G. Kuehn, *Surf. Coat. Technol.* **2005**, 200, 565;

- 
- [110] N. Lopattananon, A. S. Hayes, R. F. Jones, Proc Int Conf Fibre Reinforced Composites, **2000**, 345;
- [111] K. Yoshimura, T. Minaguchi, H. Nakano, T. Tatsuta, O. Tsuji, J. Photopolym. Sci. Technol. **2001**, 13, 13;
- [112] R. Chen, M. S. Silverstein. J. Polym. Sci. Part A. Polym. Chem. **1996**, 34, 207;
- [113] M. A. Golub, T. Wydeven, L. S. Finney, Polym. Prepr. (Am. Chem. Soc. Div. Polym. Chem.), **1995**, 36, 107;
- [114] H. Jianga, J. T. Grantb, K. Eyinka, S. Tullisa, J. Enlowa, T. J. Bunning, Polymer, **2005**, 46, 8178;
- [115] R. Hansen, H. Schonhorn, J. Polym. Sci. B4, **1966**, 4, 203;
- [116] A. Denaro, K. Hough, Electrochim. Acta, **1973**, 18, 863;
- [117] A. P. Kettle, A. J. Beck, L. O'Toole, F. R. Jones, R. D. Short, Comp. Sci. Technol. **1997**, 57, 1023;
- [118] C. Oehr, M. Müller, B. Elkin, D. Hegemann, U. Vohrer, Surf. Coat. Technol. **1999**, 116, 25;
- [119] L. Detomaso, R. Gristina, G. S. Senesi, R. d'Agostino, P. Favia, Biomaterials, **2005**, 26, 3831;
- [120] G. Habenicht, Kleben, 6th ed., Springer, Berlin, **2009**;
- [121] E. Dayss a, G. Leps a, J. Meinhardt, Surf. Coat. Technol. **1999**, 116, 986;
- [122] V. Sciarratta, U. Vohrer, D. Hegemann, M. Müller, C. Oehr, Surf. Coat. Technol. **2003**, 174, 805;
- [123] A. Eftekhari, Synthetic Metals, **2002**, 125, 295;
- [124] M. A. Garcia, J. Llopis, M. A. Villegas, S. E. Paje, J. Alloys Compd. **2001**, 323, 367;
- [125] H. T. Sun, L. Wen, Z. C. Duan, L. L. Hu, J. J. Zhang, Z. H. Jiang, J. Alloys Compd. **2006**, 414, 142;

- 
- [126] Y. Zhou<sup>a</sup>, M. H. Hong<sup>b</sup>, J. Y. H. Fu<sup>a</sup>, L. Lua, B. S. Lukyanchuk, Z. B. Wang, Journal of Alloys and Compounds, **2008**, 449, 246;
- [127] S. Y. Chou, P. R. Krauss, P. J. Renstrom, J. Vac. Sci. Technol. B, **1996**, 14, 4129;
- [128] J. R. Wendt, G. A. Vawter, R. E. Smith, M. E. Warren, J. Vac. Sci. Technol. B, **1995**, 13, 2705;
- [129] J.V. Cauich-Rodriguez et al. Biomaterials, **1996**, 17, 2259;
- [130] A. De La Rosaa, L. Heuxa, J. Y. Cavaille, Polymer **2001**, 42, 5371;
- [131] J. L. de la Fuentea, M. Wilhelm, H. W. Spiess, E. L. Madruga, M. Fernandez-Garcia, M. L. Cerrada, Polymer, **2005**, 46, 4544;
- [132] L. Labahn, R. Mix, A. Schönhals, Phys. Rev. **2009**, 79, 011801;
- [133] T. Strunskus, V. Zaporojtchenko, K. Behnke, C. von Bechtolsheim, F. Faupel, Advan. Eng. Mat. **2000**, 2, 489;
- [134] M. R. Alexander, P. V. Wright, B. D. Ratner, Surf. Interf. Anal. **1996**, 24, 217;
- [135] A. Chilcoti, B. D. Ratner in: *Surface Characterization of advanced polymers*, Editor: L. Sabbatini, P. G. Zambonin, VCH **1993**, 221.
- [136] J. Friedrich, W. Unger, A. Lippitz, I. Koprinarov, G. Kühn, St. Weidner, L. Vogel, Surf. Coat. Technol. **1992**, 59, 371;
- [137] A. Chilkoti, B. D. Ratner in “Surface Characterization of Advanced Polymers” edited by L. Sabbattini, P. G. Zambonin: **1996**, 221;
- [138] A. Chilkoti, B. D. Ratner, D. Briggs, Chem. Mater. **1991**, 3, 51;
- [139] A. Schönhals, Molecular Dynamics in Polymer Model Systems In: Broadband Dielectric Spectroscopy, F. Kremer, A. Schönhals, Eds.; Springer: Berlin, **2002**, 225;
- [140] F. Kremer, A. Schönhals, Broadband Dielectric Measurement Techniques in Broadband Dielectric Spectroscopy, edited by F. Kremer, A. Schönhals, Springer: Berlin, **2002**, 35;

- 
- [141] S. Swaraj, U. Oran, A. Lippitz, J. F. Friedrich, W. E.S. Unger, *Plasma Process. Polym.* **2007**, 4, 784;
- [142] N. Tanaka, H. Kitano, N. Ise, *Macromolecules*, **1991**, 24, 3017;
- [143] Y. Akiyama, S. Fujita, H. Senboku, C. M. Rayner, S. A. Brough, M. Arai, *J. Supercritical Fluids*, **2008**, 46, 197;
- [144] N. G. McCrum, B. E. Read, G. Williams, *Anelastic and Dielectric Effects in Polymeric Solids*. Wiley, New York (reprinted by Dover Publications), **1991**;
- [145] S. Havriliak, S. Negami, *Polymer*, **1967**, 8, 161;
- [146] F. Kremer, A. Schönhals, in *Broadband Dielectric Spectroscopy*, edited by F. Kremer, A. Schönhals, Springer: Berlin, **2002**, 59;
- [147] F. Kremer, A. Schönhals, in *Broadband Dielectric Spectroscopy*, edited by F. Kremer, A. Schönhals, Springer: Berlin, **2002**, 1;
- [148] A. De La Rosa, L. Heux, J. Y. Cavaille *Polymer*, **2000**, 41, 7547;
- [149] L. Watkins, A. Bismarck, A. F Lee, D. Wilson, K. Wilson, *Appl. Surf. Sci.* **2006**, 252, 8203;
- [150] S. J. Oh, D. R. Kinney, W. Wang, P. L. Rinaldi, *Macromolecules*, **2002**, 35, 2602;
- [151] J. P Runt, J. J. Fitzgerald (Editors) *Dielectric Spectroscopy of Polymeric Materials*, ACS books Washington DC **1997**;
- [152] F. Kremer, A. Schönhals *Broadband Dielectric Spectroscopy*, L. Hartmann, K. Fukao , F. Kremer, Eds.; Springer: Berlin, **2002**, 433;
- [153] H. Z. Vogel, *Phys.* **1921**, 22, 645 ;
- [154] G. S. Fulcher, *J. Am. Ceram. Soc.* **1925**, 8, 339 ;
- [155] G. Tammann, G. Z. Hesse *Anorg. Alleg. Chem.* **1926**, 156, 245 ;
- [156] A. Kettle, A. Becj, L. Toole, F. Jones, R. Short. *Comp. Sci. Tech.* **1996**, 57, 1023;

- 
- [157] N. Shahidzadeh, F. Arefi-Khonsari, M. M. Chehimi, J. Amouroux. *J. Surf. Sci.* **1996**, 352, 888;
- [158] A. Nakao, Y. Suzuki, M. Iwaki. *J. Colloid Interface Sci.* **1998**, 197, 257;
- [159] I. Retzko, J. F. Friedrich, A. Lippitz, W. E. S. Unger, *J. Electr. Spectr. Rel. Phenom.* **2001**, 121, 111;
- [160] R. Rochotzki, M. Nitschke, M. Artz, J. Meischner, *Phys. Stat. Sol (a)* **1994**, 145, 289;
- [161] J. E. Kennedy , J. G. Lyons , L. M. Geever , C. L. Higginbotham, *Mater. Sci. and Eng. C* **2009**, 29, 1655;
- [162] S. Munteanu, C. Vasile, *Polym. Degr. and Stab.* **2005**, 89, 501;
- [163] M. Romero-Sanchez, M. Pastor-Blas, J. Martin-Martinez, *Inter. J. of Adhesion and Adhesives* **2005**, 25, 19;
- [164] Y. M. Chung, J. G. Han, *Surf. Coat. Technol.* **2007**, 201, 5030;
- [165] J. F. Rabek, *Photodegradation*, Chapman & Hall, London, **1996**;
- [166] A. B. Gil'man, *High Energy Chemistry*, **2003**, 37, 17;
- [167] W. J. Wedenejew, L. W. Gurwitsch, W. H. Kondratjew, W. A. Medwedew; E. L. Frankewitsch, *Energien chemischer Bindungen, Ionisationspotentiale und Elektronenaffinitäten*, VEB Deutscher Verlag für Grundstoffindustrie, Leipzig, 1971.
- [168] S. Chang, T. Xie, G. Yang, *J. Appl. Polym. Sci.* **2006**, 102, 5184;
- [169] J. Friedrich, G. Kühn, R. Mix, *Progr. in Colloid Polym. Sci.* **2006**, 132, 62;
- [170] R. Kerber, *Die Makromolekulare Chemie*, **1966**, 96, 30;
- [171] H. Irai, *J. Polymer Sci. Macromolecular Reviews*, **1976**, 11, 47;
- [172] K. Gorna, S. Gogolewski. *Polym. Degr. Stab.* **2003**, 79, 475;
- [173] S. Hwang, M. Tseng, J. Shu, H. Her Yu. *Surf. Coat. Technol.* **2008**, 202, 3669;
- [174] R. Mix, J. Falkenhagen, J. F. Friedrich, Poster, conference Macro, **2010**;

- 
- [175] S. Dubinskya, G. S. Graderb, G. E. Shterb, M. S. Silverstein, Polym. Degr. Stab. **2004**, 86 171;
- [176] J. Wang, Polymer Sci. C, Polymer Letters, **1990**, 28, 317;
- [177] C. Lau, Y. Mi, Polymer **2002**, 43, 823;
- [178] R. Larrain, L. H. Tagle, F. R. Diaz, Polymer Bulletin, **1981**, 4, 487;
- [179] T. G. Fox, P. J. Flory, J. Polym. Sci. **1954**, 14,315;
- [180] H. Irai, J. Polymer Sci. Macromolecular Reviews, **1976**, 11, 47;
- [181] J. Dong, Y. Ozaki, K. Nakashima, Macromolecules, **1997**, 30, 1111;
- [182] L. Zhang, M. Mizukami, K. Kurihara, Macromol. Symposia, **2008**, 270, 40;
- [183] J. Friedrich, I. Retzko, G. Kühn, W. Unger, A. Lippitz, in: Metallized Plastics 7: Fundamentals and Applied Aspects, K. L. Mittal (ed.), VSP, Utrecht, **2001**, 117;
- [184] J. K. Stille, R. L. Sung, J. van der Kooi, J. Org. Chem. **1965**, 30, 3116;